Carnegie Mellon University

CARNEGIE INSTITUTE OF TECHNOLOGY

THESIS

SUBMITTED IN PARTIAL FULFILLMENT OF THE REQUIREMENTS

FOR THE DEGREE OF Doctor of Philosophy

TITLE Enzymatic Biosensor and Biofuel Cell Development Using Carbon Nanomaterials and Polymer-Based Protein Engineering

PRESENTED BY Alan S. Campbell

ACCEPTED BY THE DEPARTMENT OF

Biomedical Engineering

ADVISOR, MAJOR PROFESSOR	DATE
ADVISOR, MAJOR PROFESSOR	DATE
DEPARTMENT HEAD	DATE

APPROVED BY THE COLLEGE COUNCIL

DEAN	DATE

Enzymatic Biosensor and Biofuel Cell Development Using Carbon Nanomaterials and Polymer-Based Protein Engineering

Submitted in partial fulfillment of the requirements for

the degree of

Doctor of Philosophy

in

Department of Biomedical Engineering

Alan S. Campbell

B.S., Chemical Engineering, West Virginia University
M.S., Chemical Engineering, West Virginia University

Carnegie Mellon University
Pittsburgh, PA

April, 2017

ACKNOWLEDGEMENTS

There are many people to acknowledge who have helped me over my years as a PhD student. The work in this dissertation would not have been possible without the technical and personal support from these many individuals.

First, I would like to thank my advisor and committee chair Dr. Alan Russell and my advisor Dr. Mohammad Islam, who have always encouraged me to have confidence in the work I have done and what I was capable of doing. They allowed me to pursue projects that I was particularly interested in while always guiding me toward success. I firmly believe I would not have accomplished the completion of this work without their advice and example. My years working with them have catalyzed my development as a researcher and will assist me throughout my career. Additionally, I would like to thank the members of my dissertation committee, Dr. Krzysztof Matyjaszewski, Dr. Todd Przybycien and Dr. Tzahi Cohen-Karni. Their guidance from my thesis proposal through my dissertation has directly helped me through constructive criticism to improve the scientific path of this dissertation.

I would also like to thank the many members, past and present, of the Russell and Islam labs that have each helped me in different ways. Jill, Rick, Hiro, Chad, Collin, Weihang, Sheiliza, Steven, Evan, Chloe, Brian, Patrick, Max and Michelle. Without question, Hiro, Chad, Jill and Evan deserve much of my gratitude as they trained me upon beginning my PhD and continued to assist in any way possible throughout my research endeavors. I am thankful to all of the great researchers I have had the opportunity to work with throughout my time at CMU. I would also like to thank Dr. Conrad Zapanta who was always willing to provide advice in all aspects of my PhD experience.

Most importantly, I would like to thank my parents, family and friends, particularly Chelsi, for their personal and emotional support during my time in graduate school. Their words of encouragement and constant support made this all possible. Of utmost importance was Chelsi, as she was always the one person to listen and unconditionally support or motivate me to accomplish everything I was capable. Again, this would not have been possible without her.

Finally, I would like to acknowledge the CMU Deans for funding the Center for Polymer-Based Protein Engineering and part of this research along with the National Science Foundation (CBET-1066621; CBET-1335417; CMMI-1335417), Heinz Endowment (E0530) and the Pennsylvania Infrastructure Technology Alliance program.

ABSTRACT

The development of enzymatic biosensors and enzymatic biofuel cells (EBFCs) has been a significant area of research for decades. Enzymatic catalysis can provide for specific, reliable sensing of target analytes as well as the continuous generation of power from physiologically present fuels. However, the broad implementation of enzyme-based devices is still limited by low operational/storage stabilities and insufficient power densities. Approaches to improving upon these limitations have focused on the optimization of enzyme activity and electron transfer kinetics at enzyme-functionalized electrodes. Currently, such optimization can be performed through enzyme structural engineering, improvement of enzyme immobilization methodologies, and fabrication of advantageous electrode materials to enhance retained enzyme activity density at the electrode surface and electron transfer rates between enzymes and an electrode. In this work, varying electrode materials were studied to produce an increased understanding on the impacts of material properties on resulting biochemical, and electrochemical performances upon enzyme immobilization and an additional method of electroactive enzyme-based optimization was developed through the use of polymer-based protein engineering (PBPE). First, graphene/single-wall carbon nanotube cogels were studied as supports for membrane- and mediator-free EBFCs. The high available specific surface area and porosity of these materials allowed the rechargeable generation of a power density within one order of magnitude of the highest performing glucose-based EBFCs to date. Second, two additional carbon nanomaterial-based electrode materials were fabricated and examined as EBFC electrodes. Graphene-coated single-wall carbon nanotube gels and gold nanoparticle/multi-wall carbon nanotube-coated polyacrylonitrile fiber paddles were utilized as electroactive enzyme supports. The performance

comparison of these three materials provided an increased understanding of the impact of material properties such as pore size, specific surface area and material surface curvature on enzyme biochemical and electrochemical characteristics upon immobilization. Third, PBPE techniques were applied to develop enzyme-redox polymer conjugates as a new platform for enzymatic biosensor and EBFC optimization. Poly(*N*-(3-dimethyl(ferrocenyl) methylammonium bromide)propyl acrylamide) (pFcAc) was grown directly from the surface of glucose oxidase (GOX) through atom-transfer radical polymerization. Utilization of the synthesized GOX-pFcAc conjugates led to a 24-fold increase in current generation efficiency and a 4-fold increase in EBFC power density compared to native GOX. GOX-pFcAc conjugates were further examined as working catalysts in carbon paper-based enzymatic biosensors, which provided reliable and selective glucose sensitivities and allowed a systematic analysis of sources of instability in enzyme-polymer conjugate-based biosensors and EBFCs. The knowledge gained through these studies and the in-depth characterization of an additional layer of optimization capacity using PBPE could potentially enhance the progress of enzymatic biosensor and EBFC development.

TABLE OF CONTENTS

LIST OF TABLES

LIST OF FIGURES

Chapter 1: Introduction

1.1 Enzyme-Based Biosensors and Biofuel Cells

The catalytic and operational properties of enzymes have made them a significant research target for an array of applications.[1-5] Their unique combination of efficient, selective catalysis and benign operational conditions make them ideally suited for particular uses with decades of research already devoted to expanding and optimizing their industrial, medical and analytical capabilities.[5-9] The innovation of the first enzyme electrode by Clark and Lyons in 1962 marked the advent of research into the development of enzyme-based bioelectronics that has produced a variety of impactful devices and technologies.[1, 10, 11] Since this initial discovery, investigations into enzymatic biosensors and enzymatic biofuel cells (EBFCs) have yielded hundreds of scientific publications and patents with several devices already on the market, however, there yet remain persistent operational, applicability, and feasibility issues to address for their broad implementation.[12-15]

1.1.1 Operation and development of enzymatic biosensors and biofuel cells

In general, enzymatic biosensors and EBFCs operate through the oxidation and/or reduction of physiologically-present molecules at or near an electrode surface *via* enzymatic catalysis.[1, 16] Both systems rely on the consistent turnover of target substrate coupled with efficient electron transfer between the working enzyme and the electrode surface.[14] This electron transfer can be either oxidative or reductive toward the working enzyme (*i.e.* oxidative = electron transfer from enzyme/solution to electrode; reductive = electron transfer from electrode to enzyme/solution) dependent on the selected enzyme and device configuration.[17] The work presented here was primarily aimed at investigation of oxidative, or anodic, enzymatic systems. It is worth noting, that much research has also been performed on the development of microbial-

based biosensors and biofuel cells, which utilize whole cells as working catalysts. The redox reactions occurring within these systems can be enzymatic; however, whole microorganisms are necessary for operation.[18-20] In this report, I focus exclusively on enzymatic biosensors and EBFCs that use independent electroactive enzymes as the working catalysts. Owing to the broad selection of available working enzymes, an array of substrates can be specifically targeted depending on the system of interest.[21, 22] Applications ranging from the sensing of, or current generation by varying sugars and alcohols to DNA, RNA and antibodies have been explored; however, perhaps the most prevalent and impactful are glucose-driven systems, which were the target of this work.[21-30]

Electrochemical enzymatic biosensors rely on specific substrate turnover with reaction rates and resulting electrochemical responses directly correlated to substrate concentrations.[1] Fluctuations in biosensor output can be monitored through changes in cell voltage (potentiometric), electrode conductance (conductometric) or current response (amperometric) with most reported systems focusing on amperometric measurements.[31] Amperometric responses are generally produced through an externally applied voltage relative to a known reference electrode such as a saturated calomel electrode (SCE) or an Ag/AgCl electrode.[32] The system developed by Clark and Lyons consisted of an enzymatic layer entrapped over an oxygen-sensing electrode by a semipermeable membrane.[10] In this case, the working enzyme was glucose oxidase (GOX), which catalyzed the oxidation of β-D-glucose by molecular oxygen to glucono-δ-lactone and hydrogen peroxide.[10, 33] Amperometrically detected fluctuations in oxygen concentration caused by the enzymatic reaction, coupled with glucose oxidation were correlated to changing glucose concentrations. This technology was soon expanded to systems with multiple electrodes for improved reliability against interfering agents and to hydrogen

peroxide-based sensors to directly monitor the enzymatic reaction product.[34, 35] These types of sensors that target the detection of enzymatic reaction product or co-substrate were first-generation glucose biosensors (**Figure 1.1A**).[1] Similar systems are still a topic of investigation due to their simple and easily miniaturized sensing methodology, but are susceptible to unreliability stemming from fluctuations in bulk oxygen concentration and oxidation of other physiologically present species at the high applied working potentials required for hydrogen peroxide oxidation.[1, 36-38]

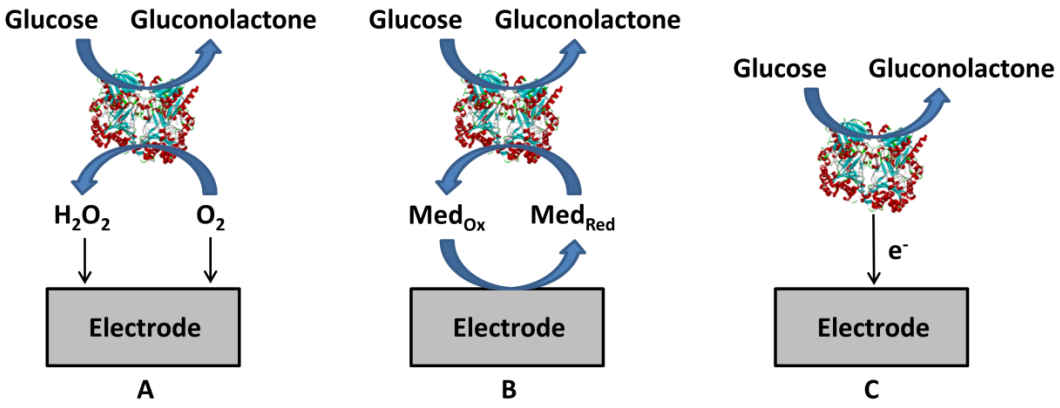

Figure 1.1 Schematic representation of amperometric glucose-driven enzymatic biosensor generations. A) First-generation glucose biosensors detect glucose concentration through oxidation or reduction of enzymatic reaction product or co-substrate at the electrode surface. B) Second-generation glucose biosensors detect glucose concentration by MET between the enzyme active site and the electrode upon substrate turnover. C) Third-generation glucose biosensors detect glucose concentration by DET between the enzyme active site and the electrode. Enzymatic reaction of GOX depicted. Med_{Ox} and Med_{Red} signify oxidized and reduced forms of electron mediator, respectively.

To increase reliability, groups have investigated the use of externally added, non-physiological redox-active compounds to shuttle electrons between the working enzyme and the electrode through what was termed mediated electron transfer (MET).[39-41] These second-

generation glucose biosensors use redox species such as ferrocene-, osmium-, cobaltocene-, or quinone-containing compounds as intermediates between enzymatic reaction and electron transduction at the electrode (**Figure 1.1B**).[39, 42] Redox mediators have been incorporated at enzyme-modified electrodes in a variety of ways to combat use-specific challenges, but are yet prone to interference by oxygen as a competitive oxidant and to increased instabilities due to the additional redox components/steps.[1, 43] Thus, much research has been performed on the fabrication of third-generation glucose biosensors capable of direct electron transfer (DET) between the enzyme active site and an electrode (**Figure 1.1C**).[44-46] However, reliable DET has been reported for only a few electroactive enzymes due to the dense protein layer surrounding many enzyme active sites.[45-47] The primary target of work in this area has been the development of electrode materials and enzyme immobilization strategies that allow close interaction between the enzyme active site and the electrode to reduce the necessary electron transfer distance.[45, 48] This mediator-less operation is an active topic of current research.

Shortly after the emergence of the first enzyme electrode, Yahiro *et al.* reported on the first glucose-driven EBFC in 1964.[49] This EBFC was composed of a GOX-catalyzed, iron powder-mediated anode and a platinum-based cathode.[49] Several early EBFCs operated with similar configurations using MET at an enzyme-modified anode and a non-enzymatic, reducing platinum-cathode.[13] The first EBFC to use both an enzyme-modified anode and an enzyme-modified cathode was reported by Laane *et al.* in 1984, which utilized the enzyme chloroperoxidase to catalyze the reduction of hydrogen peroxide generated by gold-based catalytic activity at the cathode.[50] Since these pioneering studies, many varying configurations of glucose-driven EBFCs have been reported with fully enzymatic catalysis at both electrodes and with varying electron transfer methodologies similar to enzymatic biosensors (**Figure 1.1**).

Common oxygen reducing cathodic working enzymes reported include the multicopper oxidases laccase and bilirubin oxidase (BOD).[51, 52] In general, glucose driven EBFCs convert the chemical energy present in glucose into electrical power through glucose oxidation at an enzyme-modified anode and the reduction of a final electron acceptor (generally molecular oxygen) at an enzyme-modified cathode (**Figure 1.2**).[14] The transfer of electrons between the enzyme active sites and electrodes has been achieved through oxygen-mediated electron transfer, MET and DET.[13, 14] On average, EBFCs generate lower power densities compared to their conventional counterparts (*i.e.* solid oxide fuel cells, lithium ion batteries, direct methanol/ethanol fuel cells, etc.), but their mild optimal operating conditions, inherent biocompatibility and high specificity provide for an ease of miniaturization and hold promise toward the powering of implantable or wearable devices.[8, 11, 13, 53, 54]

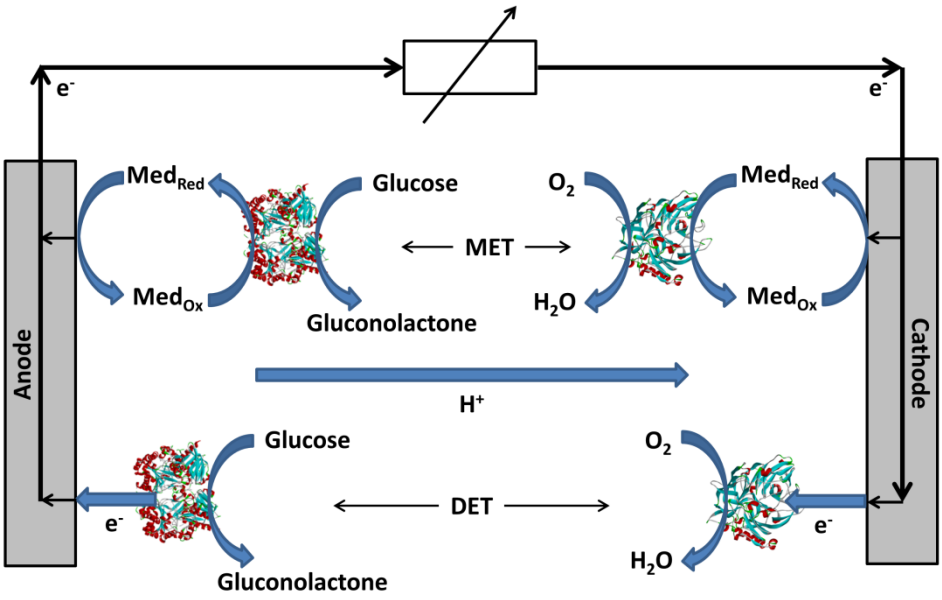

Figure 1.2 Schematic representation of glucose-driven EBFC. Current generation by enzymatic oxidation of glucose and electron transfer at an enzyme-modified anode followed by transduction of electric current through an external circuit (depicted as variable resistor) and electron transfer and oxygen reduction at an enzyme-modified cathode. Electron transfer depicted as either DET or MET with GOX at anode and BOD at cathode.

Enzymatic biosensors and EBFCs operate according to similar methodologies, but differ in terms of performance metrics. The performances of enzymatic biosensors are mainly reported in terms of sensitivity (*i.e.* change in current density per change in glucose concentration; mA μM^{-1} cm^{-2}), linear range (*i.e.* glucose concentration range in which a linear current density response is observed), limit of detection (*i.e.* lowest glucose concentration capable of being detected as a function of sensor sensitivity and signal-to-noise ratio), selectivity (*i.e.* response to glucose relative to other potential substrates) and response time (*i.e.* time between actual change in glucose concentration and steady current response observed).[21] The sensitivities of GOX-based biosensors are commonly reported between 10-50 μA mM^{-1} cm^{-2} with some systems reaching above 100 μA mM^{-1} cm^{-2} over linear ranges of 1 μM to 10 mM glucose.[55-63] These values are applicable to diabetes patient monitoring as the average blood glucose level is around 5.5 mM.[1, 64] Enzymatic biosensor limits of detection as low as 0.1 μM glucose have been reported with response times less than 1 s.[58, 63, 65, 66] The superb selectivity of GOX has also afforded excellent sensitivity in the presence of other sugars.[33, 55] Conversely, EBFC performances are mainly reported in terms of maximum power density (*i.e.* the amount of power produced per unit area; mW cm^{-2}) and open-circuit voltage (*i.e.* observed difference in redox potential between anode at cathode with no current; OCV).[22] Power densities on the order of several mW cm^{-2} have recently been reported with OCVs near 1 V, which is roughly the maximum theoretical voltage attainable in a glucose/O_2 fuel cell as governed by the thermodynamic redox potentials of the reactions occurring at the anode and cathode.[11, 13, 67-70] Such values have prompted the *in vivo* study of several such systems.[53, 71, 72]

A major determining factor in the performance of either system type is the observed active enzyme density at the electrode surface.[43, 52, 73] This measure is defined as the rate of

substrate turnover observed as electric current per unit area and is dependent on the enzyme loading (*i.e.* amount of working enzyme immobilized at or near the electrode surface per unit area) the specific substrate turnover rate (*i.e.* rate of target substrate oxidation/reduction of each immobilized enzyme (k_{cat})) and the rate/efficiency of electron transfer between the enzyme and the electrode. The electrochemically observed rate is a function of losses within the system as well as overall rate limiting steps. These losses and rates are the main focus of developmental research into enzymatic biosensors and EBFCs as they are directly determined by the selection of system components and their method of combination.[13, 14, 43]

Another key issue in the viable implementation of enzymatic biosensors and EBFCs is stability, both during operation and during storage.[11-13, 15] Enzymatic biosensors must relay reliable, consistent information regardless of storage time or sensing conditions while continuous glucose sensors must perform the same action while persisting in the test environment throughout operation.[15, 74] EBFCs take these demands one step further with the need for constant power generation.[12] Currently, the stability of these enzyme-based systems is one of the major hurdles yet to be overcome, which must occur for their broad applicability. In order to achieve a greater understanding of the factors that influence performance and stability of enzyme-modified electrodes, I focused on the investigation of GOX-based systems as GOX is the most widely studied electroactive enzyme used in enzymatic biosensors and EBFCs, and thus provided a high level of impact for future works as well as a high degree of comparison with previous reports.[16]

1.1.2 Glucose oxidase

Fungal β-D-glucose:oxygen 1-oxidoreductase (EC 1.1.3.4), more commonly referred to as GOX is a dimeric, flavin-containing glycoprotein composed of 2 identical subunits, each with a

molecular weight of ~80 kDa (**Figure 1.3**).[75] The activity of GOX toward β-D-glucose oxidation is extremely selective with the next fastest sugar oxidation (*i.e.* mannose) proceeding at a rate less than 1 % of that for β-D-glucose.[33, 75] This trait is advantageous for the design and operation of enzymatic biosensors and leads to increased selectivity compared to alternative working enzymes such as glucose dehydrogenases.[76, 77] The primary sequence and crystal structure of GOX from *A. niger* have been determined and investigations into the likely mechanism of action for glucose oxidation and the subsequent reduction of varying electron acceptors have been reported.[33, 78-81] GOX-catalyzed glucose oxidation and oxidant reduction obey the Ping Pong Bi Bi mechanism occurring at the flavin adenine dinucleotide (FAD)-based active site of GOX (**Figure 1.3B**).[33, 82] The re-oxidation of this cofactor can be achieved by molecular oxygen, quinones or 1-electron acceptors such as ferrocene, each with their own reaction kinetics.[33, 83-85] The FAD-based active site is in close proximity to 3 amino acids: Glu412, His516 and His559 with His516 participating in the likely glucose oxidation mechanism.[33, 80] This reaction scheme proceeds through deprotonation of the C1-hydroxyl group of glucose by His516 coordinated with a direct hydride transfer from the C1-hydroxyl group to FAD.[33, 86] The thermodynamically determined redox potential of this reaction is roughly -0.4 V versus Ag/AgCl, which makes GOX an advantageous anodic working enzyme for EBFCs when combined with oxygen reducing enzymes such as laccase or BOD that possess redox potentials close to 0.5 V versus Ag/AgCl.[11, 87] The well characterized structure, mechanism and electrochemical characteristics of GOX along with its beneficial properties toward enzymatic biosensors and EBFCs have made GOX the most widely applied electroactive enzyme from the first report of an enzyme electrode through today.

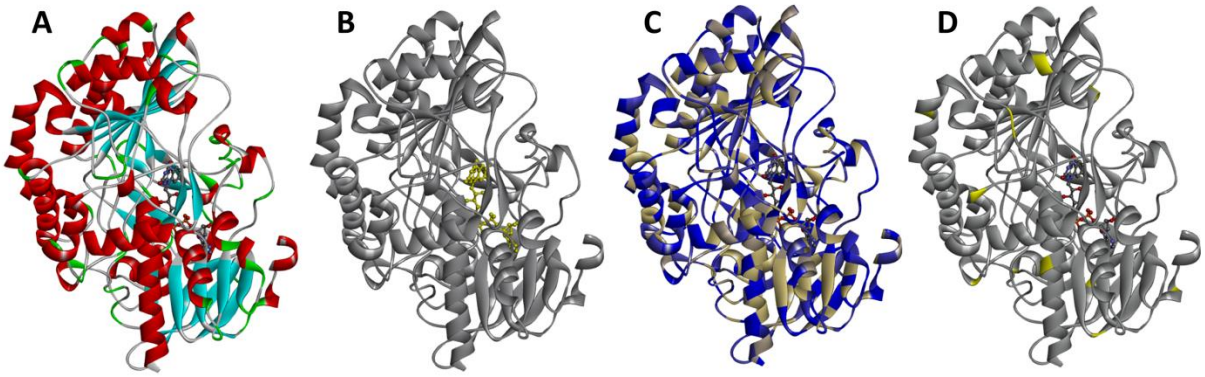

Figure 1.3 Structure and features of glucose oxidase from *Aspergillus niger*. A) GOX monomer from *A. niger*. B) GOX monomer from *A.* niger with FAD highlighted (yellow). C) GOX monomer from *A. niger* with hydrophobic residues highlighted (blue). D) GOX monomer from *A. niger* with lysine residues highlighted (yellow).

1.2 Enzymatic modification of electrode surfaces

The successful operation of enzymatic biosensors and EBFCs heavily relies on the effective immobilization of working enzymes at or near an electrode surface, which can be achieved in a variety of ways.[43, 88] As discussed, both system types depend on consistent, reliable substrate turnover and electron transfer at the enzyme-electrode interface throughout operation. The interactions at this interface are crucial to the overall device performance and are a direct function of the utilized electrode materials and employed enzyme immobilization strategy.[88, 89] A major goal of the work presented in this dissertation was to develop an increased understanding of the impacts of electrode material properties on resulting enzyme biochemical characteristics upon immobilization and to correlate those trends to the observed electrochemical performances.

1.2.1 Enzyme immobilization approaches

In general, enzyme immobilization approaches can be divided into 3 main categories: attachment to a support, encapsulation within a carrier, and crosslinking without a support.[2, 43]

Multiple variations on and combinations of these strategies have been applied toward the development of enzymatic biosensors and EBFCs.[43] Effectual immobilization of the working enzymes serves to retain enzymatic activity at the electrode surface throughout operation and improve overall device stability by reducing the propensity of enzyme detachment and enzyme deactivation during use.[88, 90] However, the process of immobilization can also cause initial losses in enzymatic biochemical activity, so optimization of immobilization strategy is important to improving overall device performance.[91, 92]

Perhaps the most commonly applied enzyme immobilization strategy for any enzyme-based application is attachment to a solid support, as electron transfer at an electrode interface is necessary for charge collection.[2, 93] This attachment can be achieved by adsorption through hydrophobic/electrostatic interactions, by affinity binding or by covalent binding.[43] Enzyme adsorption is the most straightforward approach and benefits from a lack of additional design concerns, but is also generally non-specific, which can lead to an average of enzyme orientations at the enzyme-support interface as well as adsorption of other proteins or substances.[43, 94] For instance, hydrophobic residues on the surface of GOX are fairly evenly distributed, so directed immobilization cannot be achieved through physical adsorption (**Figure 1.3C**).[95] As the FAD-based active site of GOX is deeply buried beneath the protein surface, proper orientation minimizing the distance between FAD and an electrode is crucial toward promoting DET.[96] On the other hand, the cathodic working enzymes laccase and BOD exhibit hydrophobic or negatively charged pockets near their electron accepting sites, which has allowed for directed orientation through adsorption.[97-100] Studies have also shown high degrees of enzyme denaturation upon physical adsorption dependent on support properties as a result of extensive interactions with the support surface (*i.e.* multipoint attachment) and interactions with adjacent

proteins.[89, 90] Enzyme immobilization through affinity binding (*i.e.* biotin-avidin binding, metal ion-chelator interactions etc.) can alleviate some of these concerns but generally require additional enzyme-modification steps.[43, 101]

The covalent immobilization of enzymes is achieved through activation of naturally occurring functional groups on the protein surface by multi-functional reagents such as glutaraldehyde or carbodiimide followed by binding to a functional support.[91, 102-104] For example, 1-ethyl-3-(3-dimethylaminopropyl)carbodiimide (EDC) forms direct linkages between carboxylic acids and primary amines and is commonly used to attach proteins to functionalized surfaces.[105] This method of attachment can provide stronger linkages to prohibit protein leaching and decrease denaturation caused by direct surface interactions compared to physical adsorption.[89, 106] However, many proteins, such as GOX, exhibit multiple, distributed surface functionalities, making directed orientation difficult to achieve (**Figure 1.3D**). Creative methods aimed at achieving directed, covalent binding have focused on such methods as the reconstitution of apo-enzyme onto materials pre-functionalized with cofactor and enzyme immobilization onto surfaces pre-functionalized with substrate.[25, 107, 108]

The entrapment of working enzyme within a carrier matrix at an electrode surface can serve to retain enzymatic activity within the target system while maintaining or even enhancing enzyme functionality, but can also hinder substrate diffusion.[109-112] Careful design of the entrapment matrix is necessary for efficient operation. These matrices can consist of networks or gels made up of crosslinked, electrospun or electropolymerized polymers, nanofibers or other nanomaterials, etc.[6, 67, 112, 113] Matrix physical properties such as porosity, hydrophobicity, stiffness and density govern the resulting diffusional/biochemical activity characteristics but effective electron transfer pathways must also be established for efficient operation.[109, 114-

118] Several groups have fabricated entrapment matrices consisting of conductive materials or with redox-functionalized components in order to meet this need.[67, 117, 119-121] The surrounding of working enzymes with conductive material has been shown to reduce orientation effects (*i.e.* achieve electron transfer with the enzyme active site despite orientation).[96, 122, 123] Polymer-based systems are some of the most advantageous due to their flexibility and capability for tunable functionalization to bind proteins as well as mediator molecules.

Finally, crosslinked protein aggregates have also been reported, generally in combination with entrapment or binding to a surface.[43, 124-127] Kim *et al.* reported significant increases in both GOX and laccase weight-based specific activities upon precipitation, crosslinking and adsorption onto polyaniline (PANI) fibers. This method can help to concentrate enzymatic activity at a surface but can lead to losses in molecule specific biochemical activities caused by distortion of protein structure from extensive or intramolecular linkages.[88] To reduce these effects, carrier proteins such as serum albumins have commonly been introduced to form a crosslinked protein matrix around the working enzymes.[128, 129] Many reported systems have utilized a combination of these approaches to reach optimal performances.[1, 22, 43] Post-immobilization modifications such as coatings, membranes, etc. can be applied to any fabricated enzyme-based material to reduce leaching and prevent interference from compounds present in operational solution.[67, 130-133] The applied immobilization approach acts in concert with the selected support or entrapment material to yield the observed performance.

1.2.2 Enzyme-modified electrode materials

The overall goal of enzyme immobilization in enzymatic biosensors and EBFCs is to retain the maximum enzymatic activity possible within a given volume, while enhancing stability, retention and functionality. To achieve these goals, nanostructured materials such as

carbon nanotubes (CNTs), graphene and metal nanoparticles have been intensely studied.[134-144] These materials possess high specific surface areas (SSA) available for enzyme interaction to promote large active enzyme loadings upon attachment and generally exhibit tunable surface functionalities, high conductivities and robust mechanical characteristics.[140, 142] Their nanoscale dimensions also hold promise toward the development of DET-type systems; with some debate over whether GOX-nanomaterial DET has been observed.[138, 145, 146] Such nanostructured materials can further be used to fabricate 3-dimensional, porous structures for greater loadings caused by entrapment of the working enzymes in the conductive network.[67, 69, 73, 119, 147, 148] To date, 3-dimensional nanomaterial-based systems have produced some of the highest performing enzymatic biosensors and EBFCs.[44, 67-70]

An excellent example of these types of systems can be found in the work reported by Cosnier *et al*., which presented an EBFC consisting of GOX and catalase entrapped within a compressed multi-wall carbon nanotube (MWCNT) disk as an anode and a similar laccase-MWCNT disk as a cathode.[67] Both functionalized electrodes were partially coated with silicone and a cellulose membrane to enhance stability. Catalase served to eliminate the build-up of hydrogen peroxide during operation to improve GOX stability. This EBFC showed a maximum power density of 1.25 mW cm^{-2} and an OCV of 0.95 V with 96% and 22% of initial power density retained after 30 days and 1 year of storage, respectively.[67, 149] This performance was also successfully exhibited as an implanted device within a rat model.[72] Incorporation of a naphthoquinone mediator within the anodic network increased the power output by 23% but also decreased the observed OCV to 0.76 V and resulted in decrease to 40% initial power retained after only 7 days.[68] These redox mediators served to increase the attainable current density due to improved electron transfer rates, but decreased the achievable

maximum potential difference between anode and cathode. These trends highlighted some of the advantages and drawbacks to MET in EBFCs.[39]

Alternatively, the utilization of conductive or redox-functionalized polymer networks for working enzyme entrapment has proven effective at improving observed enzymatic biosensor and EBFC performances and stabilities.[114, 115, 117, 150] Crosslinked polymer networks of inherently conducting polymers such as poly(3,4-ethylenedioxythiophene) (PEDOT), polypyrrole (PPY), PANI or polyacetylene can provide conductive networks of entrapped electroactive enzyme with high specific retained activities as the protein structures are not confined to a surface.[114, 151-154] These materials conduct electrons along a π-conjugated polymer backbone, to effectively "wire" electroactive enzymes to an electrode.[114] Enzyme retention within the networks can be enhanced through covalent binding to the polymer backbone or optimization of crosslinking extent.[155, 156] Similarly, the "wiring" of enzymes at an electrode surface has been achieved using crosslinked networks of redox-functionalized polymers such as poly(4-vinylpyridine) (PVP), poly(*N*-vinylimidazole) (PVI) or polyethylenimine (PEI). [117, 157-159] In these systems, redox centers such as ferrocene, osmium or quinones incorporated into side chains covalently bound to the polymer backbones transfer electrons between the enzyme active sites and the electrode *via* electron self-exchange.[117] Such polymer materials are effective at improving observed current densities and device responses due to the rapid rates of electron transfer within the network and the tunability of the redox moieties themselves.[115, 160-164] However, conventional polymerization methods limit the tailorability and optimization capacity of the polymer networks.

For each immobilization approach and support/entrapment material, the resulting device characteristics are a function of the interactions at the enzyme-material interface.[89-91] These

interactions are governed by the support properties such as porosity, pore size, SSA, surface curvature and surface chemistry.[89, 90, 92, 165] The observed current densities depend on not only the rates of electron transfer but also the retained biochemical activities. As a result, careful selection of fabrication conditions is crucial to optimal performance. The influence of enzyme-material interactions on enzyme biochemical characteristics upon immobilization has been well characterized (*i.e.* impact of material properties on immobilized enzyme kinetic parameters), but the extension of these trends to observed electrochemical performances was not extensively covered, which was a major focus of the work presented in this dissertation. [89, 90, 92, 165]

1.3 Electron transfer pathways at enzyme-modified electrodes

In all enzymatic biosensors and EBFCs, the efficient transfer of electrons between the working enzymes and an electrode surface is crucial to effective operation. The optimization of enzyme-electrode electron transfer pathways has been an area of avid research for many years with new and innovative materials and methods constantly being developed.[39, 46, 117, 138, 166, 167] In general, the electrochemical oxidation or reduction of an enzyme active site can be achieved by MET or DET, but with varying mechanisms dependent on the system components and method of fabrication with drawbacks and advantages to each approach.

1.3.1 Mediated electron transfer

The incorporation of redox mediators into enzyme-based systems can improve observed current densities by increasing electron transfer rates and efficiencies between the enzyme active sites and the electrode surface.[39, 68, 117, 168] Utilization of MET can improve performance by increasing the rates of active site oxidation/reduction while decreasing unwanted oxidation/reduction of natural substrates (*i.e.* oxygen reduction by GOX). This method allows for enzymatic biosensor operation at lower applied working potentials compared to first-generation

biosensors, which has led to increased reliability and specificity.[1] However, the operation of EBFCs through MET requires the redox potentials of utilized mediators to lie within the bounds of working anodic/cathodic enzyme working potentials, which decreases the maximum theoretical OCV. Reliance on these intermediate groups also decreases overall stability due to potential losses through mediator leaching or inactivation.[39] The method of mediator incorporation into enzymatic systems must thus be carefully designed to prevent this leaching, not only to maintain device performance but also to protect the working environment as many such compounds can be toxic.[1, 169]

Mediator functionality can be incorporated into enzymatic biosensors and EBFCs through a variety of methods. The most standard approach is the use of freely diffusing, small-molecule mediator compounds or their concurrent entrapment or adsorption along with working enzymes.[39, 68, 69] These types of systems generally require the use of coatings to limit leaching; however, loss of mediator functionality at the electrode surface can still be a major issue.[12, 13, 68, 69, 169] Thus, mediator groups have been covalently attached to the enzyme surface directly or through polymer tethers to form electron relays capable of intermolecular or intramolecular electron transfer with the enzyme active site.[160, 162, 163, 170, 171] Redox-functionalized enzymes have exhibited improved current densities relative to unmodified versions with electron transfer rates dependent on mediator type, tether length and polymer tether type.[162, 170] Further, the mechanism of electron transfer (*i.e.* intramolecular or intermolecular) has been shown to depend on tether length.[162] Specifically, mediators bound directly to the surface of GOX achieved re-oxidation of FAD intramolecularly as did tethered mediators with chains longer than 10 bonds, while shorter chains re-oxidized FAD within adjacent GOX molecules intermolecularly due to differences in chain mobility.[162, 170]

Successful immobilization of redox-functionalized enzymes can help to reduce losses through leaching, but intramolecular electron transfer between the enzyme active site and bound mediators has been found to be rate limiting.[170, 172] Optimization of enzymatic biosensors or EBFCs based on redox-functionalized enzymes has been limited to mediator-specific tailoring and variation in tether type and length while tether attachment site and density were difficult to control.[160, 162, 163, 170, 171]

Another common approach is the entrapment of working enzymes within polymer networks or hydrogels with redox groups covalently bound to the polymer backbones.[13, 117, 159, 173] Redox polymer-based systems conduct electrons *via* the self-exchange of electrons or holes between colliding reduced and oxidized redox centers to effectively "wire" enzymes to an electrode.[117, 159] As such, the electron transfer rates depend directly on the mobility, hydration and spacing of these tethered redox groups.[117, 160, 174] Pioneering work in this area was performed by Heller *et al.* who developed various ferrocene- and osmium-based polymers with differing redox potentials, electron diffusion coefficients and self-exchange rates.[13, 117, 150, 160, 175-178] Generally, rates of enzymatic substrate turnover (k_{cat}) and electron self-exchange through redox-polymer networks are much higher than rates of enzyme active site re-oxidation.[117, 170] Crosslinked redox polymer networks can provide high retained biochemical activities with efficient means of charge collection with some system stabilities limited by loss of mediator functionality during operation through mediator decomposition.[161, 179, 180] Tailorability of these systems is similar to redox tethers at enzyme surfaces with higher densities of redox groups within the network. Conventional polymerization methods limit optimization capacity and tailorability of enzyme-polymer

interactions, thus the development of a new, enzyme-redox polymer platform for use in enzymatic biosensors and EBFCs was a major target of the work presented in this dissertation.

1.3.2 Direct electron transfer

The ideal result of enzymatic biosensor and EBFC fabrication would be stable enzyme immobilization at an electrode while retaining complete enzymatic biochemical activity and achieving efficient, non-rate limiting DET. This configuration would be optimal as rate losses from hindered electrochemical kinetics and voltage losses from the utilization of electron transfer mediators would be eliminated; however, successful realization of these enzyme-modified surfaces has been extremely difficult to achieve for some enzymes.[138, 167] DET with electroactive enzymes was first reported in 1978 by Berezin *et al.* who showed successful reduction of a fungal laccase and subsequent oxygen reduction at an electrode surface.[181] Since this report, DET with cathodic enzymes such as laccase and BOD with nanostructured surfaces has been further developed and combined with enzyme orientation studies to improve the performance of enzyme-modified cathodes.[97, 98, 182-186]

Establishment of reliable DET with GOX is more difficult to achieve due to the deeply buried FAD-based active site more than 15 Å below the protein surface.[46, 47, 146, 187] Many reports have claimed successful DET with GOX while others have reported that true DET with GOX at nanomaterial surfaces may not be possible.[69, 138, 145, 146, 188-191] A distinction needs to be made to define GOX DET and how it can be confirmed as many such studies have not provided an adequate level of proof. DET of FAD within immobilized GOX can be successfully observed through several electrochemical characterization methods such as cyclic voltammetry (CV); however, the observation of reversible electron transfer *via* the appearance of faradaic peaks does not, on its own, prove DET with GOX, merely FAD. Here, I define “GOX”

as the biochemically active enzyme that oxidizes β-D-glucose to glucono-δ-lactone at its FAD-based active site.

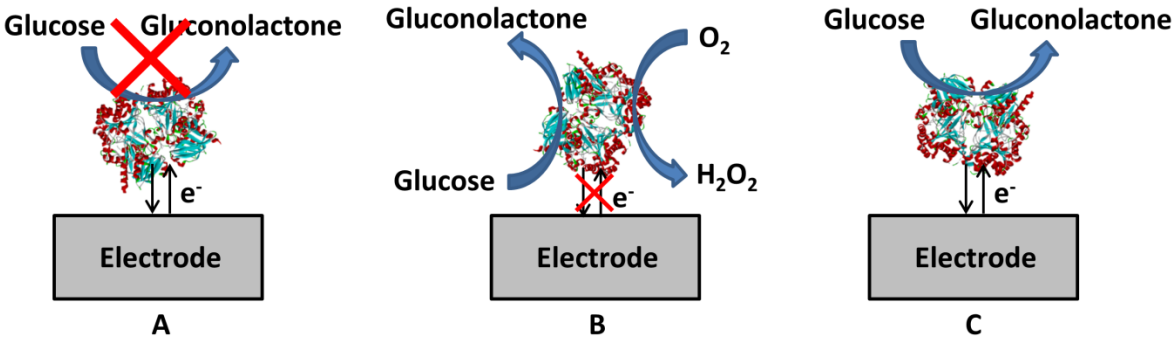

Figure 1.4 Schematic representation of GOX DET. A) Immobilization of GOX at an electrode resulting in reversible electron transfer with FAD but biochemically inactive GOX. B) Immobilization of GOX at an electrode resulting in biochemically active GOX but incapable of electron transfer to electrode. C) DET of GOX immobilized at an electrode with biochemically active GOX and subsequent electron transfer with electrode surface.

Stevenson *et al*. reported an elegant study that showed CV traces of immobilized FAD (without protein) were identical to those of immobilized GOX without substrate.[145]. This result suggested that studies claiming to have observed DET with GOX may have, in fact, characterized DET with free FAD that had detached from GOX or with FAD contained within deformed, inactive GOX.[145] The successful immobilization of biochemically active GOX can be confirmed through observation of an anodic current shift in CV traces upon introduction of glucose in de-oxygenated solution.[145] Observed current fluctuations in oxygen-containing solution do not adequately confirm DET as oxygen and hydrogen peroxide are electrochemically active. Ye *et al.* reached a similar conclusion with GOX immobilized at graphene surfaces, claiming the presence of 2 distinct GOX populations: closely associated, inactive GOX that exhibited electron transfer with contained FAD (**Figure 1.4A**), and a second GOX layer that

remained biochemically active but was not capable of electron transfer with the electrode surface (**Figure 1.4B**).[146] Confirmation of GOX molecules capable of both, electron transfer with the electrode surface and glucose oxidation, is necessary for definitive DET (**Figure 1.4C**).

However, several studies have adequately shown successful DET with GOX in enzymatic biosensors and EBFCs.[67, 107, 138, 192] In particular, the inclusion of catalase within the system presented by Cosnier *et al*. coupled with the high observed current density confirmed DET with GOX as produced hydrogen peroxide would have rapidly been eliminated by catalase.[67] However this DET was not ideal as the addition of anodic mediator improved the current output.[67, 68] Covalent attachment of FAD to surfaces followed by reconstitution of apo-GOX has also been shown to allow successful DET with GOX at CNT surfaces.[107, 192, 193] Unfortunately, direct interactions with solid surfaces can also lead to increased protein denaturation and subsequent biochemical activity losses.[89, 91, 92] For instance, the level of current density reached by Cosnier *et al*. required the use of extremely high GOX concentrations, which showed limited retained specific biochemical activity within the fabricated electrode.[67] Such factors have prompted many groups to focus on developing new immobilization approaches and electrode materials as well as on alternate electron transfer methodologies such as stable and tailorable MET.

1.4 Polymer-based protein engineering

The polymer-modification of proteins was first reported in 1977 by Davis *et al.* who studied the impact of poly(ethylene glycol) (PEG) attachment on the immunogenicity and circulation lifetime of bovine serum albumin and catalase.[194, 195] Since these studies, protein modification through the attachment or growth of polymers has greatly expanded in terms of both the utilized extent of protein PEGylation and the available methods of polymer-based

protein engineering (PBPE).[196] The attachment of pre-synthesized polymers to proteins through a "grafting to" approach eliminates the need for protein exposure to harsh polymerization conditions (*i.e.* temperature or organic solvent); however, polymer conjugation density, attachment site specificity and protein-polymer conjugate purification can all be hindered. Conversely, polymer growth directly from the protein surface through a "grafting from" approach can allow controllable polymer densities but restricts polymerization conditions to those that will not harm protein structure or function. Both approaches have proven capable of improving enzyme stability and enhancing functionality.[197-202]

PBPE utilizes controlled radical polymerization (CRP) methods to synthesize well-defined, tailorable polymers with control over product molecular weight or degree of polymerization (DP).[203] The most promising of these methods include stable free radical polymerization (SFRP) (such as nitroxide mediated polymerization (NMP)), atom-transfer radical polymerization (ATRP), and reversible addition-fragmentation chain transfer (RAFT) polymerization.[203-208] In particular, ATRP and RAFT polymerization have been widely applied to the tunable generation of enzyme-polymer conjugates with enhanced activities, stabilities and functionalities through a "grafting from" approach.[209-214] This method proceeds through initial modification of the protein surface with ATRP initiator molecules or RAFT chain transfer agents followed by polymer growth from these initiator sites. [209, 210, 214] For example, accessible lysines on the surface of a protein (**Figure 1.3D**) can be targeted using NHS-functionalized initiator molecules for predictable surface modification.[215, 216] The large library of available monomers, including functional or stimuli-responsive polymer types can provide for the rational engineering of enzyme function through PBPE.[200, 209, 210, 215, 217-222] Such modification has been shown to increase enzyme stability under adverse

conditions such as extreme pH and temperature, as well as impart additional functionalities incorporated into the polymer coating.[200, 215, 218, 223, 224] In terms of enzymatic biosensors and EBFCs, the incorporation of redox-functionality into the grown polymer side-chains could provide tailorable performance of the resulting enzyme-redox polymer conjugates. The encapsulation of individual working enzymes by a dense redox polymer coating could provide enhanced electron transfer efficiencies despite orientation upon immobilization. The development of such methods would result in an additional layer of optimization capability in the design of enzymatic biosensors and EBFCs. Thus, the investigation of these possibilities was a significant target of the work presented in this dissertation.

Chapter 2: Membrane/Mediator-Free Rechargeable Enzymatic Biofuel Cell Utilizing Graphene/Single-Wall Carbon Nanotube Cogel Electrodes

2.1 Introduction

The prospect of sustainable energy generation from readily available and renewable biofuels through the use of enzymatic biofuel cells (EBFCs) has been the target of significant research in recent years.[22, 225-228] EBFCs utilize enzymes to convert the chemical energy in fuels such as glucose,[67, 69, 119] fructose[25, 26, 229] or alcohols[27, 28, 98] into electrical power *via* oxidation of fuel at the anode and reduction of an oxidant (typically molecular oxygen) at the cathode. The mild operating conditions and inherent biocompatibility of the enzyme-based systems, along with the high specificity of enzymes, leading to membrane-less platforms and thus an ease of miniaturization, make EBFCs ideal candidates for the continuous powering of implantable devices.[53, 71, 72] However, EBFCs currently suffer several key limitations including limited power output, instability over time and lack of reusability, which must be overcome to make their utilization a reality.

The low power output and short lifetime of EBFCs stems from multiple factors, with the main contributors being poor electron transfer from enzyme active site to electrode, and low levels of active enzyme loading onto the electrodes. Attempts to solve these issues have been focused on design improvements to electrode materials and enzyme immobilization strategies. As the redox active sites of many electroactive enzymes are buried deeply within the 3-dimensional protein shell, it is difficult to establish direct electron transfer (DET) to the electrode.[145, 166] For example, the flavin adenine dinucleotide cofactor (FAD)-based active site of glucose oxidase (GOX), the most commonly studied anodic enzyme, is located roughly 15 Å below the protein surface, resulting in a large electron transfer resistance.[47] There have been two broadly investigated methods aimed at improving electron transfer efficiency. First, small

molecules have been used as mediators (*i.e.* osmium- or ferrocene-containing complexes, 2,2'-azino-bis(3-ethylbenzthiazoline)-6-sulfonic acid (ABTS), etc.)[69, 160, 230-233] that serve to mediate electron transfer from active site to electrode. Second, electrode materials that possess large available surface areas and are capable of close communication with the enzyme active site, such as carbon nanotubes, graphene or metal nanoparticles, have been utilized to increase active enzyme loading density and enhance electron transfer rates from enzyme to electrode.[67, 69, 119, 134]

Mediated electron transfer (MET) type systems have been proven to possess enhanced electron transport capabilities and thus higher power outputs compared to identical setups without mediators, but also have several drawbacks.[68, 232, 234] For MET to be feasible, the redox potentials of the applied mediators must lay within the bounds of the anodic and cathodic enzyme prosthetic site redox potentials, thus reducing the maximum theoretical open-circuit voltage (OCV) of the overall system. Additionally, the leakage and instability of mediator groups adds toxicity and further power instability concerns for the EBFC, respectively. For instance, a naphthoquinone mediator was shown to increase EBFC power output by 23% compared to an identical EBFC without a mediator. However, power stability and OCV of the mediated systems were markedly decreased to 40% power retained and 0.76 V, respectively, after 7 days, compared to 96% power retained and 0.95 V, respectively, after 30 days in the non-mediated system.[67, 68] The presence of free mediator, by design or by leaching from the electrode due to their low molecular weight, can also increase potentially harmful effects *in vivo* and necessitate the use of a membrane to separate anodic and cathodic compartments, which adds to system complexity.[69] Thus, there exists a large drive to develop improved EBFCs with increased power densities utilizing materials capable of promoting electron transfer without the

need for these types of externally added redox mediators.[166, 228] In this report, we define systems operating without the addition of external redox mediators as “mediator-free”.

Nanostructured materials such as nanotubes[134, 135] and nanoparticles[133, 136, 137] are well suited to enhance observed current densities.[138-140] Carbon nanotubes (CNTs) are particularly advantageous materials for this purpose because of their high electrical conductivity, nanometer scale dimensions, electrochemical stability and high aspect ratios.[67, 140] Nevertheless, many configurations utilizing CNTs have still required the use of mediators to achieve optimal performance and there is much debate over whether CNT-based systems are truly capable of achieving DET with FAD-containing enzymes such as GOX.[69, 145, 146, 232] However, CNT-based or CNT-decorated systems have boasted some of the highest reported power densities to date[68-70, 232] even without the use of mediators.[67] Power densities of mediator-free, CNT-based EBFCs have reached up to 1.25 mW cm^{-2}, which corresponded to 1.66 mW mL^{-1} and 33 mW g^{-1} of GOX, for a system composed of enzyme-modified compressed disks of multi-wall CNTs.[67] The electron transfer rate constant (k_s), which is a key measure of electron transfer efficiency, in systems using GOX immobilized on CTs has been shown to reach up to 13 s^{-1}.[69]Graphene has also attracted significant interest as an electrode material for enzyme-based systems due to its excellent thermal and electrical conductivity, good biocompatibility and high specific surface area.[69, 144, 235] CNTs, graphene and other nanomaterials can further be manipulated to form 3-dimensional, porous structures that allow for high enzyme loading and connectivity with an ease of substrate diffusion through formed networks.[67, 119] Incorporation of large amounts of enzyme within such a network serves to surround the enzyme with conductive material to reduce the loss of electrons to outside electron acceptors (*i.e.* molecular oxygen) and potentially reduce the leaching of enzyme during

operation. Previous reports have investigated such 3-dimensional systems; however, most have exhibited reduced available surface area and enzyme activity after fabrication[67] or required the use of external mediators.[68, 69, 119] Unfortunately, due to the fabrication process and porosity, these electrodes cannot simply be reused by replacing degraded enzymes with fresh, active enzymes.

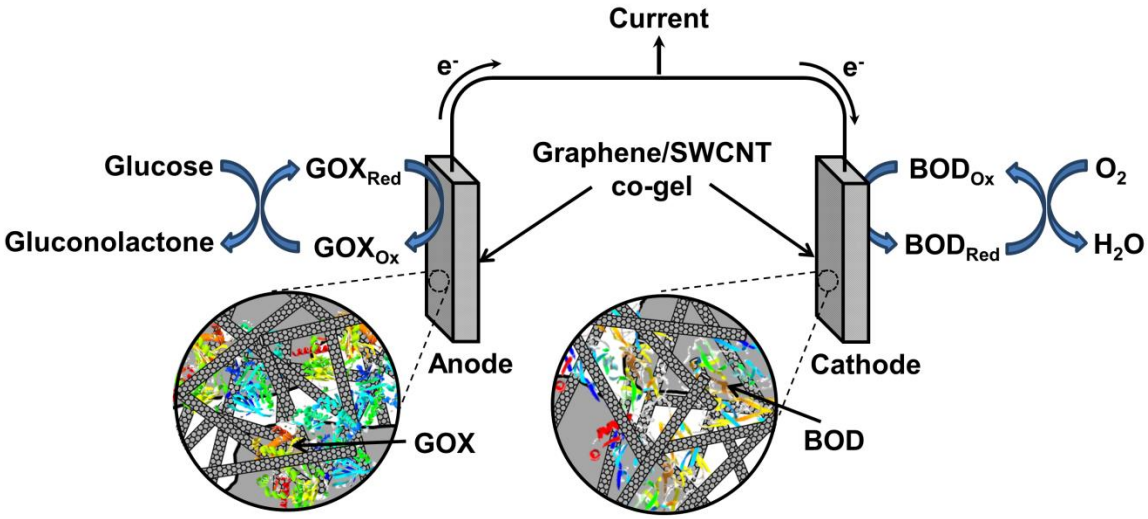

Figure 2.1 Schematic representation of graphene/SWCNT cogel-based EBFC. Immobilized GOX at the anode oxidizes glucose to gluconolactone and transfers electrons to the cogel electrode. Electrons are transferred to BOD at the cathode, which then reduces molecular oxygen to water.

Herein, we report on the development of the first glucose-based, mediator-free EBFC utilizing free-standing cogels of graphene and single-wall carbon nanotubes (SWCNTs) as electrodes (**Figure 2.1**). The graphene/SWCNT cogels were fabricated by mixing suspensions of graphene oxide and individually dispersed SWCNTs at suitable concentrations that led to percolating networks of interspersed graphene and SWCNTs (**Figure 2.2**). These gels possessed high specific surface area (SSA), porosity, and electrical conductivity that allowed high enzyme loading, unhindered substrate transport to the working enzymes and efficient charge collection

from the working enzymes. GOX from *Aspergillus niger* was used as the anodic enzyme of interest and the multicopper oxidase bilirubin oxidase (BOD) from *Myrothecium sp.* was the cathodic enzyme. We further determined the electrochemical characteristics of both anode and cathode individually as well as the simple, membrane- and mediator-free full cell. Finally, we examined the reusability of the electrodes by washing away degraded enzymes and then reloading the electrodes with fresh, active enzymes.

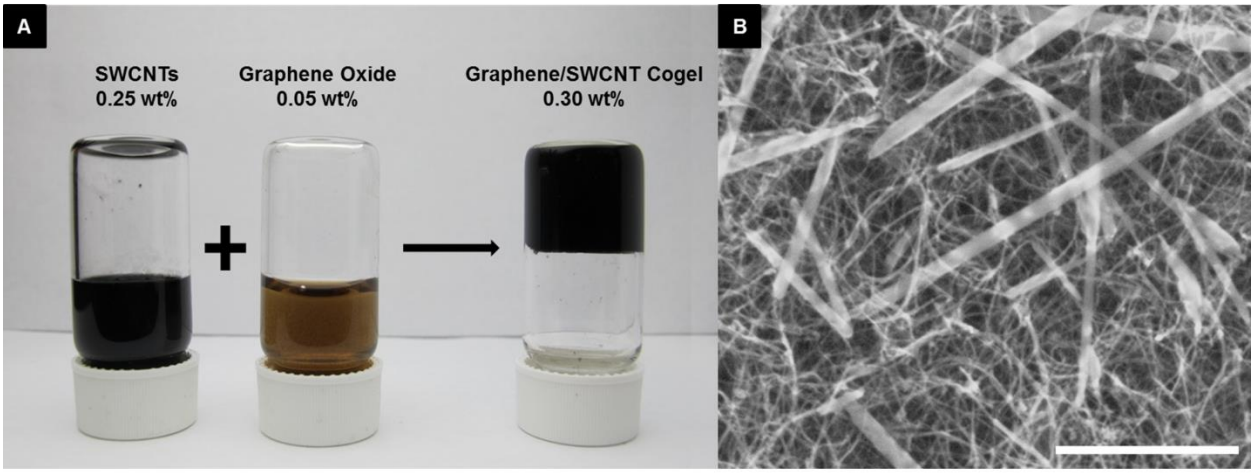

Figure 2.2 Graphene/SWCNT cogel. A) Graphene/SWCNT cogel was formed by mixing individually dispersed SWCNTs with graphene oxide in a 5:1 ratio by weight. B) SEM micrograph of graphene/SWCNT aerogel with scale bar representing 5 µm.

2.2 Materials and Methods

2.2.1 Materials

Ultrapure Milli-Q grade water (resistivity of 18.2 MΩ·cm) was used for all experiments. SWCNTs batch CG 200 with average diameter of 1 nm and average length of 1 µm were purchased from Southwest Nanotechnologies Inc. Graphite flakes were purchased from Bay Carbon Inc. GOX from *Aspergillus niger* (100-250 units mg^{-1}), hydrogen peroxide and horseradish peroxidase were purchased from Sigma Aldrich. BOD from *Myrothecium sp.* (2.7

units mg^{-1}) was purchased from Amano Enzyme Inc. All chemicals were of analytical grade and used as received. Sodium phosphate buffer (0.1 M, pH 7.0), used for preparation of enzyme solutions and testing of electrodes, was prepared from phosphate salts.

2.2.2 Equipment

Sonication and centrifugation of nanotube solutions were carried out using a Thermo Fisher 500 probe tip sonicator and a Beckman Coulter L-100K ultracentrifuge, respectively. Adsorption spectra of SWCNT solutions were measured using a Varian Cary 5000 UV-vis NIR spectrophotometer. Fluorescence spectra were collected using a visible spectrum capable Horiba Jobin Yvon Nanolog spectrofluorometer with samples placed in a 1 cm path length quartz cell (Starna). Entrance slit width was 10 nm, emission slit width was 5 nm, excitation was centered at 280 nm and emission signal was collected from 300-400 nm with a 1 s integration time and 2 nm step size. The excitation and emission gratings were blazed at 500 nm and had 1200 grooves mm^{-1}. Data was plotted as corrected signal intensity over corrected lamp intensity to account for variations in gratings and excitation intensity. Critical point drying of ethanol saturated gels was performed on an Autosamdri 815 critical point dryer (Tousimis Research Corporation). Aerogel surface area was measured through nitrogen adsorption and desorption at 77 K using a Gemini VII 2390 surface area analyzer (Micromeritics) using the Brunauer-Emmett-Teller (BET) theory.[236] Pore volume and pore size distribution were calculated from the measured desorption isotherms using the Barret-Joyner-Halenda (BJH) calculation scheme. The characteristic morphologies of the aerogels were imaged using scanning electron microscopy (SEM; FEI Quanta 600) at 10 kV. Electrical conductivities of the gels were measured by 2-probe contact direct current measurements using a Fluke 287 True RMS multimeter.

All electrochemical measurements were performed using a conventional 3-electrode electrochemical cell utilizing a KCl saturated Ag/AgCl electrode and a 0.5 mm platinum wire electrode as reference and counter electrodes, respectively, and the gel electrode under study was used as the working electrode. Biofuel cell performance was monitored using a Fluke 287 True RMS multimeter with an IET Labs RS-200 resistance decade box used to manually vary EBFC resistance. GOX kinetic analysis was performed using the standard GOX ABTS activity assay at varying glucose concentrations, monitoring change in absorbance at 415 nm.

2.2.3 Fabrication of graphene/SWCNT cogels

SWCNT dispersions were prepared as described previously.[237-240] Briefly, we first sonicated SWCNTS in sodium dodecylbenzenesulfonate (NaDDBS) solution (1.0 wt%) at a SWCNT:NaDDBS ratio of 1:10 at 60 W for 2 h and removed aggregates through centrifugation at 3500 rpm for 15 min. We then determined the concentration of dispersed SWCNTs through UV-Vis spectroscopy using an extinction coefficient of 2.6 abs mL mg^{-1} mm^{-1} at 901 nm and the Beer-Lambert law.[237] We synthesized graphene oxide *via* modified Hummers' method.[241, 242] The graphene oxide was then thoroughly washed by multiple water rinse and centrifugation steps. Subsequently, we added graphene oxide to the dispersed SWCNT suspension at a graphene oxide:SWCNT ratio of 1:5, briefly sonicated to mix and concentrated to ~0.3 wt% carbon-based materials *via* slow water evaporation at 60 °C. To form the desired shape, we degassed and pipetted the solution into 2 mm thick rectangular molds. The mixed suspension of graphene oxide and SWCNTs gelled within a few minutes to 2 hours. We allowed these graphene oxide/SWCNT cogels to set for roughly 12 h to improve their mechanical integrity. We removed the NaDDBS surfactant from the cogels by repeated washing with ultrapure water and 1 washing with nitric acid (1 M) for 20 min followed by thorough washing with ultrapure water to

neutralize acid within the cogels. The graphene oxide was then converted to graphene by hydrothermal reduction of graphene oxide/SWCNT cogels at 185 °C for 18 h. Finally, water was exchanged with ethanol at increasing concentrations up to 100% and the cogels were transformed into aerogels *via* critical point drying. We further reduced graphene using pyrolysis at 900 °C for 6 h to yield the final graphene/SWCNT aerogels. The fabrication process of graphene/SWCNT cogels and aerogels is summarized in **Figure 2.2**. We refer to an interspersed network of graphene and SWCNT in any liquid as a cogel and in air as an aerogel. All graphene/SWCNT cogel-based electrodes used in this study had a cross-sectional area of ~0.3 cm^2 and were ~0.2 cm thick.

2.2.4 Preparation and test of EBFCs

To load enzymes into the cogel electrodes, we incubated individual graphene/SWCNT aerogels in 2 mL of enzyme (GOX or BOD) solution (1 mg mL^{-1} in 0.1 M sodium phosphate buffer (pH 7.0) for 4 h at 4 °C. To induce complete loading of these electrodes with enzyme solution, without collapsing the cogels, we applied a weak pulsed vacuum for several minutes using a benchtop vacuum pump prior to incubation. We then individually washed each enzyme-loaded cogel in 5 mL of 0.1 M sodium phosphate buffer (pH 7.0) for 10 min to remove weakly bound enzyme. To characterize the distribution of GOX within the porosity of the cogel matrix, we examined graphene/SWCNT cogels with and without GOX functionalization using fluorescence spectroscopy. GOX-modified cogels were sliced to isolate the outside of the cogels exposed to enzyme solution during incubation from the inside portion not directly exposed. The slices were then dispersed into 0.1 M sodium phosphate buffer (pH 7.0) *via* physical agitation and sonication to form a homogenous solution. Fluorescence spectra were collected and compared to that of graphene/SWCNT cogel without enzyme functionalization as well as

graphene/SWCNT cogel dispersed into solution with a known GOX concentration equal to that determined through electrochemical GOX loading analysis. Finally, we carried out EBFC measurements in glucose-containing (100 mM) air-saturated 0.1 M sodium phosphate buffer (pH 7.0; 200 mL) under stirring with enzyme-loaded cogel electrodes securely attached to wire leads *via* copper clips that were minimally exposed to buffer solution. Reloading of EBFC electrodes was carried out after 20 min incubation in nitric acid (1 M) and thorough washing with ultrapure water.

2.3 Results and Discussion

2.3.1 Material characterization

We have previously shown that suspensions of SWCNTs can undergo sol-gel transition to form robust, 3-dimensional networks owing to van der Waals forces acting between individually dispersed nanotubes.[237-239, 243, 244] Aerogels of CG 200 SWCNTs prepared using this process typically had electrical conductivities of κ ~1 S cm^{-1} and high SSA of ~1290 m^2 g^{-1}, which made them highly attractive as EBFC electrodes.[237] However, the majority of pores within the reported SWCNT gels had diameters of ~2-8 nm, which was likely too small for efficient internalization of globular proteins such as GOX (8 x 7 x 8 nm).[237, 245] We hypothesized that a network of micrometer-sized graphene sheets and SWCNTs would likely possess larger pores throughout the formed matrix and thus enhance globular protein internalization.

Consequently, we fabricated free-standing, 3-dimensional graphene/SWCNT cogels (**Figure 2.2**) having a density of 7.1 mg mL^{-1} and examined their pore/surface area characteristics and morphologies *via* BET and SEM, respectively (**Figure 2.3** and **Figure 2.2B**). As expected, more than 70% of total pore volume in the graphene/SWCNT cogels was made up

of pores having a radius greater than 10 nm, as calculated from BET surface area measurements according to the BJH calculation scheme (**Figure 2.3**), meaning a large majority of the electrode material was potentially accessible to the diffusion of electroactive enzymes. The micron-scale graphene sheets, which formed scroll-like structures[246] within the SWCNT matrix, were easily discernable in SEM images from the nano-sized SWCNTs (**Figure 2.2B**). The final graphene/SWCNT aerogels possessed moderate electrical conductivity (κ = 0.2 S cm^{-1}) and ultrahigh surface area (SSA = 846 m^2 g^{-1}), and were further functionalized *via* physical adsorption of GOX or BOD to form EBFC anodes or cathodes, respectively.

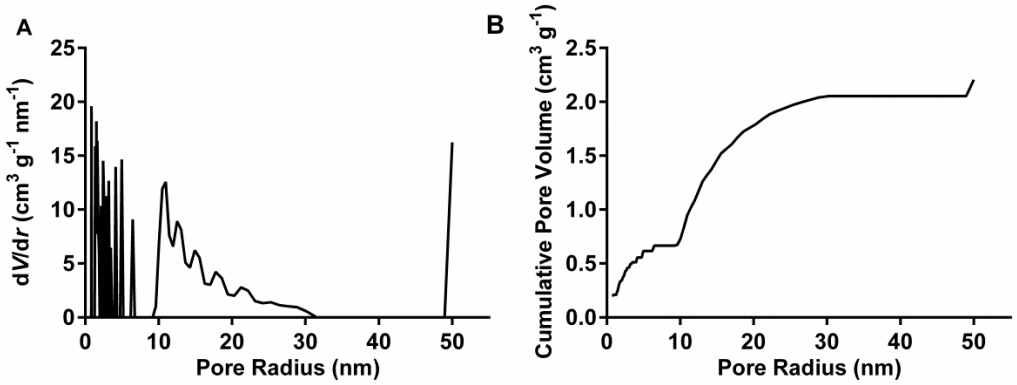

Figure 2.3 Pore size analysis of graphene/SWCNT cogel. A) Pore size distribution of graphene/SWCNT cogel. B) Cumulative pore volume with increasing pore size of graphene/SWCNT cogel. Pore size information from BJH calculation scheme of BET surface area analysis.

2.3.2 Characterization of GOX-modified graphene/SWCNT cogel anodes

The GOX-catalyzed oxidation of glucose proceeds as follows:

$$\mathrm{GOX_{FAD}} + \mathrm{glucose} \rightarrow \mathrm{GOX_{FADH_2}} + \mathrm{gluconolactone} \quad (2.1)$$

$$\mathrm{GOX_{FADH_2}} \rightarrow \mathrm{GOX_{FAD}} + 2\mathrm{H^+} + 2\mathrm{e^-} \quad (2.2)$$

In **Equation (2.2)**, the re-oxidation of the FAD-based GOX active site can be facilitated by an electrode, molecular oxygen or an externally added redox mediator. Upon GOX functionalization, we electrochemically characterized the cogel anodes to evaluate their performance. OCV evolutions of the cogel with and without immobilized GOX were examined to evaluate overpotentials within the system (**Figure 2.4**). The OCV of the GOX-modified anode in the presence of 10 mM glucose was -0.05 ± 0.01 V versus Ag/AgCl. The thermodynamically determined redox potential of the FAD/$FADH_2$ redox couple has been shown to be approximately -0.36 V versus Ag/AgCl.[11] The overpotential between the thermodynamically determined and experimentally observed redox potentials suggested decreases in native enzyme activity due to partial denaturation upon physical adsorption or blockage of electrically connected FAD sites to glucose binding.[91, 247] Nevertheless, the observed decrease in OCV upon anode functionalization indicated successful adsorption of enzyme and electron transfer between the active site and electrode.

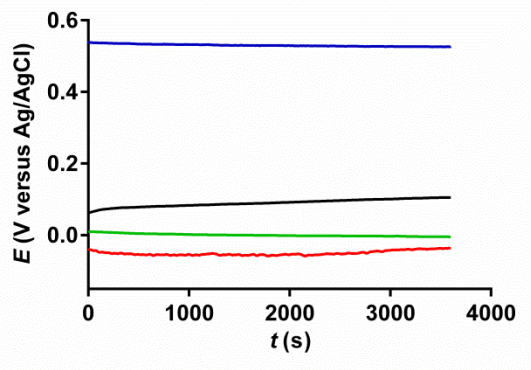

Figure 2.4 Open circuit voltages of graphene/SWCNT cogel-based anode and cathode. OCV evolution of BOD-modified graphene/SWCNT cogel cathode (blue), graphene/SWCNT cogel cathode without BOD-modification (black), GOX-modified graphene/SWCNT cogel anode (red) and graphene/SWCNT cogel anode without GOX-modification (green). Anodic measurements carried out with 10 mM glucose in argon-saturated solution and cathodic measurements carried out in O_2-saturated solution. Experiments performed in 0.1 M sodium phosphate buffer (pH 7.0).

Cyclic voltammetry (CV) measurements of the GOX-modified graphene/SWCNT cogel anodes showed obvious oxidation and reduction peaks at -0.34 V and -0.51 V versus Ag/AgCl, respectively, which indicated quasi-reversible electron transfer between the FAD-based active site of GOX and the electrode surface (**Figure 2.5A**).

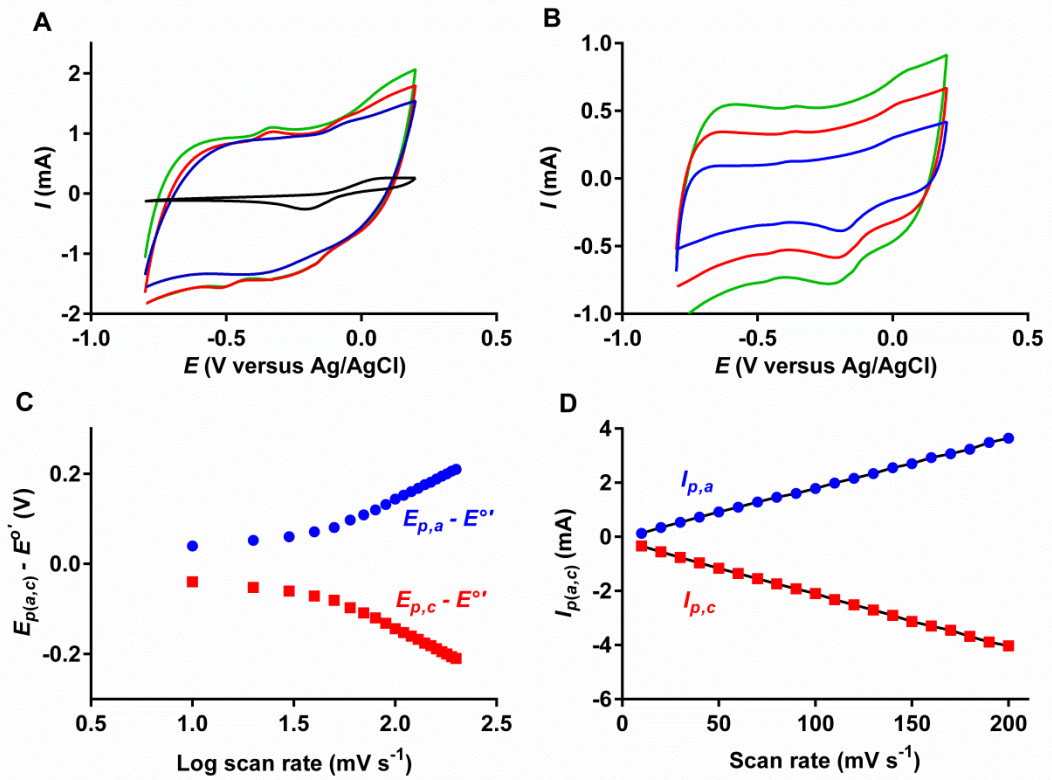

Figure 2.5 Electrochemical performance of graphene/SWCNT cogel-based anode. A) Characteristic CV traces of bare copper clip (black), graphene/SWCNT cogel anode without GOX-modification (blue), GOX-modified graphene/SWCNT cogel anode (red) and GOX-modification graphene/SWCNT cogel anode with 10 mM glucose (green) at a scan rate of 50 mV s^{-1}. B) Characteristic CV traces of GOX-modified graphene/SWCNT cogel anode at varying scan rates of 10 mV s^{-1} (blue), 20 mV s^{-1} (red) and 30 mV s^{-1} (green). C) Dependence of anodic (blue circle) and cathodic (red square) peak potentials on the logarithm of scan rate for GOX-modified graphene/SWCNT cogel anodes at varying scan rates. D) Dependence of anodic (blue circle) and cathodic (red square) peak currents on scan rate for GOX-modified graphene/SWCNT cogel anodes at varying scan rates. Experiments performed in argon-saturated 0.1 M sodium phosphate buffer (pH 7.0).

Additionally, the current response increased slightly upon the addition of glucose into the system, which suggested some level of GOX activity. This result further confirmed the successful incorporation of GOX into the cogel network as the discussed faradaic response was absent in CV scans of graphene/SWCNT cogel anodes without GOX-modification (**Figure 2.5A**) and no current shifts were observed upon the addition of glucose to control materials (*i.e.* graphene/SWCNT cogel and copper clip without GOX-modification) (**Figure 2.6**).

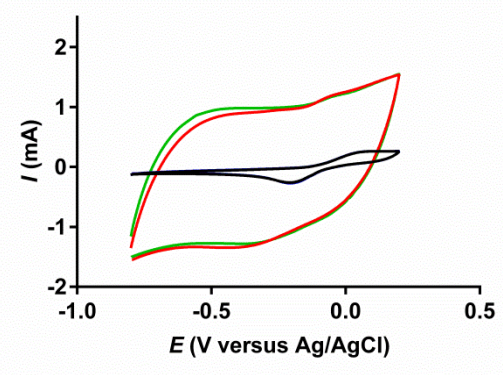

Figure 2.6 Electrochemical performances of anodic system control materials. Characteristic CV traces of bare copper clip (black), bare copper clip with 10 mM glucose (blue), graphene/SWCNT cogel anode without GOX-modification (red) and graphene/SWCNT cogel anode without GOX-modification with 10 mM glucose (green). Experiments performed in 0.1 M sodium phosphate buffer (pH 7.0) at a scan rate of 50 mV s^{-1}.

However, these results alone did not sufficiently prove that we observed DET between biocatalytically-active GOX and the cogel electrode. Stevenson *et al.* recently reported significant evidence that DET with biocatalytically active GOX at CNTs was not possible and that electrochemical responses observed in DET claiming studies were a result of free FAD adsorbed onto the CT surfaces.[145] This conclusion was also reached by Ye *et al.* concerning graphene surfaces.[146] Stevenson *et al.* further suggested that the appearance of anodic current upon glucose addition in argon-saturated solution was likely the most appropriate signature of

DET with an FAD-containing enzyme such as GOX.[145] To study the potential DET of GOX immobilized onto graphene/SWCNT cogels in depth, we performed amperometry along with additional CV traces on GOX-modified graphene/SWCNT cogel anodes (**Figure 2.7**). We observed a slow anodic shift in current upon the addition of glucose to GOX-modified graphene/SWCNT cogel anodes in argon-saturated solution (**Figure 2.7A**) and in O_2-saturated solution (**Figure 2.7B**) with applied voltage held at the observed anodic formal potential (-0.42 V versus Ag/AgCl). The appearance of this shift in argon-saturated solution suggested DET between GOX and the cogel electrode. We further examined the response of GOX-modified graphene/SWCNT cogel anodes to glucose addition by measuring CV characteristics at a scan rate of 5 mV s^{-1}. In both argon- and O_2-saturated solution, anodic current increased upon the addition of glucose, which indicated current generation through the oxidation of glucose by electrically connected GOX (**Figure 2.7C,D**). Also, we noted a significant decrease in the cathodic peak current in O_2saturated solution, which we attributed to a decrease in local O_2 concentration due to the GOX-catalyzed reduction of O_2 to hydrogen peroxide (**Figure 2.7D**). To ensure this cathodic peak and amperometric shift were not results of O_2 reduction at the electrode surface uncoupled from GOX kinetics, we performed CV traces of graphene/SWCNT cogel anodes without GOX-modification in both argon- and O_2-saturated solutions and observed no change (**Figure 2.7E**). From these results, we postulated that DET between GOX and graphene/SWCNT cogels was observed and, independent of these findings, we defined the system to be mediator-free, as no external redox mediators were added at any point.

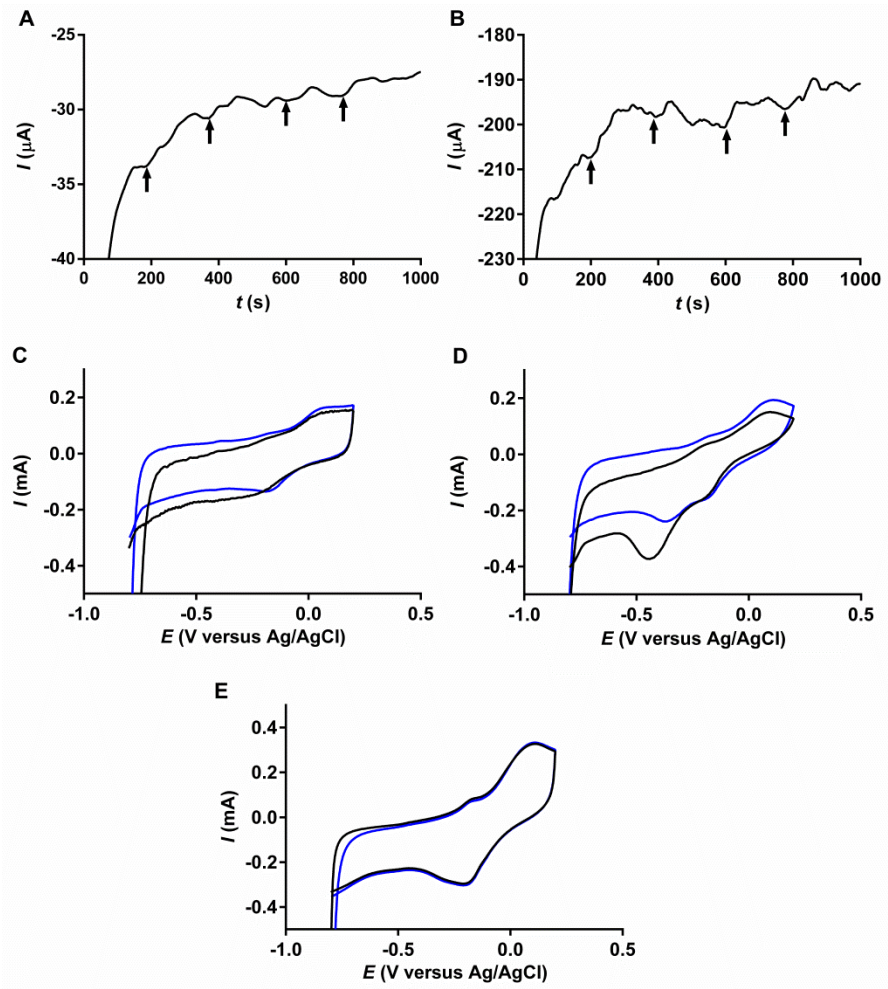

Figure 2.7 Characterization of GOX electron transfer with graphene/SWCNT cogel electrodes. A) Typical amperometric profile of GOX-modified graphene/SWCNT cogel anodes in argon saturated solution with applied potential held at -0.42 V versus Ag/AgCl (5 mM glucose injection indicated by arrow). B) Typical amperometric profile of GOX-modified graphene/SWCNT cogel anodes in O_2-saturated solution with applied potential held at -0.42 V versus Ag/AgCl (5 mM glucose injection indicated by arrow). C) Characteristic CV traces of GOX-modified graphene/SWCNT cogel anodes in argon saturated solution before (black) and after (blue) 10 mM glucose injection. D) Characteristic CV traces of GOX-modified graphene/SWCNT cogel anodes in O_2 saturated solution before (black) and after (blue) 10 mM glucose injection. E) Characteristic CV traces of graphene/SWCNT cogel anodes without GOX-modification in argon-saturated solution (black) and O_2-saturated solution. Experiments performed in 0.1 M sodium phosphate buffer (pH 7.0). CV traces performed at a scan rate of 5 mV s^{-1}.

We further investigated the electron transfer between immobilized GOX/FAD and graphene/SWCNT cogels by measuring the CV characteristics of the GOX-modified anode at varying scan rates (**Figure 2.5B**). The observed dependence of anodic and cathodic peak potentials on the logarithm of scan rate from 10 to 100 mV s^{-1} was examined (**Figure 2.5C**) and used to determined anodic electrochemical parameters according to:[248, 249]

$$E_{p,c} = E'^{\circ} - \left[\frac{RT}{\alpha nF}\right] \ln\left[\frac{\alpha Fn}{RTk_s} v\right] \quad (2.3)$$

$$E_{p,c} = E'^{\circ} + \left[\frac{RT}{(1-\alpha)nF}\right] \ln\left[\frac{(1-\alpha)Fn}{RTk_s} v\right] \quad (2.4)$$

In **Equation (2.3)** and **Equation (2.4)**, E'° is the formal potential of the system equal to the average of anodic and cathodic peak potentials, α designates the charge transfer coefficient of the system, v is the scan rate used, n is the number of electrons transferred in the reactions, k_s is the heterogeneous electron transfer rate constant and T, R and F are temperature, the ideal gas constant and Faraday's constant, respectively. Based on these equations, n and α were calculated from the slopes of the linear trends observed at high scan rates (**Figure 2.5C**). Specifically, the fit lines passing through these points gave linear trends whose slopes were equivalent to $-2.3RT/[\alpha nF]$ for the cathodic peaks and $2.3RT/[(1-\alpha)nF]$ for the anodic peaks (**Equation (2.3)** and **Equation (2.4)**).[248] Thus, α and n were found to be 0.5 and 0.54, respectively. The calculated α value was similar to other studies reported.[134, 190] However, the calculated value of n was markedly lower than the theoretical value for the conversion of FAD to $FADH_2$ in GOX (*i.e.* 2), which suggested potentially hindered electron transport. Further, the k_s of the anodic system was calculated according to:[248]

$$\log k_s = \alpha \log(1-\alpha) + (1-\alpha)\log\alpha - \log\left(\frac{RT}{nFv}\right) - \alpha(1-\alpha)\left(\frac{nF\Delta E_p}{2.3RT}\right) \quad (2.5)$$

From **Equation (2.5)**, the k_s of the graphene/SWCNT cogel-based system was estimated to be 0.23 ± 0.01 s^{-1}, which was slightly lower than similar reports due to increased separation of peak potentials.[147, 189, 190]

The anodic and cathodic peak currents of GOX-modified graphene/SWCNt cogel anodes increased linearly with scan rate (**Figure 2.5D**). This result implied that the system was limited by the electron transfer occurring at the enzyme-electrode interface rather than by diffusion. Further, we used the slopes of these trends to estimate the loading of electroactive species immobilized onto the electrode surface according to:[32]

$$I_p = \frac{n^2 F^2 \Gamma A}{4RT} v \tag{2.6}$$

In **Equation (2.6)**, Γ signifies the surface coverage of electroactive species (*i.e.* FAD),[234] A is the surface area available for electroactive species adsorption and I_p is the peak current. The estimated SSA coverage of $FAD/FADH_2$ was 1.44×10^{-12} mol cm^{-2} or 1.73×10^{-8} mol cm^{-2} of cross-sectional area, which indicated the efficient internalization of GOX into the cogel matrix resulting in high loadings. Assuming an average diameter of 8 nm for each GOX molecule, the calculated loading corresponded to more than 20% of available cogel SSA being occupied by electroactive GOX presuming two molecules of FAD indicated one GOX molecule. This loading was almost 2 orders of magnitude higher than similar 3-dimensional structures based on Pd aerogels or graphene foams decorated with SWCNTs.[69, 119] Using the apparent concentration of immobilized GOX, we determined the retained GOX kinetics upon immobilization. Specifically, the catalytic rate constant (k_{cat}) of immobilized GOX was 46 ± 3 s^{-1} compared to 316 ± 16 s^{-1} for native GOX (**Figure 2.8**). This decrease has been commonly reported for immobilized enzymes due to partial denaturation at the enzyme-nanosupport

interface upon attachment.[91, 141] Despite the reduction of catalytic efficiency, k_{cat} was greater than the observed k_s, which suggested an electron transport limited system.

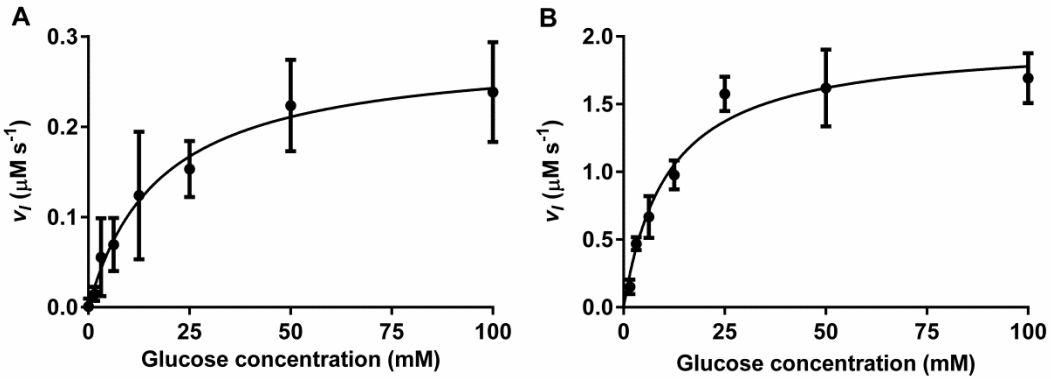

Figure 2.8 Kinetic analysis of immobilized and native GOX. A) Initial rate of reaction at varying substrate concentration for GOX physically adsorbed onto graphene/SWCNT cogels. B) Initial rate of reaction at varying substrate concentration for native GOX. Experiments performed in 0.1 M sodium phosphate buffer (pH 7.0). Error bars represent 1 standard deviation between 6 trials.

We analyzed tryptophan fluorescence within GOX-modified cogels to evaluate the presence of internalized GOX. Tryptophan has been reported to exhibit an emission peak between ~308-355 nm depending on local environment.[250, 251] Thus, detection of tryptophan fluorescence within the cogel network would correspond to internalized enzyme. The observed peak fluorescence varied depending on location of analyzed cogel slice (*i.e.* cogel interior versus exterior) with peak intensity indicative of GOX amount present (**Figure 2.9**). The interior slice of the GOX-modified graphene/SWCNT cogel anode exhibited a similar but slightly higher peak signal intensity compared to the sample that contained a known concentration of GOX equal to the electrochemically determined GOX loading. This result was expected as not all of the internalized GOX would be capable of electron transfer to and from the cogel electrode due to enzyme orientation effects, resulting in increased distance between FAD and the nanomaterial

surface. We found the extent of these orientation effects and potential GOX agglomeration to be much greater at the exterior of the electrode, evident from the increased fluorescence peak intensity of the exterior slice (**Figure 2.9**). These results confirmed distribution of GOX within the entirety of the graphene/SWCNT cogel and showed the presence of GOX that was not capable of electron transfer with the cogel network along with electroactive GOX.

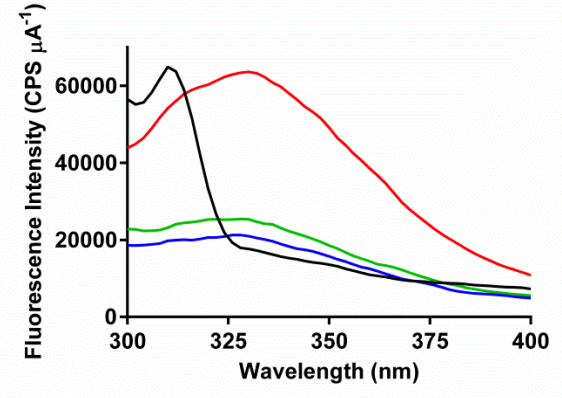

Figure 2.9 Tryptophan fluorescence spectra of dispersed graphene/SWCNT cogels with and without GOX-modification. Corrected signal intensity over corrected lamp intensity of graphene/SWCNT cogel without GOX modification (black), graphene/SWCNT with known concentration of native GOX added equal to electrochemically determined GOX loading (blue) and GOX-modified graphene/SWCNT cogel anodes exterior slice (red) and interior slice (green). Experiments performed in 0.1 M sodium phosphate buffer (pH 7.0).

2.3.3 Characterization of BOD-modified graphene/SWCNT cogel cathodes

BOD is a multicopper oxidase that, when utilized as a cathodic working enzyme, accepts electrons from an electrode at its T1 copper site and transfer those electrons approximately 13 Å along a His-Cys-His chain to its T2/T3 copper site where molecular oxygen is reduced to water in a 4-electron transfer mechanism according to:[182, 252]

$$O_2 + 4H^+ + 4e^- \rightarrow 2H_2O \qquad (2.7)$$

The observed OCV of the BOD-modified graphene/SWCNT cogel cathode was 0.53 ± 0.01 V versus Ag/AgCl, which was in agreement with reported OCVs in similar studies (**Figure 2.4**).[253] This value was slightly more positive than the thermodynamically determined value of the T1 copper site of BOD, which has been reported to be approximately 0.47 V versus Ag/AgCl.[87] The observed increase in OCV compared to bare graphene/SWCNT cogel cathodes under similar conditions confirmed the presence of immobilized BOD and, more importantly, showed the efficient electron transfer between enzyme active site and electrode. Lower overpotentials were likely achieved for BOD compared to GOX due to the closer proximity of the T1 electron acceptor site to the surface of BOD relative to the FAD active site of GOX.[252]

To further confirm the presence of electrically connected enzyme on the cathode, we examined BOD-modified graphene/SWCNT cogel cathodes using CV. CV sweeps did not yield any redox transformation evident by the lack of faradaic current response, which was consistent with previous reports on the electrochemical activity of BOD and other multicopper oxidases (**Figure 2.10**).[185, 254] However, upon addition of molecular oxygen to the BOD-modified system, a significant decrease in cathodic current was observed with an onset potential of oxygen reduction of ~0.4 V versus Ag/AgCl. This result showed the capability of immobilized BOD to achieve DET and efficiently reduce oxygen to water at the cogel electrode surface.[119, 255, 256]We stress that no response to the addition of molecular oxygen occurred in our system without BOD-modification, which showed that the immobilized enzyme was solely responsible for O_2 reduction (**Figure 2.11**).

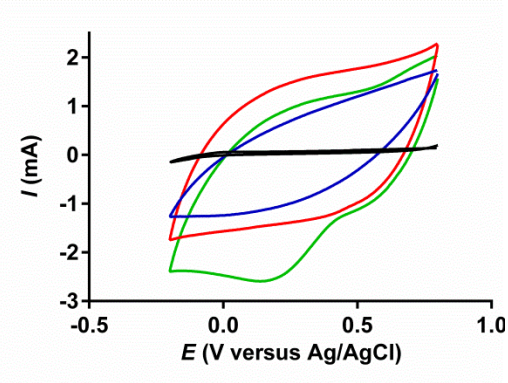

Figure 2.10 Electrochemical performance of graphene/SWCNT cogel-based cathode. Characteristic CV traces of bare copper clip (black), graphene/SWCNT cogel cathode without BOD-modification (blue) and BOD-modified graphene/SWCNT cogel cathode (red) in argon-saturated solution and BOD-modified graphene/SWCNT cogel cathode in O_2-saturated solution (green) at a scan rate of 50 mV s^{-1}. Experiments performed in 0.1 M sodium phosphate buffer (pH 7.0).

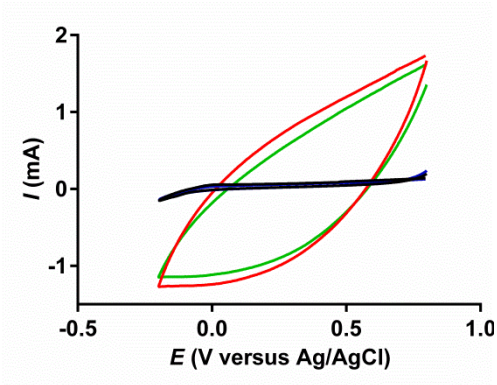

Figure 2.11 Electrochemical performances of cathodic system control materials. Characteristic CV traces of bare copper clip in argon-saturated solution (black), bare copper clip in O_2-saturated solution (blue), graphene/SWCNT cogel cathode without BOD-modification in argon-saturated solution (red) and graphene/SWCNT cogel cathode without BOD-modification in O_2-saturated solution (green). Experiments performed in 0.1 M sodium phosphate buffer (pH 7.0) at a scan rate of 50 mV s^{-1}.

2.3.4 Characterization of graphene/SWCNT cogel-based EBFC performance

We set up EBFC using a single GOX-loaded graphene/SWCNT cogel anode and a single BOD-loaded graphene/SWCNT cogel cathode (**Figure 2.1**), and tested power output through the manual variation of circuit resistance while measuring voltage output. The performance of an EBFC can be expressed through the use of two main characteristics: OCV and power density. For our mediator-free graphene/SWCNT-based system, the OCV was 0.61 ± 0.05 V and the cross-sectional power density was 0.19 ± 0.03 mW cm^{-2} operating at 0.44 V (**Figure 2.12**).

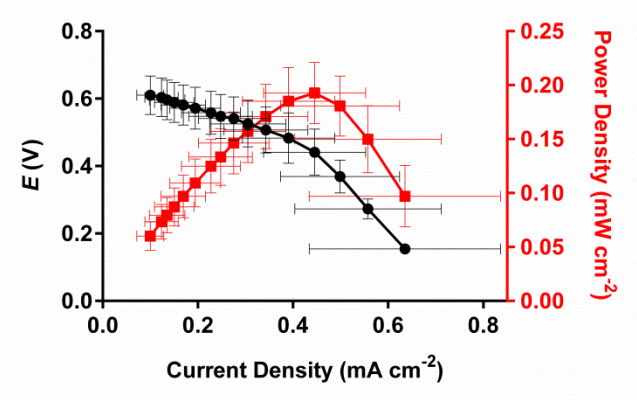

Figure 2.12 Performance of graphene/SWCNT cogel-based EBFC. Graphene/SWCNT cogel-based EBFC performance and cell-polarization curves. Experiments performed in air-saturated 0.1 M sodium phosphate buffer (pH 7.0). Error bars represent 1 standard deviation of 3 trials.

This power output corresponded to 0.08% of native GOX activity relative to GOX turning over glucose at the experimentally determined k_{cat} of native enzyme and GOX loading. In other words, we found the experimental power density to have an efficiency of 0.08% of the maximum, corresponding to the calculated amount of GOX per unit area generating current from glucose at the reported k_{cat} of native GOX. The observed percentage activity was in agreement with similar EBFC systems.[67] The experimental full-cell OCV was in good agreement with the difference between OCVs of the individual anode and cathode (i.e., -0.05 V and 0.53 V versus

Ag/AgCl, respectively) as expected. The polarization curve showed the maximum power output corresponded to a current density that was lower than the onset of concentration losses caused by limited diffusion of reactants and products (i.e., increased negative slope at high current density) (**Figure 2.12**).[225] Further, we tested the operation of the EBFC at pH 5.5 for optimal GOX biocatalytic activity, but observed essentially no change from the EBFC performance at pH 7.0 (**Figure 2.13**).This result confirmed that the overall system was limited by electron transfer at the anode and not intrinsic enzyme activity.

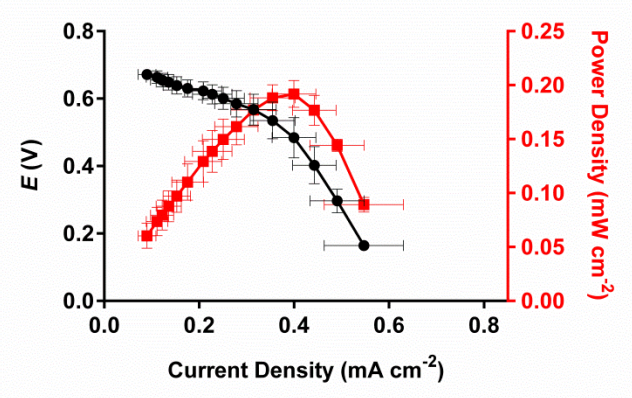

Figure 2.13 Graphene/SWCNT cogel-based EBFC performance under optimal GOX conditions. Graphene/SWCNT cogel-based EBFC performance and cell-polarization curves at optimal GOX pH. Experiments performed in air-saturated 0.1 M sodium phosphate buffer (pH 5.5) with 100 mM glucose. Error bars represent 1 standard deviation of 3 trials.

We further verified that the oxidation of glucose by GOX generated the observed current in the system through a series of control experiments without GOX-modification. First, we immersed the copper leads alone in the EBFC solution with no graphene/SWCNT cogels or enzyme and tested for current generation. Then, we examined the performance of EBFCs with bare graphene/SWCNT cogels without any adsorbed enzyme as an anode and a cathode, followed by tests using a bare cogel as the anode and a BOD-modified cogel as the cathode. The

resulting performance and polarization curves exhibited negligible current generation, which confirmed a GOX-driven system (**Figure 2.14**).

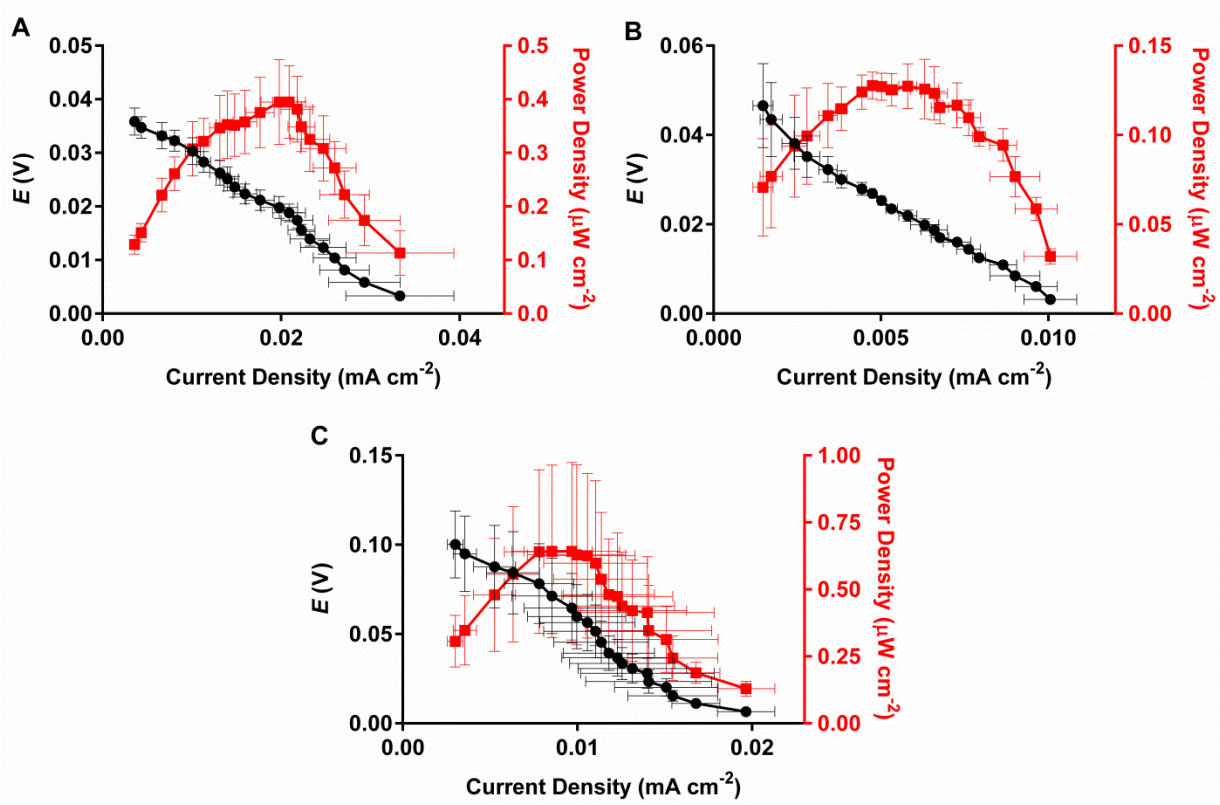

Figure 2.14 Graphene/SWCNT cogel-based EBFC performance without GOX-modification. A) Graphene/SWCNT cogel-based EBFC performance and cell-polarization curves using copper leads alone. B) Graphene/SWCNT cogel-based EBFC performance and cell-polarization curves using non-modified anode and cathode. C) Graphene/SWCNT cogel-based EBFC performance and cell-polarization curves using non-modified anode and BOD-modified cathode. Experiments performed in air-saturated 0.1 M sodium phosphate buffer (pH 7.0) with 100 mM glucose. Error bars represent 1 standard deviation of 3 trials.

An interesting question that has never been addressed for EBFCs was whether the electrodes can be reloaded when the enzymes degrade. The robustness and simple loading procedure of our system allowed us to clean and then "refill" the electrodes with active enzymes. Rejuvenation of power output by cyclic removal of degraded enzyme with acid and replenishing

the system with fresh, active enzyme generated a power density of 0.15 ± 0.02 mW cm^{-2} (**Figure 2.15**).

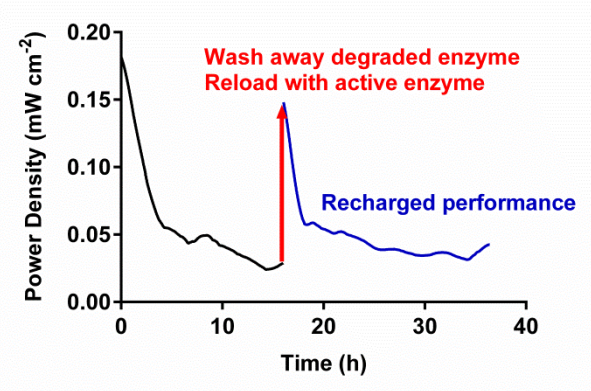

Figure 2.15 Continuous performance and recharging of graphene/SWCNT cogel-based EBFC. Performance of graphene/SWCNT cogel-based EBFC over time. Acid washing of degraded enzyme and reloading with active enzyme after 18 h (red) followed by repeated performance (blue). Experiments performed in air-saturated 0.1 M sodium phosphate buffer (pH 7.0). with 100 mM glucose.

Conventionally, the power densities of fuel cells have been reported in cm^{-2} as the flow of current is a flux through the electrode surface. Most reported EBFC systems are essentially 2-dimensional, such as functionalized coatings on pre-existing material surfaces (i.e., glassy carbon electrodes (GCE), buckeypaper, etc.).[233, 257-259] Recently, however, EBFC systems utilizing 3-dimensional electrodes have gained increased attention and resulted in enhanced power densities due to the possibility of increased active enzyme loadings and connectivity.[67-69, 232, 260] Thus, the need to report power densities volumetrically has arisen to allow for meaningful comparisons between studies. The volumetric power density of this system utilizing ~2 mm thick graphene/SWCNT cogel electrodes was 0.65 ± 0.22 mW mL^{-1}. Further, it was important to characterize the system in terms of gravimetric power density to show the power output per mass of catalyst. The loading density of GOX onto the graphene/SWCNT co-gel anodes was estimated

through CV analysis at varying scan rates knowing each GOX molecule contains two FAD sites.[32, 189] The gravimetric power density of this system was 140 ± 20 mW g^{-1} GOX, which was more than 4-fold greater than the elegant systems based on compressed disks of multi-wall CNTs and enzymes.[67] This increase compared to the similar mediator-free system was attributed to the fabrication procedure and high porosity of our system, which allowed the majority of incorporated enzyme to have access to both the electrode surface for electron transfer and to freely diffusing substrate.

The membrane-and mediator-free EBFC we describe herein can be added to a small but growing literature on similar systems,[67, 261, 262] including a setup resulting in a nearly identical cross-sectional power density that was successfully implanted into rats.[72] Multiple other studies have been able to produce higher performing fuel cells but have also required mediated electron transfer and even setups with multiple compartments separated by a semi-permeable membrane, adding complexity and additional toxicity concerns.[68-70] Further, other mediator-free systems have commonly required more complicated electrode functionalization steps prior to enzyme immobilization[261, 262] or large amounts of bulk enzyme due to low enzyme activity retention.[67] Due to the porosity, high SSA and significant electrical conductivity of the electrode materials used herein, we have been able to achieve relatively high enzyme loadings and rapid charge collection without significant loss, which resulted in a significant power density despite hindered electron transport. High enzyme loadings are relative to reported studies that used similar 3-dimensional nanomaterial networks and enzyme immobilization strategies.[69, 119] A comparison of various relevant studies focused on glucose-driven EBFCs utilizing graphene or carbon nanotube-based electrode materials is presented in **Table 2.1**. The EBFC reported herein had a power output within an order of magnitude of the

highest performing systems to date.[68-70] Our data showed that the anodic electron transfer rate constant was lower than other investigators have found,[69] leading to a clear path for further improvement in our EBFC.

Table 2.1: Performance of published glucose-driven EBFC systems utilizing graphene- or carbon nanotube-based electrode materials

Anode	Cathode	Mediator-free/MET (membrane Y/N)	OCV (V)	Power density	Ref
GOX-graphene/SWCNT cogel	BOD-graphene/ SWCNT cogel	Mediator-free (N)	0.61	0.19 mW cm^{-2} 0.65 mW mL^{-1}	This work
GOX/catalase-compressed MWCNT disk	Laccase-compressed MWCNT disk	Mediator-free (N)	0.57	0.19 mW cm^{-2} 0.16 mW mL^{-1}	[72]
PQQ-GDH-PANi/ MWCNT-Au electrode	BOD-MWCNT-Au electrode	Mediator-free (N)	0.68	0.07 mW cm^{-2}	[261]
GOX-SWCNT/PPY 3D composite	Tyrosinase-CNP/PPY composite	Mediator-free (N)	0.19	0.16 mW mL^{-1}	[262]
GOX/catalase-compressed MWCNT disk	Laccase-compressed MWCNT disk	Mediator-free (Y)	0.95	1.25 mW cm^{-2} 1.66 mW mL^{-1}	[67]
Crosslinked GOX clusters-MWCNT/Nafion	Pt/C/Nafion	Mediator-free (Y)	0.43	0.18 mW cm^{-2}	[259]
GOX/FCA-Pd aerogel	BOD-Pd/Pt aerogel	MET (N)	0.40	0.02 mW cm^{-2}	[119]
Nafion/GOX/FCA-3D graphene	Nafion/laccase-3D graphene/PTCA/DA	MET (N)	0.40	0.11 mW cm^{-2}	[235]
(MWCNT/thionine/ AuNPs)GDH	MWCNT/PLL/laccase	MET (N)	0.70	0.33 mW cm^{-2}	[263]
vaCNT/PABMSA/PQQ-GDH	vaCNT/PQQ/BOD	MET (N)	0.80	0.12 mW cm^{-2}	[264]
PPY/SWCNT/GOX	PPY/laccase/ABTS	MET (N)	0.77	1.39 mW cm^{-2} 232 mW mL^{-1}	[232]
GOX/PEDOT/MWCNT/ PVI-Os	BOD/PEDOT/MWCNT/ PAA-PVI-Os	MET (N)	0.70	2.18 mW cm^{-2} 793 mW mL^{-1}	[70]
GOX-graphene/SWCNT foam	Laccase/ABTS-graphene/ SWCNT foam	MET (Y)	1.20	2.27 mW cm^{-2}	[69]
GOX/catalase/NQ-compressed MWCNT disk	Laccase-compressed MWCNT disk	MET (Y)	0.76	1.54 mW cm^{-2} 1.92 mW mL^{-1}	[68]

MET, mediated electron transfer; OCV, open circuit voltage; MWCNT, multi-wall carbon nanotube; PQQ-GDH, pyrroloquinoline quinone dependent glucose dehydrogenase; PANi, polyaniline; PPY, polypyrrole; CNP, carbon nanopowder; FCA, ferrocenecarboxylic acid; PTCA, 3,4,9,10-perylene tetracarboxylic acid; DA, dopamine; AuNPs, gold nanoparticles; PLL, poly-L-lysine; vaCNT, vertically aligned carbon nanotube; PABMSA, poly(3-aminobenzoic acid-*co*-2-methoxyaniline-5-sulfonic acid; PEDOT, poly(3,4-dioxythiophene); PVI-Os, poly(*N*-vinylimidazole)-[Os(4,4'-dichloro-2,2'-bipyridine)$_2$]$^{+/2+}$; NQ, naphthoquinone.

2.4 Conclusions

We have developed and characterized a membrane- and mediator-free EBFC utilizing novel graphene/SWCNT cogel electrodes. The glucose/O_2-fueled system proved capable of producing a power density of 0.19 ± 0.03 mW cm^{-2}, 0.65 ± 0.22 mW mL^{-1} or 140 ± 20 mW g^{-1} GOX with an OCV of 0.61 ± 0.05 V without the addition of external redox mediators. Compared to previous studies, the EBFC we describe was a robust, high power output system despite significantly hindered anodic electron transfer. We attributed this performance to the high available surface area and porosity of the electrode material allowing for large loading of active enzymes relative to similar studies and ease of glucose diffusion through the cogel based electrode. The nanoscale structure and high electrical conductivity of the cogels facilitated electron transfer to the electrode surface and charge collection through the electrode without any toxic redox mediators. The robustness of the cogels and our custom-designed loading procedure also allowed for the reloading and reuse of the EBFC. This study demonstrated the potential of such a system and highlighted areas of possible improvement for enhanced EBFC performance. Future work will focus on increasing electron transfer efficiency and long-term stability.

Chapter 3: Improved Power Density of an Enzymatic Biofuel Cell with Fibrous Supports of High Curvature

3.1 Introduction

Immobilized enzymes are used in a wide range of applications.[2, 88] The conjugation of enzymes onto or within support materials serves to impart biological function to non-biological materials while providing enhanced enzyme stability and a means of retaining enzymatic activity at a surface.[90, 106, 142, 265] Enzyme-based biofuel cells (EBFCs) use immobilized enzymes to generate electrical power from renewable fuels.[43, 266] Such systems have been reported to generate power densities of up to 2 mW cm^{-2} from sugars such as glucose and fructose, thereby enabling the continuous powering of some implantable devices.[25, 53, 67, 68, 70, 72] For EBFCs to function effectively, the working enzymes must be immobilized at or near an electrode surface so that electron transfer between the enzyme active site and the electrode structure continues during operation. The interactions at the enzyme-support interface influence these properties and thus the overall performance, making the choice of support material crucial.[88, 89, 91]

The operation of EBFCs is based on the oxidation of a fuel at the anode and the reduction of a final electron acceptor (generally molecular oxygen) at the cathode. The capability of these devices to operate at physiological conditions and the biocompatibility of reactants and products make EBFCs ideally suited for operation *in vivo*.[91] During operation, electrons are transferred between the enzyme active site and the electrode surface either directly (direct electron transfer (DET)) or through an intermediate redox molecule (mediated electron transfer (MET)). The achievable power density of a given EBFC is a function of the efficiency of electron transfer, the degree of enzyme loading onto the electrode surface and the retained enzyme kinetics.[16, 225] In designing an EBFC support material, three key parameters for consideration are support

curvature, pore size and specific surface area (SSA). A porous material with high SSA provides ample surface area for enzyme adsorption, which can lead to high enzyme loadings. However, without appropriate pore sizes, much of the material may not be accessible to the target enzyme, effectively reducing the available surface area. Further, studies have shown a direct influence of support curvature on retained activity of immobilized enzyme.[2, 89, 91] This impact has been attributed to increased nonspecific interactions between the enzyme and surfaces with lower rates of curvature (i.e. larger diameter) as well as between adjacent enzymes leading to increased protein denaturation upon adsorption.[89, 90] Evaluating the impact of each of these design parameters is crucial to the efficient design of future EBFC systems.

To optimize power, nanomaterials have become increasingly popular electrode materials due to their high available surface area and their potential to facilitate efficient electron transfer.[140, 228] Nanomaterials have also been proven to be capable of enhancing immobilized enzyme stability while preserving enzyme function.[90, 106, 118, 142, 265, 267-275] For instance, Wu *et al.* recently reported the significantly increased stability of a GOX-based biosensor against trypsin, ethylenediaminetetraacetic acid (EDTA) and long-term storage when the enzyme was incorporated into zeolitic imidazolate framework nanocrystals.[267] Two of the most widely used classes of nanomaterial are gold nanoparticle (AuNP)- and carbon nanotube-based surfaces. Both of these nanomaterials possess excellent electrical conductivity, high SSA and an ease of functionalization making them ideal for enzyme interaction.[228] For example, Cosnier *et al.* reported one of the highest performing and most versatile EBFC systems to date based on compressed pellets of multi-wall carbon nanotubes (MWCNTs) operating *via* DET[67] and MET,[68] which was further shown to successfully function within a rat model.[72] Shleev *et al.* have exhibited the potential of AuNP-functionalized electrodes to form intricate systems

capable of operating within the eye toward forming “smart” contact lenses.[276, 277] Similarly, our group has investigated the capability of these materials to form high-performing biosensors and EBFCs. Our studies showed the capability of carbon nanotube- and AuNP-based materials to form highly porous networks, which allowed high enzyme loadings and reliable operation without the need for external mediators.[191, 278, 279] Despite significant research into developing efficient EBFCs, the application of EBFCs is currently limited due to challenges stemming from poor electron transfer efficiency and enzyme stability at the enzyme-nanomaterial interface.[14] A thorough understanding of the impact of electrode material characteristics such as surface curvature, SSA and pore size on resulting EBFC performance was the goal of the work described herein.

Gold/MWCNT fiber paddle electrodes[191] and graphene-coated single-wall carbon nanotube (SWCNT) gel electrodes[238, 280] were modified with electroactive enzymes and their electrochemical properties determined. Glucose oxidase (GOX) and bilirubin oxidase (BOD) were used as anodic and cathodic catalysts, respectively. Both of these model electroactive enzymes are used throughout EBFC and biosensor research and have been thoroughly characterized.[47, 77, 182, 281] Gold/MWCNT fiber paddle electrodes were fabricated *via* the electrospinning of polyacrylonitrile (PAN) fibers containing gold salt followed by reduction and deposition of AuNPs and subsequent coating with MWCNTs.[191] Graphene-coated SWCNT gels were formed by mixing suspensions of individually dispersed SWCNTS and slowly decreasing water content until percolation occurred, forming a network of interconnected SWCNTs that was then coated with a continuous graphene layer through the cyclization and reduction of glucose.[238, 280] These two systems were characterized in terms of anodic and cathodic electrochemistry as well as EBFC performance. We also determined how material

morphology and surface properties impacted performance of each electrode. The objectives of this study were to provide an in-depth, side-by-side comparison of two materials with varying surface curvature, SSA and pore size to aid in the efficient design of future EBFC and biosensor systems.

3.2 Materials and Methods

3.2.1 Materials

Ultrapure milliQ grade water (resistivity of 18.2 MΩ·cm) was used for all experiments. Sodium phosphate buffer (0.1 M, pH 7.0) was prepared from phosphate salts and used for the preparation of enzyme solutions and testing of electrodes. GOX Type VII from *Aspergillus niger* (100-250 units mg^{-1}) was purchased from Sigma-Aldrich. BOD from *Myrothecium sp.* (2.7 U mg^{-1}) was purchased from Amano Enzyme Inc. MWCNTs with average diameter of 11.5 nm and average length of 30 μm were purchased from Cheap Tubes, Inc. CoMoCAT SWCNTs (batch CG 200) with average diameter of 1 nm and average length of 1 μm were purchased from Southwest Nanotechnologies Inc. All chemicals were of analytical grade and used as received.

3.2.2 Electrode fabrication

We prepared gold/MWCNT fiber paddle electrodes[191] and graphene-coated SWCNT gel electrodes[238, 240, 280] as previously described. To obviate the need for surfactant, we performed the electrophoretic deposition of MWCNTs used in the fabrication of gold/MWCNT fiber paddle electrodes with 0.02 mg mL^{-1} MWCNTs in 33% ethanol.[191] For testing, we formed graphene-coated SWCNT gel electrodes in 2 mm thick rectangular molds and cut ≈0.5 cm^2 sections.

To form enzyme-modified anodes and cathodes, we incubated individual electrodes in 1 mg mL^{-1} enzyme solution (GOX or BOD in 0.1 M sodium phosphate buffer (pH 7.0)) for 4 h at 4

°C to allow enzyme attachment *via* physical adsorption. Using a bench-top vacuum pump, we applied a weak pulsed vacuum for several minutes prior to incubation of graphene-coated SWCNT gels to enhance enzyme internalization. Then, we briefly washed each electrode to remove loosely bound enzyme prior to individual electrochemical examination or EBFC testing.

3.2.3 Material microstructural characterization

SSA of graphene-coated SWCNT gels was measured through nitrogen adsorption and desorption at 77 K using a Gemini VII 2390 surface area analyzer (Micromeritics) using the Brunauer, Emmett and Teller (BET) theory.[236] Pore volume and pore size distribution were calculated from the measured desorption isotherms using the density functional theory (DFT) calculation scheme.[237] Scanning electron microscope (SEM) images were taken using a FEI/Aspex Explorer and FEI Quanta 600 scanning electron microscope for the gold/MWCNT fiber paddle and graphene-coated SWCNT gel, respectively. Transmission electron microscope (TEM) images were collected using a FEI Titan 83 TEM.

3.2.4 Electrode characterization

Total GOX loadings were determined using a standard bicinchoninic acid (BCA) assay kit (ThermoFisher Scienctific). GOX-modified electrodes were incubated at room temperature with shaking at 100 rpm in 1 wt% sodium dodecylbenzenesulfonate (NaDDBS) for 4 h and supernatant tested for protein concentration. All electrochemical measurements were performed using a conventional three-electrode electrochemical cell utilizing a KCl saturated Ag/AgCl electrode and a 0.5 mm diameter platinum wire electrode as reference and counter electrodes, respectively. Gold/MWCNT fiber paddle electrochemically active surface area was measured through the electrochemical oxidation/reduction of ferrocenecarboxylic (FeCOOH) acid at the electrode surface *via* cyclic voltammetry (CV).[279] EBFC performance characteristics were

evaluated in 200 mL of air-saturated 0.1 M sodium phosphate buffer (pH 7.0) containing 0.1 M glucose under stirring and using a Fluke 287 True RMS multimeter with an IET Labs RS-200 resistance decade box to manually vary circuit resistance.

3.3 Results and Discussion

3.3.1 Material characterization

The performance characteristics of enzyme-nanomaterial conjugates greatly depend on the surface properties of the nanomaterial.[89, 91] Enzyme loading and substrate accessibility are a function of available surface area and porosity while specific enzyme activity and stability depend on enzyme conformation at the nanomaterial surface, which can be impacted by support surface curvature, enzyme orientation and binding affinity.[192, 228] All of these interactions coupled with the electron transfer characteristics of the system are the target design parameters of enzyme-based bioelectronics. Many studies have shown the impact of material characteristics on enzyme biochemical activity and stability, but the effect of these material properties on enzyme electrochemical activity has not been adequately described.[2, 89, 91] Toward this goal we fabricated two differing electrode systems based on commonly used classes of nanomaterials to determine their capabilities as electroactive enzyme supports and to compare their varying performance characteristics as a function of material properties. The chosen electrode materials were gold/MWCNT fiber paddles and graphene-coated SWCNT gels, which possessed extremely different surface curvature, pore sizes and SSA. The surface curvature of materials such as carbon nanotubes and electrospun fibers are determined by diameter, with larger diameter materials possessing a lower degree of curvature.[89-91]

We found both electrode materials consisted of interconnected, porous networks of individual polymer fibers or SWCNTs (**Figure 3.1**). SEM images of gold/MWCNT fiber paddles

showed ≈1 µm diameter PAN fibers coated with 0.5 – 0.7 µm AuNPs and with 11.5 nm diameter MWCNTs (**Figure 3.1A-C**). Pore sizes between adjacent fibers were on the order of several micrometers, which allowed unhindered access to both substrate and adsorbing enzyme.[245] Imaging of graphene-coated SWCNT gels revealed a percolating network of 1 nm diameter SWCNTs (**Figure 3.1D**) coated with multiple layers of graphene (**Figure 3.1E**). This structure was consistent with previous reports of similar materials.[238, 280]

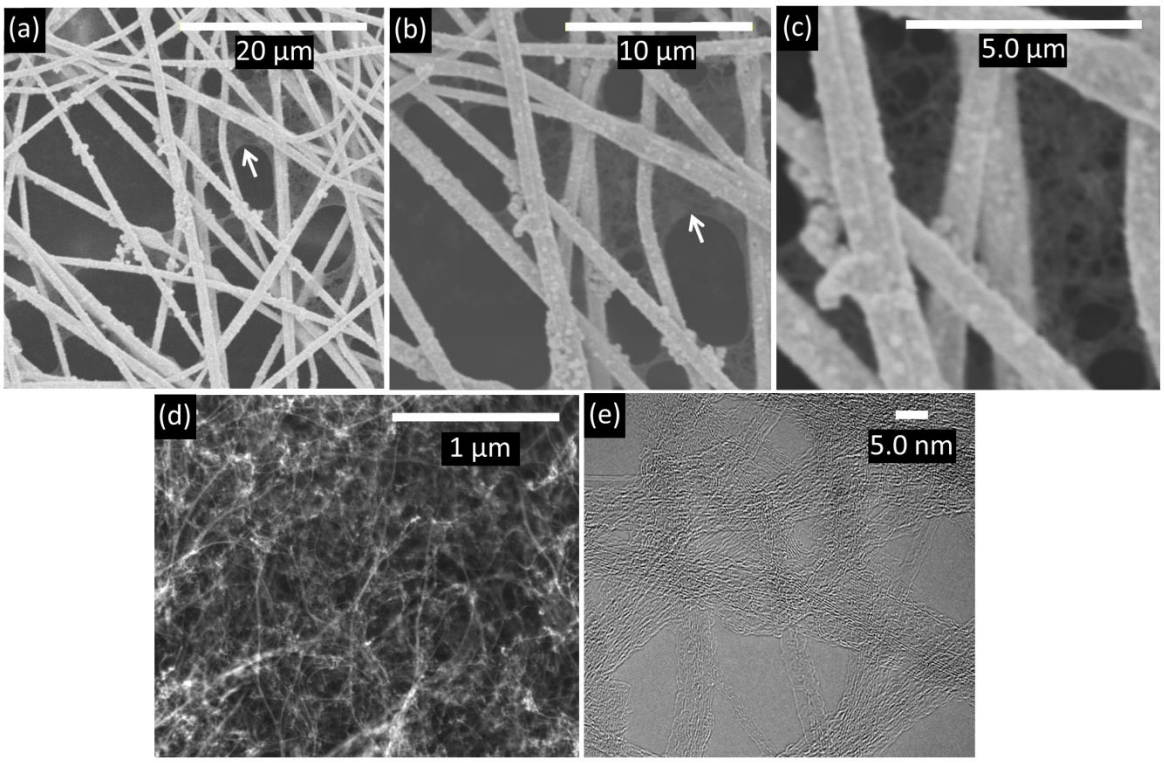

Figure 3.1 Morphological examination of electrode materials. A-C) SEM images of gold/MWCNT fiber electrode at varying magnifications. White arrows indicate formation of MWCNT-interconnection between neighboring fibers. D) SEM image of graphene-coated SWCNT gel. E) TEM image of graphene-coated SWCNT gel.

The SSA of the gold/MWCNT fiber paddles was too low to be reliably measured by a BET system. Hence, we probed the electrochemically active surface area (ECSA) of the

gold/MWCNT fiber paddles through the oxidation and reduction of the small redox molecule FeCOOH *via* CV (**Figure 3.2A,B**).[279] At high scan rates, the anodic and cathodic peak currents increased linearly with scan rate, which indicated a surface-limited system.[32] The slopes of these curves were used to calculate the FeCOOH loading at the electrode surface, which yielded a calculated ECSA of 3.6 m^2 g^{-1} that qualitatively reflected the SSA of the paddles.[32] The ECSA of a material depends on the conducting nature of the electrode being studied and is thus a measure of surface area available for interaction with redox molecules.[282] In this study, the ECSA is comparable to the SSA of the material as only the surface area capable of electron transfer with redox molecules would yield electrochemically active immobilized enzyme or substrate reduction/oxidation. For simplicity and comparison with graphene-coated SWCNT gels, we refer to the ECSA of the gold/MWCNT fiber paddles as SSA. We examined the SSA of the graphene-coated SWCNT gels using BET analysis of nitrogen adsorption and desorption and modeled pore distribution using the DFT calculation scheme (**Figure 3.2C,D**).[236, 237] These gels possessed a SSA of 686 m^2 g^{-1} with the majority of the total pore volume made up of pores less than 15 nm in radius. Some of the pores were too small to allow unhindered internalization of enzymes such as GOX (8 x 7 x 8 nm) throughout the gel structure.[245] Both materials were further modified *via* physical adsorption of GOX and BOD and electrochemically characterized.

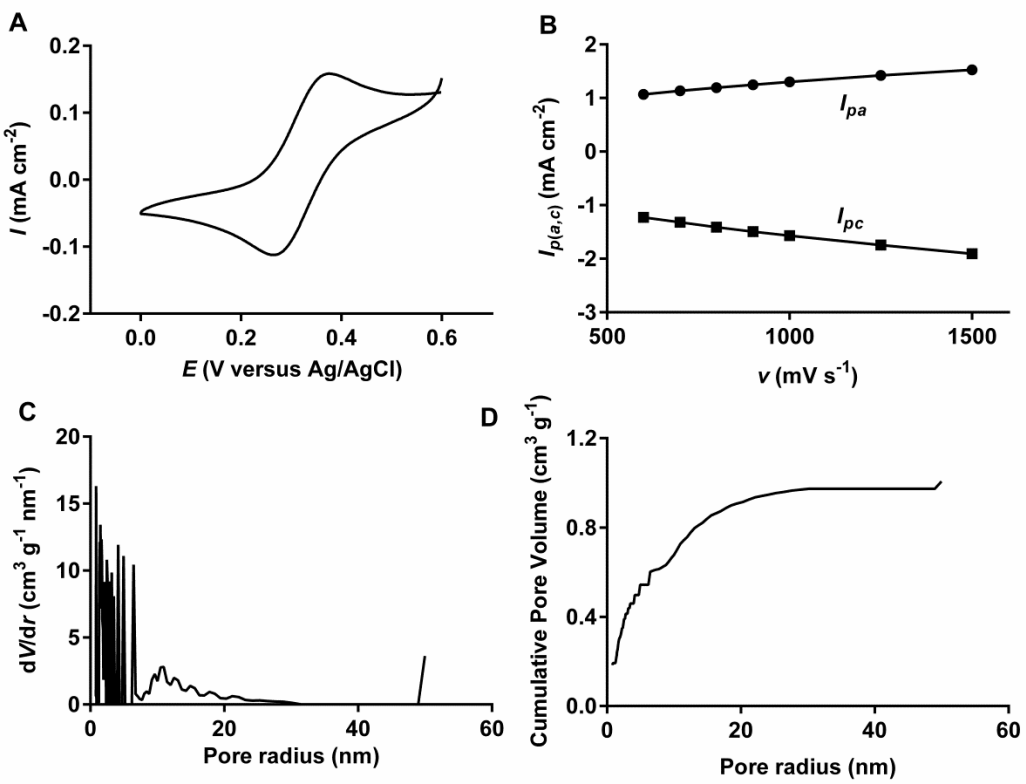

Figure 3.2 Specific surface area analysis of electrode materials. A) Representative CV trace of FeCOOH at gold/MWCNT fiber paddle electrode at a scan rate of 5 mV s^{-1}. B) Dependence of anodic (filled circle) and cathodic (filled square) peak current densities on scan rate at high scan rates of FeCOOH at gold/MWCNT fiber paddle electrodes. CV experiments performed in argon saturated 0.1 M sodium phosphate buffer (pH 7.0). C) Pore-size distribution of graphene-coated SWCNT gels. D) Cumulative pore volume with increasing pore size of graphene-coated SWCNT gels. Pore-size information from DFT calculation scheme of BET surface area analysis.

3.3.2 Anodic system comparison

The anodic enzyme GOX catalyzes the two-electron oxidation of glucose to gluconolactone and the subsequent reduction of molecular oxygen to hydrogen peroxide. EBFC anodes utilize the oxidation half of this reaction to generate electrical current through the transfer of electrons to an electrode surface by DET or MET instead of to oxygen. Alternatively,

oxidation of generated hydrogen peroxide can occur at the electrode surface effectively using molecular oxygen as a natural electron mediator.[145, 188]

We electrochemically characterized GOX-modified anodes formed from each of the two electrode materials. CV traces of GOX-modified anodes of both materials showed obvious oxidation and reduction peaks with formal potentials of -0.43 V versus Ag/AgCl (**Figure 3.3**). This formal potential was indicative of quasi-reversible oxidation/reduction of the flavin adenine dinucleotide cofactor (FAD)-based active site of GOX. The identical formal potential of the two systems suggested a similar conformation of electrochemically active GOX at the enzyme-nanomaterial interface in both systems. Graphene-coated SWCNT gel anodes exhibited a significantly higher capacitive current response than our gold/MWCNT fiber paddle anodes. We believe this property reflected the larger SSA of the graphene-coated SWCNT gel as opposed to our gold/MWCNT fiber paddles (**Figure 3.3**).[283]

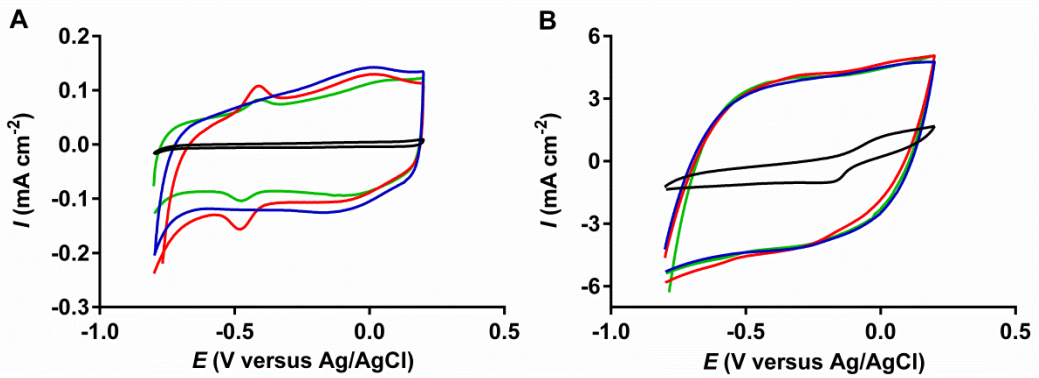

Figure 3.3 Electrochemical performance of anodic systems. A) Characteristic CV traces of bare gold wire (black), gold/MWCNT fiber paddle anode without GOX-modification (blue), GOX-modified gold/MWCNT fiber paddle anode (red) and GOX-modified gold/MWCNT fiber paddle anode with 0.1 M glucose (green). B) Characteristic CV traces of bare copper clip (black), graphene-coated SWCNT gel anode without GOX-modification (blue), GOX-modified graphene-coated SWCNT gel anode (red) and GOX-modified graphene-coated SWCNT gel anode with 0.1 M glucose (green). Experiments performed in argon-saturated 0.1 M sodium phosphate buffer (pH 7.0) at a scan rate of 50 mV s^{-1}.

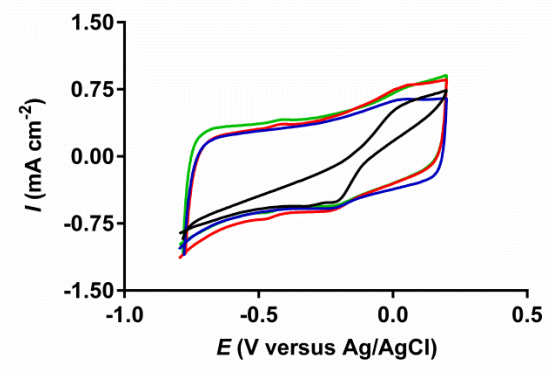

Figure 3.4 Electrochemical performance of graphene-coated SWCNT gel anode at low scan rate. Characteristic CV traces of bare copper clip (black), graphene-coated SWCNT gel anode without GOX-modification (blue), GOX-modified graphene-coated SWCNT gel anode (red) and GOX-modified graphene-coated SWCNT gel anode with 0.1 M glucose (green). Experiments performed in argon-saturated 0.1 M sodium phosphate buffer (pH 7.0) at a scan rate of 5 mV s^{-1}.

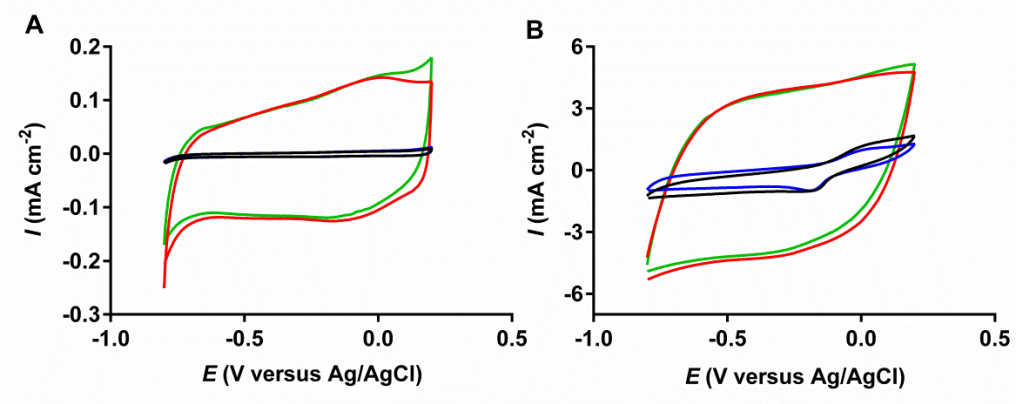

Figure 3.5 Electrochemical performance of anodic control materials. A) Characteristic CV traces of bare gold wire (black), bare gold with 0.1 M glucose (blue), gold/MWCNT fiber paddle anode without GOX-modification (red) and gold/MWCNT fiber paddle anode without GOX-modification with 0.1 M glucose (green). B) Characteristic CV traces of bare copper clip (black), bare copper clip with 0.1 M glucose (blue), graphene-coated SWCNT gel anode without GOX-modification (red) and graphene-coated SWCNT gel anode without GOX-modification with 0.1 M glucose (green). Experiments performed in argon-saturated 0.1 M sodium phosphate buffer (pH 7.0) at a scan rate of 50 mV s^{-1}.

To better exhibit the faradaic peaks of GOX at graphene-coated SWCNT gels, we additionally performed the CV analysis at a lower scan rate of 5 mV s^{-1}, which yielded identical results (**Figure 3.4**). Upon the addition of glucose to either GOX-modified anode, we observed no appreciable shift in current response. This result demonstrated that no current generation was being driven by DET and suggested that current was produced *via* hydrogen peroxide oxidation using oxygen as a natural electron mediator (**Figure 3.3**). No faradaic peaks or shifts in current were observed in trials with materials lacking GOX modification (**Figure 3.5**).

By performing CV scans at varying scan rates, we were able to determine the loading of FAD at the anodic material surface and the heterogeneous electron transfer rate constant (k_s)(**Figure 3.6**). We calculated the loadings of FAD using the dependence of anodic and cathodic peak currents with increasing scan rate (**Figure 3.6A,C**). The linearity of this plot indicated that the efficacies of both systems were limited by the rate of electron transfer to the electrode surface rather than diffusion.[32] Gold/MWCNT fiber paddle anodes had an electrochemical loading of 3.92 x 10^{-10} mol FAD cm^{-2} whereas graphene-coated SWCNT gel anodes had an electrochemical loading of 1.99 x 10^{-11} mol FAD cm^{-2} (where the area was the cross-sectional area of the electrode). We examined the accuracy of these values in representing the total GOX loading by removing adsorbed enzymes from GOX-modified electrodes using the surfactant NaDDBS and testing the resulting supernatants *via* standard BCA assay. The resulting total GOX loadings were 2.60 x 10^{-10} mol GOX cm^{-2} and 1.57 x 10^{-11} mol GOX cm^{-2} for gold/MWCNT fiber paddle anodes and graphene-coated SWCNT gel anodes, respectively. These values were slightly higher than the apparent loadings determined electrochemically assuming two FAD molecules corresponded to each GOX molecule. The increased total loading compared to the electrochemically determined loading is likely due to one or both FAD sites in some

adsorbed GOX molecules not being electrochemically connected to the electrode surface, which is consistent with similar materials.[146] These loading results suggested extensive GOX coverage throughout the gold/MWCNT fiber paddles, but limited internalization into the graphene-coated SWCNT gels, meaning that GOX was likely only adsorbed at the outer gel surface.

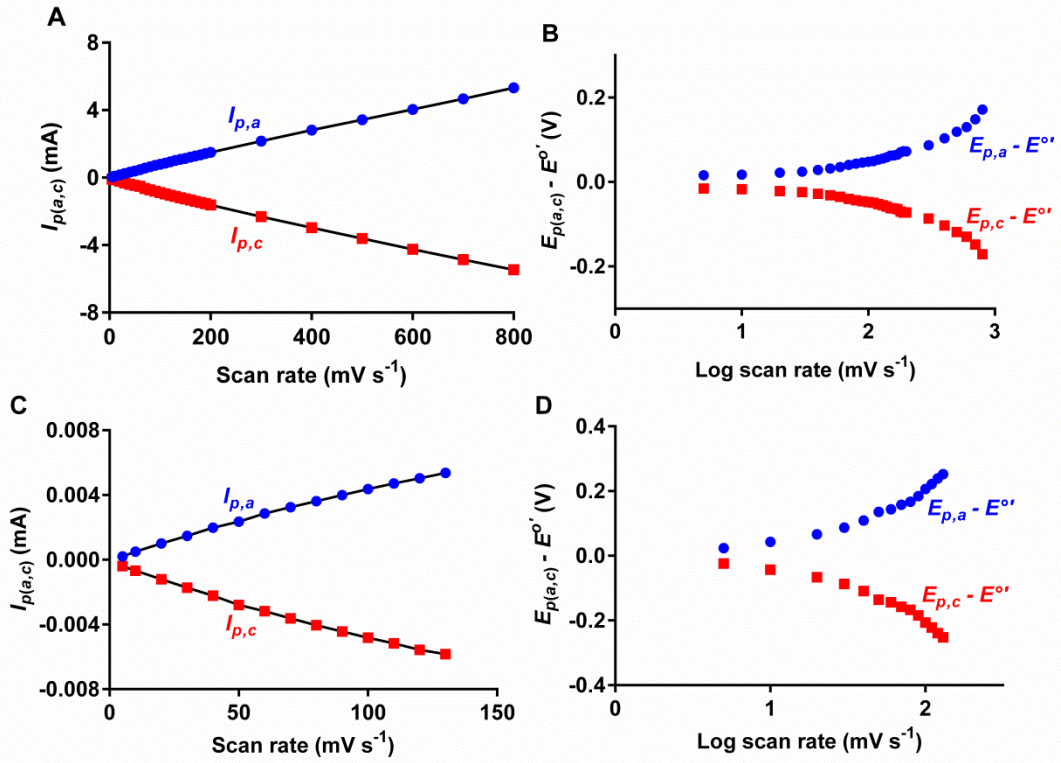

Figure 3.6 Loading and electron transfer rate analysis of anodic systems. A) Dependence of anodic (blue circle) and cathodic (red square) peak current densities on scan rate for GOX-modified gold/MWCNT fiber paddle anodes at varying scan rates. B) Dependence of anodic (blue circle) and cathodic (red square) peak potentials on the logarithm of scan rate for GOX-modified gold/MWCNT fiber paddle anodes at varying scan rates. C) Dependence of anodic (blue circle) and cathodic (red square) peak current densities on scan rate for GOX-modified graphene-coated SWCNT gel anodes varying scan rates. B) Dependence of anodic (blue circle) and cathodic (red square) peak potentials on the logarithm of scan rate for GOX-modified graphene-coated SWCNT gel anodes at varying scan rates. Experiments performed in argon-saturated 0.1 M sodium phosphate buffer (pH 7.0).

We further calculated the k_s for each system using the dependence of anodic and cathodic peak potentials on the logarithm of scan rate (**Figure 3.6B,D**).[248, 284] We found the k_s values to be 0.95 ± 0.01 s^{-1} and 0.98 ± 0.07 s^{-1} for gold/MWCNT fiber paddle anodes and graphene-coated SWCNT gel anodes, respectively. Electron transfer resistances between adsorbed FAD and the electrode surface were clearly similar in both systems, which further suggested similar conformations of electrochemically active GOX at the electrode surfaces.

The appearance of faradaic peaks in CV traces of GOX-modified materials confirmed the presence of electrochemically active FAD at the electrode surface, but these data alone did not definitively prove that GOX was biochemically active (**Figure 3.3**).[145] To examine if biochemically active GOX was successfully adsorbed onto the electrode materials, we monitored the current output of each GOX-modified anode upon the successive addition of glucose (**Figure 3.7**). When the potential of the each anode was held at 0.8 V versus Ag/AgCl in an oxygen saturated solution, an obvious increase in anodic current was observed (**Figure 3.7A,C**). This response corresponded to the electrochemical oxidation of hydrogen peroxide produced by GOX, which confirmed the presence of biochemically active GOX turning over glucose in both systems under study.[1, 191]

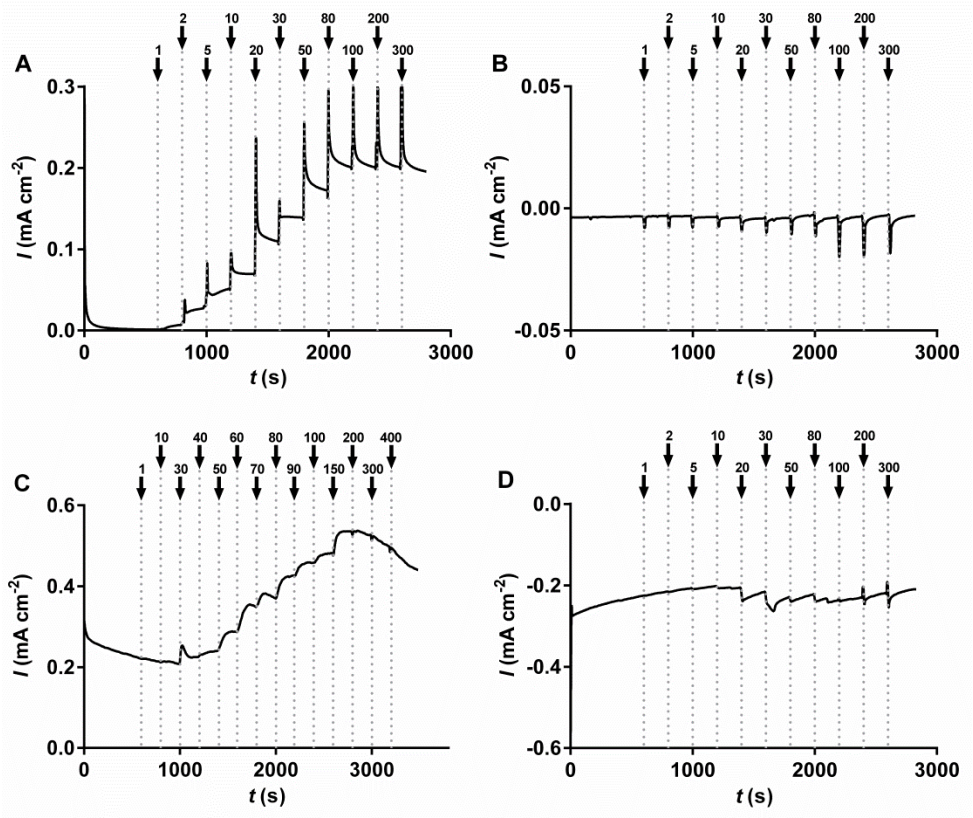

Figure 3.7 Amperometric performance of anodic systems. A) Typical amperometric profile of GOX-modified gold/MWCNT fiber paddle anode in O_2-saturated solution with potential held at 0.8 V versus Ag/AgCl. B) Typical amperometric profile of GOX-modified gold/MWCNT fiber paddle anode in argon-saturated solution with potential held at -0.43 V versus Ag/AgCl. C) Typical amperometric profile of GOX-modified graphene-coated SWCNT gel anode in O_2-saturated solution with potential held at 0.8 V versus Ag/AgCl. D) Typical amperometric profile of GOX-modified graphene-coated SWCNT gel anode in argon-saturated solution with potential held at -0.43 V versus Ag/AgCl. Glucose injections indicated by arrows with resulting glucose concentration given in mM. Experiments performed in 0.1 M sodium phosphate buffer (pH 7.0).

Examination of the increasing current density upon glucose addition allowed the calculation of maximum current density (J_{max}) and apparent Michaelis-Menten constant (K_M^{app}) for both systems (**Figure 3.7**). The GOX-modified gold/MWCNT fiber paddle anodes yielded a J_{max} of 0.23 ± 0.01 mA cm^{-2} and an apparent K_M^{app} of 18.8 ± 2.6 mM glucose, whereas the GOX-

modified graphene-coated SWCNT gel anodes achieved a J_{max} of 0.57 ± 0.03 mA cm^{-2} with an apparent K_M^{app} of 33.8 ± 4.8 mM glucose. Coupled with the calculated total GOX loadings, these J_{max} values become 8.85 x 10^8 mA mol^{-1} of GOX and 3.63 x 10^{10} mA mol^{-1} of GOX for the gold/MWCNT fiber paddle anodes and the graphene-coated SWCNT gel anodes, respectively. The higher current generation rate per mol of GOX immobilized onto the graphene-coated SWCNT gel electrodes suggested much greater biochemical activity at the electrode surface. This finding was consistent with reports stating that enzymes adsorbed onto curved nanomaterials retain more activity on supports with smaller diameters.[89, 90] Interestingly, GOX adsorbed onto the graphene-coated SWCNT gel electrode also exhibited an increased K_M^{app}, which was indicative of interference with substrate binding by the smaller diameter SWCNTs. The detection of hydrogen peroxide oxidation showed the capability of both material systems to perform as functioning enzyme-based electrodes. However, when the working electrode potential was held at the observed FAD formal potential (-0.43 V versus Ag/AgCl) in argon-saturated solution, no sustained current response was observed for either anode material (**Figure 3.7C,D**) (small peaks observed resulted from mixing effects). The absence of a current response upon glucose injection under these conditions confirmed the inability of either electrode material to collect electrons from the GOX active site *via* DET. In contrast, in a previous study, we showed the capability of a similar anodic material made up of a graphene/SWCNT cogel to achieve DET with GOX.[278] The larger pore sizes of the cogel material aided in greater GOX internalization compared to the graphene-coated SWCNT gels, suggesting that GOX must be entirely surrounded by a nanoscale conducting material, such as SWCNTs, in order to exhibit DET, which was consistent with previous reports.[96, 123, 285]

We further characterized the GOX-modified anodes in terms of open circuit voltage (OCV) to analyze the extent of overpotentials that limited the rate of electron transfer between GOX and each electrode material (**Figure 3.8**). Analysis of the GOX-modified gold/MWCNT fiber paddle anodes in an argon-saturated solution with 0.1 M glucose resulted in an OCV of 0.18 V versus Ag/AgCl, which was significantly higher than the thermodynamically determined value of -0.36 V versus Ag/AgCl.[11]

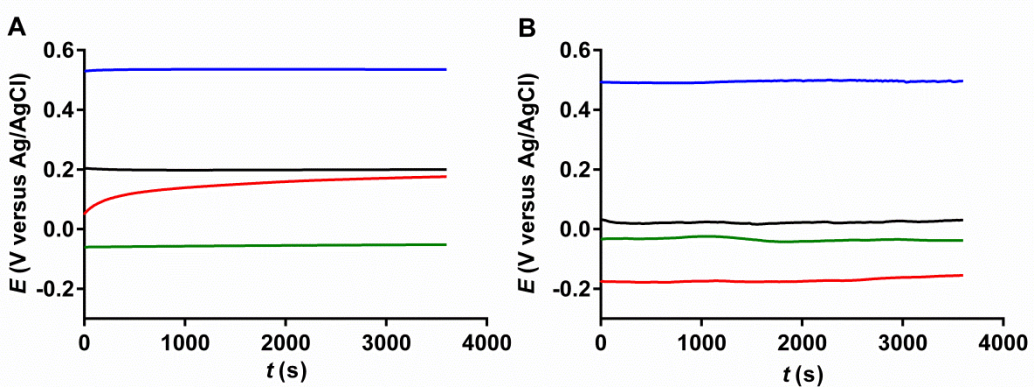

Figure 3.8 Open-circuit voltage analysis of electrode materials. A) OCV measurements of gold/MWCNT fiber paddle anode without GOX-modification (green), GOX-modified gold/MWCNT fiber paddle anode (red), gold/MWCNT fiber paddle cathode without BOD-modification (black) and BOD-modified gold/MWCNT fiber paddle cathode (blue). B) OCV measurements of graphene-coated SWCNT gel anode without GOX-modification (green), GOX-modified graphene-coated SWCNT gel anode (red), graphene-coated SWCNT gel cathode without BOD-modification (black) and BOD-modified graphene-coated SWCNT gel cathode (blue). Experiments performed in 0.1 M sodium phosphate buffer (pH 7.0) containing substrate: anodic in argon saturated solution with 0.1 M glucose; Cathodic in O_2-saturated solution.

We hypothesize that at least some of this effect was caused by oxygen reduction at the gold/MWCNT fiber paddle anode surface at voltages of ~0 V versus Ag/AgCl and lower (**Figure 3.9A**). Since OCV is a measure of the voltage at which no current is observed, at voltages below this threshold, oxygen that remained or diffused into the argon-saturated solution was likely

reduced to water and generated cathodic current. GOX-modified gold/MWCNT fiber paddle anodes yielded decreased cathodic current due to the local depletion of oxygen and production of hydrogen peroxide *via* GOX reaction. However, reduction of remaining oxygen or produced hydrogen peroxide still occurred (**Figure 3.9B**). Examination of the GOX-modified graphene-coated SWCNT gel anodes under the same conditions resulted in an OCV of -0.15 V versus Ag/AgCl (**Figure 3.8B**). The observed overpotentials could also have been caused by partial GOX denaturation or steric hindrance of its active site upon immobilization yielding reduced activity and electron transfer resistances between the buried FAD-based active site of GOX and the electrode surface, which contributed to the deterrence of electron transfer.[47] Larger overpotentials at the gold/MWCNT fiber paddle electrode were consistent with increased GOX deformation and hence lower biochemical activity at the larger diameter gold/MWCNT fibers.

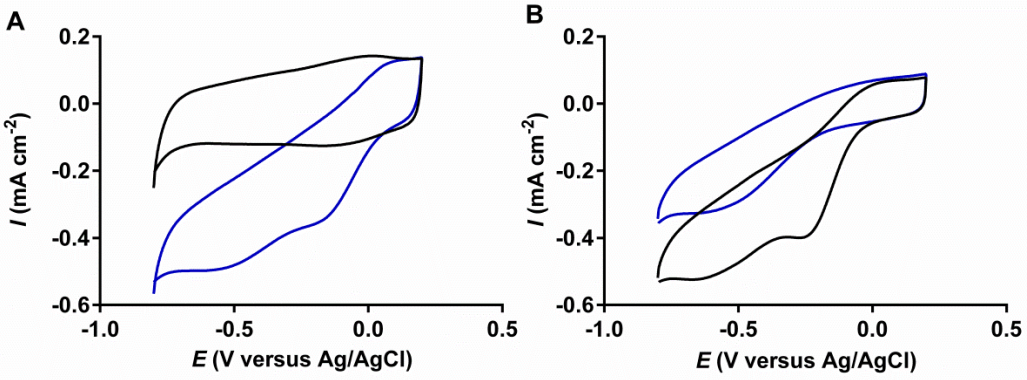

Figure 3.9 Analysis of oxygen/hydrogen peroxide reduction at gold/MWCNT fiber paddle anodes. A) Characteristic CV traces of gold/MWCNT fiber paddle anodes without GOX-modification in argon-saturated (black) and in O_2-saturated solution (blue). B) Characteristic CV traces of GOX-modified gold/MWCNT fiber paddle anodes in O_2-saturated solution (black) and GOX-modified gold/MWCNT fiber paddle anodes in O_2-saturated solution with 0.1 M glucose (blue). Experiments performed in 0.1 M sodium phosphate buffer (pH 7.0) at a scan rate of 50 mV s^{-1}.

3.3.3 Cathodic system comparison

The cathodic multicopper oxidase BOD catalyzes the 4-electron reduction of oxygen to water at its T2/T3 copper-containing active site upon accepting electrons at its T1 copper-containing active site.[182] To determine the presence of overpotentials in the cathodic systems, we analyzed BOD-modified gold/MWCNT fiber paddle cathodes and BOD-modified graphene-coated SWCNT gel cathodes according to OCV (**Figure 3.8**). The enzyme-modified cathodes yielded OCVs of 0.53 V versus Ag/AgCl and 0.50 V versus Ag/AgCl for gold/MWCNT fiber paddle cathodes and graphene-coated SWCNT gel cathodes, respectively (**Figure 3.8**). These values were consistent with the thermodynamically determined value of the T1 copper site of BOD.[87] The increase in OCV compared to non-modified control showed the presence of successfully adsorbed BOD with no appreciable overpotentials. To further examine cathodic characteristics, we performed CV scans of each cathode material before and after BOD modification (**Figure 3.10**). No faradaic peaks were observed for either material system, which is consistent with previous studies.[254, 278]

BOD-modified gold/MWCNT fiber paddle cathodes showed obvious oxygen reduction at onset potentials of 0.45 V versus Ag/AgCl and 0 V versus Ag/AgCl (**Figure 3.10A**). Non-modified gold/MWCNT fiber paddle cathodes only exhibited oxygen reduction beginning at 0 V versus Ag/AgCl consistent with anodic measurements, which confirmed BOD adsorption and DET (**Figure 3.11A**). Similarly, BOD-modified graphene-coated SWCNT gel cathodes exhibited oxygen reduction at an onset potential of 0.4 V versus Ag/AgCl whereas no oxygen reduction was observed in non-modified trials, which confirmed DET with physically adsorbed BOD (**Figure 3.10B and Figure 3.11B**).

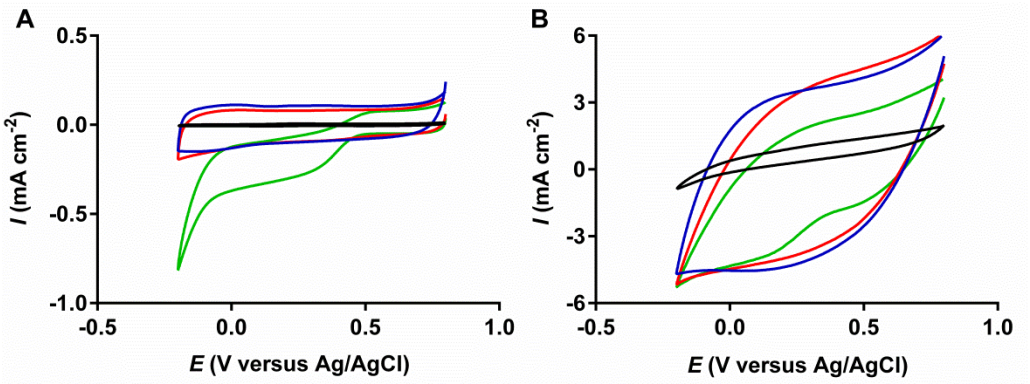

Figure 3.10 Electrochemical performance of cathodic systems. A) Characteristic CV traces of bare gold wire (black), gold/MWCNT fiber paddle cathode without BOD-modification (blue) and BOD-modified gold/MWCNT fiber paddle cathode (red) in argon-saturated solution and BOD-modified gold/MWCNT fiber paddle cathode in O_2-saturated solution (green). B) Characteristic CV traces of bare copper clip (black), graphene-coated SWCNT gel cathode without BOD-modification (blue) and BOD-modified graphene-coated SWCNT gel cathode (red) in argon-saturated solution and BOD-modified graphene-coated SWCNT gel cathode in O_2-saturated solution (green). Experiments performed in 0.1 M sodium phosphate buffer (pH 7.0) at a scan rate of 50 mV s^{-1}.

The capability of both cathodic materials to achieve DET with adsorbed BOD was additionally confirmed *via* amperometry (**Figure 3.12**). We observed a rapid increase in cathodic current upon oxygen bubbling into argon-saturated solution for both gold/MWCNT fiber paddle cathodes and graphene-coated SWCNT gel cathodes. Larger current density at the graphene-coated SWCNT gel electrode suggested increased loading and/or biochemical activity of BOD. Combined, these results highlighted the capability of BOD to achieve efficient DET with AuNP- and carbon nanotube-based materials whereas this functionality was not observed for surface adsorbed GOX. Efficient electron transfer from the BOD active site to electrodes with these types of materials was consistent with previous findings.[97, 148, 256, 278]

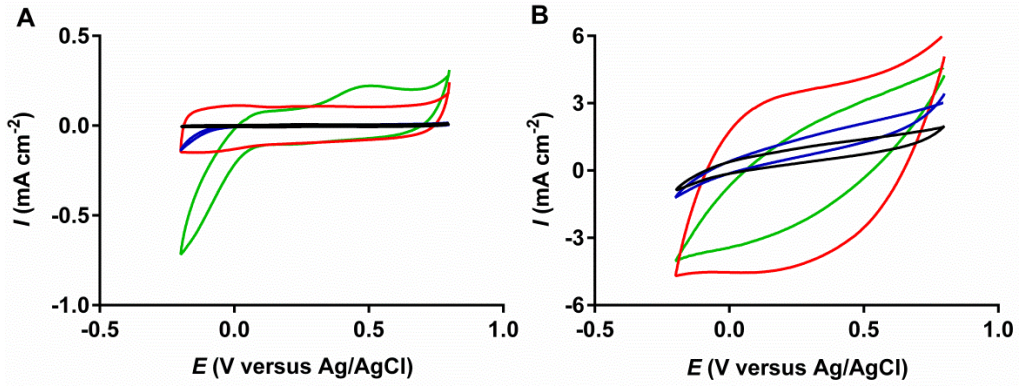

Figure 3.11 Electrochemical performance of cathodic control materials. A) Characteristic CV traces of bare gold wire in argon-saturated solution (black), bare gold with in O_2-saturated (blue), gold/MWCNT fiber paddle cathode without BOD-modification in argon-saturated solution (red) and gold/MWCNT fiber paddle cathode without BOD-modification in O_2-saturated solution (green). B) Characteristic CV traces of bare copper clip in argon-saturated solution (black), bare copper clip in O_2-saturated solution (blue), graphene-coated SWCNT gel cathode without BOD-modification in argon-saturated solution (red) and graphene-coated SWCNT gel cathode without BOD-modification in O_2-saturated solution (green). Experiments performed in 0.1 M sodium phosphate buffer (pH 7.0) at a scan rate of 50 mV s^{-1}.

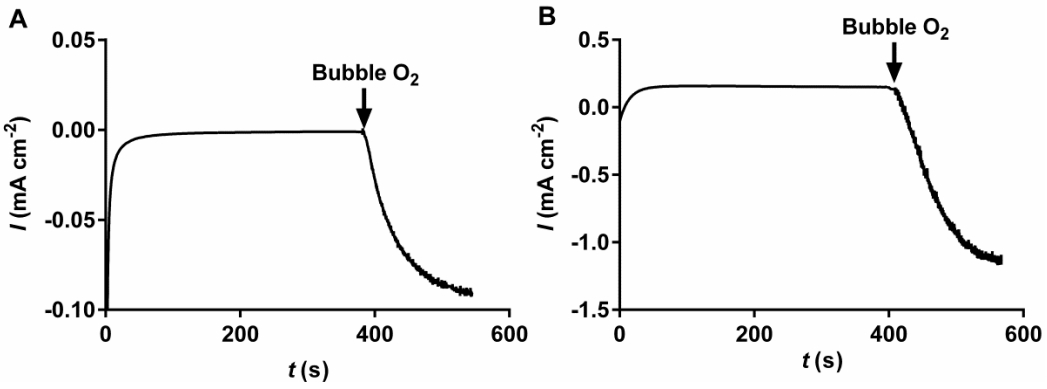

Figure 3.12 Amperometric performance of cathodic systems. A) Typical amperometric profile of BOD-modified gold/MWCNT finer paddle cathode in argon-saturated solution with potential held at 0.2 V versus Ag/AgCl. B) Typical amperometric profile of BOD-modified graphene-coated SWCNT gel cathode in argon-saturated solution with potential held at 0.2 V versus Ag/AgCl. Beginning of O_2 bubbling indicated by arrows. Experiments performed in 0.1 M sodium phosphate buffer (pH 7.0).

3.3.4 EBFC comparison

We separately examined symmetric EBFCs consisting of a single GOX-modified anode and a single BOD-modified cathode using either gold/MWCNT fiber paddle electrodes or graphene-coated SWCNT electrodes. All trials consisted of the manual variation of circuit resistance and the monitoring of resulting cell voltages in air-saturated 0.1 M sodium phosphate buffer (pH 7.0) containing glucose (0.1 M). Gold/MWCNT fiber paddle electrode-based systems yielded a maximum power density of 0.42 ± 0.06 μW cm^{-2} and full-cell OCV of 0.22 ± 0.02 V (**Figure 3.13A**). Graphene-coated SWCNT gel-based systems generated ~10 times larger maximum power density of 3.56 ± 1.09 μW cm^{-2} but identical full-cell OCV of 0.22 ± 0.03 V (**Figure 3.13B**). Recall that the graphene-coated SWCNT gel electrodes had ~10 times lower GOX loading. The identical OCV values confirmed similar electron transfer limitations in both systems where the increased power density of the graphene-coated SWCNT gel-based system was consistent with a higher degree of GOX biochemical activity at the anode. Further, when the EBFC systems were examined without enzyme-modification, we observed negligible power density, which confirmed GOX and BOD were solely responsible for power generation (**Figure 3.14**). Individual characterization of the anodic and cathodic components of each system showed EBFCs made up of either material to be limited at the anode as electron transfer was not hindered by cathodic overpotentials and efficient DET with BOD was observed.

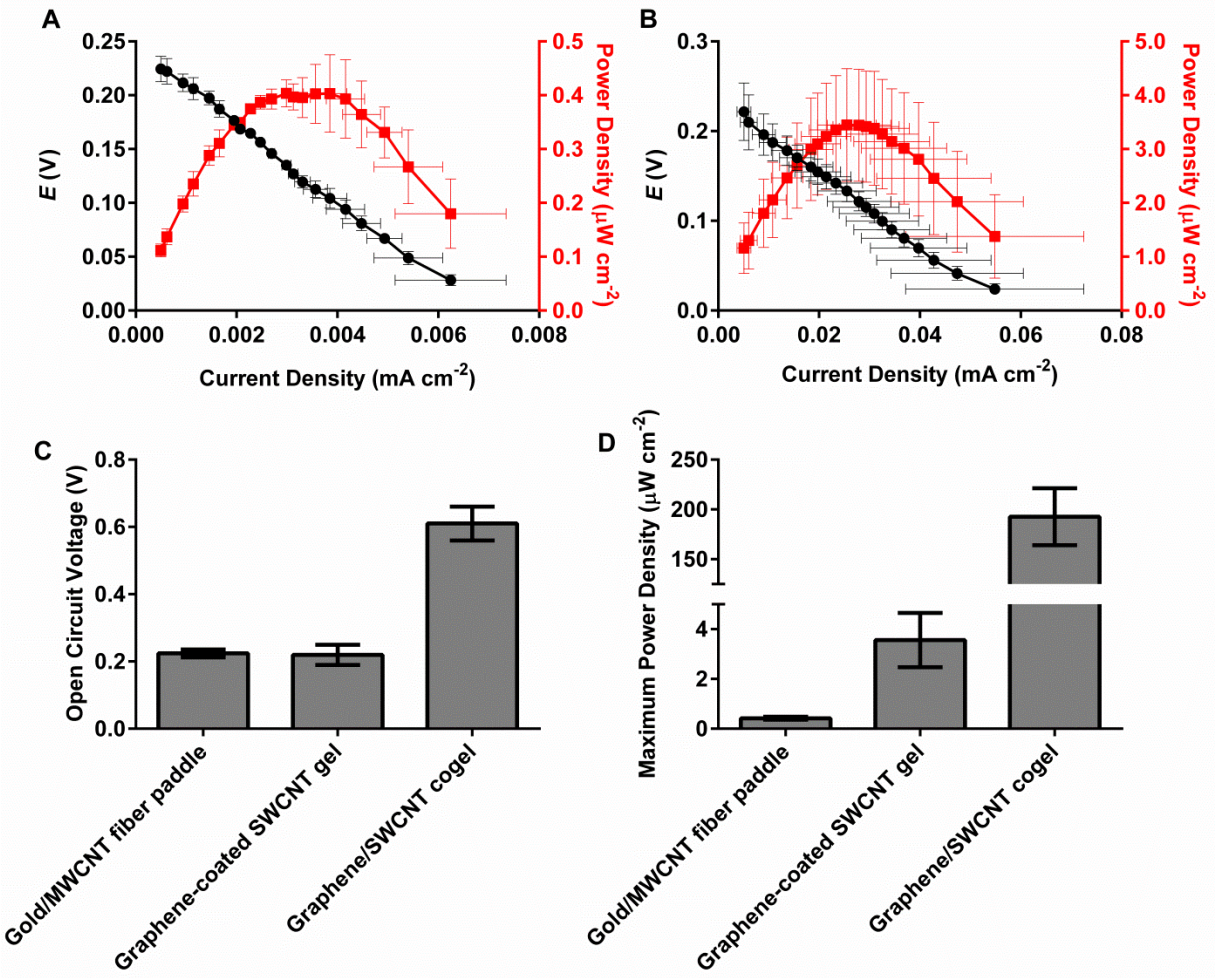

Figure 3.13 EBFC performance comparison of electrode materials. A) Gold/MWCNT fiber paddle-based EBFC performance and cell-polarization curves. B) Graphene-coated SWCNT gel-based EBFC performance and cell-polarization curves. Experiments performed in air-saturated 0.1 M sodium phosphate buffer (pH 7.0) with 0.1 M glucose. C) OCV comparison of gold/MWCNT fiber paddle-, graphene-coated SWCNT gel- and graphene/SWCNT cogel-based EBFCs. D) Maximum power density comparison of gold/MWCNT fiber paddle-, graphene-coated SWCNT gel- and graphene/SWCNT cogel-based EBFCs. Error bars represent 1 standard deviation of 3 trials.[278]

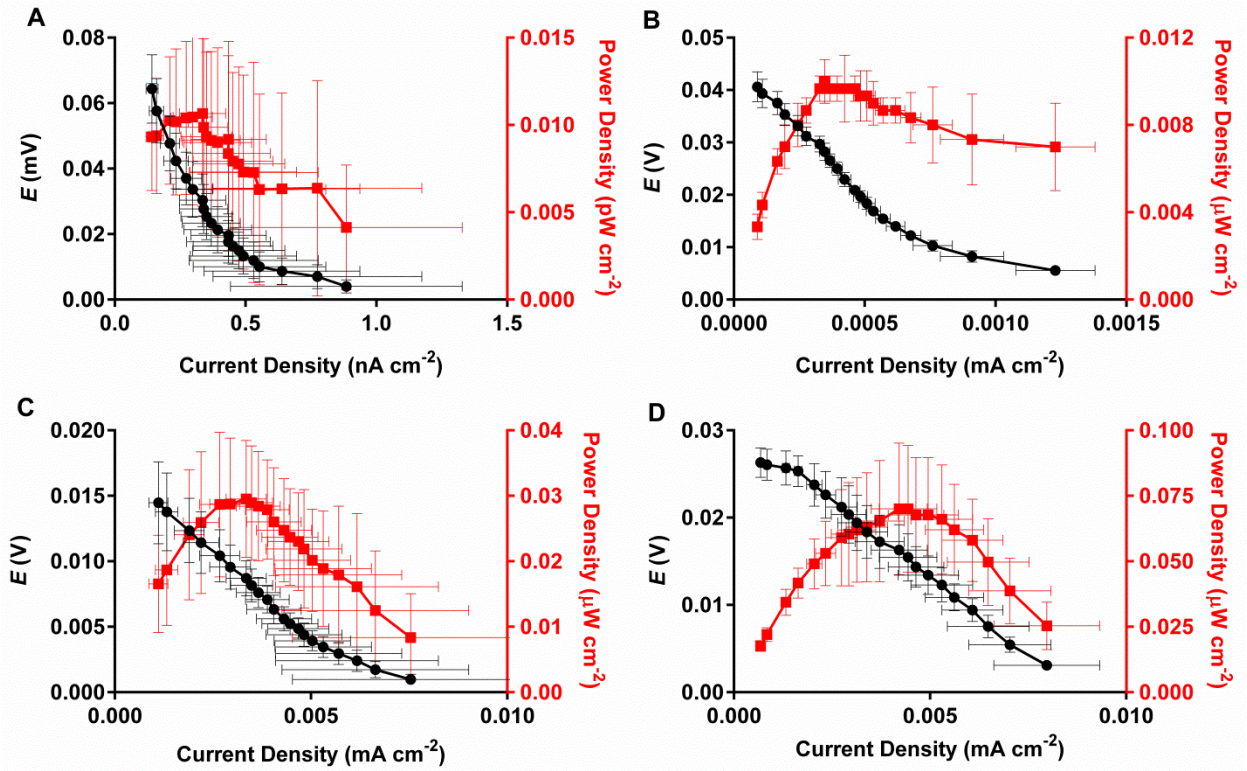

Figure 3.14 Control EBFC performance. A) EBFC performance and polarization curves using bare gold wire. B) Gold/MWCNT fiber paddle electrodes without enzyme-modification-based EBFC performance and polarization curves. C) EBFC performance and polarization curves using bare copper clips. D) Graphene-coated SWCN gel electrodes without enzyme-modification-based EBFC performance and polarization curves. Experiments performed in air-saturated 0.1 M sodium phosphate buffer (pH 7.0) with 0.1 M glucose. Error bars represent 1 standard deviation of 3 trials.

For comparison, we calculated the theoretical power density of each system based on the electrochemically determined GOX loading and operating voltage that correlated to the maximum power density. Assuming GOX operation at the previously determined native k_{cat}, experimental maximum power densities corresponded to 0.03% and 4.28% of theoretical values for gold/MWCNT fiber paddle- and graphene-coated SWCNT gel-based systems, respectively.[278] This result showed that despite allowing a 20-fold higher GOX loading due to

unhindered internalization by larger pore sizes, the gold/MWCNT fiber paddle-based system yielded a ~10 fold lower maximum power density than the graphene-coated SWCNT gel-based system. Enzymes immobilized onto curved nanomaterials have been shown to lose a greater percentage of enzymatic activity when adsorbed onto supports with lower degrees of curvature (i.e., larger diameter). This has been attributed to increased interaction between hydrophobic portions of the enzyme surface and the hydrophobic nanomaterial surface leading to a greater degree of enzyme deformation upon adsorption.[89] Thus, it was possible that the larger diameter PAN fibers coated with AuNPs and MWCNTs in the gold/MWCNT fiber paddle system caused relatively greater GOX denaturation upon adsorption compared to the graphene-coated SWCNT gel system. The 40-fold greater current generation rate per mol of GOX observed at the graphene-coated SWCNT gel anode was consistent with higher GOX specific activity at the electrode material of higher curvature. These results highlighted the importance of not only targeting high working enzyme loadings, but also providing maximum retained activity and charge collection capability.

The two EBFC systems described in this study allowed us to delve into the interactions of electroactive enzymes with commonly used electrode materials. We recently described an EBFC that had significantly higher power density that is included in **Figure 5C,D**.[278] The increased power density of this graphene/SWCNT cogel-based EBFC was driven by a GOX loading 2 to 3 orders of magnitude greater than the systems discussed in this study, but with GOX fully internalized into a three-dimensional conducting matrix. The increased GOX loading was possible due to the high SSA of the graphene/SWCNT cogels (846 m^2 g^{-1}) coupled with pore sizes that allowed unhindered access of GOX throughout the electrode material (70% of pores greater than 10 nm).[278] The encapsulation of GOX into the electrode structure allowed some

measure of DET to be achieved, but yielded decreased current generation efficiency (0.08% relative to native GOX at the observed loading) compared with the graphene-coated SWCNT gel-based system, which possessed a comparable SSA (686 m^2 g^{-1})[278] This result emphasized the need for electrode materials to possess not only high SSA, but also appropriate pore sizes to maximize enzyme accessible surface area. The high anodic loading allowed this system to produce a power density within one order of magnitude of the highest performing systems reported to date.[67-70, 278] Together, the data we have generated on these three EBFC designs has taught us that ample SSA for enzyme adsorption, appropriate pore size for enzyme/substrate internalization and high surface curvature for retained enzyme activity were critical elements in driving efficacy.

3.4 Conclusions

We have thoroughly characterized and compared glucose-driven EBFCs based on two vastly differing materials. We showed that gold/MWCNT fiber paddle electrodes and graphene-coated SWCNT gel electrodes were capable of generating power densities of 0.42 ± 0.06 μW cm^{-2} and 3.56 ± 1.09 μW cm^{-2} with OCVs of 0.22 ± 0.02 V and 0.22 ± 0.03 V, respectively, upon modification with GOX and BOD. We found that electroactive enzyme performance was a function of support curvature, pore size distribution and SSA. This work highlighted the potential of both materials to operate as enzyme-modified electrodes, and also demonstrated the limitations of each with DET between GOX and electrode surfaces remaining one of the most challenging hurdles in EBFC design. Future work will be focused on improving anodic electron transfer efficiency of GOX.

Chapter 4: Polymer-Based Protein Engineering Grown Ferrocene-containing Redox Polymers Improve Current Generation in an Enzymatic Biofuel Cell

4.1 Introduction

Enzymatic biofuel cells (EBFCs) have been intensely studied as prospective power sources for the future of implantable devices.[13, 53] These fuel cells capitalize on the biocompatibility, specificity and mild operating conditions of enzymes to generate electrical power from physiologically present fuels without added toxicity concerns.[225, 286] The general operation of an EBFC consists of two separate redox reactions occurring at enzyme-modified electrodes connected through an external circuit.[16, 22] The magnitude of power capable of being produced is governed by the density of current generated and the potential difference between the anodic and cathodic redox reactions.[16, 17] A major limiting factor in these systems is the inefficient generation of current at the anode.[12, 14]

The density of current produced (J_{max}) at enzyme-modified anodes is proportional to the density of anodic working enzyme activity. This activity density depends on the loading of working enzyme incorporated onto the electrode material per unit area and the rates of two reactions: the turnover of substrate (*i.e.*, fuel) by the anodic working enzymes and the transfer of electrons from the active sites of these enzymes to the supporting electrode material. Consequently, there are two main strategies to improving anodic J_{max} in EBFCs. One approach is to maximize enzyme loading density through the design of electrode materials with greatly increased available surface area for enzyme attachment through the incorporation of nanomaterials such as metal nanoparticles, graphene and carbon nanotubes.[137, 140, 287] These materials have further been fabricated into three-dimensional conducting matrices with extremely high specific surface area (SSA), which have produced some of the highest performing EBFCs to date with power densities reaching 2 mW cm^{-2}.[67-69]

The other approach to improving anodic J_{max} is to enhance the observed reaction rates of the immobilized enzyme. The turnover rate constants (k_{cat}) of enzymes are impacted by the process of immobilization dependent on the characteristics of the support material, as well as on the immobilization method employed.[89, 91, 288, 289] Similarly, the heterogeneous electron transfer rate constants (k_s) of electroactive enzymes are a function of support material, immobilization method and target working enzyme.[258, 288, 290] Much of the resistance to electron transfer limiting k_s in such systems stems from the location of the enzymatic active sites being deeply buried within the protein shell.[145, 166] The transfer of electrons to the electrode surface also must compete with electron transfer to the natural enzyme co-substrate. Thus, the observed J_{max} is generally limited by inefficient electron transfer between the enzyme active sites and the electrode surface. Attempts to mitigate electron transfer resistances have focused on the use of small molecule redox mediators and directed orientation immobilization strategies.[39, 68, 163] Also, polymer nanocomposite materials containing carbon nanotubes or metal nanoparticles have been shown to facilitate direct electron transfer (DET) with electroactive enzymes due to the capability of these nanomaterials to interact with the enzyme active site.[291-295]

In mediated electron transfer (MET) type systems, the anodic working enzymes are re-oxidized by small molecule redox mediators that then transfer electrons to the electrode. These mediators are capable of reaching the buried active site more readily than the electrode materials, thus, increasing the percentage of available electrons that are transferred to the circuit rather than the natural electron acceptor. For instance, Reuillard *et al.* reported that the addition of free naphthoquinone to a glucose oxidase (GOX)/multi-walled carbon nanotube (MWCNT)-based anode resulted in a 14-fold increase in current output.[68] However, the use of free mediators

within EBFCs raises additional toxicity and stability concerns, and also necessitates membrane separation of anode and cathode.[39, 69]

To minimize the rate at which mediator leaches into solution, groups have incorporated redox moieties into polymer networks to effectively "wire" redox enzymes to electrodes[11, 160] Specifically, the incorporation of anodic working enzymes into ferrocene, osmium and quinone containing polymer networks have been shown to enhance electron transfer efficiency between the enzymes and the electrode surfaces without the presence of freely diffusing mediator molecules.[158, 296, 297] Polymer-based protein engineering (PBPE) using atom transfer radical polymerization (ATRP) offers a method to tailor enzyme function through tunable modification of the enzyme surface with rationally designed functional polymers. ATRP is a type of controlled radical polymerization that provides the formation of polymers with low polydispersity indices (PDI), enzyme-friendly reaction conditions and a large library of available monomers including ferrocene-containing monomers.[197, 218, 298-300] A large density of polymer can be grown from the surface of target enzymes using the "grafting-from" method in which polymerization is initiated directly from the enzyme surface eliminating steric limitations of pre-grown polymers.[211] Application of these methodologies to model enzymes has been shown to not only enhance enzyme activity and stability, but also allow predictable engineering of enzyme function through modification with temperature and pH responsive polymers.[215, 217, 218, 222] However, the impact of redox mediator-containing polymers grown from the surface of enzymes has not been previously investigated.

Herein, we report on the functionalization of the anodic working enzyme GOX with ferrocene-containing redox polymers through PBPE (**Figure 4.1**). We chose GOX because it is notoriously difficult to achieve DET between the flavin adenenine dinucleotide (FAD) cofactor

active site within GOX and an electrode surface.[138, 145, 146] Poly(*N*-(3-dimethyl(ferrocenyl)methylammonium bromide)propyl acrylamide) (pFcAc) was grown from covalently attached, water-soluble initiator molecules on the surface of GOX in a "grafting from" approach using surface initiated-ATRP (SI-ATRP).

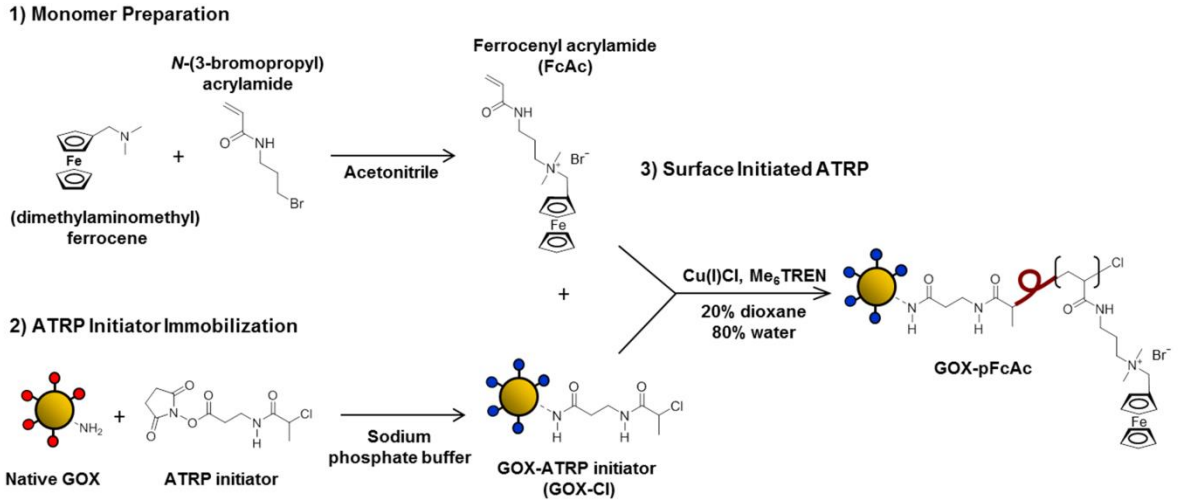

Figure 4.1 Schematic representation of GOX-pFcAc formation using PBPE. 1) Preparation of FcAc monomer. 2) ATRP initiator modification of native GOX. 3) "Grafting from" ATRP reaction to produce GOX-pFcAc conjugates

The GOX-pFcAc conjugates were subsequently immobilized through physical adsorption onto paddle-shaped electrodes made up of electrospun polyacrylonitrile fibers coated with gold nanoparticles (AuNPs) and MWCNTs. We have previously reported on the fabrication and characterization of these gold/MWCNT fiber paddles modified with native GOX.[191, 288] GOX-pFcAc conjugates and GOX-pFcAc-gold/MWCNT fiber paddle electrodes were thoroughly characterized in terms of biochemical and electrochemical properties. We further determined the EBFC performance of GOX-pFcAc-gold/MWCNT fiber paddle anodes when coupled with gold/MWCNT fiber paddle cathodes modified with bilirubin oxidase (BOD) prepared as previously described.[288] The objectives of this study were to examine the

capabilities of PBPE to promote the effective "wiring" of the buried GOX active sites to an external electrode by thorough characterization and comparison of the performance of GOX-pFcAc conjugates to that of native GOX.

4.2 Materials and Methods

4.2.1 Materials

Sodium phosphate buffer (0.1 M, pH 7.0) prepared from phosphate salts and ultrapure milliQ grade water (resistivity of 18.2 MΩ·cm) was used in all experiments unless otherwise stated. GOX type X-S from *Aspergillus niger* and horseradish peroxidase type VI-A were purchased from Sigma Aldrich. BOD from *Myrothecium* sp. was purchased from Amano Enzyme Inc. Tris[2-(dimethylamino)ethyl]amine (Me_6TREN) was synthesized as described previously.[301] MWCNTs with average diameter of 11.5 nm and average length of 30 μm were purchased from Cheap Tubes, Inc. Dialysis tubing (25 kDa molecular weight cutoff, Spectra/Por®, Spectrum Laboratories Inc.) was purchased from Fisher Scientific. All chemicals were of analytical grade and used as received.

4.2.2 Synthesis of *N*-(3-dimethyl(ferrocenyl)methylammonium bromide)propyl acrylamide

We first mixed 3-bromopropylamine hydrobromide (10 g, 45.6 mmol) and trimethylamine (15.9 mL, 114 mmol) in 100 mL ultrapure water and slowly added acryloyl chloride (4.1 mL, 50.7 mmol) at 0 °C. After stirring at room temperature for 1 h, the mixture was cooled to 0 °C and adjusted to pH 7.0 using 6 N hydrochloric acid. We extracted *N*-(3-bromopropyl) acrylamide with four additions of ethyl acetate (50 mL) and washed the organic phase twice with saturated $NaHCO_3$ aq. (50 mL), twice with 10 wt% citric acid aq. (50 mL) and twice with saturated NaCl aq. (50 mL). The organic phase was then dried over anhydrous $MgSO_4$ and evaporated to remove ethyl acetate; yield 8.0 g (90%). ^{1}H NMR (300 MHz, C*D*Cl_3),

δ 2.14 (m, 2H, *J* = 6.6 Hz, $NHCH_2C\mathit{H}_2CH_2Br$), 3.44 – 3.52 (m, 4H, $NHC\mathit{H}_2CH_2C\mathit{H}_2Br$), 5.67 (dd, 1H, *J* = 1.5 and 10.2 Hz, alkene), 5.98 (broad s, 1H, amide proton), 6.12 (dd, 1H, *J* = 10.2 and 17.1 Hz, alkene) and 6.31 (dd, 1H, *J* = 1.5 and 17.1 Hz, alkene) ppm. Next, a mixture of *N*-(3-bromopropyl) acrylamide (2.4 g, 12.5 mmol) in acetonitrile (25 mL) was added to a solution of (dimethylaminomethyl)ferrocene (3.0 g, 12.5 mmol) in acetonitrile (25 mL) and stirred at 60°C overnight. After the mixture had cooled to room temperature, we added diethyl ether (300 mL) and stored the solution at 4 °C overnight. *N*-(3-dimethyl(ferrocenyl)methylammonium bromide)propyl acrylamide (FcAc) was finally filtered and washed with diethyl ether; yield 3.2 g (59%), mp. 124 – 127 °C. ^{1}H NMR (300 MHz, $C\mathit{D}Cl_3$), δ 2.22 (m, 2H, *J* = 5.7 Hz, $NHCH_2C\mathit{H}_2CH_2Br$), 3.10 (s, 6H, $CH_2\ N^+(C\mathit{H}_3)_2CH_2$), 3.52 (t, *J* = 5.7 Hz, 2H, $NHCH_2CH_2C\mathit{H}_2N^+$), 3.84 (t, 2H, *J* = 5.7 Hz $NHC\mathit{H}_2CH_2CH_2N^+$), 4.29 – 4.57 (11H, Ferrocene and $C\mathit{H}_2$ between Ferrocene and ammonium) 5.63 (d, 1H, *J* = 10.2 Hz, alkene), 6.34 (d, 1H, *J* = 16.5 Hz, alkene) and 6.57 (dd, 1H, *J* = 10.2 and 16.5 Hz, alkene), 8.33 (broad s, 1H, amide proton) ppm. IR (KBr) 3453, 3384, 3267, 3053, 3012, 2956, 1675, 1658, 1621, 1542, 1463, 1445, 1407, 1312, 1230, 1103, 1003, 987, 864, 845, 812 and 514 cm^{-1}. ^{1}H NMR spectra were recorded on a spectrometer (300 MHz, Bruker Avance) in the NMR facility located in the Center for Molecular Analysis, Carnegie Mellon University, with $CDCl_3$. Routine FT-IR spectra were measured by KBr pellet method using a Nicolet IR200 FT-IR spectrometer (Thermo Scientific) located in the Department of Chemistry, University of Pittsburgh.

4.2.3 Preparation of GOX-pFcAc conjugates

Synthesis of ATRP initiating molecules was carried out as previously described.[215, 218] Synthesized initiating molecules (50 mg, 0.18 mmol) and GOX (300 mg, 0.002 mmol protein, 0.06 mmol primary amine) were dissolved in 0.1 M sodium phosphate buffer (pH 8.0)

and stirred for 3 h at 4 °C. The solution was then dialyzed against 0.1 M sodium phosphate buffer (pH 7.0) for 48 h at 4 °C. We determined the resulting initiator modified GOX (GOX-Cl) concentration and number of initiating sites per GOX molecule *via* standard bicinchonic acid (BCA) assay kit (Thermofisher Scientific) and fluorescamine protein assay, respectively. We modeled the expected sites of modification using computational analysis *via* lysine available surface area and predicted pKa UV-vis spectra were recorded using a UV-vis spectrometer (Lambda 2, Perkin Elmer).

To synthesize GOX-pFcAc conjugates, the GOX-Cl initiator complex (110 mg, 0.017 mmol initiator) and FcAc (73 mg, 0.17 mmol) were first dissolved in a 20 mL mixture of 80% ultrapure water and 20% 1,4-dioxane and bubbled with argon for 1 h. In a separate flask, Me_6TREN (5.36 µL, 0.02 mmol) was dissolved in ultrapure water (2 mL) and bubbled with Argon for 10 min. Copper(I) chloride (1.98 mg, 0.02 mmol) was then added to the Me_6TREN solution and bubbled with argon for 50 min prior to the addition of the GOX-Cl/FcAc solution to the copper/Me_6TREN solution. Upon combining the two solutions, the reaction mixture was incubated at 4 °C for 5 h with stirring. The resulting solution was purified by dialysis against 0.1 M sodium phosphate buffer (pH 7.0) using 25 kDa molecular cutoff dialysis tubing for 48 h at 4 °C (final 2 h of dialysis against ultrapure water) and then lyophilized.

4.2.4 Fluorescamine protein assay

The GOX-Cl sample solution (150 µL, 3 mg mL^{-1}) in 0.1 M sodium phosphate buffer (pH 8.0) was mixed with fluorescamine solution (50 µL, 3 mg mL^{-1}) in DMSO and incubated at room temperature for 15 min. Fluorescence of the sample with excitation at 365 nm and emission at 470 nm was measured using a Synergy H1 Hybrid Multi-Mode microplate reader (Biotek). The number of initiating sites per GOX molecule was determined by comparison of the

fluorescence to a standard curve. The standard curve was obtained from native GOX prepared as above with varying concentration ratio in 0.1 M sodium phosphate buffer (pH 8.0).

4.2.5 Computational analysis of ATRP initiator modification of GOX

Computational analysis of GOX from *Aspergillus niger* structure was used to evaluate lysine and *N*-terminus reactivity. The crystal structure of the monomer of GOX is readily available from the Protein Data Bank (PDB code: 1GAL).

Accessible surface area (ASA) of free amine residues was calculated using the ASA-View (DSSP algorithm).[302] Values of ASA are presented as a ratio relative to the surface area that was presented when residue X was in the extended state of Ala-X-Ala. When residue X was completely surrounded by its neighboring residues, its relative solvent accessibility was 0. The threshold for exposed lysine residues was defined as the average protein lysine accessibility of 0.4.[303] Reactivity of free amine residues was determined by pKa calculations using PROPKA 2.0.[304] This program predicts pKa values for all ionizable groups present in a target protein by empirically establishing relationships based on desolvation effects, hydrogen-bonding and charge-charge interactions.

4.2.6 GOX-pFcAc conjugate characterization

We determined the enzyme content of lyophilized GOX-pFcAc powder using the standard BCA assay kit. Hydrodynamic diameters (D_h) of native GOX and GOX-pFcAc were determined *via* dynamic light scattering (DLS) using a Nanoplus zeta/nano particle analyzer (Particulate Systems). GOX and GOX-pFcAc kinetic analysis was performed using the standard GOX 2,2’-azino-bis(3-ethylbenthiazoline)-6-sulfonic acid (ABTS) activity assay.

4.2.7 Electrode fabrication

We prepared gold/MWCNT fiber paddle electrodes as previously described.[191, 288] Enzyme-modified electrodes were formed by incubating individual gold/MWCNT fiber paddle electrodes in 1 mg mL^{-1} enzyme solution (10 mL, GOX, BOD or GOX-pFcAc) in 0.1 M sodium phosphate buffer (pH 7.0) at 4 °C for 4 h to allow for physical adsorption of enzyme/conjugate. Electrodes modified with both native GOX and FcAc monomer were formed by similar incubation with both 1 mg mL^{-1} GOX and 0.26 mg mL^{-1} FcAc monomer. We then gently washed each fiber paddle to remove loosely bound enzyme prior to individual electrode characterization of EBFC testing. Scanning electron microscope (SEM) images were taken using a Hitachi S-2460N SEM.

4.2.8 Electrode characterization

Total GOX loadings were determined as previously described.[288] We performed all electrochemical measurements using a conventional three-electrode electrochemical cell utilizing a KCl saturated Ag/AgCl reference electrode and a 0.5 mm diameter platinum wire counter electrode. EBFC performances were tested in 200 mL of air saturated 0.1 M sodium phosphate buffer (pH 7.0) containing 0.1 M glucose with stirring. A Fluke 287 True RMS multimeter was used to measure circuit voltage with circuit resistance varied manually with an IET Labs RS-200 resistance decade box.

4.3 Results and discussion

4.3.1 Preparation of GOX-pFcAc conjugates

PBPE has proven capable of adding functionality to enzymes through modification of the enzyme surface with stimuli responsive polymers.[215, 217, 218, 222] We investigated the extension of these capabilities to ferrocene-containing redox polymers grown from the anodic

working enzyme GOX (**Figure 4.1**). To ensure highly modified enzyme-polymer conjugates, we utilized a water-soluble, NHS-functionalized ATRP initiator to react with primary amines on the surface of GOX.[215] Each GOX dimer possessed 32 available primary amines including the *N*-termini.[47] Upon ATRP initiator modification, we determined that there was an average of 25 initiating sites per GOX molecule using a fluorescamine protein assay. Thus, there were 25 separate sites on each enzyme from which pFcAc polymers could be grown. We modeled the expected sites of initiator modification using computational analysis of predicted primary amine accessible surface area (ASA) and pKa (**Figure 4.2**).[302, 304]

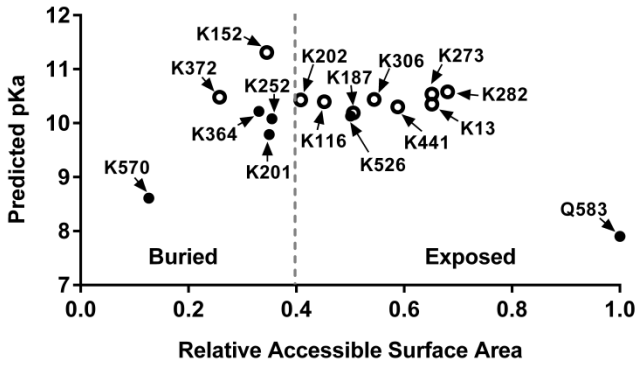

Figure 4.2 Modeling of expected ATRP initiator modification sites within GOX monomer. ASA relative to residue X in fully extended state of Ala-X-Ala. Threshold for exposed lysine residues defined as the average protein lysine accessibility. Residues within 4 Å of active site marked with filled circle.

This analysis showed 6 lysine residues per monomer were buried with a relative ASA below 0.4, which is the average value for lysines within proteins.[303] Thus, it was predicted that the 10 exposed primary amines per monomer (ASA greater than 0.4; **Figure 4.2**) were modified in each GOX molecule. Discrepancy between predicted (20 accessible) and observed (25 modified) number of initiator sites per GOX molecule was likely due to the computer analysis using a static model with actual ASA fluctuating in solution. Nevertheless, it was

predicted that at least one lysine per monomer as well as the *N*-termini within 4 Å of the GOX active site were modified, which may lead to interference with biocatalytic activity but would also be conducive to charge collection (**Figure 4.2**).

GOX-pFcAc conjugates were prepared using a "grafting-from" approach in which FcAc monomers were extended from the chlorine functionalized ATRP initiators.[218] Enzyme content of the prepared GOX-pFcAc was determined using a standard BCA protein assay kit. From this information, and assuming all initiating sites participated in polymerization, we estimated the molecular weight of the conjugates to be approximately 204 kDa, assuming equivalent polymerization from each ATRP initiator modified GOX molecule (GOX Mw = 160 kDa; FcAc Mw = 435.19 Da).[77] Details for BCA determined molecular weight calculations are provided in our previous reports.[215, 217] The structure of pFcAc grown from free ATRP initiator without NHS functionality was confirmed *via* ^{1}H NMR (**Figure 4.3**).

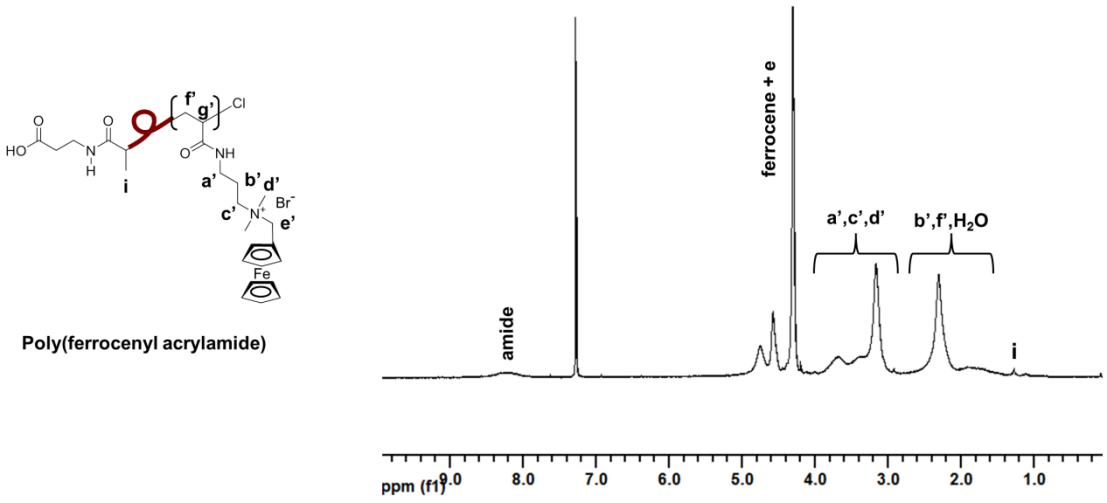

Figure 4.3 ^{1}H NMR spectra of pFcAc polymer in C*D*Cl$_3$. ^{1}H NMR spectra and corresponding protons of pFcAc polymer.The FT-IR spectra of native GOX exhibited strong absorbance at 3298 cm^{-1} attributed to N-H stretching, along with characteristic peaks at 1654 cm^{-1} and 1542 cm^{-1} assigned to the amide I band (C=O stretching of peptide bonds) and to the amide II band

(N-H bending and C-N stretching of peptide groups), respectively (**Figure 4.4**).[295] Analysis of pFcAc free polymer showed a broad N-H stretching peak at 3430 cm^{-1}. The FT-IR spectra of GOX-pFcAc displayed a combination of the features of its components (*i.e.* native GOX and pFcAc) including characteristic amide peaks at 1654 cm^{-1} and 1545 cm^{-1} (**Figure 4.4**). These results suggested the successful functionalization of GOX with pFcAc chains while maintaining the secondary structure of the enzyme.[291, 295]

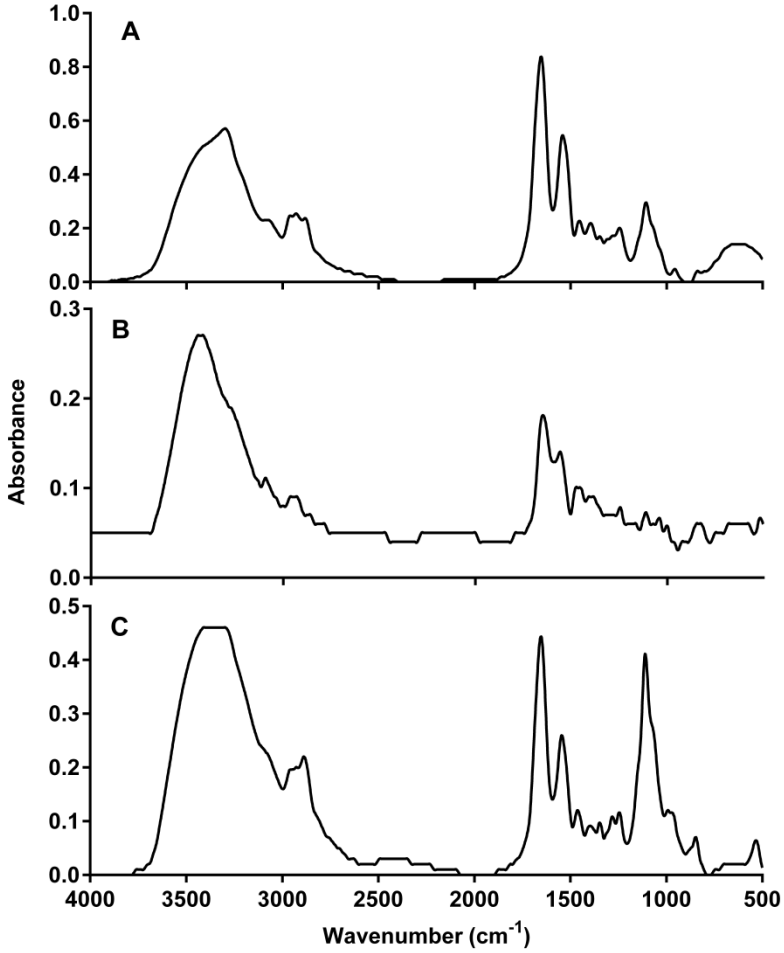

Figure 4.4 Component FT-IR analysis. A) FT-IR spectra of native GOX. B) FT-IR spectra of pFcAc polymer. C) FT-IR spectra of GOX-pFcAc conjugate.

4.3.2 Characterization of GOX-pFcAc conjugates

We characterized our GOX-pFcAc conjugates in terms of their retained native activity using the standard GOX ABTS activity assay. Monitoring initial rates of reaction (v_i) at varying glucose concentrations, we determined the k_{cat} and Michaelis-Menten constant (K_M) of both native and modified GOX (**Figure 4.5**). GOX and GOX-pFcAc produced k_{cat} values of 471.8 ± 6.9 s^{-1} and 48.0 ± 0.9 s^{-1}, respectively. The ten-fold decrease in k_{cat} was indicative of hindered substrate turnover by GOX-pFcAc.

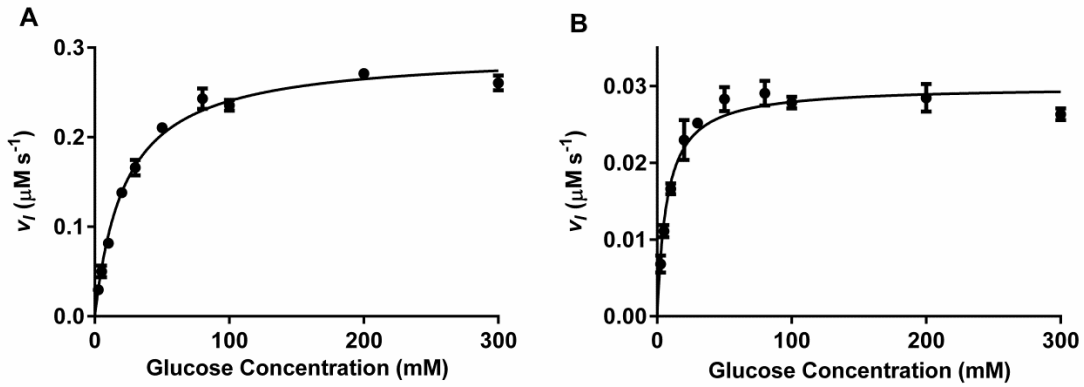

Figure 4.5 Kinetic analysis of native GOX and GOX-pFcAc. A) Initial rate of reaction at varying glucose concentrations of native GOX. B) Initial rate of reaction at varying glucose concentrations of GOX-pFcAc. Experiments performed in 0.1 M sodium phosphate buffer (pH 7.0). Error bars represent 1 standard deviations of 3 trials.

Upon examination using DLS, we found a large degree of aggregation in aqueous samples of GOX-pFcAc with particle sizes reaching 6 – 7 μm compared to the average determined particle size of GOX of 11.6 ± 3.6 nm. We further discovered that GOX activity was inhibited by increasing concentrations of FcAc monomer, which likely contributed to the observed loss of activity (**Figure 4.6**). The K_M of an enzyme is the substrate concentration at which the reaction rate is half of theoretical maximum. This value is driven by the tightness of substrate binding to the enzyme. The K_M values of GOX and GOX-pFcAc were found to be 23 ±

1 mM glucose and 7 ± 1 mM glucose, respectively. This result suggested GOX-pFcAc possessed a high affinity for glucose, despite substantially hindered substrate turnover. GOX-pFcAc conjugates were subsequently incorporated into gold/MWCNT fiber paddle electrodes *via* physical adsorption.

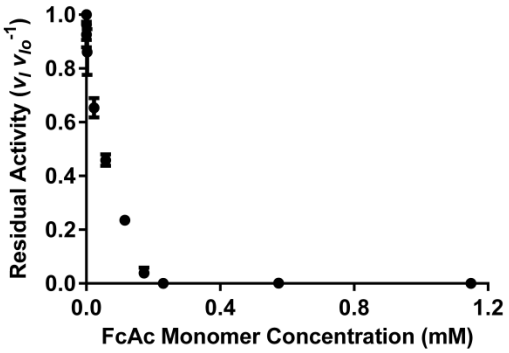

Figure 4.6 Residual activity analysis of native GOX in varying concentrations of FcAc monomer. Residual activity was determined relative to activity with no FcAc monomer present. Experiments performed in 0.1 M sodium phosphate buffer (pH 7.0). with 0.3 M glucose. Error bars represent 1 standard deviation of 3 trials.

4.3.3 Characterization of GOX-pFcAc-modified electrodes

We have previously reported on the fabrication and thorough electrochemical characterization of native GOX physically adsorbed onto gold/MWCNT fiber paddle electrodes.[191, 288] Briefly, the electrodes were prepared by the electrospinning of polyacrylonitrile fibers containing gold salt followed by reduction and deposition of AuNPs with subsequent electrodeposition of MWCNTs.[191, 288] In depth characterizations of the resulting electrode morphology can be found in our previous reports.[191, 288] Characteristic SEM images of gold/MWCNT fiber paddle electrodes before and after GOX-pFcAc functionalization showed retention of electrode morphology upon conjugate immobilization (**Figure 4.7**).

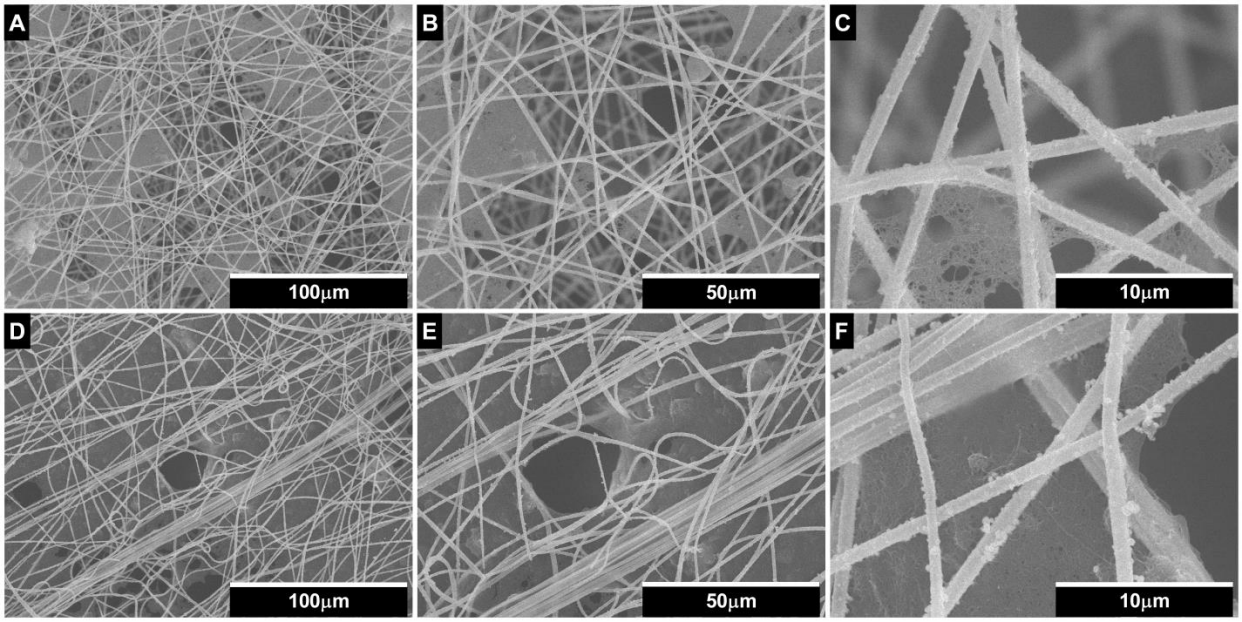

Figure 4.7 Morphological examination of gold/MWCNT fiber paddle electrodes. A-C) SEM images of gold/MWCNT fiber paddle electrode at varying magnifications. D-F) SEM images of GOX-pFcAc-gold/MWCNT fiber paddle electrodes at varying magnifications.

Cyclic voltammetry (CV) traces of gold/MWCNT fiber paddle anodes showed a single reduction peak at 0.5 V versus Ag/AgCl, which was attributed to further gold salt reduction to AuNPs within the fibers (**Figure 4.8**).[305, 306] GOX-pFcAc-gold/MWCNT fiber paddle anodes exhibited obvious oxidation and reduction peaks having a formal potential of 0.44 V versus Ag/AgCl and peak separation of 0.02 V indicating reversible electron transfer between ferrocene and the anode surface (**Figure 4.8A**). Upon the addition of 0.01 M glucose to solution, an obvious shift in anodic current was observed, which signified MET between bioactive GOX and the electrode through attached pFcAc polymer. The observed formal potential was stable over a wide range of pH, which was consistent with the pH independence of ferrocene redox activity (**Figure 4.8B**).[307] The slightly increasing formal potential exhibited at pH lower than

4.0 could result from a greater resistance to oxidation caused by positively charged GOX under those conditions (GOX p*I* = 4.2).[308]

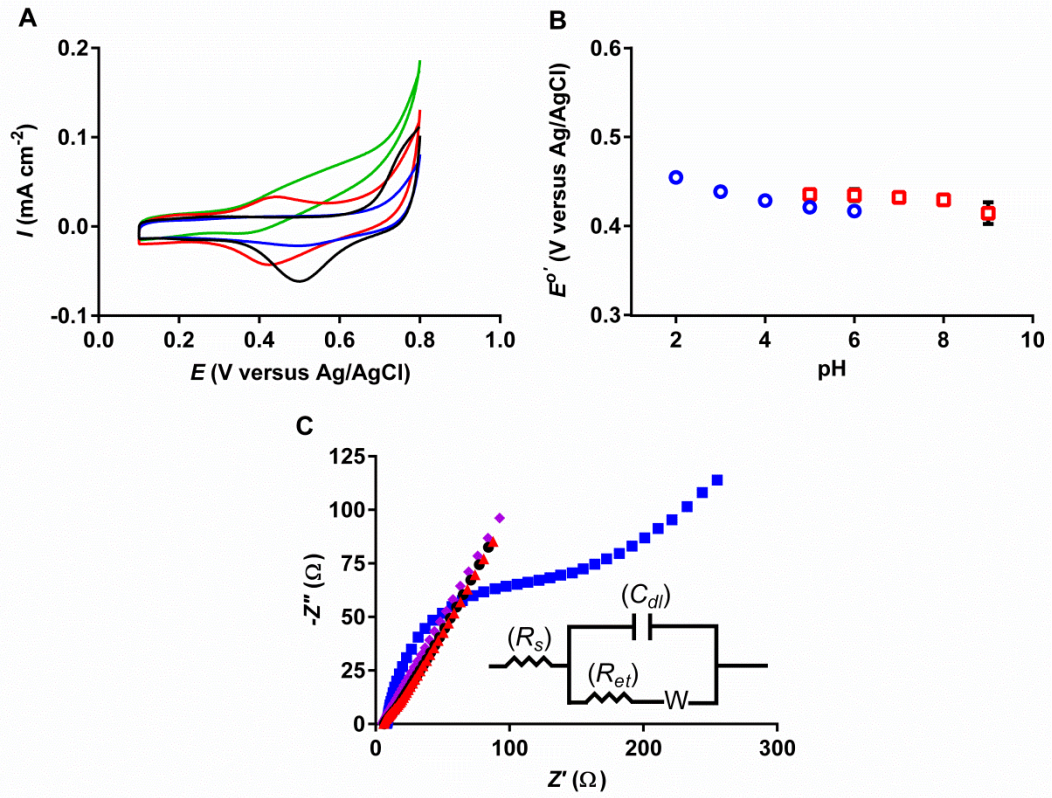

Figure 4.8 Electrochemical performance of GOX-pFcAc-gold/MWCNT fiber paddle anodes. A) Characteristic CV traces of gold/MWCNT fiber paddle anode of gold/MWCNT fiber paddle anode (black), GOX-gold/MWCNT fiber paddle anode (blue), GOX-pFcAc-gold/MWCNT fiber paddle anode (red) and GOX-pFcAc-gold/MWCNT fiber paddle anode with 10 mM glucose in 0.1 M sodium phosphate buffer (pH 7.0). B) GOX-pFcAc gold/MWCNT fiber paddle anode formal potential at varying buffer pH in either 0.1 M sodium phosphate buffer (pH 5.0-9.0)(red square) or 0.1 M citrate buffer (pH 2.0-6.0). Error bars represent 1 standard deviation of 3 trials. C) Nyquist plots of electrochemical impedance spectra for gold/MWCNT fiber paddle anode (black circle), GOX-gold/MWCNT fiber paddle anode (blue square) FcAc monomer-gold/MWCNT fiber paddle anode (purple diamond) and GOX-pFcAc-gold/MWCNT fiber paddle anode (red triangle) in 0.1 M KCl with 1.0 mM $Fe(CN)_6^{3-/4-}$ at 0.2 V versus Ag/AgCl. Inset: equivalent circuit used to fit data. CV experiments performed in argon-saturated solution at a scan rate of 10 mV s^{-1}.

We performed electrochemical impedance spectroscopy (EIS) to examine the surface characteristics of the gold/MWCNT fiber paddle anodes with various adsorbed materials (**Figure 4.8C**). Nyquist plots of the impedance spectra showed nearly straight trends for gold/MWCNT fiber paddle anodes and FcAc monomer-gold/MWCNT fiber paddle anodes, which were characteristic of diffusion limited systems.[309] Upon adsorption of native GOX, an insulating protein layer was formed at the electrode surface, evident from the appearance of the semicircular portion of the resulting spectrum (**Figure 4.8C**). The diameter of this semicircular region corresponded to the resistance to electron transfer of GOX-gold/MWCNT fiber paddle anodes with the $Fe(CN)_6^{3-/4-}$ redox probe. We then fit this data to an equivalent circuit (**Figure 4.8C inset**) to determine the corresponding electron transfer resistance (R_{et}), which was calculated to be 96.8 ± 2.8 Ω.[310] The Randles equivalent circuit incorporated (R_{et}), electrolyte/solution resistance (R_s), double layer capacitance (C_{dl}) and Warburg impedance (W).[310] EIS examination of GOX-pFcAc-gold/MWCNT fiber paddle anodes revealed a R_{et} of 3.5 ± 0.2 Ω, which proved decreased resistance to electron transfer by modification of GOX with pFcAc (**Figure 4.8C**).

Next, we examined the properties of the GOX-pFcAc-gold/MWCNT fiber paddle anodes by running CV traces at varying scan rates (**Figure 4.9**). The dependence of ferrocene faradaic peak current on scan rate allowed for the calculation of ferrocene loading at the anode surface for GOX-pFcAc-gold/MWCNT fiber paddle anodes and gold/MWCNT fiber paddles modified with both native GOX and free FcAc monomer (GOX/FcAc monomer-fiber paddle anodes; **Figure 4.9A,C**; **Table 4.1**) (Wang, 2000). The FcAc monomer concentration used for GOX/FcAc monomer-gold/MWCNT fiber paddle anodes was selected according to the estimated molar ratio consistent with the native GOX concentration in the incubation. The linear dependence of peak

current on scan rate showed that both systems were limited by electron transfer at the ferrocene-electrode interface rather than by diffusion (**Figure 4.9A,C**).[32] Additionally, we determined the total GOX loading at the anodes by removing adsorbed GOX or GOX-pFcAc using sodium dodecylbenzenesulfonate surfactant and calculating the enzyme content of the resulting supernatant *via* standard BCA assay kit (**Table 4.1**). The roughly 2-fold greater ferrocene loading and 1.6-fold greater total GOX loading observed for GOX-pFcAc conjugates compared to the GOX/FcAc monomer mixture suggested polymerization of pFcAc from the surface of GOX allowed ferrocene groups preferential interaction with the anode surface due to the lack of native GOX adsorption while also providing greater GOX retention at the anode surface. Further, the total GOX loading of GOX-pFcAc was found to be similar to that of native GOX absorbed with no FcAc present (**Table 4.1**).[288]

Table 4.1: Functional parameters of GOX-pFcAc-gold/MWCNT fiber paddle anodes

Gold/MWCNT fiber paddle anode	Ferrocene loading x 10^{-10} (mol cm^{-2})	Total GOX loading x 10^{-10} (mol cm^{-2})	k_s (s^{-1})	J_{max} (mA cm^{-2})	K_M^{app} (mM glucose)
GOX	N/A	2.60 [288]	0.95 ± 0.01 [288]	0.24 ± 0.01	41 ± 7
GOX-pFcAc	6.24	2.25	2.86 ± 0.46	0.50 ± 0.02	50 ± 8
GOX/pFcAc monomer	3.18	1.37	5.35 ± 0.41	0.18 ± 0.01	52 ± 8

[a] J_{max} and K_M^{app} values relative to amperometry in O_2-saturated solution with cell potential held at 0.8 V versus Ag/AgCl

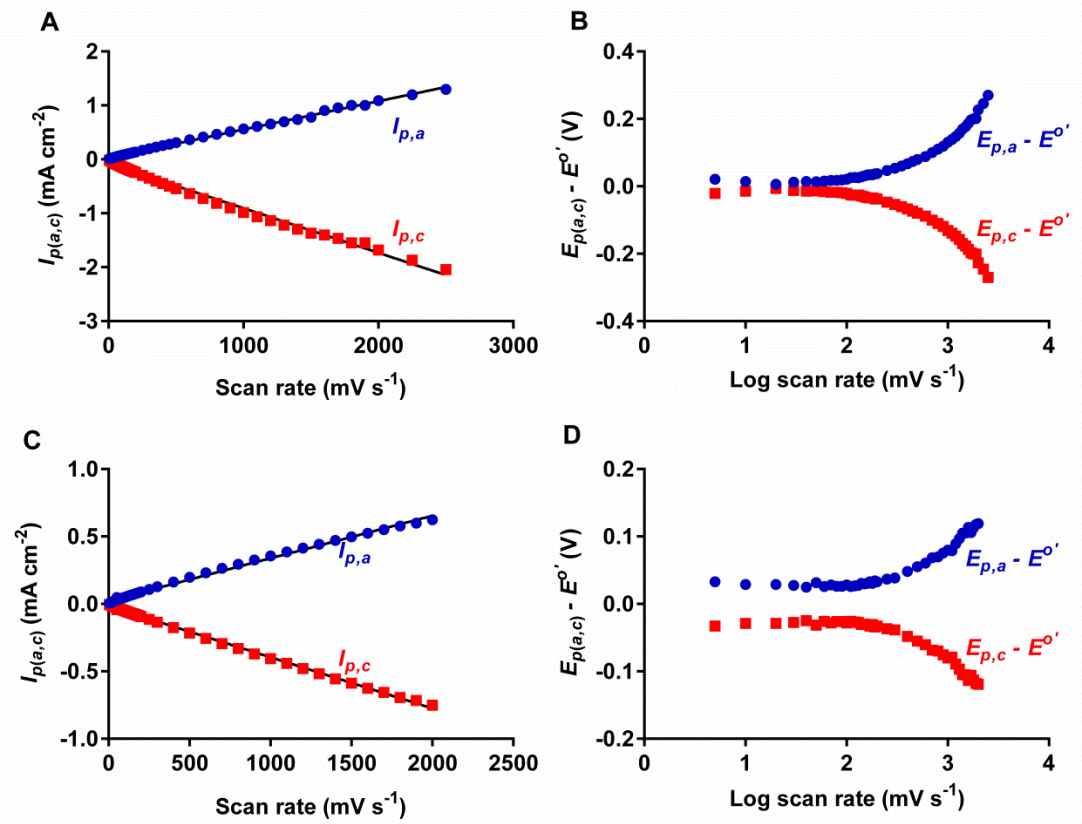

Figure 4.9 CV characterization of GOX-pFcAc-gold/MWCNT fiber paddle anode. A) Dependence of anodic (blue circle) and cathodic (red square) peak currents on scan rate for GOX-pFcAc-gold/MWCNT fiber paddle anodes. B) Dependence of anodic (blue circle) and cathodic (red square) peak potentials on the logarithm of scan rate for GOX-pFcAc-gold/MWCNT fiber paddle anodes. C) Dependence of anodic (blue circle) and cathodic (red square) peak currents on scan rate for GOX/FcAc monomer-gold/MWCNT fiber paddle anodes. D) Dependence of anodic (blue circle) and cathodic (red square) peak potentials on the logarithm of scan rate for GOX/FcAc monomer-gold/MWCNT fiber paddle anodes. Experiments performed in argon-saturated 0.1 M sodium phosphate buffer (pH 7.0).

The dependence of ferrocene faradaic peak potential on the logarithm of scan rate allowed for the determination of k_s in each configuration (**Figure 4.9B,D**; **Table 4.1**).[248, 284] The 1.9-fold lower k_s of GOX-pFcAc-gold/MWCNT fiber paddle anodes compared to GOX/FcAc monomer-gold/MWCNT fiber paddle anodes suggested slightly increased electron

transfer resistances stemming from polymerized pFcAc despite the increased ferrocene loading. The observed k_s of GOX-pFcAc was 3-fold higher, however, compared to GOX-gold/MWCNT fiber paddle anodes determined by the dependence of GOX faradaic peak potential on the logarithm of scan rate.[278]

We characterized electrical current generation *via* biocatalytic turnover of glucose in GOX-pFcAc-gold/MCWNT fiber paddle anodes through amperometry at varying glucose concentrations and cell potentials (**Figure 4.10**). Monitoring the increases in current density in argon-saturated solution with the cell potential held at the determined formal potential of pFcAc (0.44 V versus Ag/AgCl) provided characterization of glucose oxidation by GOX and MET through ferrocene to the electrode surface (**Figure 4.10A**).

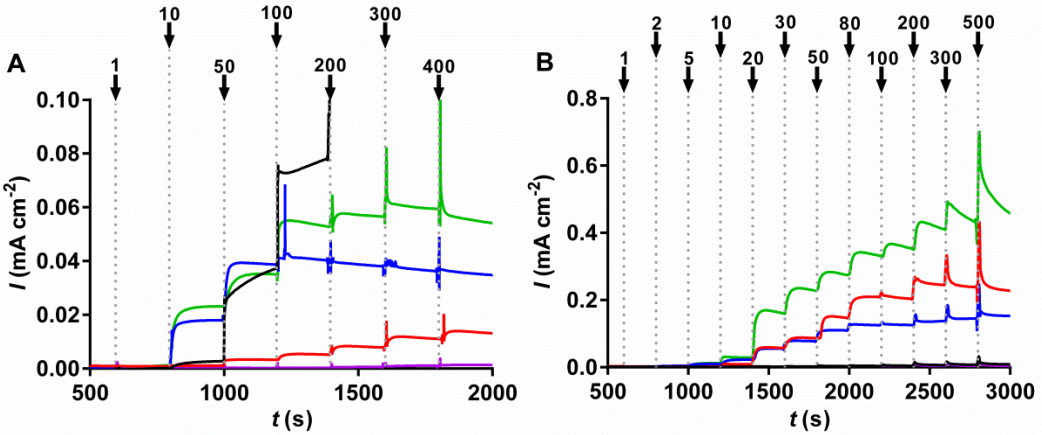

Figure 4.10 Amperometric performance of GOX-pFcAc-gold/MWCNT fiber paddle anodes. Typical amperometric profiles of gold/MWCNT fiber paddle anode (black), FcAc monomer-gold/MWCNT fiber paddle anode (purple), GOX-gold/MWCNT fiber paddle anode (red), GOX/FcAc monomer-gold/MWCNT fiber paddle anode (blue), and GOX-pFcAc-gold/MWCNT fiber paddle anode (green) upon successive glucose additions in A) argon-saturated solution with cell potential held at 0.44 V versus Ag/AgCl, and B) O_2-saturated solution with cell potential held at 0.8 V versus Ag/AgCl. Experiments performed in 0.1 M sodium phosphate buffer (pH 7.0). Glucose injections indicated by arrows with values representative of final glucose concentration in mM upon injection.

The highest current density was observed for non-functionalized gold/MWCNT fiber paddle anodes due to the direct oxidation of glucose by AuNPs at this potential (**Figure 4.11**).[311, 312] However, this activity was eliminated upon adsorption of FcAc monomer and inhibited upon adsorption of native GOX (**Figure 4.10A**).

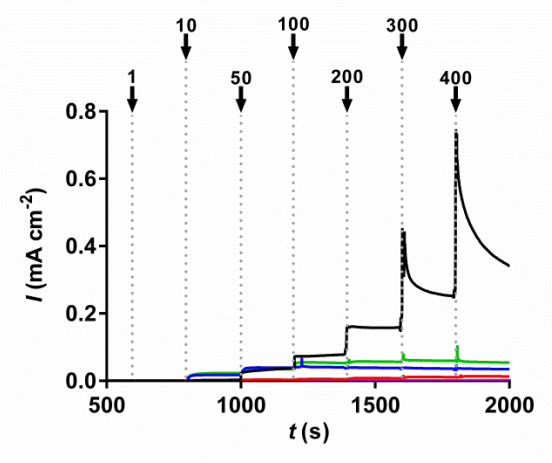

Figure 4.11 Amperometric evaluation of gold electrochemistry within GOX-pFcAc-gold/MWCNT fiber paddle anodes. Typical amperometric profiles of gold/MWCNT fiber paddle anode (black), FcAc monomer-gold/MWCNT fiber paddle anode (purple), GOX-gold/MWCNT fiber paddle anode (red), GOX/FcAc monomer-gold/MWCNT fiber paddle anode (blue), and GOX-pFcAc-gold/MWCNT fiber paddle anode (green) upon successive glucose additions in argon-saturated solution with cell potential held at 0.44 V versus Ag/AgCl. Experiments performed in 0.1 M sodium phosphate buffer (pH 7.0). Glucose injections indicated by arrows with values representative of final glucose concentration in mM upon injection.

GOX-pFcAc- and GOX/FcAc monomer-gold/MWCNT fiber paddle anodes exhibited reproducible current responses upon successive glucose injections (**Figure 4.10**). The steady-state current densities reached after glucose injection allowed the calculation of apparent Michaelis-Menten kinetics characteristic of MET (**Figure 4.12**). The apparent Michaelis-Menten constants (K_M^{app}) for the enzyme within GOX-pFcAc-gold/MWCNT and GOX/FcAc monomer-gold/MWCNT fiber paddles anodes were 19 ± 10 mM glucose and 13 ± 5 mM glucose,

respectively, which showed similar affinities for glucose in both configurations. The maximum current density (J_{max}) of MET for GOX-pFcAc-gold/MWCNT fiber paddle anodes was somewhat higher at 0.09 ± 0.01 mA cm^{-2} than that for GOX/FcAc monomer-gold/MWCNT fiber paddle anodes at 0.05 ± 0.01 mA cm^{-2} revealing a slightly decreased resistance to electron transfer between FAD in GOX and the electrode surface through the ferrocene moieties. Apparent activity from GOX-gold/MWCNT fiber paddle anodes under these conditions was attributed to retained AuNPs glucose oxidation at due to incomplete coverage by enzyme alone (**Figure 4.12A**).

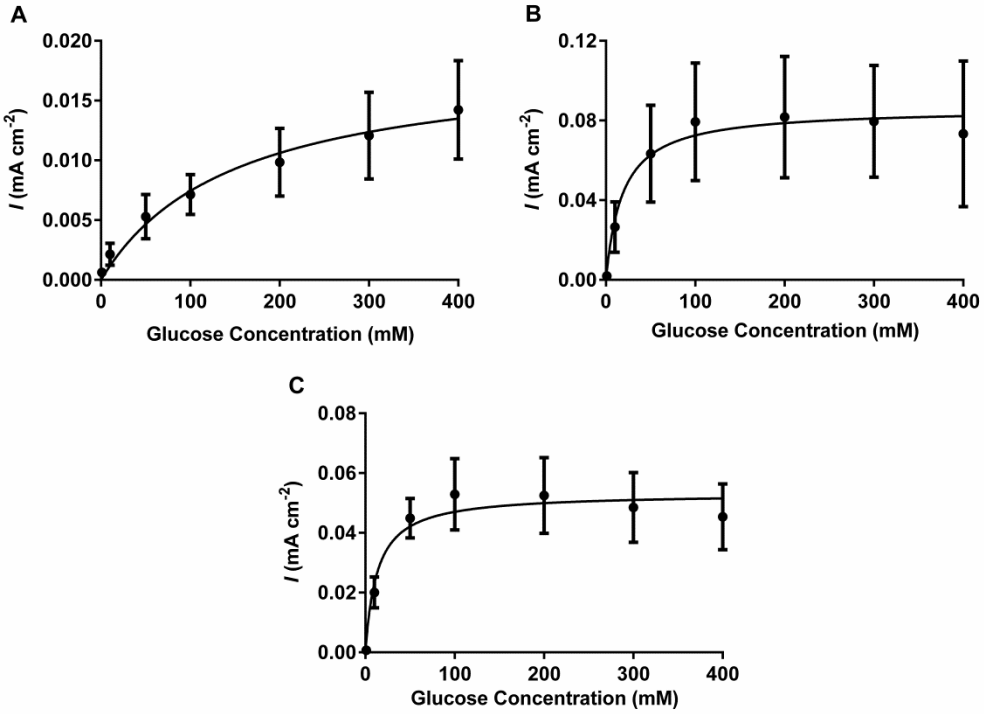

Figure 4.12 Apparent MET kinetic analysis of GOX-pFcAc-gold/MWCNT fiber paddle anodes. A) Apparent MET kinetic analysis from amperometry of GOX-gold/MWCNT fiber paddle anodes. B) Apparent MET kinetic analysis from amperometry of GOX-pFcAc-gold/MWCNT fiber paddle anodes. C) Apparent MET kinetic analysis from amperometry of GOX/FcAc monomer-gold/MWCNT fiber paddle anodes. Experiments performed in argon-saturated 0.1 M sodium phosphate buffer (pH 7.0) with cell potential held at 0.4 V versus Ag/AgCl. Error bars represent 1 standard deviation of 3 trials.

We previously reported on electrical current generation by GOX-gold/MWCNT fiber paddles in O_2-saturated solution with cell potential held at 0.8 V versus Ag/AgCl.[288] At this potential, hydrogen peroxide produced from GOX was oxidized at the electrode surface, effectively using oxygen as a natural electron mediator. In configurations containing ferrocene, MET was also observed at these conditions, which allowed for a measure of total current generation capabilities (**Figure 4.10B**). [1, 191]Again, examination of increasing current density upon successive glucose injections provided for calculation of apparent Michaelis-Menten kinetics (**Figure 4.13**; **Table 4.1**). Glucose oxidation by AuNPs was not observed under these conditions (**Figure 4.10B**). The increased K_M^{app} for all configurations was indicative of similar GOX/substrate interactions at each functionalized anode. GOX-pFcAc-gold/MWCNT fiber paddle anodes exhibited the highest overall J_{max} despite a ten-fold lower k_{cat} than native GOX and a nearly 2-fold lower k_s than ferrocene at GOX/FcAc monomer-gold/MWCNT fiber paddle anodes (**Table 4.1**). The decreased overall current generation of GOX/FcAc monomer-gold/MWCNT fiber paddle anodes compared to GOX-gold/MWCNT fiber paddle anodes was consistent with the inhibition of native GOX biocatalytic activity (**Figure 4.6**)

Assuming the determined k_{cat} values were the maximum rates of electron production from the 2-electron oxidation of glucose, the maximum specific current generation rates for GOX and GOX-pFcAc were 9.10×10^7 A mol GOX^{-1} and 9.25×10^6 A mol GOX^{-1}, respectively. Combining these rates with the calculated total GOX loadings, the maximum theoretical J_{max} values for GOX-gold/MWCNT fiber paddle anodes and GOX-pFcAc-gold/MWCNT fiber paddle anodes became 23.7 mA cm^{-2} and 2.1 mA cm^{-2}, respectively. Thus, the current generation efficiency of GOX-pFcAc-gold/MWCNT fiber paddle anodes calculated as the percent of J_{max} observed relative to the maximum possible J_{max} was 24%, whereas the same value for GOX-

gold/MWCNT fiber paddle anodes was only 1%. These results highlighted the effective "wiring" of the GOX active site to the electrode by pFcAc grown from the surface of GOX while also maintaining a portion of native GOX activity. The dramatic increase observed in anodic efficiency motivated us to examine the performance of GOX-pFcAc-gold/MCWNT fiber paddle anodes in an EBFC.

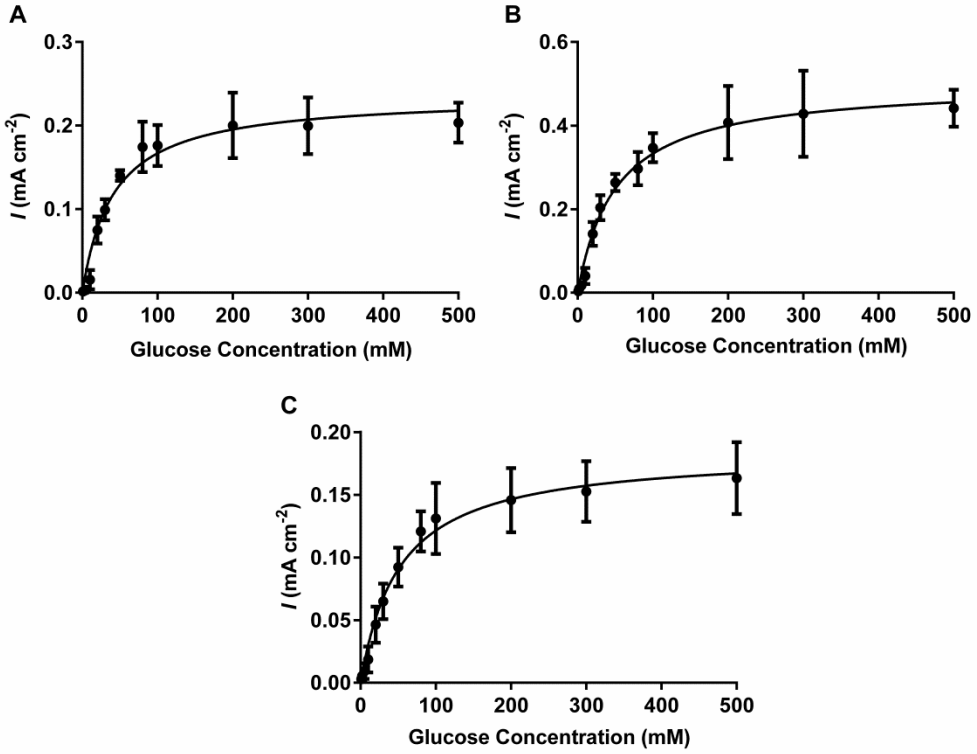

Figure 4.13 Apparent total kinetic analysis of GOX-pFcAc-gold/MWCNT fiber paddle anodes. A) Apparent total kinetic analysis from amperometry of GOX-gold/MWCNT fiber paddle anodes. B) Apparent total kinetic analysis from amperometry of GOX-pFcAc-gold/MWCNT fiber paddle anodes. C) Apparent total kinetic analysis from amperometry of GOX/FcAc monomer-gold/MWCNT fiber paddle anodes. Experiments performed in O_2-saturated 0.1 M sodium phosphate buffer (pH 7.0) with cell potential held at 0.8 V versus Ag/AgCl. Error bars represent 1 standard deviation of 3 trials.

4.3.4 GOX-pFcAc-based EBFC performance

GOX-pFcAc-based EBFCs were constructed with a single GOX-pFcAc-gold/MWCNT fiber paddle anode and single BOD-gold/MWCNT fiber paddle cathode connected through an external circuit without membrane separation. BOD is a multicopper oxidase that catalyzes the reduction of oxygen to water and is commonly used as a cathodic working enzyme in EBFCs due its proven capability of DET.[100, 182] The performances of all EBFCs were tested through the manual variation of circuit resistance while monitoring circuit voltage (**Figure 4.14**).

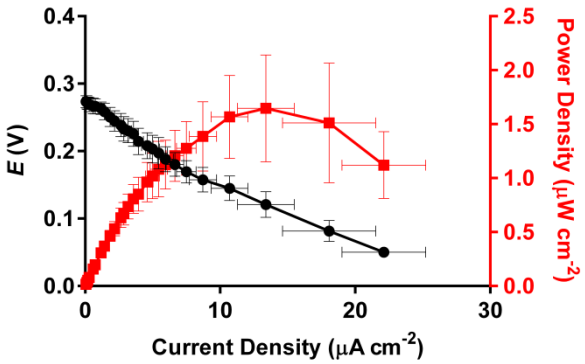

Figure 4.14 EBFC performance of GOX-pFcAc-gold/MWCNT fiber paddle anodes. Performance and cell-polarization curves of EBFCs with GOX-pFcAc-gold/MWCNT fiber paddle anodes and BOD-gold/MWCNT fiber paddle cathodes. Experiments were performed in air-saturated 0.1 M sodium phosphate buffer (pH 7.0) with 0.1 M glucose. Error bars represent 1 standard deviation of 3 trials.

For EBFCs utilizing GOX-pFcAc-gold/MWCNT fiber paddle anodes, the observed maximum power density was 1.66 ± 0.47 μW cm^{-2}, which was 4-fold greater compared to EBFCs using GOX-gold/MWCNT fiber paddle anodes.[288] Further, the open circuit voltage (OCV) of EBFCs with GOX-pFcAc-gold/MWCNT fiber paddle anodes was 0.27 ± 0.01 V, which was similar to those modified with native GOX.[288] These results showed the capability of pFcAc modification through PBPE to increase current density without limiting the cell

voltage, a common disadvantage in MET-type systems.[39, 68] Further, EBFCs constructed with GOX/FcAc monomer-gold/MWCNT fiber paddle anodes exhibited maximum power densities of only 4 ± 2 nW cm^{-2} with decreased performance likely a result of inhibited GOX activity by free FcAc and detachment of free FcAc in the membrane-less system (**Figure 4.15**). Non-functionalized gold/MWCNT fiber paddle anodes were previously shown to demonstrate negligible power generation.[288] These results confirmed the benefits of pFcAc "wiring" GOX to the electrode surface and thus increasing electron transfer rates for greater power generation despite decreased GOX biocatalytic activity.

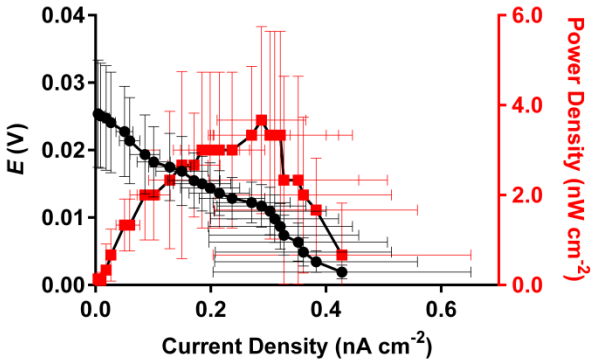

Figure 4.15 EBFC performance of GOX/FcAc monomer-gold/MWCNT fiber paddle anodes. Performance and cell-polarization curves of EBFCs with GOX/FcAc monomer-gold/MWCNT fiber paddle anodes and BOD-functionalized gold/MWCNT fiber paddle cathodes. Experiments performed in air-saturated 0.1 M sodium phosphate buffer (pH 7.0) with 0.1 M glucose. Error bars represent 1 standard deviation of 3 trials.

A major issue in the development of EBFCs has been the instability of power generation over time.[12, 228, 313] The use of free redox-mediators within EBFCs introduces additional stability concerns due to the tendency of these small molecule mediators to diffuse away from the working system.[39] The output power density of our EBFCs utilizing GOX-pFcAc-

gold/MWCNT fiber paddle anodes steadily decreased during continuous operation (**Figure 4.16A**).

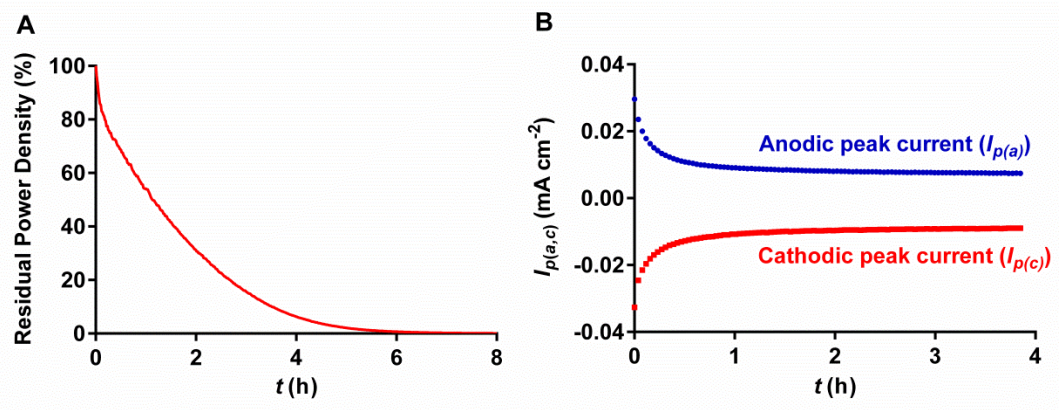

Figure 4.16 Electrochemical stability of GOX-pFcAc-gold/MWCNT fiber paddle anodes. A) Characteristic residual power density of EBFC with GOX-pFcAc-gold/MWCNT fiber paddles anodes and BOD-gold/MWCNT fiber paddle cathodes under continuous operation. Residual power density relative to maximum power density at t = 0. Experiments performed in air-saturated 0.1 M sodium phosphate buffer (pH 7.0) with 0.1 M glucose. B) Dependence of anodic (blue circle) and cathodic (red square) peak currents on time for consecutive CV traces of GOX-pFcAc-gold/MWCNT fiber paddle anodes. Experiments performed in argon-saturated 0.1 M sodium phosphate buffer (pH 7.0) at a scan rate of 10 mV s^{-1}.

This instability was likely caused due to enzyme activity and electron transfer functionality loss at the modified gold/MWCNT fiber paddle anodes. Indeed, consecutive CV traces of GOX-pFcAc-gold/MWCNT fiber paddle anodes confirmed a continuous decrease in ferrocene faradaic current density, which suggested either detachment of GOX-pFcAc from the electrode surface over time, loss of electron transfer efficiency through pFcAc or a combination of these factors (**Figure 4.16 and Figure 4.17**).[39, 180] This configuration did not solve the issue of power generation stability, but conjugation of redox polymer directly to the enzyme surface provides the potential for simultaneous covalent attachment of working enzyme coupled with redox mediator for increased stability, which will be a goal of our future work.

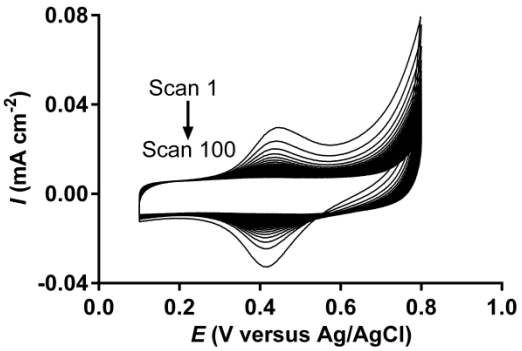

Figure 4.17 Electrochemical stability of GOX-pFcAc-gold/MWCNT fiber paddle anodes. Consecutive CV traces of GOX-pFcAc-gold/MWCNT fiber paddle anodes. Experiments performed in argon-saturated 0.1 M sodium phosphate buffer (pH 7.0) at a scan rate of 10 mVs^{-1}.

The characterizations described in this study allowed us to evaluate the use of PBPE to grow ferrocene-containing redox polymers from the surface of GOX *via* "grafting from" SI-ATRP as a new method toward the development of MET-type EBFC anodes. Indeed, the prepared GOX-pFcAc-gold/MWCNT fiber paddle anodes exhibited a dramatically increased current generation efficiency compared to unmodified GOX despite a lower biocatalytic turnover rate. This improvement in performance provided a 4-fold increase in EBFC power density over native GOX with a large loss of power generation observed when free FcAc monomer was adsorbed along with GOX. Our immediate next steps are to fully characterize EBFC stability and to report on strategies we are developing to overcome the low stability observed within our systems.

4.4 Conclusions

We have developed and thoroughly characterized a GOX-based electrode system formed by the growth of poly(*N*-(3-dimethyl(ferrocenyl)methylammonium bromide)propyl acrylamide) from the enzyme surface *via* PBPE techniques followed by the physical adsorption of these GOX-pFcAc conjugates onto gold/MWCNT fiber paddle electrodes. The final GOX-pFcAc-

gold/MWCNT fiber paddles anodes proved capable of MET through the covalently attached redox polymer chains while maintaining GOX biocatalytic activity. The effective "wiring" of GOX through pFcAc led to a 24-fold increase in current generation efficiency compared to native GOX adsorbed onto the same electrode material. This performance enhancement extended to the capability of GOX-pFcAc-gold/MWCNT fiber paddle anodes coupled with BOD-gold/MWCNT fiber paddle cathodes to produce a 4-fold greater EBFC power density (1.7 μW cm^{-2}) compared to GOX-gold/MWCNT fiber paddle anodes without the presence of free mediator and thus no need for compartmentalization. With a variety of potential polymer types, mediator groups and working enzymes to select from, PBPE represents a powerful new tool in the development enzyme-mediator conjugate synthesis toward improved MET-type EBFCs.

Chapter 5: Intramolecular Direct Electron Transfer through Poly-Ferrocenyl Glucose Oxidase Conjugates to Carbon Electrodes: 1. Sensor Sensitivity, Selectivity and Longevity

5.1 Introduction

Reliable, accurate determination of glucose concentrations is of high importance in a range of applications including food processing and diabetes management. [1, 15, 38] In particular, enzyme-based biosensors have been intensely studied due to their superb selectivity, specificity and sensitivity. [21, 43, 314] Enzyme-based amperometric biosensors electrochemically detect a target analyte using an enzyme as the recognition element coupled with transduction of the biocatalytically generated electrons into an electric current at an electrode surface with an applied potential.[21] Commonly, glucose oxidase (GOX) is used as the working enzyme to catalyze glucose oxidation at its flavin adenine dinucleotide cofactor (FAD)-based active site according to:

$$\mathrm{GOX_{FAD}} + \mathrm{glucose} \rightarrow \mathrm{GOX_{FADH_2}} + \mathrm{gluconolactone} \quad (5.1)$$

$$\mathrm{GOX_{FADH_2}} + \mathrm{O_2} \rightarrow \mathrm{GOX_{FAD}} + \mathrm{H_2O_2} \quad (5.2)$$

The development of enzyme-based glucose biosensors began with the work of Clark and Lyons, who in 1962 proposed the detection of glucose through monitoring of oxygen depletion at an oxygen reducing electrode caused by this GOX mediated reaction.[10] Similar systems were later developed based on detection of hydrogen peroxide.[35] These types of biosensors, that depend on the detection of enzymatic reaction product or co-substrate, were first-generation glucose biosensors.[1] Selectivity and sensitivity issues caused by oxidation of other physiologically present species at the high working potentials required and reliance on oxygen concentration, respectively, led researchers to develop second-generation glucose biosensors. These types of devices rely on redox mediators such as ferrocene-, osmium- or quinone-

containing compounds to shuttle electrons between the enzyme active site and the electrode surface [33, 55] according to:

$$\mathrm{GOX_{FADH_2}} + 2\mathrm{Med_{Ox}} \rightarrow \mathrm{GOX_{FAD}} + 2\mathrm{Med_{Red}} + 2\mathrm{H^+} \quad (5.3)$$

$$2\mathrm{Med_{Red}} \xrightarrow{\text{electrode}} 2\mathrm{Med_{Ox}} + 2\mathrm{e^-} \quad (5.4)$$

where Med_{Ox} and Med_{Red} represent the oxidized and reduced versions of the selected mediator, respectively. Utilization of these mediators allowed for operation at working potentials closer to the redox potential of the working enzyme, but freely diffusing redox groups also posed significantly increased stability and toxicity concerns.[1] Unfortunately, the dense protein layer surrounding the GOX active site hinders reliable electron transfer directly from the active site to an electrode (third-generation glucose biosensors).[44]

The limited applicability of second-generation glucose biosensors using diffusive mediators resulted in the development of systems that utilized enzymes entrapped within redox containing polymer networks [160, 315] as well as electron relays attached directly to the enzyme surface. [122, 162, 163, 170, 316] Conjugation of redox groups to the backbone of an enzyme-containing polymer network or directly to an enzyme surface served to reduce leaching of the potentially toxic molecules while still promoting improved electron transfer efficiencies. [1, 117, 170] In particular, ferrocene-based systems have been intensely studied for both cases due to the chemical stability, pH and oxygen independence and well characterized, reversible electron transfer kinetics of ferrocene. [168] A wide array of ferrocene-containing polymer systems has been reported with varying polymer types and configurations that effectively "wire" the entrapped enzymes to the electrode by conducting electrons through the polymer network *via* self-exchange of electrons or holes between colliding reduced and oxidized redox centers. [117, 159] Individual electron relays attached to the surface of GOX such as ferrocene-

monocarboxylic acid or ferrocene-acetic acid were shown to promote intramolecular electron transfer from the FAD-cofactor-based active site of GOX to the attached ferrocene groups and subsequently to an electrode. [122, 170]

We previously reported initial findings on a combination of these approaches in which we grew ferrocene-containing polymers directly from the surface of GOX using polymer-based protein engineering (PBPE).[317] Briefly, poly(*N*-(3-dimethyl(ferrocenyl) methylammonium bromide)propyl acrylamide (pFcAc) was grown from GOX in a "grafting from" approach *via* atom transfer radical polymerization (ATRP). The resulting GOX-pFcAc conjugates yielded a 24-fold increase in current generation efficiency and a 4-fold increase in enzyme-based biofuel cell (EBFC) power density.[317] PBPE represents a well-controlled method to tailor enzyme function through modification with a wide library of designed, functional polymers.[196, 200, 209, 215, 217-223, 317] For GOX-pFcAc-based electrodes, modification of the enzyme surface with polymer chains that contained pendant ferrocene groups at each monomer provided the possibility of both intramolecular electron transfer as well as electron conduction *via* self-exchange through the grown polymer chains and neighboring GOX-pFcAc conjugates.

Herein, we report on the thorough characterization of a GOX-pFcAc-based glucose biosensor operating using a combination of intramolecular electron transfer and self-exchange electron conduction mechanisms (**Figure 5.1**). Human serum albumin (HSA) was crosslinked along with GOX-pFcAc within a viscous chitosan solution and drop cast onto carbon paper strips. HSA was chosen as a carrier protein to promote an extensively crosslinked network and inhibit GOX-pFcAc leaching while reducing local GOX concentrations to limit potential H_2O_2 local accumulation and reduce GOX structural changes.[128, 129] Utilization of GOX-pFcAc conjugates allowed the use of simple carbon paper-based electrodes without a complicated

immobilization procedure. The objectives of this study were to electrochemically characterize GOX-pFcAc-HSA-carbon paper electrodes and evaluate their glucose sensing capabilities and longevity during storage and operation.

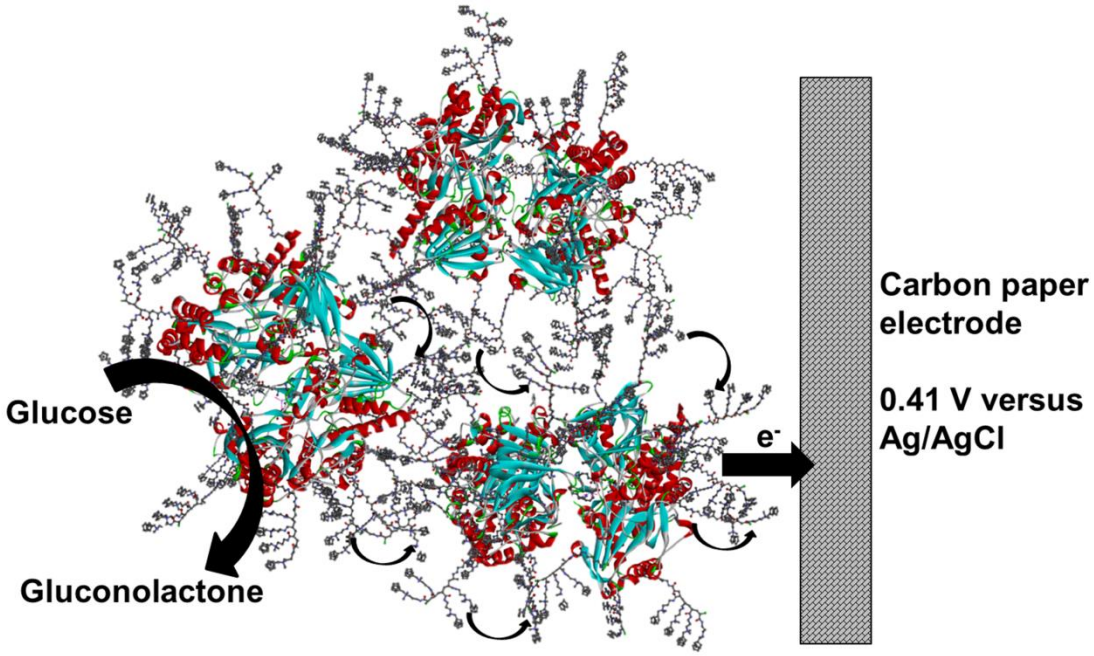

Figure 5.1 Schematic representation of GOX-pFcAc-based sensing. Intramolecular electron transfer through GOX-pFcAc conjugates *via* self-exchange through covalently coupled ferrocene compounds to carbon paper electrodes.

5.2 Materials and Methods

5.2.1 Materials

Sodium phosphate buffer (0.1 M, pH 7.0) prepared from phosphate salts using ultrapure milliQ grade water (18.2 MΩ·cm) was used in all experiments unless otherwise stated. GOX type X-S from *Aspergillus niger*, albumin from human serum, chitosan (medium molecular weight), poly-L-lysine (70-150 kDa) and heat inactivated serum from human male AB plasma were purchased from Sigma Aldrich. AvCarb© MEGL370 carbon paper was purchased from

Fuel Cell Earth. Succinate succinimidyl polyethylene glycol (NHS-PEG-NHS; MW 5000) was purchased from NANOCS. All chemicals were of analytical grade and used as received.

5.2.2 Biosensor fabrication

We prepared GOX-pFcAc conjugates as previously described.[317] Chit-GOX-pFcAc-HSA-carbon paper electrodes were formed by drop casting 20 µL of 5 mg mL^{-1} NHS-PEG-NHS, 10 mg mL^{-1} HSA and 1 mg mL^{-1} GOX-pFcAc (GOX:HSA 1:30 molar ratio) in viscous chitosan solution onto 2 x 0.5 cm carbon paper strips and drying at 4°C overnight. For electrodes modified with native GOX, the same concentrations were used. Viscous chitosan solution was prepared by stirring 1 wt % chitosan in 1% acetic acid solution at 60 °C for 4 h. Enzyme-functionalized electrodes without chitosan coating were formed by dissolving the enzyme/crosslinker mixture in 0.1 M sodium phosphate buffer (pH 7.0) rather than viscous chitosan solution.

5.2.3 Biosensor characterization

We performed all electrochemical measurements using a conventional three-electrode electrochemical cell utilizing a KCl-saturated Ag/AgCl reference electrode and a 0.5 mm diameter platinum wire counter electrode. Reported current densities are relative to the geometric surface area of dried, drop cast solution. Initial glucose concentration of heat treated human AB serum was determined using a TRUEresult® glucose test meter and TRUEtest glucose test strips from NIPRO diagnostics.

5.3 Results and Discussion

5.3.1 Characterization of Chit-GOX-pFcAc-HSA-carbon paper electrodes

We previously showed the capability of GOX-pFcAc conjugates to improve electron transfer efficiency in enzyme-modified electrodes.[317] The performance of these conjugates led us to investigate their application toward enzyme-based glucose biosensors (**Figure 5.1**). GOX-pFcAc conjugates were fabricated through PBPE by attaching water soluble, NHS-functionalized ATRP initiators to primary amines on the GOX surface (*i.e.* accessible surface lysines and *N*-termini) and growing pFcAc by "grafting from" ATRP as described previously.[317] The resulting GOX-pFcAc conjugates were crosslinked along with HSA by a dual NHS-functionalized PEG linker within a viscous chitosan solution at a molar ratio of 30:1 HSA:GOX. Crosslinking with inert carrier proteins has been shown to improve retained enzymatic activity through reduction of intramolecular linkages that could cause extensive conformational changes and through limitation of local H_2O_2 accumulation that could lead to GOX deactivation.[43, 128, 129, 318, 319] Analysis by SDS-PAGE confirmed crosslinking with the appearance of broad, streaked bands in lanes that included crosslinker (**Figure 5.2**). The viscous chitosan solution slowed the precipitation of GOX-pFcAc conjugates, which allowed for more consistent electrode preparation. GOX-pFcAc-HSA or Chit-GOX-pFcAc-HSA solutions were subsequently drop cast onto carbon paper strips and dried overnight prior to use.

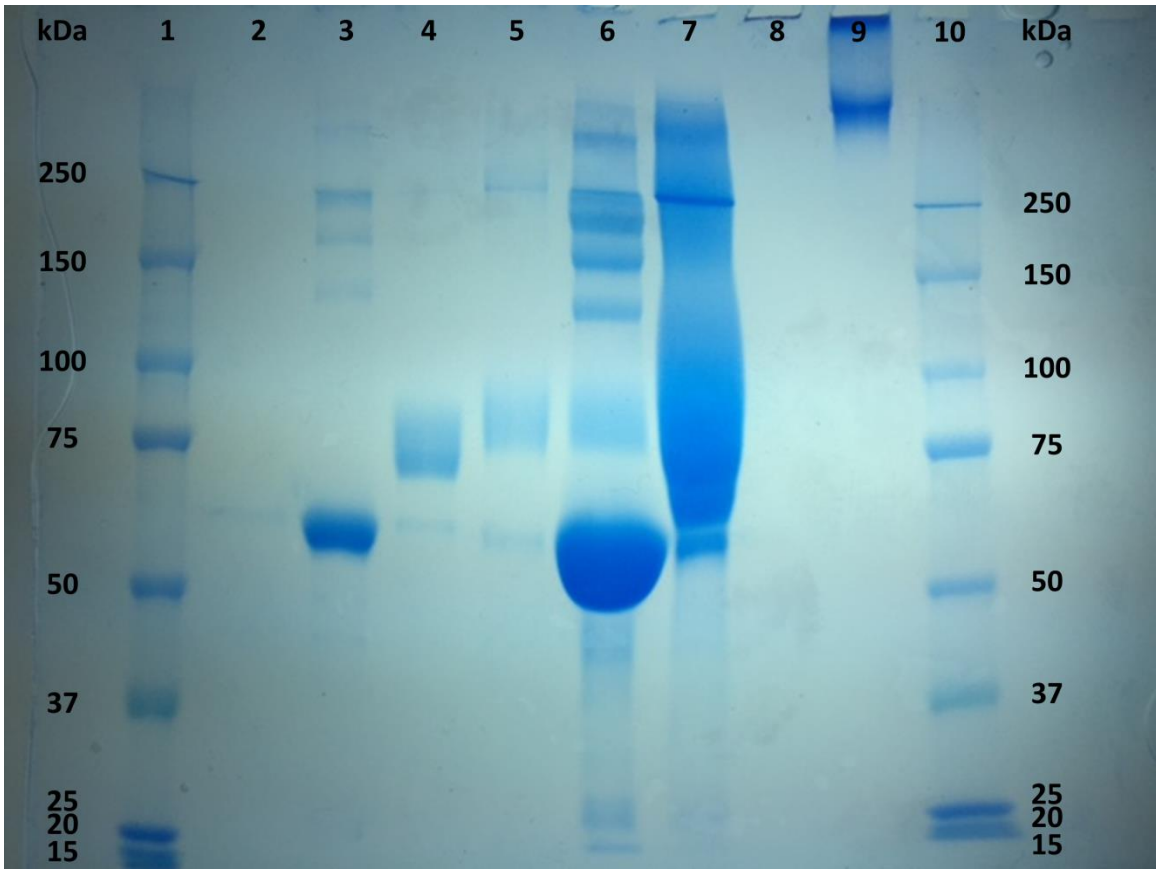

Figure 5.2 SDS-PAGE analysis of protein crosslinking. Lane 1: protein ladder; Lane 2: 5 mg mL^{-1} NHS-PEG-NHS; Lane 3: 1 mg mL^{-1} HSA; Lane 4: 1 mg mL^{-1} GOX; Lane 5: 1 mg mL^{-1} GOX-pFcAc; Lane 6: 10 mg mL^{-1} HSA and 1 mg mL^{-1} GOX-pFcAc; Lane 7: 10 mg mL^{-1} HSA, 1 mg mL^{-1} GOX-pFcAc and 5 mg mL^{-1} NHS-PEG-NHS; Lane 8: 1 mg mL^{-1} poly-L-lysine; Lane 9: 1 mg mL^{-1} poly-L-lysine and 5 mg mL^{-1} NHS-PEG-NHS; Lane 10: protein ladder.

Redox-polymer networks conduct electrons *via* self-exchange of electrons or holes between colliding reduced and oxidized redox species whereas intramolecular electron transfer within redox-modified enzymes is achieved through re-oxidation of the enzyme active site by redox groups bound to the enzyme surface near the active site.[117, 170] Reports claim that conduction by electron hopping is rarely observed in either case and that intramolecular electroactivity relies on the location of a few key redox groups close to the FAD-based active site of GOX rather than the number of redox-modified sites.[117, 170] Our previous characterization

of GOX-pFcAc conjugates suggested the presence of pFcAc chains within 4 Å of the GOX active site and confirmed multiple pendant ferrocene groups per chain.[317] Thus, we hypothesized that GOX-pFcAc conjugates were capable of intramolecular electron transfer between the FAD-based GOX active site and covalently bound pFcAc chains followed by electron self-exchange through the GOX-pFcAc conjugates to an electrode surface.

Cyclic voltammetry (CV) traces of control and enzyme-modified carbon paper electrodes confirmed heterogeneous electron transfer between GOX-pFcAc conjugates and the electrode surface (**Figure 5.3**). GOX-pFcAc-HSA-carbon paper electrodes and Chit-GOX-pFcAc-HSA-carbon paper electrodes showed clear oxidation and reduction peaks with peak separations of 0.08 V and 0.07 V, respectively, characteristic of quasi-reversible electron transfer. Both electrode types exhibited a formal potential of 0.41 V versus Ag/AgCl (**Figure 5.3A**). This result suggested the presence of chitosan during fabrication did not significantly impact electron transfer between GOX-pFcAc and the carbon paper surface. Indeed, linear sweep voltammetry (LSV) analysis of GOX-pFcAc-HSA-carbon paper electrodes and Chit-GOX-pFcAc-HSA-carbon paper electrodes yielded matching glucose oxidation onset potentials, which proved that the incorporation of chitosan during fabrication did not introduce additional overpotentials within the network (**Figure 5.3B**). An obvious oxidative shift was observed upon the injection of 10 mM glucose to Chit-GOX-pFcAc-HSA-carbon paper electrode CV trials, which indicated turnover of glucose by bioactive GOX and subsequent electron transfer through pFcAc to the carbon paper electrodes (**Figure 5.3A**).

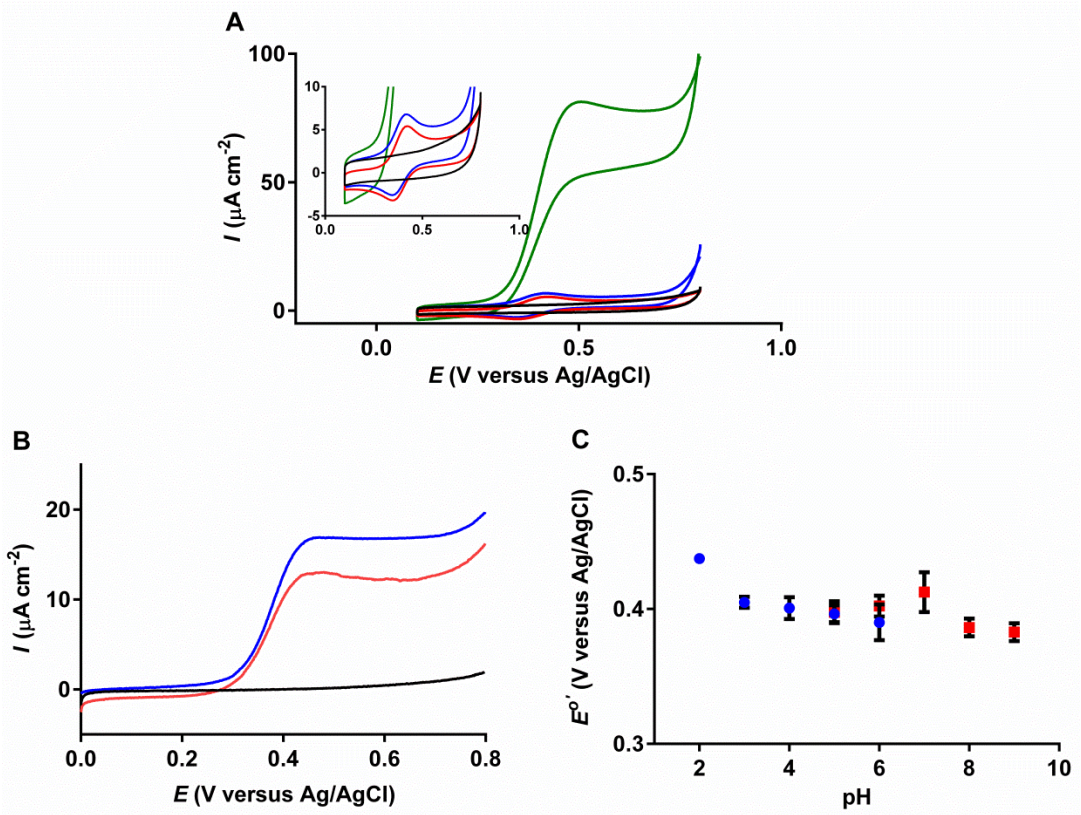

Figure 5.3 Electrochemical characterization of Chit-GOX-pFcAc-HSA-carbon paper electrodes. A) Typical CV traces of carbon paper electrode (black), GOX-pFcAc-HSA-carbon paper electrode (red), Chit-GOX-pFcAc-HSA-carbon paper electrode (blue) and Chit-GOX-pFcAc-HSA-carbon paper electrode with 10 mM glucose (green) in argon-saturated 0.1 M sodium phosphate buffer (pH 7.0) at a scan rate of 10 mV s^{-1}. Inset: low current density range of typical CV traces. B) Typical LSV traces of carbon paper electrode (black), GOX-pFcAc-HSA-carbon paper electrode (red) and Chit-GOX-pFcAc-carbon paper electrode (blue) in argon-saturated 0.1 M sodium phosphate buffer (pH 7.0) with 10 mM glucose at a scan rate of 1 mV s^{-1}. C) Chit-GOX-pFcAc-HSA-carbon paper electrode formal potential at varying buffer pH in either 0.1 M sodium phosphate buffer (pH 5.0-9.0)(red square) or 0.1 M citrate buffer (pH 2.0-6.0)(blue circle). Error bars represent 1 standard deviation of 3 trials.

The observed formal potential of Chit-GOX-pFcAc-HSA-carbon paper electrodes was found to be stable over a wide range of pH, consistent with the pH-independent oxidation and reduction of ferrocene (**Figure 5.3C**).[307, 320] The slight increase in formal potential exhibited

below pH 3.0 could have been caused by an increase in oxidation resistance due to positively charged GOX under those conditions (GOX p*I* = 4.2).[308] The insensitivity of such ferrocene-based glucose biosensors to variations in pH leads to increased reliability compared to first-generation GOX-based glucose biosensors, which vary in response with pH as a result of proton exchange during the complete enzymatic reaction (**Equation (5.1)** and **Equation (5.2)**).[320] The confirmation of GOX bioactivity coupled with successful electron transfer through GOX-pFcAc conjugates to carbon paper electrodes motivated us to investigate Chit-GOX-pFcAc-HSA-carbon paper electrodes as enzyme-based glucose biosensors.

5.3.2 Chit-GOX-pFcAc-HSA-carbon paper glucose sensing

We determined the glucose sensing behavior of the enzyme-modified electrodes using amperometry at varying glucose concentrations with cell voltage held at the observed formal potential of pFcAc at pH 7.0 (0.41 V versus Ag/AgCl) (**Figure 5.4**). Stepwise, reproducible increases in current density upon glucose injection were observed in assays using either GOX-pFcAc-HSA-carbon paper biosensors or Chit-GOX-pFcAc-HSA-carbon paper biosensors, but not when testing GOX-HSA-carbon paper biosensors (**Figure 5.4A**). Negligible current generation by native GOX at carbon paper electrodes under these conditions confirmed electron transfer through pFcAc rather than by oxidation of biocatalytically produced H_2O_2 as in first-generation glucose biosensors.[1, 317] In each assay, the solution was stirred briefly upon each glucose injection and capacitive current influence from carbon paper was removed through background subtraction of steady-state current density with no glucose present.

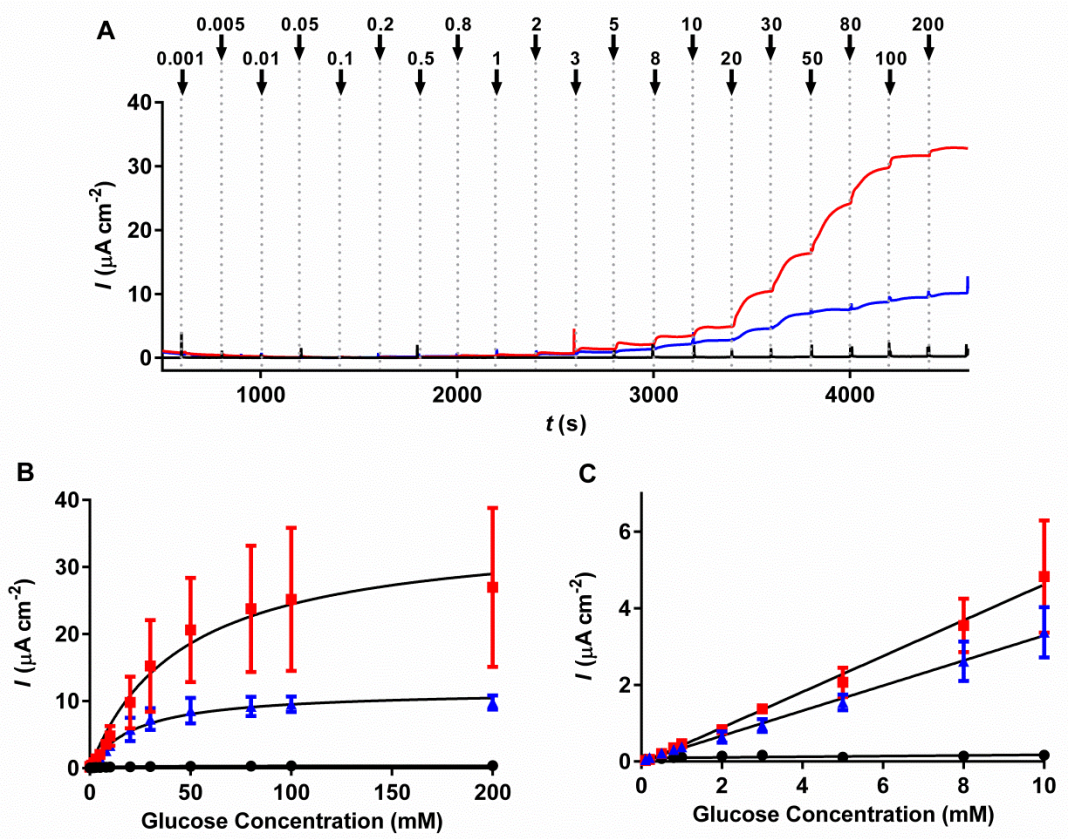

Figure 5.4 Glucose sensing analysis of Chit-GOX-pFcAc-HSA-carbon paper biosensors. A) Typical amperometric sensing evaluation of GOX-HSA-carbon paper biosensor (black), GOX-pFcAc-HSA-carbon paper biosensor (red) and Chit-GOX-pFcAc-HSA-carbon paper biosensor (blue) in air-saturated 0.1 M sodium phosphate buffer (pH 7.0) with brief stirring upon glucose injection. Potential held at 0.41 V versus Ag/AgCl. Glucose injections indicated by arrows with resulting concentrations given in mM. B) Average current density 20 to 10 s prior to subsequent glucose injection at each corresponding glucose concentration (data fit to Michaelis-Menten kinetics model). C) Linear fit of average current density data. Error bars represent 1 standard deviation of 3 trials.

We used the average steady-state current density response upon glucose addition to calculate apparent Michaelis-Menten kinetics of heterogeneous electron transfer (**Figure 5.4B**). Steady-state responses to glucose additions were reached within 2 min. GOX-pFcAc-HSA-carbon paper biosensors and Chit-GOX-pFcAc-HSA-carbon paper biosensors exhibited apparent

Michaelis-Menten constants (K_M^{app}) of 45.7 ± 12.4 mM glucose and 22.3 ± 2.7 mM glucose, respectively, which was characteristic of a greater affinity for glucose binding within the chitosan-containing network. Chit-GOX-pFcAc-HSA-carbon paper biosensors also showed a much more consistent response evident by the lower magnitude of standard deviation between trials (**Figure 5.4B**). The GOX-pFcAc-HSA-carbon paper biosensors were, however, capable of generating a higher maximum current density (J_{max}) (35.60 ± 3.84 μA cm^{-2}) than Chit-GOX-pFcAc-HSA-carbon paper biosensors (11.63 ± 0.45 μA cm^{-2}). GOX-HSA-carbon paper biosensors showed dramatically lower responses to glucose than GOX-pFcAc conjugate-based biosensors with a K_M^{app} of 11.3 ± 2.9 mM glucose and J_{max} of 0.38 ± 0.03 μA cm^{-2} (**Figure 5.4B**).

Biosensor responses were linear over the concentration range 0.1 – 10 mM glucose, which spanned normal physiological conditions (4.4 – 6.6 mM) (**Figure 5.4C**).[1] GOX-pFcAc-HSA-carbon paper biosensors yielded an average glucose sensitivity of 0.47 ± 0.03 μA mM^{-1} cm^{-2} (R^2 = 0.9236) whereas Chit-GOX-pFcAc-HSA-carbon paper biosensors showed an average glucose sensitivity of 0.33 ± 0.01 μA mM^{-1} cm^{-2} (R^2 = 0.9536). GOX-HSA-carbon paper biosensors exhibited much lower responses with an average glucose sensitivity of only 8.3 ± 2.9 nA mM^{-1} cm^{-2} (R^2 = 0.2255). The relatively low impact of chitosan on biosensor sensitivity coupled with increased response reproducibility led us to further investigate Chit-GOX-pFcAc-HSA-carbon paper biosensors. We estimated the limit of detection for Chit-GOX-pFcAc-HSA-carbon paper biosensors to be 0.07 mM glucose based on the signal-to-noise ratio. The observed glucose sensing metrics were similar to previously described glucose biosensors utilizing redox-polymers.[173, 321-323]

We tested the physiologic applicability of the Chit-GOX-pFcAc-HSA-carbon paper biosensors by examining glucose sensing in human serum (**Figure 5.5**). Compared to sensing in buffered solution, experiments carried out in human serum or whole blood contain many sources of interference and instability including interactions with proteins, enzyme inhibition by transition metal ions and interfering oxidation reactions at the electrode surface.[324-326] Indeed, glucose sensing characteristics in human AB serum were far less reproducible than in buffered solution (**Figure 5.5**). Nevertheless, we observed both J_{max} and the average glucose sensitivity to be greater than assays in buffered solution with values of 110.5 ± 7.9 μA cm^{-2} and 29.38 ± 13.71 μA mM^{-1} cm^{-2} (R^2 = 0.2610), respectively. The observed K_M^{app} also decreased to 6.9 ± 1.5 mM glucose. These results were likely due to the constant stirring during the amperometric evaluation required to maintain serum dispersion. Further, the reported linear range of glucose concentrations (3.89 – 4.79 mM total glucose including 3.79 mM glucose initially as determined using a commercial glucose test meter) resulted in an extremely low correlation coefficient (R^2 = 0.2610), which limit reliable glucose concentration determination (**Figure 5.5C**). However, Chit-GOX-pFcAc-HSA-carbon paper biosensors clearly retained GOX bioactivity and electron transfer capabilities throughout the serum sensing evaluation (**Figure 5.5**).

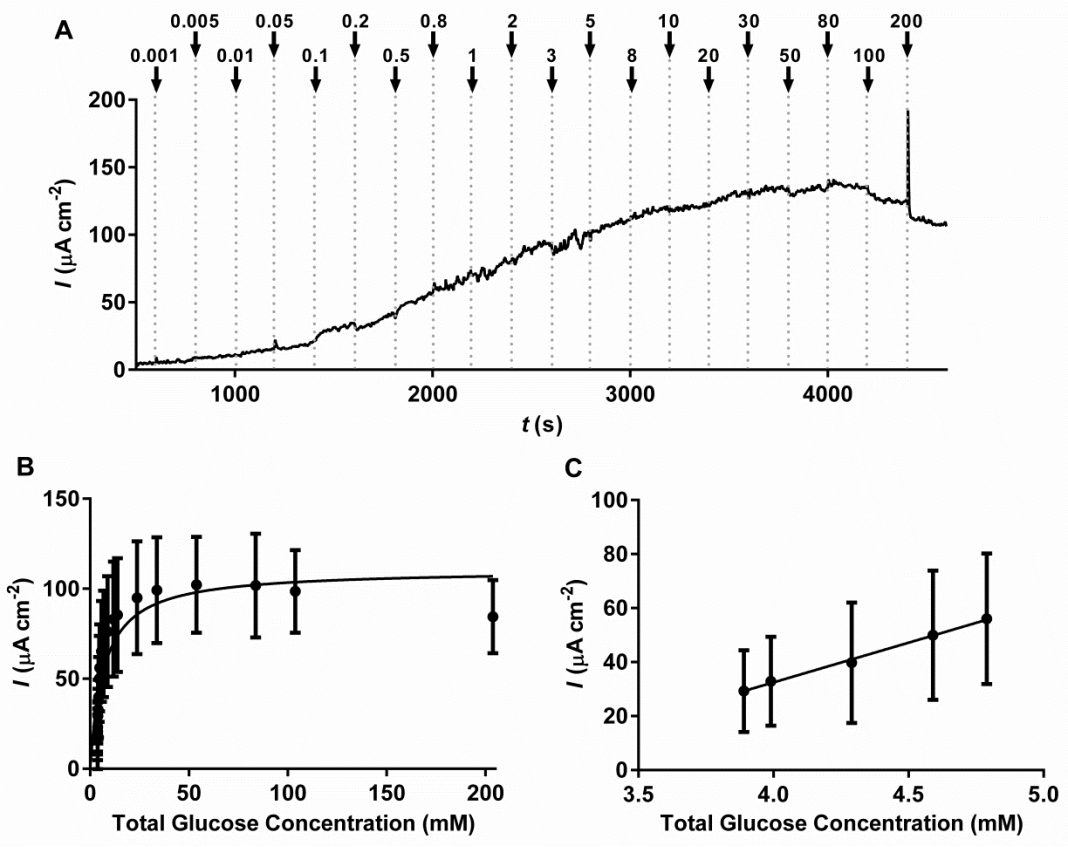

Figure 5.5 Glucose sensing analysis of Chit-GOX-pFcAc-HSA-carbon paper biosensors in human serum. A) Typical amperometric sensing evaluation of Chit-GOX-pFcAc-HSA-carbon paper biosensors in air-saturated serum from human AB plasma under constant stirring. Potential held at 0.41 V versus Ag/AgCl. Glucose injections indicated by arrows with resulting concentrations given in mM. B) Average current density 20 to 10 s prior to subsequent glucose injection at each corresponding glucose concentration (data fit to Michaelis-Menten kinetics model). C) Linear fit of average current density data. Error bars represent 1 standard deviation of 3 trials.

GOX is commonly used for the development of glucose biosensors due to its superior selectivity toward glucose compared to other glucose oxidizing enzymes such as glucose dehydrogenase.[38] Chit-GOX-pFcAc-HSA-carbon paper glucose sensors exhibited superb selectivity when challenged with other sugars (**Figure 5.6**). This characteristic would prove beneficial toward physiologic application to limit response fluctuations caused by other sugars.

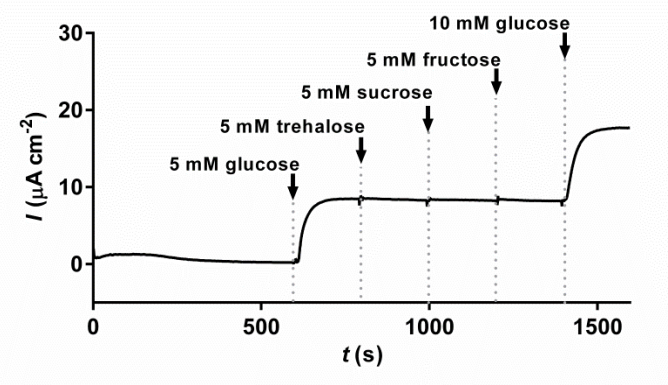

Figure 5.6 Selectivity of Chit-GOX-pFcAc-HSA-carbon paper biosensor glucose sensing. Typical amperometric evaluation of Chit-GOX-pFcAc-HSA-carbon paper biosensors in air-saturated 0.1 M sodium phosphate buffer pH 7.0 with constant stirring upon injections of varying sugars. Potential held at 0.41 V versus Ag/AgCl. Injections indicated by arrows with resulting concentrations given in mM.

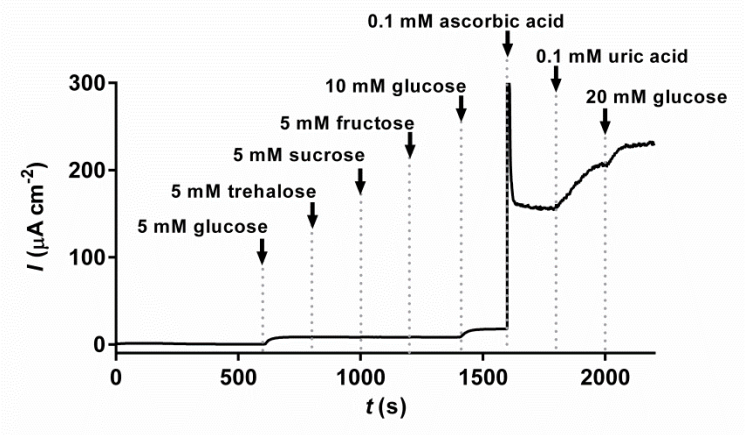

Figure 5.7 Interference impacts on Chit-GOX-pFcAc-HSA-carbon paper biosensor glucose sensing. Typical amperometric evaluation of Chit-GOX-pFcAc-HSA-carbon paper biosensors in air-saturated 0.1 M sodium phosphate buffer pH 7.0 with constant stirring upon injections of varying sugars and interfering agents. Potential held at 0.41 V versus Ag/AgCl. Injections indicated by arrows with resulting concentrations given in mM.

However, physiologically present interfering agents (*i.e.* ascorbic acid and uric acid) had a significant impact on current generation (**Figure 5.7**). Ascorbic acid and uric acid were both

likely oxidized by the electrode material or ferrocene groups at the applied potential [327, 328]. Thus, additional design concerns would need to be implemented prior to operation in physiological samples.

5.3.3 Response and longevity tailoring of Chit-GOX-pFcAc-HSA-carbon paper biosensors

Utilization of GOX-pFcAc conjugates capable of both intramolecular re-oxidation of the FAD-based GOX active site and electron transfer by self-exchange through pFcAc allowed for a simple fabrication approach to form carbon paper-based glucose biosensors. Consequently, we were able to predictably tailor the response of Chit-GOX-pFcAc-HSA-carbon paper biosensors by varying the GOX-pFcAc concentration during fabrication (**Figure 5.8A**). All other fabrication parameters were held constant. The resulting peak current density at 10 mM glucose injection resembled a first order increase with increasing GOX-pFcAc concentration (**Figure 5.8B**).

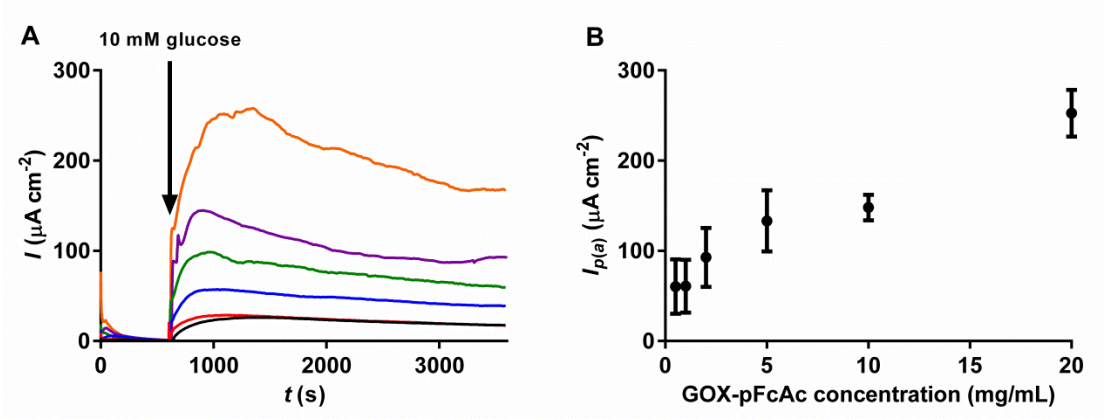

Figure 5.8 Amperometry of Chit-GOX-pFcAc-HSA-carbon paper biosensors with varying GOX concentration in fabrication. A) Typical amperometric evaluation of Chit-GOX-pFcAc-HSA-carbon paper biosensors fabricated using 20 mg mL^{-1} (orange), 10 mg mL^{-1} (purple), 5 mg mL^{-1} (green), 2 mg mL^{-1} (blue), 1 mg mL^{-1} (red) or 0.5 mg mL^{-1} (black) upon 10 mM glucose injection in air-saturated 0.1 M sodium phosphate buffer (pH 7.0). B) Average peak current density of Chit-GOX-pFcAc-HSA-carbon paper biosensors with varying GOX concentration in fabrication upon 10 mM glucose injection. Error bars represent 1 standard deviation of 3 trials.

This type of trend was characteristic of intramolecular electron transfer as intermolecular electron transfer rates would likely increase more rapidly with GOX-pFcAc concentration.[162, 170] In our system, intermolecular electron transfer would occur if a pFcAc group attached to one GOX molecule were to re-oxidize the active site of another GOX molecule. As such, we would expect the observed current density to resemble a second order increase with increasing GOX-pFcAc concentration due to not only an increasing density of GOX molecules individually generating current but also an increasing rate of GOX active site re-oxidation. The capability to reliably vary the biosensor response during fabrication could prove useful when tailoring a single system for multiple applications. Although current density response by Chit-GOX-pFcAc-HSA-carbon paper biosensors was tailorable in magnitude, the rate of current loss relative to peak current density was independent of GOX-pFcAc concentration, which indicated similar instability sources between assays (**Figure 5.9**).

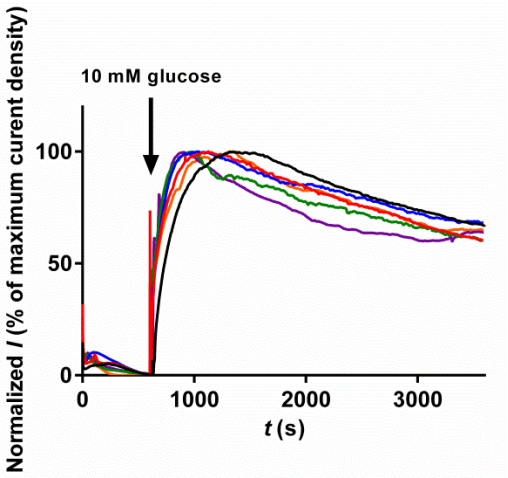

Figure 5.9 Longevity analysis of Chit-GOX-pFcAc-HSA-carbon paper biosensors with varying GOX-pFcAc concentration in fabrication. Typical amperometric evaluation of Chit-GOX-pFcAc-HSA-carbon paper biosensors fabricated using 20 mg mL^{-1} (orange), 10 mg mL^{-1} (purple), 5 mg mL^{-1} (green), 2 mg mL^{-1} (blue), 1 mg mL^{-1} (red) or 0.5 mg mL^{-1} (black) upon 10 mM glucose injection in air-saturated 0.1 M sodium phosphate buffer (pH 7.0). Current density normalized to maximum current density recorded during each trial.

We similarly investigated Chit-GOX-pFcAc-HSA-carbon paper biosensor response by varying the volume of solution drop cast onto carbon paper strips during fabrication (**Figure 5.10A**). All other constituent concentrations were held constant. However, the resulting peak current densities appeared independent of drop volume (**Figure 5.10B**). Combined, these results suggested that the Chit-GOX-pFcAc-HSA-carbon paper biosensors current density response depended directly on the immobilized density of GOX-pFcAc. Again, we observed similar longevity profiles despite changes in drop volume indicative of matching activity losses during operation (**Figure 5.11**).

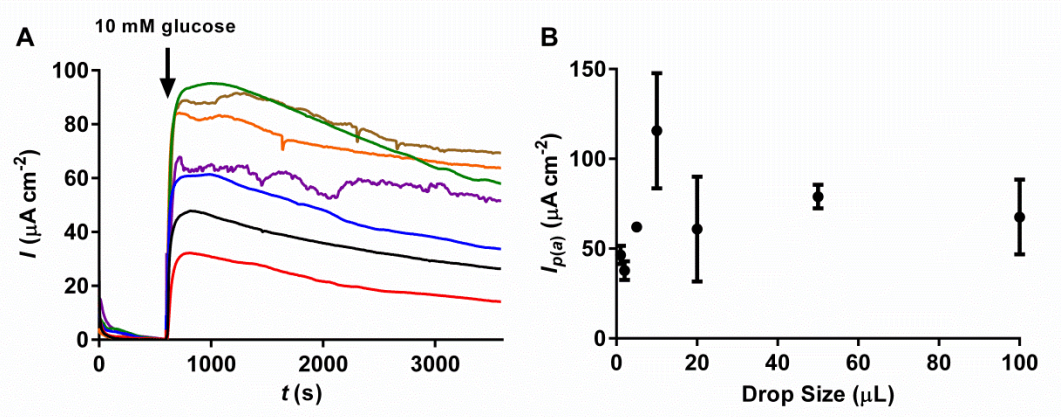

Figure 5.10 Amperometry of Chit-GOX-pFcAc-HSA-carbon paper biosensors with varying drop volume in fabrication. A) Typical amperometric evaluation of Chit-GOX-pFcAc-HSA-carbon paper biosensors fabricated using a drop cast volume of 100 µL (brown), 50 µL (orange), 20 µL (purple), 10 µL (green), 5 µL (blue), 2 µL (red) or 1 µL (black) upon 10 mM glucose injection in air-saturated 0.1 M sodium phosphate buffer (pH 7.0). B) Average peak current density of Chit-GOX-pFcAc-HSA-carbon paper biosensors with varying drop size in fabrication upon 10 mM glucose injection. Error bars represent 1 standard deviation of 3 trials.

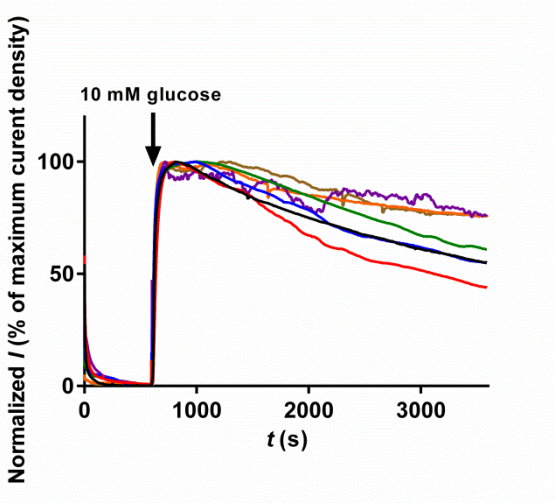

Figure 5.11 Longevity analysis of Chit-GOX-pFcAc-HSA-carbon paper biosensors with varying drop volume in fabrication. Typical amperometric evaluation of Chit-GOX-pFcAc-HSA-carbon paper biosensors fabricated using a drop cast volume of 100 µL (brown), 50 µL (orange), 20 µL (purple), 10 µL (green), 5 µL (blue), 2 µL (red) or 1 µL (black) upon 10 mM glucose injection in air-saturated 0.1 M sodium phosphate buffer (pH 7.0). Current density normalized to maximum current density recorded during each trial.

The use of paper-based glucose test strips as disposable, single use devices for determining glucose concentrations is widespread in home glucose monitoring.[329] This application places particular emphasis on reproducibility between test strips after storage. We tested the impact of dry storage by examining the resulting current density upon 10 mM glucose injection after varying periods of dry storage at 4 °C. Our Chit-GOX-pFcAc-HSA-carbon paper biosensors exhibited excellent storage stability with no significant loss of function after 4 weeks (**Figure 5.12**). Naturally, the application of our system towards continuous glucose monitoring requires the development of a deep, mechanistic understanding of the observed stability losses observed during continuous operation. We present those data in the next paper in this series.

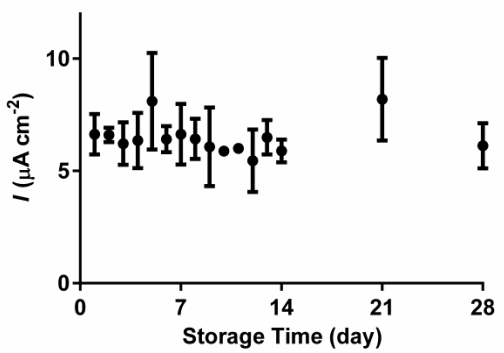

Figure 5.12 Storage stability evaluation of Chit-GOX-pFcAc-HSA-carbon paper biosensors. Average amperometric current density of Chit-GOX-pFcAc-HSA-carbon paper biosensors upon 10 mM glucose injection after electrode storage. Biosensors stored dry at 4 °C. Sensing performed in air-saturated 0.1 M sodium phosphate buffer (pH 7.0) with brief stirring upon injection. Potential held at 0.41 V versus Ag/AgCl. Error bars represent 1 standard deviation of 3 trials.

Herein, we investigated the tailoring of glucose current density response through the variation of biosensor fabrication parameters. This capability was afforded by the combination of intramolecular electron transfer by electron relays bound at the GOX surface and electron self-exchange through multiple redox moieties per chain with multiple chains bound to individual conjugates as well as electron self-exchange through adjacent conjugates. The performance of this configuration was particularly promising due to the high degree of potential optimization capable of being carried out at the level of individual conjugates. This work can be expanded and optimized using the high level of control represented by PBPE. Specifically, PBPE techniques allow the tailoring of polymer chain length and attached chain density, which can be extended to vary the enzyme to polymer ratio within the system of interest. Further, the pendant chain length and spacing between pendant redox groups along the polymer backbone can be tailored to modify redox group mobility, electron self-exchange rates and intramolecular electron transfer rates. The proof of performance presented here thus opens the door for new developments in

high performance enzyme-based bioelectronics through PBPE, which will be the target of future studies.

5.4 Conclusions

We have fabricated and thoroughly characterized a glucose biosensing platform based on GOX-pFcAc conjugates generated using PBPE. Chit-GOX-pFcAc-HSA-carbon paper biosensors were formed through the crosslinking of GOX-pFcAc conjugates along with HSA by a dual NHS-functionalized PEG linker within viscous chitosan solution and subsequent drop casting onto carbon paper strips. The combination of intramolecular electron transfer between the FAD-based GOX active site and pFcAc with electron self-exchange through pFcAc within the crosslinked network yielded a glucose sensitivity of 0.33 ± 0.01 μA mM^{-1} cm^{-2} and superb selectivity when challenged with sugars other than glucose. The biosensor response to glucose concentration was dependent on fabrication design and the sensor was stable through long-term storage. This report showed the glucose sensing capabilities of a system that merged the properties of redox polymer-containing networks with those of redox relay-functionalized enzymes. The combination of electron transfer mechanisms within individual conjugates represents a highly tailorable system with multiple degrees of potential optimization through PBPE.

Chapter 6: Intramolecular Direct Electron Transfer through Poly-Ferrocenyl Glucose Oxidase Conjugates to Carbon Electrodes: 2. Mechanistic Understanding of Long-Term Stability

6.1 Introduction

Many advances in enzyme-based biosensing technologies have been made in recent decades.[1, 21, 43, 314] Despite strides forward in sensor sensitivity, miniaturization and electron transfer modalities, a persistent deficiency in long-term stability limits the feasibility of many continuous-glucose monitoring systems.[15, 55, 74] True continuous-glucose monitoring devices should be capable of reliable determination of glucose concentrations while persisting in the test environment (*i.e.* physiological solution) for such a time as to make their use economically viable. A general sensing method displayed by enzyme-based amperometric biosensors proceeds by enzyme-catalyzed oxidation of the target substrate followed by transduction of the generated electrons into a detectable current at an electrode surface.[21] This sensing mechanism must produce a consistent response to changes in glucose concentration over time through limited deterioration of observed glucose turnover/electron transfer rates at an enzyme-functionalized electrode.[330] The most widely utilized enzyme for glucose biosensing is glucose oxidase (GOX), which catalyzes glucose oxidation according to:

$$\mathrm{GOX_{FAD}} + \mathrm{glucose} \rightarrow \mathrm{GOX_{FADH_2}} + \mathrm{gluconolactone} \qquad (6.11)$$

Enzymatic glucose oxidation is facilitated by the reduction of the flavin adenine dinucleotide cofactor (FAD)-based active site of GOX (**Equation (6.1)**).[77] Transduction of the resulting electrons into electric current must subsequently be achieved through electron transfer between reduced GOX and an electrode, which can occur through a variety of means.[1] The location of FAD deeply buried beneath the protein surface makes direct electron transfer difficult

to reliably achieve.[44] The most straightforward alternate approach is the utilization of the natural electron acceptor of GOX, oxygen by:

$$\mathrm{GOX_{FADH_2}} + \mathrm{O_2} \rightarrow \mathrm{GOX_{FAD}} + \mathrm{H_2O_2} \tag{6.2}$$

$$\mathrm{H_2O_2} \xrightarrow{\text{electrode}} \mathrm{O_2} + 2\mathrm{H^+} + 2\mathrm{e^-} \tag{6.3}$$

This path of electron conduction effectively uses oxygen as a natural electron mediator leading to the oxidation of hydrogen peroxide at positively charged electrodes (**Equation (6.3)**) and is one example of a first-generation glucose biosensor.[1, 35] Concurrent fluctuations in oxygen concentration caused by the GOX-catalyzed reaction can also be monitored through oxygen-reducing electrodes.[10, 21] Alternatively, small molecule redox mediators such as ferrocene-, osmium- or quinone-containing compounds can take the place of oxygen as electron mediators for current generation at lower working potentials (second-generation glucose biosensors).[33, 39, 55, 163] Ferrocene-based systems have been avidly researched due to reversible electrochemical kinetics, chemical stability and pH independence.[168, 180] The functionalization of enzyme-based biosensing systems with ferrocene redox mediator moieties has been achieved through several approaches including the use of freely diffusing ferrocene redox mediators, the immobilization of GOX within ferrocene-modified polymer networks and the conjugation of ferrocene-containing molecules directly to the GOX surface.[115, 122, 160, 162, 170, 315, 316] Each of these methods follows the general electron transduction scheme of:

$$\left(\mathrm{GOX_{FADH_2}}\right)\mathrm{Fc} \xrightarrow{\text{electrode}} \left(\mathrm{GOX_{FADH_2}}\right)\mathrm{Fc^+} + \mathrm{e^-} \tag{6.4}$$

$$\left(\mathrm{GOX_{FADH_2}}\right)\mathrm{Fc^+} \rightarrow (\mathrm{GOX^*_{FADH}})\mathrm{Fc} + \mathrm{H^+} \tag{6.5}$$

$$(\mathrm{GOX^*_{FADH}})\mathrm{Fc} \xrightarrow{\text{electrode}} (\mathrm{GOX^*_{FADH}})\mathrm{Fc^+} + \mathrm{e^-} \tag{6.6}$$

$$(\mathrm{GOX^*_{FADH}})\mathrm{Fc^+} \rightarrow (\mathrm{GOX_{FAD}})\mathrm{Fc} + \mathrm{H^+} \tag{6.7}$$

Individual ferrocene moieties (denoted Fc) serve to mediate electron transfer between FAD and an electrode through ferrocene oxidation into the ferrocenium ion (denoted Fc^+) by an applied working potential.[33] This ferrocene mediated oxidation of FAD can be achieved by diffusive mediators or through ferrocene redox groups conjugated to an external polymer backbone or directly to the GOX surface.[1] FAD oxidation by ferrocene groups conjugated to the surface of each respective GOX molecule has been termed "intramolecular electron transfer".[162]

Each enzyme-based biosensing approach is vulnerable to both general and individual sources of instability. Loss of enzyme activity at the electrode surface is a vital concern to be addressed in the design of any enzyme-based biosensor. This decrease in the rate of glucose turnover per unit area can occur through leaching of GOX molecules from the system or through deactivation/denaturation of GOX molecules during device storage and operation. Variations in active GOX density would lead to unreliable glucose sensing responses.[21, 288] First-generation glucose biosensors that depend on the detection of oxygen or hydrogen peroxide are further susceptible to sensitivity variations caused by fluctuating oxygen concentrations as well as selectivity issues resulting from the oxidation of physiologically present interfering agents (*i.e.* ascorbic acid, uric acid, etc.) at the required working potentials.[1] Hydrogen peroxide has been shown to also cause loss of GOX activity.[319] Any change in response output over time would necessitate additional design considerations to ensure consistent, accurate glucose readings.

Second-generation glucose biosensing systems that utilize diffusive redox mediators are prone to leaching of the small molecule redox groups due to their diffusive nature, which not only reduces the rates of mediated electron transfer (MET) over time, but also raises toxicity concerns.[1] Thus, the conjugation of these redox groups onto polymer backbones or the

working enzymes themselves could serve to limit leaching while retaining mediating capabilities.[39, 115, 117, 159] However, efficiency of the electron transfer pathways by intramolecular electron transfer and electron self-exchange through adjacent mediator groups must be maintained to avoid losses in transfer rates and thus observed current densities. These losses could occur through degradation of the selected mediator or decreased mobility of pendant redox chains.[117, 180] Ideally, an enzyme-based biosensing system should be easily tailorable to identify and address sources of instability.

Enzyme modification through polymer-based protein engineering (PBPE) has proven capable of tailoring enzyme function by tunable engineering of the enzyme surface with responsive or active polymers.[196, 200, 209, 215, 217-220, 317, 331] Utilization of atom transfer radical polymerization (ATRP) can provide precise control over the extent of enzyme-polymer modification and resulting enzyme-polymer conjugate characteristics.[197, 300] Using these methods, we designed a GOX-polymer conjugate system based on poly(*N*-(3-dimethyl(ferrocenyl)methylammonium bromide)propyl acrylamide) (pFcAc) grown from ATRP initiator sites attached directly to the GOX surface that proved capable of enhancing electron transfer efficiency in GOX-functionalized electrodes.[317] The method of electron transfer employed by these GOX-pFcAc conjugates combined intramolecular electron transfer to oxidize the FAD-based active site with electron self-exchange through the pFcAc chains on the surface of the GOX conjugates (**Equation (6.4) and Equation (6.6)**). We recently described the use of GOX-pFcAc conjugates as sensitive glucose-based biosensors and herein we report on the systematic analysis of potential sources of operational instability within the GOX-pFcAc-modified electrodes observed during characterization of glucose sensing capabilities. Chit-GOX-pFcAc-HSA-carbon paper biosensors were formed through the crosslinking of GOX-pFcAc

conjugates along with human serum albumin (HSA) within chitosan (Chit)-containing solution and subsequent drop casting onto carbon paper strips. These biosensors were capable of electron transduction *via* both pFcAc mediated intramolecular electron transfer through GOX-pFcAc conjugates (**Equations (6.4)-(6.7)**) and oxygen mediated electron transfer (**Equations (6.2)-(6.3)**; **Figure 6.1**). We identified the major sources of instability within the enzyme-polymer conjugate-containing network and used that knowledge to optimize stability.

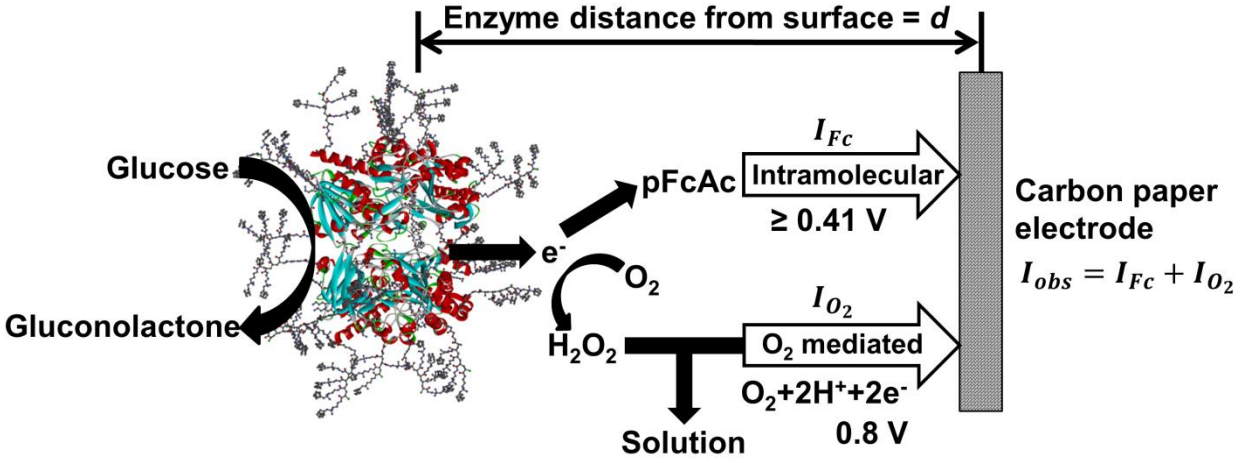

Figure 6.1 Schematic representation of electron transfer paths in GOX-pFcAc-modified biosensors. Intramolecular electron transfer coupled with electron self-exchange through GOX-pFcAc conjugates proceeded at or above 0.41 V versus Ag/AgCl (I_{Fc} = current density through ferrocene mediation). Electron transfer mediated through oxygen resulted in hydrogen peroxide oxidation at 0.8 V versus Ag/AgCl ($\boldsymbol{I_{O_2}}$= current density through oxygen mediation). I_{obs} = observed current density.

6.2 Materials and Methods

6.2.1 Materials

Sodium phosphate buffer (0.1 M, pH 7.0) prepared from phosphate salts using ultrapure milliQ grade water (18.2 MΩ·cm) was used in all experiments unless otherwise stated. GOX type X-S from *Aspergillus niger*, albumin from human serum, peroxidase from horseradish type

VI-A and chitosan (medium molecular weight) were purchased from Sigma Aldrich. AvCarb© MEGL370 carbon paper was purchased from Fuel Cell Earth. Succinate succinimidyl polyethylene glycol (NHS-PEG-NHS; MW 5000) was purchased from NANOCS. All chemicals were of analytical grade and used as received.

6.2.2 Biosensor fabrication

We prepared GOX-pFcAc conjugates as previously described.[317] Chit-GOX-pFcAc-HSA-carbon paper electrodes were formed by drop casting 20 µL of 5 mg mL^{-1} NHS-PEG-NHS, 10 mg mL^{-1} HSA and 1 mg mL^{-1} GOX-pFcAc (GOX:HSA 1:30 molar ratio) in viscous chitosan solution onto 2 x 0.5 cm carbon paper strips and drying at 4 °C overnight. For electrodes modified with native GOX, the same concentrations were used. Viscous chitosan solution was prepared by stirring 1 wt % chitosan in 1% acetic acid solution at 60 °C for 4 h. Enzyme-functionalized electrodes without chitosan coating were formed by dissolving the enzyme/crosslinker mixture in 0.1 M sodium phosphate buffer (pH 7.0) rather than viscous chitosan solution. Ellipsometry images were collected using a VCA optima series contact angle measurement system (AST products).

6.2.3 Biosensor characterization

We performed all electrochemical measurements using a conventional three-electrode electrochemical cell utilizing a KCl saturated Ag/AgCl reference electrode and a 0.5 mm diameter platinum wire counter electrode. Reported current densities are relative to the geometric surface area of dried, drop cast solution.

Protein leaching assays were performed by incubation of functionalized electrodes in 0.1 M sodium phosphate buffer (pH 7.0) with samples of supernatant taken at varying time points. Amounts of protein leached were monitored using both protein content and GOX activity assays.

Protein concentration was determined using a standard micro bicinchoninic acid (μBCA) assay kit (ThermoFisher Scientific). GOX activity in solution was determined using the standard GOX 2,2'-azino-bis(3-ethylbenzthiazoline)-6-sulfonic acid (ABTS) activity assay with native GOX and GOX-pFcAc solution kinetic parameters determined previously.[317]

6.3 Results and Discussion

6.3.1 Chit-GOX-pFcAc-HSA-carbon paper biosensor long-term stability

We previously reported on the synthesis of GOX-pFcAc conjugates by "grafting from" ATRP.[317] These conjugates were formed through the growth of pFcAc chains directly from ATRP initiator sites covalently bound to the GOX surface. The fabrication of conjugate-modified carbon paper electrodes through GOX-pFcAc and HSA crosslinking within Chit-containing solution followed by drop casting onto carbon paper strips and their thorough characterization as glucose-based biosensors were described in a related paper. The overall performance of these biosensors led us to investigate their long-term stability in order to understand potential sources of instability within enzyme-based biosensors that utilize enzyme-polymer conjugates for both glucose oxidation and electron transfer.

The stability of Chit-GOX-pFcAc-HSA-carbon paper biosensors, GOX-pFcAc-HSA-carbon paper biosensors and GOX-HSA-carbon paper biosensors in air-saturated solution was dependent on applied working potential during operation (**Figure 6.2A**). We previously observed that operation at the formal potential of pFcAc (0.41 V versus Ag/AgCl) resulted in an initial decrease in observed current density until a steady-state value was reached for biosensors with or without Chit. GOX-HSA-carbon paper biosensors produced negligible current density under these conditions.[317] This result highlighted the necessity of pFcAc modification to achieve current generation at 0.41 V versus Ag/AgCl. However, upon switching of the applied potential

to 0.8 V versus Ag/AgCl, the observed current density consistently increased for each biosensor (**Figure 6.2A**). Successive switches in applied potential maintained these trends.

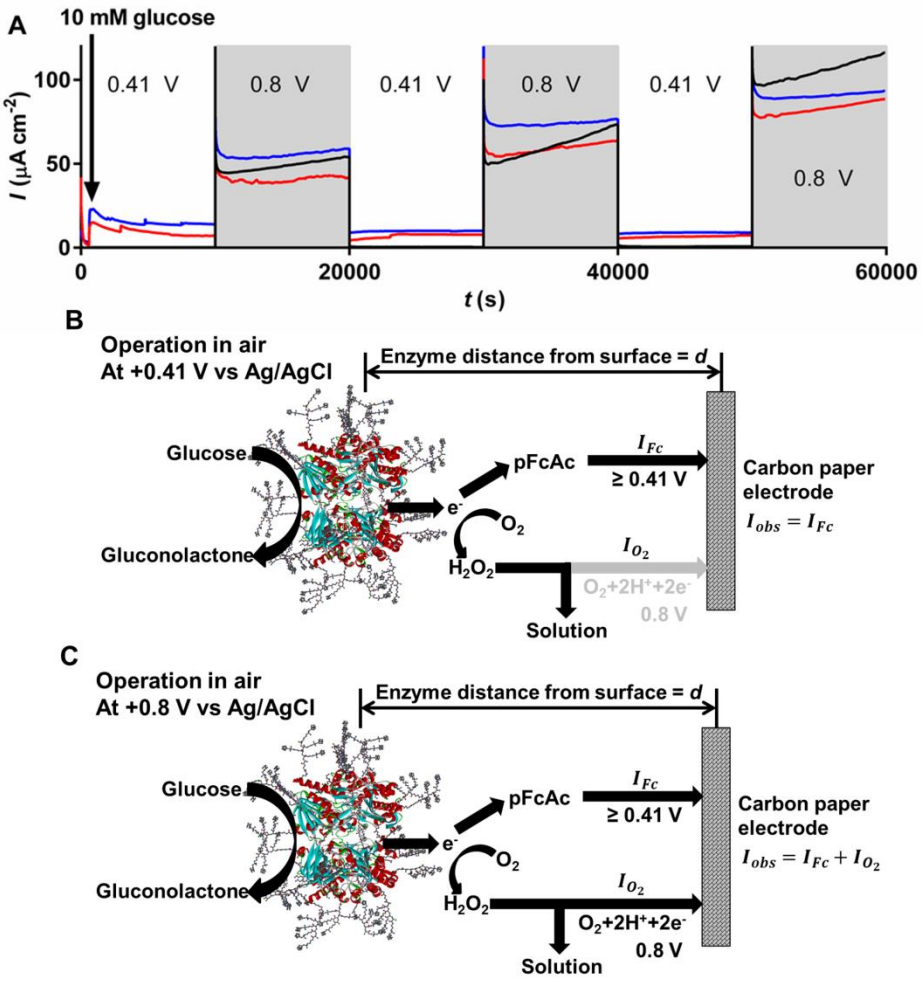

Figure 6.2 Long-term operational stability of Chit-GOX-pFcAc-HSA-carbon paper biosensors in air-saturated solution. A) Typical amperometric evaluations of GOX-HSA-carbon paper biosensor (black), GOX-pFcAc-HSA-carbon paper biosensor (red) and Chit-GOX-pFcAc-HSA-carbon paper biosensor (blue) at varying applied voltages after 10 mM glucose injection. Voltages reported versus Ag/AgCl. B) Schematic representation of available electron transfer pathways under operation at 0.41 V versus Ag/AgCl. C) Schematic representation of available electron transfer pathways under operation at 0.8 V versus Ag/AgCl. Experiments performed in 0.1 M sodium phosphate buffer (pH 7.0).

Operation at 0.41 V versus Ag/AgCl allowed ferrocene-mediated electron transfer to proceed by intramolecular oxidation of FAD by pFcAc chains and electron self-exchange through GOX-pFcAc conjugates (**Figure 6.2B**; **Equations (6.4)-(6.7)**).[117, 170] However, electron transfer through oxygen mediated hydrogen peroxide oxidation could not occur at this voltage despite the possibility of hydrogen peroxide production in the oxygen-containing solution, which was confirmed by negligible GOX-HSA-carbon paper current generation (**Figure 6.2A**).[188] The obvious initial decrease in observed current density for Chit-GOX-pFcAc-HSA-carbon paper biosensors suggested partial loss of GOX-pFcAc activity at the carbon paper electrode, which could have resulted from decreasing densities of GOX catalyzed glucose oxidation rates (GOX leaching and/or diminished turnover rate of each GOX molecule), losses in ferrocene-mediated electron transfer functionality or a combination of these factors.[317]

Upon switching of the applied voltage to 0.8 V versus Ag/AgCl, oxidation of hydrogen peroxide occurred at the carbon paper electrodes (**Figure 6.2C**; **Equation (6.3)**). Consistently increasing observed current densities for each sample under these conditions suggested retention of GOX activity during operation with native GOX-modified biosensors reaching the highest relative current density values (**Figure 6.2A**). Previous characterization of GOX-pFcAc biocatalytic glucose turnover rates showed a one order of magnitude decrease in GOX turnover number (k_{cat}) upon pFcAc functionalization, which could account for increased current generation by native GOX.[317] The impact of glucose consumption during operation was assumed to be negligible due to the total volume used in each assay (15 mL). The total consumption of glucose during the course of each assay would have resulted in changes to bulk glucose concentrations of less than 0.2 mM estimated by (overestimating constant current output of 100 μA cm^{-2}):

$$\left(\frac{100\ \mu A}{cm^2}\right)(0.093\ cm^2)(60{,}000\ s)\left(\frac{6.242\ x\ 10^{18}\ e^-}{Coulomb}\right)\left(\frac{glucose\ molecule}{2\ e^-}\right)\left(\frac{mol}{6.022\ x\ 10^{23}}\right) = 2.9\ \mu mol$$

$$\frac{(0.15 - 0.0029\ mmol\ glucose)}{0.015\ L} = 9.8\ mM\ at\ end$$

Examination of continuous biosensor operation under alternate conditions showed similar trends (**Figure 6.3**). Specifically, upon injection of a ten-fold greater glucose concentration, initial losses of current density at 0.41 V versus Ag/AgCl, and the extent of increased current density at 0.8 V versus Ag/AgCl, were both amplified (**Figure 6.3A**). Increased relative observed current densities were likely caused by increased turnover rates at the higher glucose concentration.[317] When the applied voltage was held at 0.8 V versus Ag/AgCl initially, slow increases in observed current density showed the impact of continuous operation conditions on rates of hydrogen peroxide generation and subsequent oxidation (**Equations (6.2)-(6.3)**; **Figure 6.3B**). These results highlighted the potential importance of film swelling on observed current density as increased rates of substrate diffusion and higher mobility of GOX and pFcAc pendant chains could result from greater degrees of swelling within the crosslinked film.[117] Interestingly, observed current densities upon switching of applied potential to 0.41 V versus Ag/AgCl after operation at 0.8 V versus Ag/AgCl approached zero, which may have been caused by hydrogen peroxide mediated inactivation of GOX at higher concentrations or deterioration of the ferrocene-mediated electron transfer pathway (**Figure 6.3**).

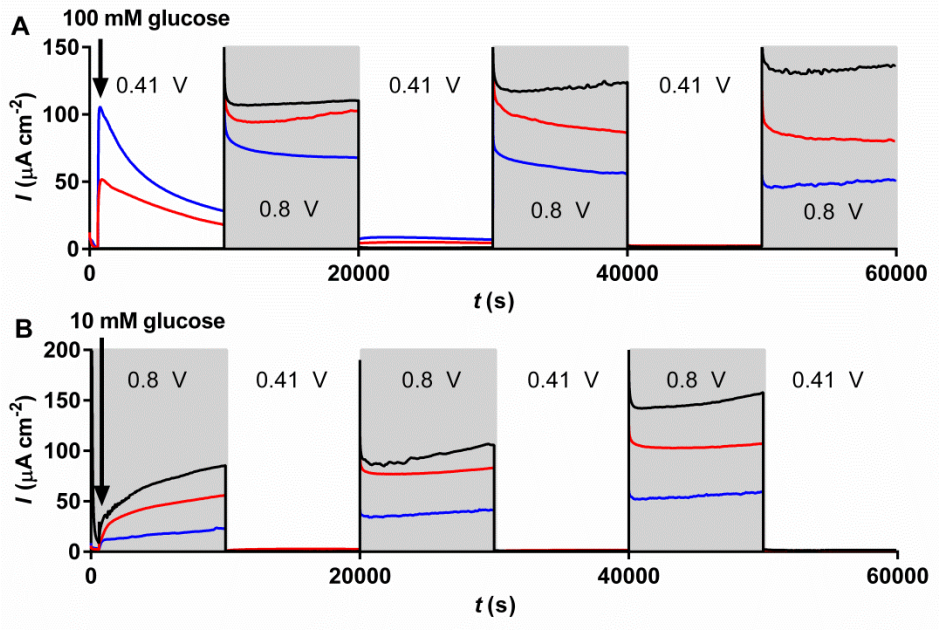

Figure 6.3 Long-term operational stability of Chit-GOX-pFcAc-HSA-carbon paper biosensors in alternate conditions. A) Typical amperometric evaluations of GOX-HSA-carbon paper biosensor (black), GOX-pFcAc-HSA-carbon paper biosensor (red) and Chit-GOX-pFcAc-HSA-carbon paper biosensor (blue) at varying applied voltages after 100 mM glucose injection. B) Typical amperometric evaluations of carbon paper electrode (black), GOX-pFcAc-HSA-carbon paper biosensor (red) and Chit-GOX-pFcAc-HSA-carbon paper biosensor (blue) at varying applied voltages after 10 mM glucose injection. Arrows indicate glucose injection. Experiments performed in air-saturated 0.1 M sodium phosphate buffer (pH 7.0). Voltages reported versus Ag/AgCl.

The overall target of GOX-pFcAc-based biosensing was stable operation through pFcAc mediated electron transfer to decrease potential interference from physiologically present compounds and reliance on oxygen. To specifically characterize this electron transfer pathway we monitored continuous operation in an argon-saturated solution, thereby removing oxygen-based chemistry from the system (**Figure 6.4A**). Chit-GOX-pFcAc-HSA-carbon paper biosensors and GOX-pFcAc-HSA-carbon paper biosensors showed a continuous decrease in observed current density despite changes in applied potential. Increased initial observed current

densities at 0.41 V versus Ag/AgCl relative to operation in air-saturated solution were indicative of greater densities of intramolecular electron transfer between FAD and attached pFcAc chains caused by eliminated competition of FAD reduction by oxygen (**Figure 6.4B**). Over time, GOX-HSA-carbon paper biosensors exhibited slowly increasing current generation at 0.8 V versus Ag/AgCl, which suggested the slow diffusion of oxygen into the test cell during the course of the investigation. The observed trends confirmed the presence of sources of instability within the ferrocene-mediated electron transfer pathway. Thus, careful examination of each source of instability to understand the mechanism of current density loss was crucial to the development of enzyme-polymer conjugate-based biosensing systems for long-term applications.

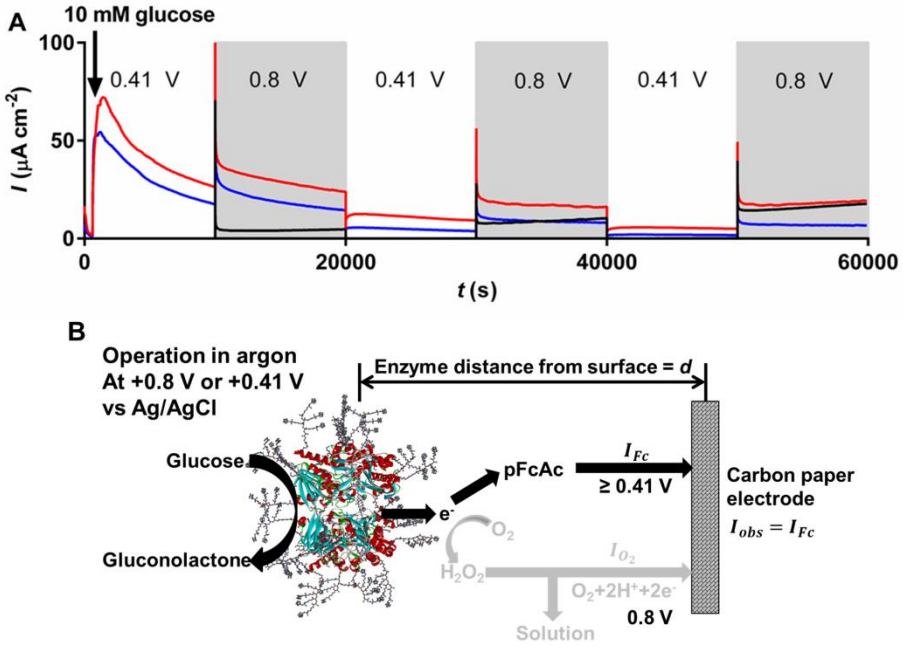

Figure 6.4 Long-term operational stability of Chit-GOX-pFcAc-HSA-carbon paper biosensors in argon-saturated solution. A) Typical amperometric evaluations of GOX-HSA-carbon paper biosensor (black), GOX-pFcAc-HSA-carbon paper biosensor (red) and Chit-GOX-pFcAc-HSA-carbon paper biosensor (blue) at varying applied voltages after 10 mM glucose injection. Voltages reported versus Ag/AgCl. B) Schematic representation of available electron transfer pathways under operation at 0.41 V or 0.8 V versus Ag/AgCl. Experiments performed in 0.1 M sodium phosphate buffer (pH 7.0).

6.3.2 General-sources of instability in Chit-GOX-pFcAc-HSA-carbon paper biosensors

Some of the major sources of instability in second-generation biosensors that rely on diffusive redox mediators are the leaching of working enzyme and small molecule mediator from the immobilization matrix during operation.[1, 39] Our system that utilizes covalently bound mediator-containing chains to the GOX surface may also have been susceptible to similar losses through conjugate leaching. We evaluated the propensity of GOX to leach from the crosslinked network by monitoring the concentration of total protein and GOX activity in solution surrounding incubated biosensors. Increases in total protein content were measured by standard μBCA assay, which reported protein concentration in solution through colorimetric analysis of bicinchoninic acid binding to Cu^{+1} formed by reduction of Cu^{+2} by protein in alkaline medium (**Figure 6.5**).[332, 333] After 24 h, total protein detected in solution corresponded to 34.0 ± 1.5 % and 26.4 ± 1.4 % of initially incorporated GOX for GOX-pFcAc-HSA-carbon paper biosensors and Chit-GOX-pFcAc-HSA-carbon paper biosensors, respectively, with the greatest increase in detected protein occurring after 30 min (**Figure 6.5A**). This result validated that the inclusion of Chit increased protein retention at the carbon paper surface. Interestingly, dissolved Chit also affected the apparent protein concentration and slightly increased estimated amounts of leached protein (**Figure 6.5B**). Since we used a ten-fold greater amount of HSA than GOX during crosslinking of each biosensor it was likely that 90% of the leached protein was HSA.

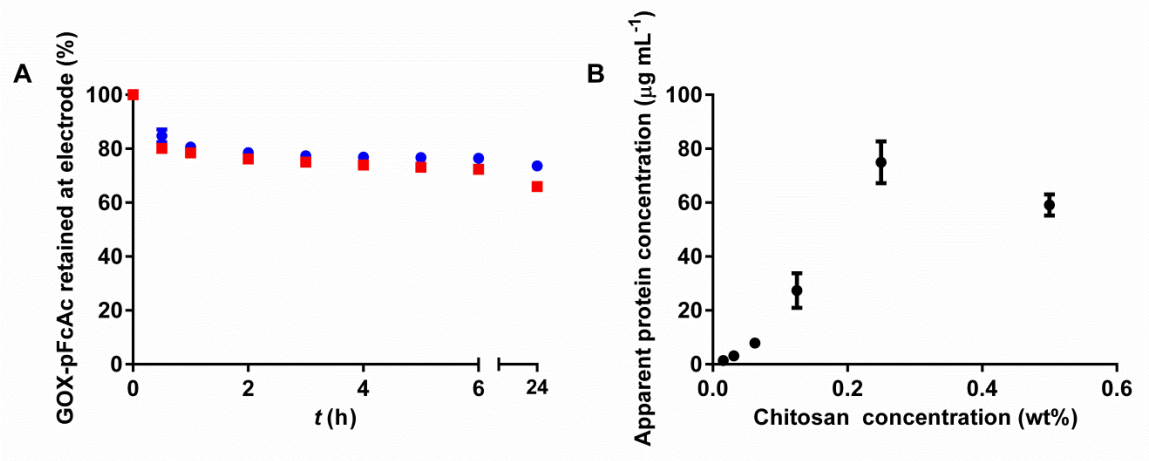

Figure 6.5 Total protein concentration leaching analysis. A) Average percentage of GOX-pFcAc retained at carbon paper electrode for GOX-pFcAc-HSA-carbon paper biosensors (red) and Chit-GOX-pFcAc-HSA-carbon paper biosensors (blue) incubated in 0.1 M sodium phosphate buffer (pH 7.0) as measured by total protein content in supernatant. B) Corresponding protein concentration of varying chitosan concentrations relative to protein standard. Protein concentrations determined *via* μBCA assay. Error bars represent 1 standard deviation of 3 trials.

To examine GOX-specific leaching, we tested for GOX activity in solution during incubation through GOX ABTS activity assay (**Figure 6.6**). Apparent GOX concentration in the supernatant was estimated using the previously determined GOX-pFcAc k_{cat} (48.0 ± 0.9 s^{-1}).[317] We observed negligible GOX-specific leaching from either GOX-pFcAc-HSA-carbon paper biosensors or Chit-GOX-pFcAc-carbon paper biosensors during incubation (**Figure 6.6**). It should be noted that the GOX activity analysis assumed the retention of GOX activity throughout biosensor fabrication and leaching analysis. Combined, these assays implied strongly that GOX leaching was not a major source of instability for Chit-GOX-pFcAc-HSA-carbon paper biosensors.

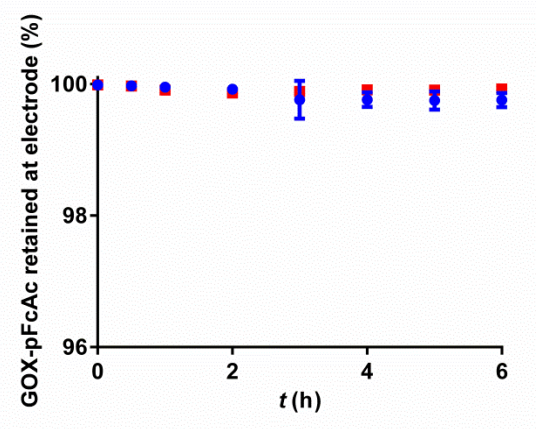

Figure 6.6 GOX activity leaching analysis. Average percentage of GOX-pFcAc retained at carbon paper electrode for GOX-pFcAc-HSA-carbon paper biosensors (red) and Chit-GOX-pFcAc-HSA-carbon paper biosensors (blue) incubated in 0.1 M sodium phosphate buffer (pH 7.0) as measured by GOX biocatalytic activity in supernatant. GOX activity measured using GOX ABTS activity assay. Error bars represent 1 standard deviation of three trials.

Increased observed current densities in all samples operating in air-saturated solution at 0.8 V versus Ag/AgCl relative to operation at 0.41 V versus Ag/AgCl implied that the biocatalytic turnover of glucose by GOX (**Equation (6.1)**) was much faster than ferrocene-mediated intramolecular electron transfer and electron-self-exchange through GOX-pFcAc conjugates (**Equations (6.4)-(6.7)**).[170] Thus, during operation in glucose-containing, argon-saturated solution, the majority of GOX molecules would be in a reduced state at any given time. To determine if deactivation of reduced GOX contributed to the observed instability of ferrocene-mediated electron transfer (**Figure 6.4A**), we tested the continuous operation of Chit-GOX-pFcAc-HSA-carbon paper biosensors in argon-saturated solution at 0.8 V versus Ag/AgCl and evaluated changes in observed current density upon removal of the applied argon blanket (**Figure 6.7**). Specifically, it has reported that the reduced form of GOX was generally more stable to fluctuations in operating conditions (*i.e.* temperature and pH), however, the reduced

form was also 100-fold more susceptible to inactivation by hydrogen peroxide.[334] Consistently reduced GOX within Chit-GOX-pFcAc-HSA-carbon paper biosensors proved to retain activity during operation in argon-saturated solution with a constant, linear increase in current density observed upon removal of the applied argon blanket (**Figure 6.7**). This consistently increasing current production, similar to continuous operation in air-saturated solution, indicated that GOX deactivation was not a major source of instability despite obviously increasing hydrogen peroxide concentrations during operation.

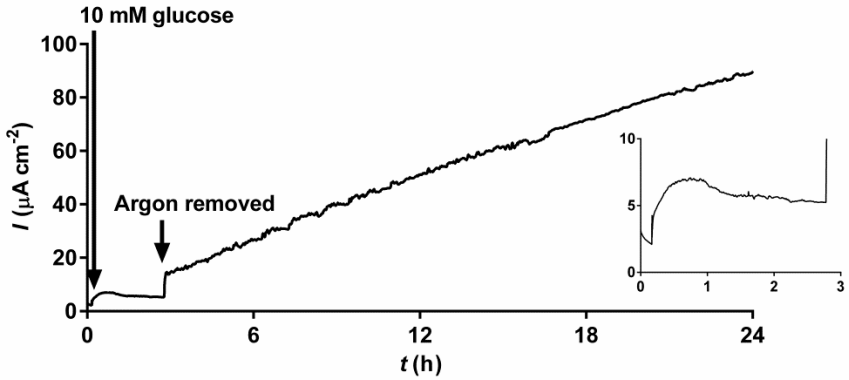

Figure 6.7 Long-term stability of reduced GOX. Typical amperometric evaluation of Chit-GOX-pFcAc-HSA-carbon paper biosensor after 10 mM glucose injection. Experiments performed in 0.1 M sodium phosphate buffer (pH 7.0). Inset: enlarged view of low current density range. Solution initially argon-saturated. Arrows indicate glucose injection and removal of argon blanket. Applied voltage held at 0.8 V versus Ag/AgCl.

Hydration and swelling of the crosslinked film could have increased current densities, observed at 0.8 V versus Ag/AgCl, over time as a result of increased substrate and GOX-pFcAc diffusion. Electron self-exchange in redox polymer networks proceeds through the propagation of electrons or holes by collisions between neighboring reduced and oxidized redox centers tethered to polymer backbones.[117, 150, 335] In such systems, electron hopping is rarely observed as hydration and swelling have been shown to increase electronic conductivity by

enhancing the mobility of the pendant redox sites over short distances. If electron hopping were dominant, the increased distances between neighboring sites resulting from swelling would lead to decreased electronic conductivities.[117] We observed the degree of swelling within our crosslinked film by examining film thickness before and after incubation in buffer (**Figure 6.8**; images depict cross-sectional film profiles with perspective parallel to carbon paper surface).

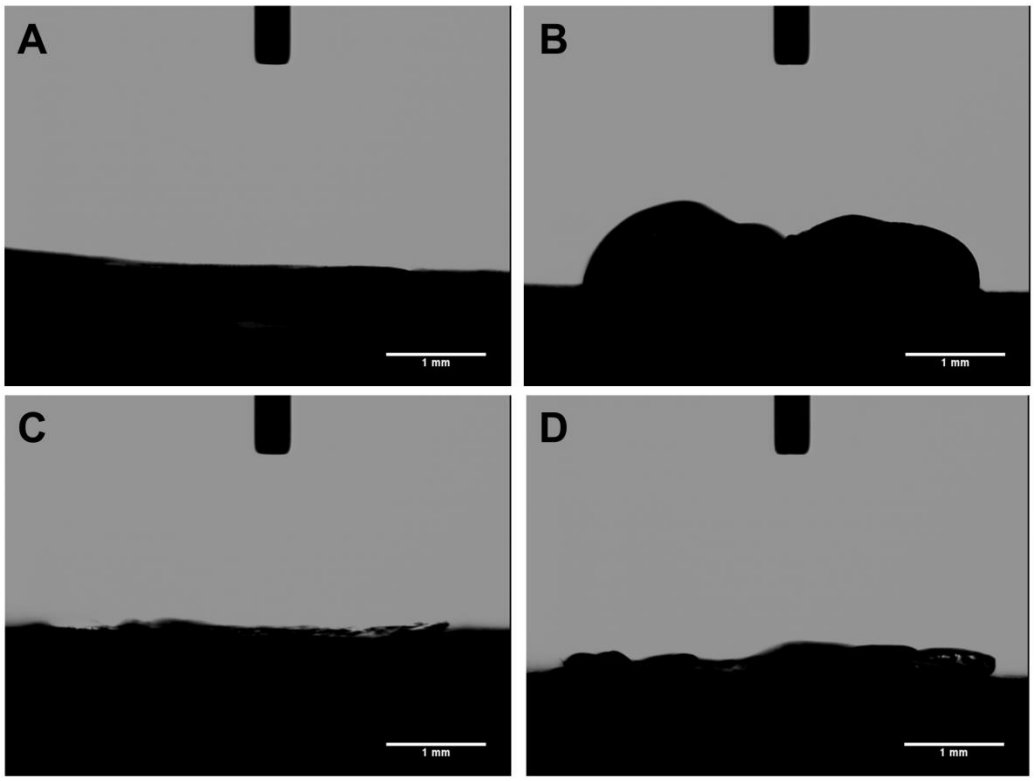

Figure 6.8 GOX-pFcAc film swelling. A) Typical film thickness of prepared GOX-pFcAc-HSA-carbon paper biosensors. B) Typical film thickness of GOX-pFcAc-HSA-carbon paper biosensors after 1 h incubation in 0.1 M sodium phosphate buffer (pH 7.0). C) Typical film thickness of prepared Chit-GOX-pFcAc-HSA-carbon paper biosensors. D) Typical film thickness of Chit-GOX-pFcAc-HSA-carbon paper biosensors after 1 h incubation in 0.1 M sodium phosphate buffer (pH 7.0). Scale bars = 1 mm.

Using the approximate size of individual GOX-pFcAc conjugates (diameter = 10.5 nm; GOX diameter ≈ 8 nm; pFcAc radius of gyration estimated by good solvent approximation ≈ 1.5

nm) [245, 336] and the known electrode area modified by drop casting (area of dried drop = 0.09 cm^2), we estimated the maximum film thickness at which GOX-pFcAc conjugates would retain constant connectivity between conjugates to be roughly 8 μm. The incorporation of Chit slowed the rate of swelling (**Figure 6.8C,D**), but the thickness of Chit-GOX-pFcAc-HSA-carbon paper biosensors exceeded 8 μm after only 1 h of incubation (**Figure 6.8D**).

To determine if loss of connectivity between conjugates impacted current generation, we examined the performance of Chit-GOX-pFcAc-HSA-carbon paper biosensors after varying periods of storage in 0.1 M sodium phosphate buffer (pH 7.0) for up to 4 weeks (**Figure 6.9A**). Analysis of current generation at 0.41 V versus Ag/AgCl allowed specific characterization of changes in ferrocene-mediated electron transfer. Increased observed current densities after incubation showed the improvement of electron transfer rates within the crosslinked network upon hydration (**Figure 6.9A**). This result further confirmed that biosensor performance was not significantly affected by conjugate leaching. Combination of the observed extent of swelling and improved current densities upon hydration agreed with reported improvements in electronic conductivities of redox polymer networks, but also suggested an important role of conjugate diffusion within the crosslinked network as neighboring GOX-pFcAc conjugates would likely not be in continuous contact during operation. We further examined the impact of film hydration *via* polarization analysis before and after 1 day of wet storage (**Figure 6.9B**). We observed obvious decreases in overpotential after film swelling. In other words, a lower applied voltage would be necessary to achieve the same current density after hydration, which was characteristic of improved electron transfer efficiencies. These results are very promising in terms of long-term storage stability, but perhaps at the expense of reliability. Thus, complete hydration of the biosensor would be required prior to continuous sensing. Overall, Chit-GOX-pFcAc-HSA-

carbon paper biosensors showed electron transfer characteristics similar to redox polymer networks as well as diffusive electron mediation through GOX-pFcAc conjugates, without significant leaching or deactivation of enzyme-polymer conjugate.

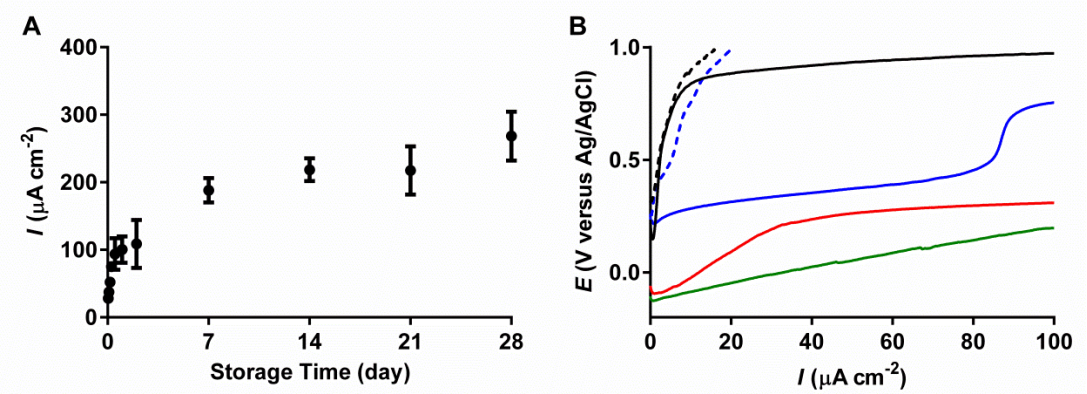

Figure 6.9 Impact of film swelling on Chit-GOX-pFcAc-HSA-carbon paper biosensor performance. A) Average current density produced by Chit-GOX-pFcAc-HSA-carbon paper biosensors upon 10 mM glucose injection at 0.41 V versus Ag/AgCl after wet storage in 0.1 M sodium phosphate buffer (pH 7.0) at 4 °C. B) Typical polarization curves of carbon paper electrode (black), Chit-GOX-pFcAc-HSA-carbon paper biosensor (blue) and Chit-GOX-pFcAc-HSA-carbon paper biosensor after 1 day storage in 0.1 M sodium phosphate buffer (pH 7.0) without (red) and with 10 mM glucose (green). Polarization determination performed without (dotted line) or with (solid line) 10 mM glucose. Experiments performed in air-saturated 0.1 M sodium phosphate buffer (pH 7.0).

6.3.3 Ferrocene-specific instability in Chit-GOX-pFcAc-HSA-carbon paper biosensors

GOX-pFcAc conjugate-based biosensors showed continuously decreasing current generation when ferrocene-mediated electron transfer (**Equations (6.4)-(6.7)**) was specifically characterized (**Figure 6.4**), but proved resistant to general sources of activity loss. To identify sources of instability in ferrocene-meditated electron transfer, we carried out successive cyclic voltammetry (CV) scans under varying conditions (**Figure 6.10**).The reproducibility of CV traces varied depending on the pH and electrolyte.

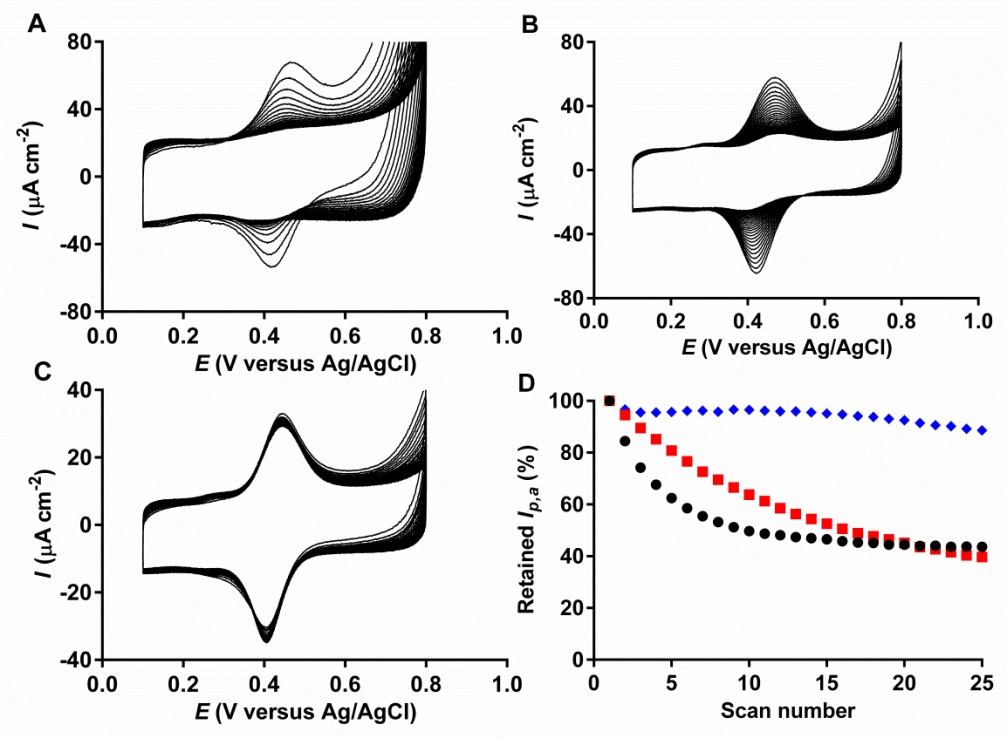

Figure 6.10 Instability of reversible electron transfer with ferrocene. A) 25 successive CV traces of Chit-GOX-pFcAc-HSA-carbon paper biosensor in 0.1 sodium phosphate buffer (pH 7.0). B) 25 successive CV traces of Chit-GOX-pFcAc-HSA-carbon paper biosensor in 0.1 sodium phosphate buffer (pH 5.0). C) 25 successive CV traces of Chit-GOX-pFcAc-HSA-carbon paper biosensor in 0.1 sodium sulfate buffer (pH 7.0). D) Retained anodic peak current density relative to scan 1 for Chit-GOX-pFcAc-HSA-carbon paper biosensors in 0.1 M sodium phosphate buffer (pH 7.0) (black circles), 0.1 M sodium phosphate buffer (pH 5.0) (red squares) and 0.1 M sodium sulfate buffer (pH 7.0) (blue diamonds). Experiments performed in argon-saturated solution at a scan rate of 10 mV s^{-1}.

Under normal operating conditions (0.1 M sodium phosphate buffer (pH 7.0)), Chit-GOX-pFcAc-HSA-carbon paper biosensors exhibited rapidly reducing peak current densities with each successive scan (**Figure 6.10A,D**). This result indicated a rapid loss in reversible electron transfer between the electrode and pFcAc chains. The observed loss was slowed when tested in 0.1 M sodium phosphate buffer (pH 5.0) (**Figure 6.10B,D**) and was nearly stable when

tested in 0.1 M sodium sulfate buffer (pH 7.0) (**Figure 6.10C,D**), which suggested instability of ferrocene-electrode electron transfer was a function of electrolyte conditions. These losses were consistent with the decomposition of ferrocenium in the presence of nucleophiles and nucleophilic anion uptake in the polymer structure.[161, 179, 180] Sodium phosphate buffer contained nucleophilic dibasic sodium phosphate, which was present in higher concentrations at pH 7.0 relative to pH 5.0 and would thus lead to a higher degree of ferrocenium instability. Studies have reported on nucleophilic anion uptake in the presence of secondary amino groups leading to film collapse in ferrocene-modified thin films *via* film dehydration.[161, 179] Similar instabilities have been reported for some ferrocene-containing redox polymer systems while others exhibited successful function in phosphate-containing solution, which suggested that the mechanism of ferrocenium activity loss was dependent on polymer structure.[116, 337, 338]

The impact of these sources of instability was further confirmed when Chit-GOX-pFcAc-HSA-carbon paper biosensors were tested in non-nucleophilic sodium sulfate buffer (**Figure 6.10C,D**), which showed relatively stable ferrocene oxidation and reduction. Thus, we concluded that ferrocenium degradation during operation led to consistently decreased overall rates of ferrocene-mediated electron transfer in the crosslinked film, which was evident in argon-saturated solution (**Figure 6.4**), but did not impact oxygen-mediated current generation (**Figure 6.2A,C**). This mechanism of instability was likely a function of the amount of time each ferrocenium ion persisted in the system (*i.e.* magnitude of difference in rates of ferrocene oxidation by electrode and ferrocene reduction through intramolecular electron transfer). Indeed, CV analysis of Chit-GOX-pFcAc-HSA-carbon paper biosensors in 0.1 M sodium phosphate buffer (pH 7.0) at differing scan rates showed instability of reversible electron transfer of pFcAc

to be dependent on the time ferrocenium was present rather than the number of successive oxidation and reduction cycles (**Figure 6.11**).

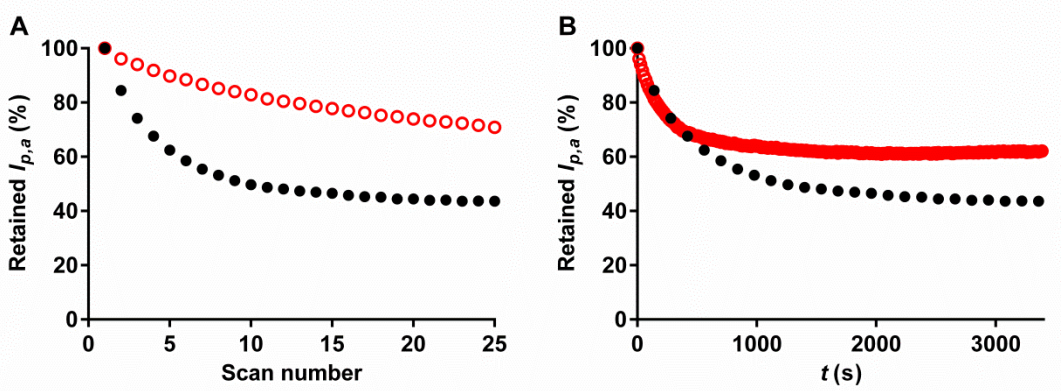

Figure 6.11 Influence of scan rate on GOX-pFcAc long-term electron transfer stability. A) Retained percentage of peak anodic current density relative to scan number of Chit-GOX-pFcAc-HSA-carbon paper biosensors at a scan rate of 10 mV s^{-1} (black) and 100 mV s^{-1} (red). B) Retained percentage of peak anodic current density relative to time of Chit-GOX-pFcAc-HSA-carbon paper biosensors at a scan rate of 10 mV s^{-1} (black) and 100 mV s^{-1} (red). Experiments performed in argon-saturated 0.1 M sodium phosphate buffer (pH 7.0)

These results highlighted the necessity of increased rates of intramolecular electron transfer to reduce the persisting lifetime of ferrocenium during operation. Intramolecular electron transfer rates of surface bound ferrocene-containing compounds have been shown to generally be much lower than GOX-catalyzed glucose turnover and electron self-exchange through polymer networks.[170] Ferrocene-mediators bound to the surface of GOX through flexible chains have exhibited varying rates of intramolecular or intermolecular electron transfer dependent on chain length and thus mobility.[162] To characterize Chit-GOX-pFcAc-HSA-carbon biosensors operating at rapid rates of ferrocene-mediated electron transfer, we examined long-term operation at varying applied voltages in argon-saturated solution with freely diffusing FcAc (**Figure 6.12**). Maximum current density and long-term stability of current output were increased

under operation at both 0.41 V and 0.8 V versus Ag/AgCl (**Figure 6.12A**). These trends were indicative of increased rates of FAD oxidation by the freely diffusing FcAc relative to pFcAc bound to the GOX surface comparable to oxygen-mediated electron transfer (**Figure 6.12B**) (FcAc was incorporated into the tested solution at a concentration similar to dissolved oxygen). Increased stability may also have been influenced by the higher overall concentration of ferrocene in the tested environment, which could reduce the impact of ferrocenium degradation. The increased potential long-term stability of Chit-GOX-pFcAc-HSA-carbon paper biosensors indicated a path toward improvement for sensing systems based on enzyme-polymer conjugates.

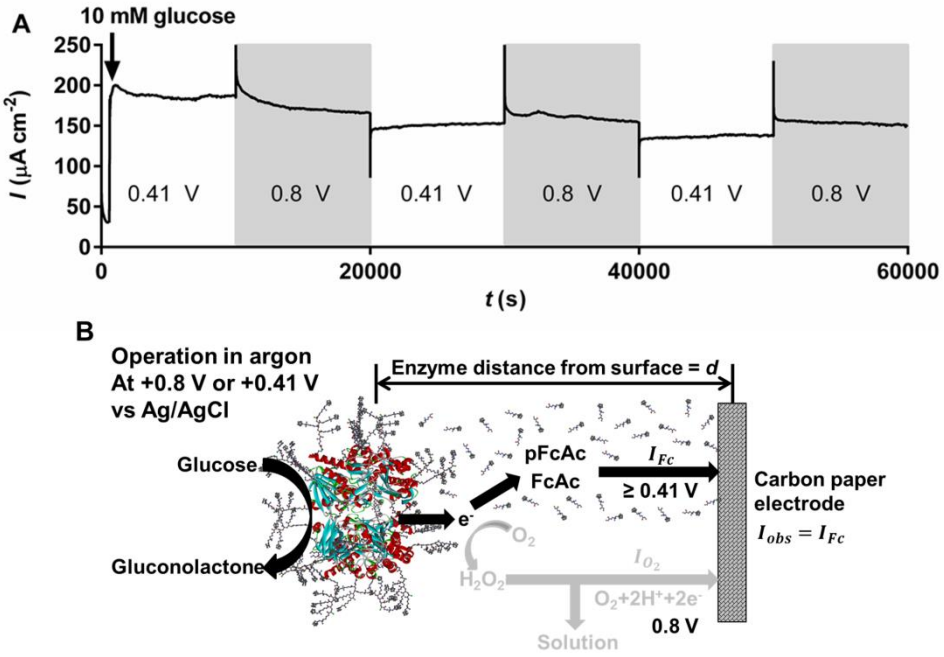

Figure 6.12 Long-term operational stability of Chit-GOX-pFcAc-HSA-carbon paper biosensor with freely diffusing FcAc. A) Typical amperometric evaluation of Chit-GOX-pFcAc-HSA-carbon paper biosensor at varying applied voltages after 10 mM glucose injection with 0.2 mM FcAc. Voltages reported versus Ag/AgCl. Experiment performed in argon-saturated 0.1 M sodium phosphate buffer (pH 7.0). B) Schematic representation of available electron transfer pathways under operation at 0.41 V or 0.8 V versus Ag/AgCl with freely diffusing FcAc.

We characterized the long-term operational stability of Chit-GOX-pFcAc-HSA-carbon paper biosensors and identified their major sources of instability as well as resistances to some general sources of instability exhibited by other enzyme-based biosensing systems. These results showed the potential of enzyme-polymer conjugate-based biosensors toward continuous glucose sensing coupled with the thorough evaluation of glucose sensing characteristics reported in our prior study. Chit-GOX-pFcAc-HSA-carbon paper biosensors exhibited performance characteristics similar to those in redox polymer networks and diffusionally mediated systems, but without leaching of conjugate or GOX deactivation from within the crosslinked network. Our characterization of this system was mostly performed in neutral, phosphate-containing solutions as reliable operation under these conditions would be important in predicting potential physiological applications. Our suspicions of a nucleophile-based instability would need to be addressed, and current work focused on engineering of grown polymer structures that could enhance intramolecular electron transfer rates and inherent mediator stability. The knowledge gained in this study will advance the next-generation electroactive enzyme-polymer conjugates synthesized using PBPE for biosensing applications.

6.4 Conclusions

We have characterized the long-term operational stability of Chit-GOX-pFcAc-HSA-carbon paper biosensors and we have identified major sources of instability as well as advantageous operational characteristics. GOX-pFcAc conjugates generated through PBPE using ATRP were crosslinked, along with HSA in a Chit-containing solution, and drop cast onto carbon paper strips to form glucose-based biosensors that exhibited characteristics of systems based on redox polymer networks as well as those using diffusional redox mediators. GOX-pFcAc conjugates did not leach from the crosslinked film and GOX retained biocatalytic activity

during operation. Crosslinked film swelling prior to use resulted in an increased glucose response. Ferrocene-mediated electron transfer rapidly degraded due to ferrocenium decomposition and nucleophilic anion uptake during operation, which is now our focus of interest as we move toward implementation of GOX-pFcAc-based biosensors. The identification of instability sources within enzyme-polymer conjugate-based biosensing systems provided us with a clear path forward in the development and optimization of such materials for continuous glucose sensing through PBPE.

Chapter 7: Future Directions and Overall Conclusions

7.1 Future Directions

The work presented in this dissertation showed the potential of 3-dimensional carbon nanomaterial-based structures and polymer-based protein engineering (PBPE) toward the development of high-performance enzymatic biosensors and enzymatic biofuel cells (EBFCs). The tailorability of these approaches provides many additional possibilities for future development. The combination of enzyme-polymer conjugates synthesized using PBPE with electrode materials designed to maximize accessible surface area could promote optimized biosensor and EBFC performance and stability. In particular, PBPE presents an incredible amount of control over resulting conjugate characteristics. The development of PBPE methods with electroactive enzymes and redox polymers could lead to systems with rationally tailored degrees of polymerization (DP), redox-containing side chain lengths and spacing along the polymer backbone, polymer chain density on the enzyme surface and predictable modification of targeted sites as well as incorporation of block copolymer systems for additional solubility or immobilization functionality. Future work in these areas should focus on optimization of enzyme-polymer conjugate characteristics and the incorporation of these conjugates into suitable, advantageous electrode support materials.

7.1.1 PBPE of GOX

The modification of glucose oxidase (GOX) through PBPE presented in this dissertation focused on the use of ferrocene-containing polymers. One of the main limiting issues with this system was the solubility of the grown polymer, which hindered precise control over certain polymer characteristics such as DP.[317] The future development of these methods should focus on rationally tailorable polymer systems with facile control over both polymer and resulting

enzyme-polymer conjugate characteristics. Toward this goal, we synthesized a GOX-polymer conjugate that utilized a naphthoquinone (NQ)-based redox mediator by first controllably growing poly(2-(dimethylamino)ethyl methacrylate) (pDMAEMA) and subsequently functionalizing the terminal amine of each side chain with 6-bromomethyl-1,4-naphthoquinone to form GOX-pNQ conjugates (**Figure 7.1**). This method could allow greater control over conjugate characteristics as tailorable enzyme-pDMAEMA conjugates have been reported.[215, 219] NQ is an advantageous and tailorable mediator for anodic enzyme-based systems as its redox potential can be similar to that of the GOX active site.[33, 68, 163]

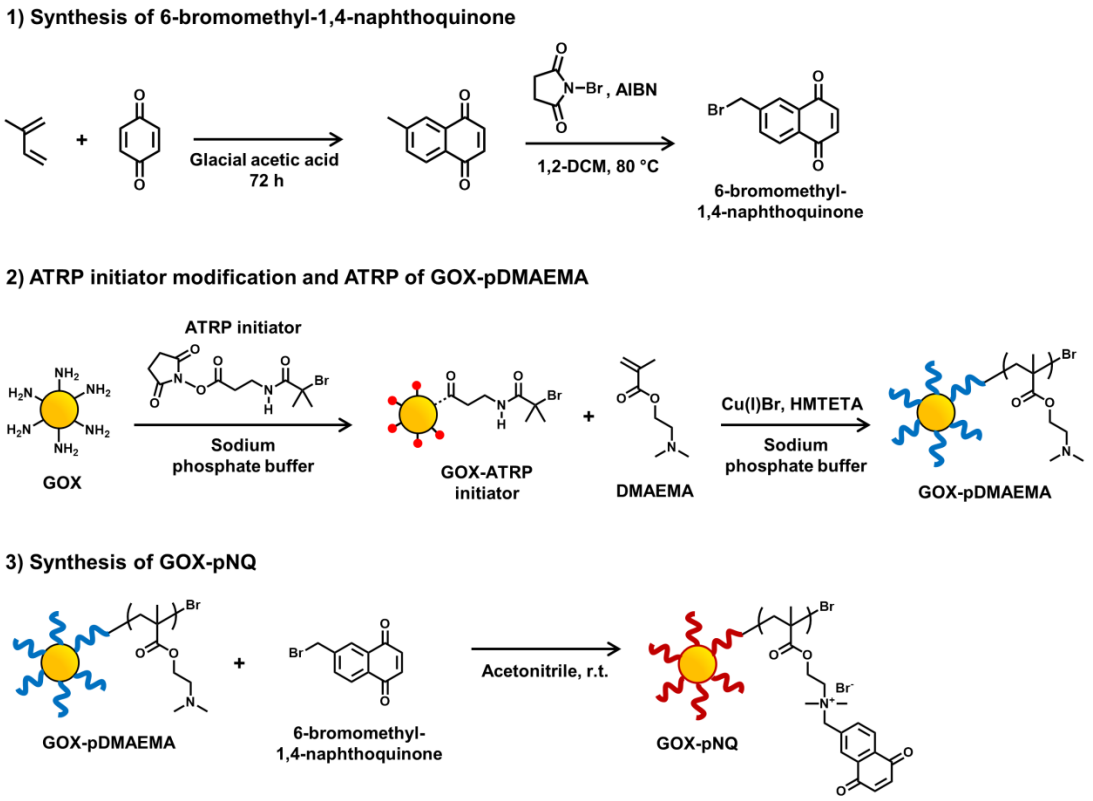

Figure 7.1 Schematic representation of GOX-pNQ conjugate synthesis. 1) Preparation of 6-bromomethyl-1,4-naphthoquinone. 2) ATRP initiator modification of native GOX and "grafting from" ATRP reaction to produce GOX-pDMAEMA conjugates. 3) Formation of GOX-pNQ conjugates.

DMAEMA (Sigma Aldrich; passed over a column of basic alumina prior to use) was polymerized from the surface of GOX from *Aspergillus niger* (Type X-S, Sigma Aldrich), modified with ATRP initiator, in a "grafting from" method using 1,1,4,7,10,10-hexamethyltriethylenetetramine (HMTETA; Sigma Aldrich) as ligand for the copper catalyst with a targeted DP of 50 (*i.e.* 50:1 molar ratio of DMAEMA monomer to –Br initiator in polymerization) (**Figure 7.1**).[215] GOX-pDMAEMA conjugates were isolated by dialysis and lyophilization with enzyme content of resulting powder determined using a standard BCA protein assay kit. The successful formation of GOX-pDMAEMA conjugates was confirmed by dynamic light scattering (DLS; Nanoplus zeta/nano particle analyzer (Particulate Systems)) and through gel permeation chromatography (GPC; Waters 2695 Series with a data processor, equipped with 3 columns (Waters Ultrahydrogel Linier, 500 and 250)) analysis of pDMAEMA cleaved by acid hydrolysis.[215] DLS measurements showed an increase in average hydrodynamic diameter (d_{hyd}) upon polymerization with GOX-pDMAEMA conjugates d_{hyd} = 36.6 ± 12.3 nm compared to native GOX d_{hyd} = 7.3 ± 0.2 nm. Evaluation of cleaved pDMAEMA by GPC yielded a narrow elution peak indicative of an average obtained DP of 43.7 with a narrow polydispersity index (PDI) of 1.23. The polymer structures of GOX-pDMAEMA conjugates and cleaved –pDMAEMA were confirmed by ^{1}H NMR in D_2O (**Figure 7.2**). These results suggested a well-controlled polymerization.

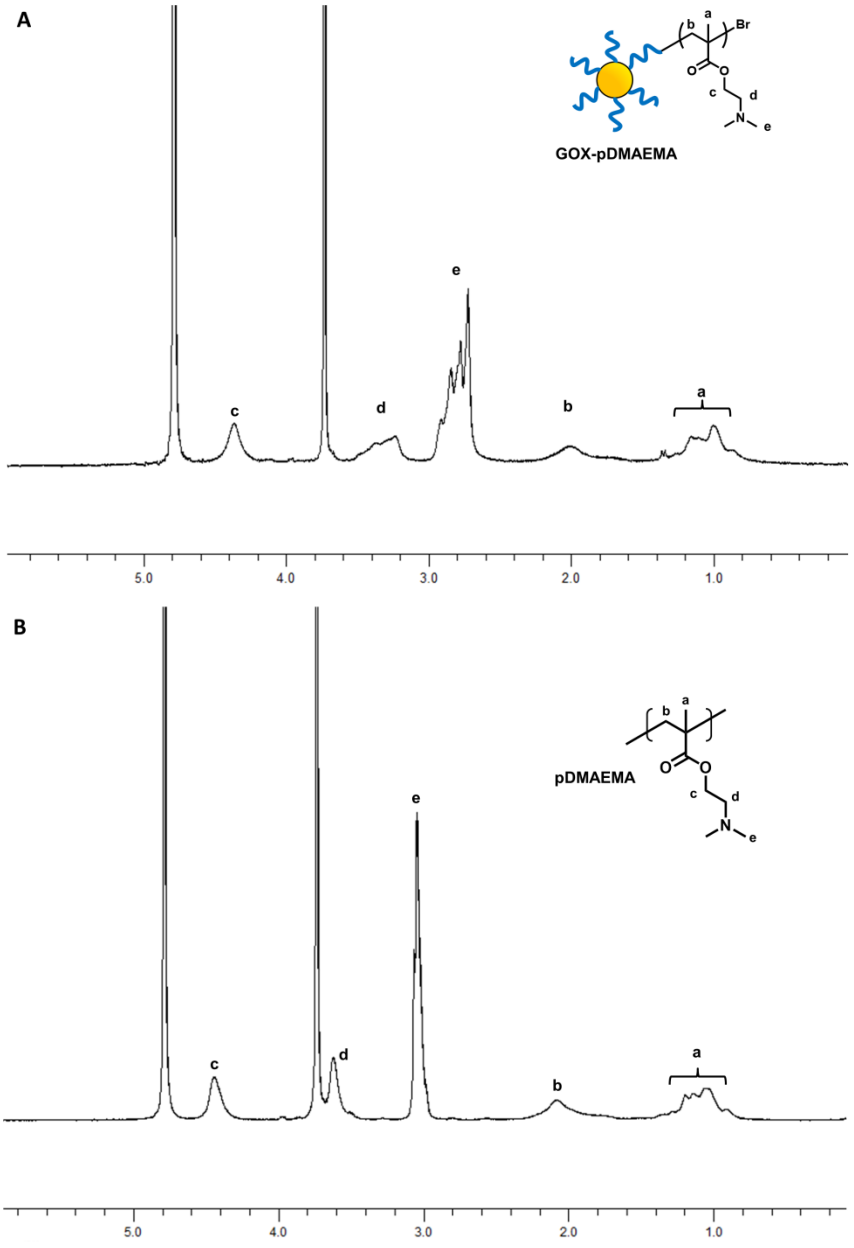

Figure 7.2 ^{1}H NMR spectra pDMAEMA materials. A) ^{1}H NMR spectra of GOX-pDMAEMA in D_2O. B) ^{1}H NMR spectra of cleaved –pDMAEMA in D_2O.

Upon determination of the successful synthesis of GOX-pDMAEMA conjugates, it was important to evaluate retained biochemical kinetics as polymer-modification of proteins can impact enzymatic activity.[317] Indeed, the solution biochemical activities of GOX-pDMAEMA differed from that of native GOX (**Figure 7.3**). GOX biochemical kinetics were determined

using the standard GOX 2,2'-azino-bis(3-ethylbenzthiazoline)-6-sulfonic acid (ABTS) activity assay with change in solution absorbance monitored at 415 nm. We found the k_{cat} and K_M of native GOX to be 637.6 ± 16.7 s^{-1} and 37.3 ± 3.8 mM glucose (**Figure 7.3A**), respectively, whereas the k_{cat} and K_M of GOX-pDMAEMA was 80.6 ± 1.7 s^{-1} and 27.5 ± 2.5 mM glucose (**Figure 7.3B**), respectively. This decrease in k_{cat} was indicative of hindered glucose turnover; however, many GOX-based systems have exhibited overall limitations based on electron transfer kinetics and efficiencies with lower rates than our determined biochemical activities.[12, 13]

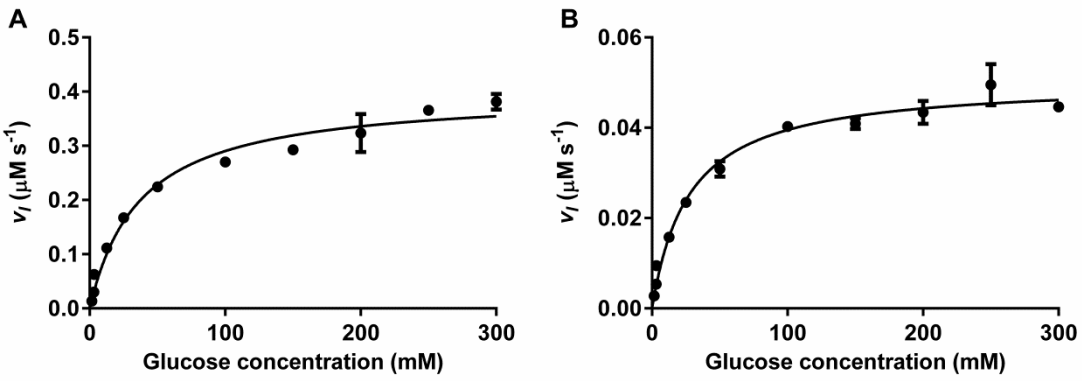

Figure 7.3 Kinetic analysis of native GOX and GOX-pDMAEMA. A) Initial rate of reaction at varying glucose concentrations of native GOX B) Initial rate of reaction at varying glucose concentrations of GOX-pDMAEMA. Experiments performed in 0.1 M sodium phosphate buffer (pH 7.0)

GOX-pDMAEMA conjugates were subsequently functionalized with 6-bromomethyl-1,4-naphthoquinone to form GOX-pNQ conjugates (**Figure 7.1**). Estimated by mass yield of GOX-pNQ product, we determined roughly 74% of the available side chains were successfully NQ-functionalized. Biochemical kinetic parameters and hydrodynamic diameters were unable to be determined due to the low solubility of GOX-pNQ conjugates. We characterized successful NQ-functionalization and GOX secondary structure retention through FT-IR (**Figure 7.4**; Perkin Elmer Frontier).

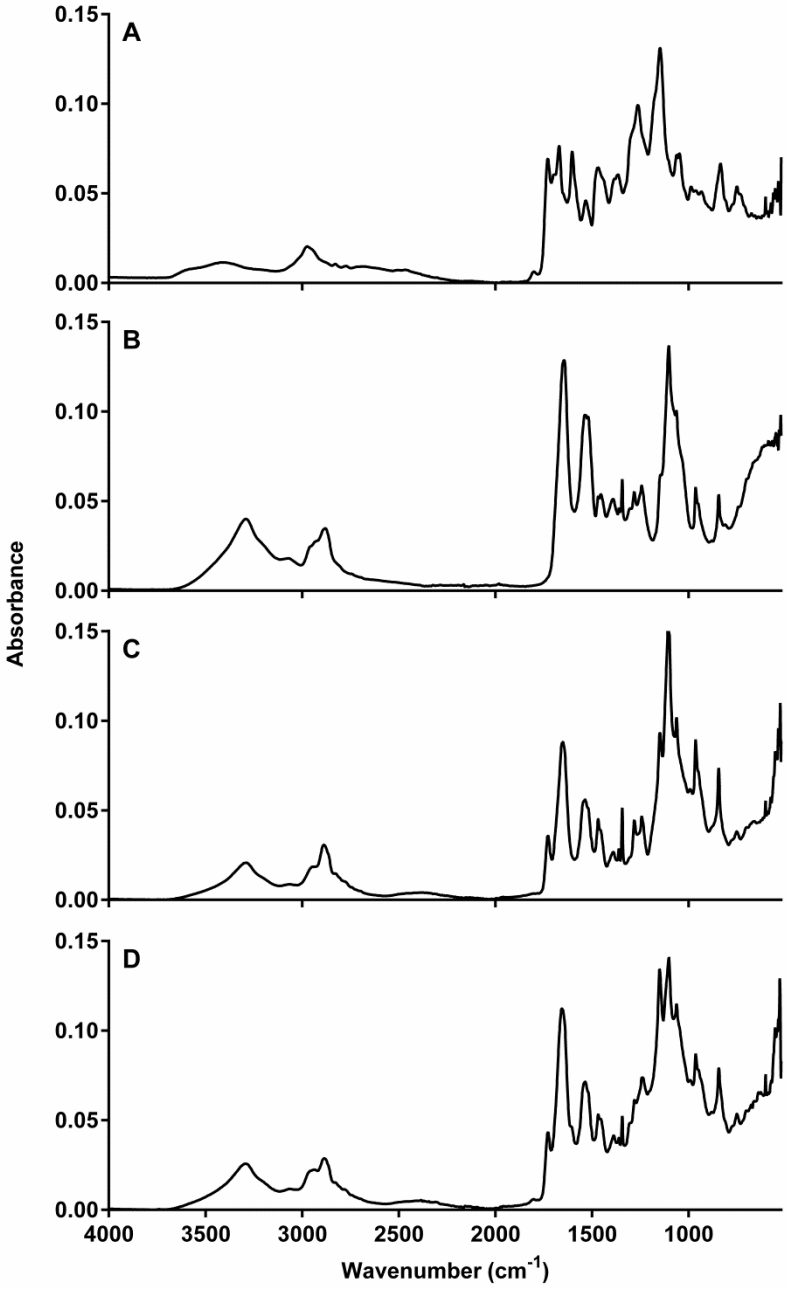

Figure 7.4 Component FT-IR analysis. A) FT-IR spectra of free pNQ polymer. B) FT-IR spectra of native GOX. C) FT-IR spectra of GOX-pDMAEMA. D) FT-IR spectra of GOX-pNQ.

The FT-IR spectra of free pNQ polymer synthesized similarly to GOX-pNQ conjugates but with free ATRP initiator exhibited absorbance peaks at 1727 cm^{-1} and 1601 cm^{-1}, characteristic of C=O stretching within ester groups of the methacrylate polymer side chains and

v(C=C) stretching of the naphthoquinone, respectively (**Figure 7.4A**).[339] Native GOX FT-IR spectra showed characteristic absorbance peaks at 1644 cm^{-1} and 1535 cm^{-1} assigned to the amide I band (C=O stretching of peptide bonds) and to the amide II band (N-H bending and C-N stretching of peptide groups) within GOX, respectively (**Figure 7.4B**).[295] FT-IR analysis of GOX-pDMAEMA conjugates (**Figure 7.4C**) and GOX-pNQ conjugates (**Figure 7.4D**) displayed a combination of the features of their components with un-shifted amide II peaks in both (GOX-pDMAEMA and GOX-pNQ amide II = 1535 cm^{-1}), slightly shifted amide I peaks in both (GOX-pDMAMEA amide I = 1650 cm^{-1} and GOX-pNQ amide I = 1657 cm^{-1}), un-shifted methacrylate ester peaks in both (GOX-pDMAEMA and GOX-pNQ methacrylate ester C=O stretching = 1727 cm^{-1}) and a characteristic shoulder of pNQ v(C=C) stretching in GOX-pNQ at 1605 cm^{-1}. These results suggested the successful functionalization of GOX with each targeted polymer while conserving the secondary structure of the enzyme.[291, 295]

Enzyme-modified electrodes were fabricated by crosslinking GOX-pNQ (1 mg mL^{-1}) along with human serum albumin (HSA; 10 mg mL^{-1}; Sigma Aldrich) by a dual NHS-functionalized poly(ethylene glycol) (PEG) linker (NHS-PEG-NHS; 5 mg mL^{-1}; NANOCS) within 1 wt% chitosan (Chit) solution followed by drop-casting (20 µL) of the resulting dispersion onto carbon paper strips (AvCarb© MEGL370; Fuel Cell Earth) and drying at 4 °C overnight. Cyclic voltammetry (CV) traces of control and enzyme-modified carbon paper electrodes exhibited multiple faradaic peak couples for each material (**Figure 7.5**). Chit-GOX-HSA-carbon paper electrodes and Chit-GOX-pDMAEMA-HSA-carbon paper electrodes were fabricated in an identical approach to Chit-GOX-pNQ-HSA carbon paper electrodes. Control CV scans of bare carbon paper showed a pair of redox peaks with a formal potential of 0.08 V versus

Ag/AgCl, which suggested the presence of impurities within the carbon paper. These peaks appeared in CV scans of each material (**Figure 7.5A**).

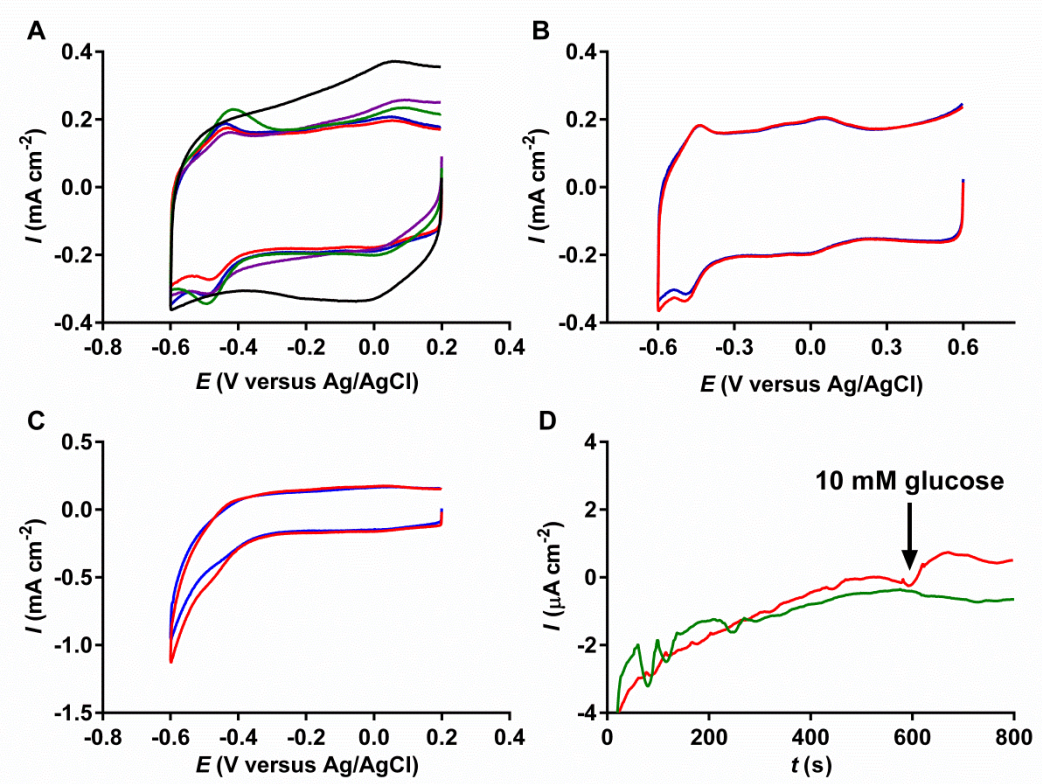

Figure 7.5 Electrochemical characterization of Chit-GOX-pNQ-HSA-carbon paper electrodes. A) Typical CV traces of carbon paper electrode (black), Chit-GOX-HSA-carbon paper electrodes (green), Chit-GOX-pDMAEMA-HSA-carbon paper electrodes (purple), Chit-GOX-pNQ-HSA-carbon paper electrodes (red) and Chit-GOX-pNQ-HSA-carbon paper electrodes with 10 mM glucose (blue) in argon-saturated solution. B) Typical CV traces with extended voltage range of Chit-GOX-pNQ-HSA-carbon paper electrodes (red) and Chit-GOX-pNQ-HSA-carbon paper electrodes with 10 mM glucose (blue) in argon-saturated solution. C) Typical CV traces of Chit-GOX-pNQ-HSA-carbon paper electrodes (red) and Chit-GOX-pNQ-HSA-carbon paper electrodes with 10 mM glucose (blue) in air-saturated solution. D) Characteristic amperometric evaluation of Chit-GOX-HSA-carbon paper electrode (green) and Chit-GOX-pNQ-HSA-carbon paper electrode (red) in air-saturated solution upon 10 mM glucose injection (indicated by arrow). Experiments performed in 0.1 M sodium phosphate buffer (pH 7.0). CV scans performed at a scan rate of 100 mV s^{-1}.

Chit-GOX-HSA-carbon paper electrodes displayed an additional pair of faradaic peaks having a formal potential of -0.46 V versus Ag/AgCl characteristic of electron transfer with the flavin adenine dinucleotide (FAD) cofactor of GOX, which were present in traces of all electrodes containing GOX (*i.e* GOX, GOX-pDMAEMA, and GOX-pNQ) (**Figure 7.5A**).[145] A third pair of redox peaks with a formal potential of -0.14 V versus Ag/AgCl appeared in CV scans of Chit-GOX-pNQ-HSA-carbon paper electrodes. Indeed, extended voltage range scans of Chit-GOX-pNQ-HSA-carbon paper electrodes more greatly exhibited these peaks, which suggested successful reduction/oxidation of pNQ at the electrode surface (**Figure 7.5B**).

Unfortunately, upon the addition of 10 mM glucose to trials using Chit-GOX-pNQ-HSA carbon paper electrodes, no significant anodic shifts signifying glucose oxidation and mediated electron transfer (MET) through pNQ chains were detected (**Figure 7.5A,B**). However, in air-saturated solution and at low voltages where oxygen reduction could occur, a decrease in observed reducing current was evident of retained biochemical turnover of oxygen by GOX. (**Figure 7.5C**). In other words, upon injection of 10 mM glucose into trials using Chit-GOX-pNQ-HSA-carbon paper electrodes, decreased local concentrations of oxygen were electrochemically observed, which indicated the presence of biochemically active GOX (**Figure 7.5C**). These results suggested the immobilization of active GOX at the electrode surface, but limited MET through pNQ chains. To directly analyze current generation *via* MET, we performed amperometric evaluations of Chit-GOX-HSA-carbon paper electrodes and Chit-GOX-pNQ-HSA carbon paper electrodes in air-saturated solution with applied working voltage held at 0 V versus Ag/AgCl, which was oxidative toward the observed formal potential of pNQ (*i.e.* -0.14 V versus Ag/AgCl) (**Figure 7.5D**). Upon injection of 10 mM glucose we observed a slight increase in anodic current generated by Chit-GOX-pNQ-HSA-carbon paper electrodes (**Figure**

7.5D). This trend was indicative of successful biochemical turnover of glucose by GOX and subsequent MET through pNQ chains to the electrode surface. However, the amperometric response was very low compared to other systems and to the theoretical current density possible from the known concentration of immobilized GOX, which showed large limitations to biochemical activity, electron transfer efficiency or a combination of these factors.[117, 317]

The observed biochemical and electrochemical characteristics of GOX-pNQ conjugates require additional improvement prior to impactful utilization. Nevertheless, the successful, controlled "grafting from" polymerization of pDMAEMA at the surface of GOX, followed by modification with redox mediator functionality was extremely promising toward the development of enzymatic biosensors and EBFCs. This approach could provide an additional layer of optimization capacity within such systems. Future investigations should be performed to optimize performance by careful variation of polymer and enzyme-polymer conjugate characteristics. Specifically, grown polymer DP, redox-containing side chain length and spacing along the polymer backbone, polymer chain density at the surface of GOX and targeted polymer attachment sites should be carefully varied to maximize retained biochemical activity while promoting rapid, efficient electron transfer from enzymatic FAD to an electrode. The utilized redox mediator within these polymer-based systems should be selected and tailored to the desired working redox potential with promising candidates including the studied quinone-based mediator as well as developed osmium-based materials.[117, 158, 163, 340-343] These studies can be combined with the development of ideal strategies for GOX-polymer conjugate immobilization onto suitable, high surface area electrode materials such as 3-dimensional carbon nanomaterial-based structures to yield viable enzyme-based devices.

7.1.2 PBPE of cathodic enzymes

The design of enzyme-polymer conjugates discussed in this dissertation focused on the increased electron transfer efficiency of the anodic working enzyme GOX. However, for continuous power generation using EBFCs, stable, enzyme-modified cathodes would also be required. The cathodic working enzymes bilirubin oxidase (BOD) and laccase electrochemically catalyze the 4-electron reduction of molecular oxygen to water at T2/T3 copper-containing active sites upon accepting electrons from an electrode at a T1 copper-containing active site.[182, 185, 252, 344] These enzymes are capable of achieving efficient direct electron transfer (DET) with electrode surfaces due to the location and orientation of their active sites.[100, 182-185, 344] However, these multicopper oxidases are susceptible to inactivation by anionic inhibitors present in solution such as Cl^-, F^- and OH^- as well as hydrogen peroxide.[281, 345] For instance, we observed the biochemical activity of BOD to rapidly decrease in the presence of the GOX reaction, but this loss could be mitigated by the addition of catalase to eliminate the build-up of hydrogen peroxide (**Figure 7.6**) BOD activity was measured using the standard BOD ABTS activity assay with change in solution absorbance monitored at 415 nm in the presence of 0.25 unit mL^{-1} GOX and 100 mM glucose. One unit of GOX Type X-S purchased from Sigma Aldrich is defined as the amount that will oxidize 1.0 μmole of β-D-glucose to D-gluconolactone and hydrogen peroxide per minute at pH 5.1 and 35 °C. One unit of catalase from bovine liver purchased from Sigma Aldrich is defined as the amount that will decompose 1.0 μmole of hydrogen peroxide per minute at pH 7.0 and 25 °C.

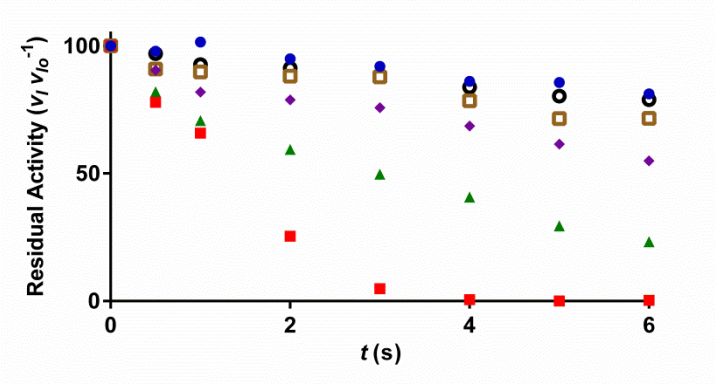

Figure 7.6 BOD activity loss in the presence of GOX reaction. BOD biochemical activity over time in the presence of GOX reaction with no catalase and no glucose (blue filled circle), no catalase (red filled square), 1.25 unit mL^{-1} catalase (green filled triangle), 2.5 unit mL^{-1} catalase (purple filled diamond), 6.25 unit mL^{-1} catalase (brown open square) and 12.5 unit mL^{-1} catalase (black open circle). Experiments performed in 0.1 M sodium phosphate buffer (pH 7.0) with 0.25 unit mL^{-1} GOX and 100 mM glucose.

Some laccases are even unstable at the OH^- concentration in neutral solution.[346, 347] Operation in near-neutral solution in the presence of anionic compounds is required for implementation in physiologic applications. Thus, we examined the activity profiles at varying pH for BOD from *Myrothecium sp.* and laccase M120 purchased from Amano Enzyme Inc. (**Figure 7.7**). Laccase was observed to exhibit optimal activity well below neutral pH (optimal k_{cat} at pH = 3.0) with nearly no activity observed at pH 7.0 (**Figure 7.7A**) while BOD maintained fairly high activities under neutral conditions (**Figure 7.7B**). All activities were measured using the standard ABTS activity assay. These characterizations highlighted the need for laccase stabilization for successful, long-term application.

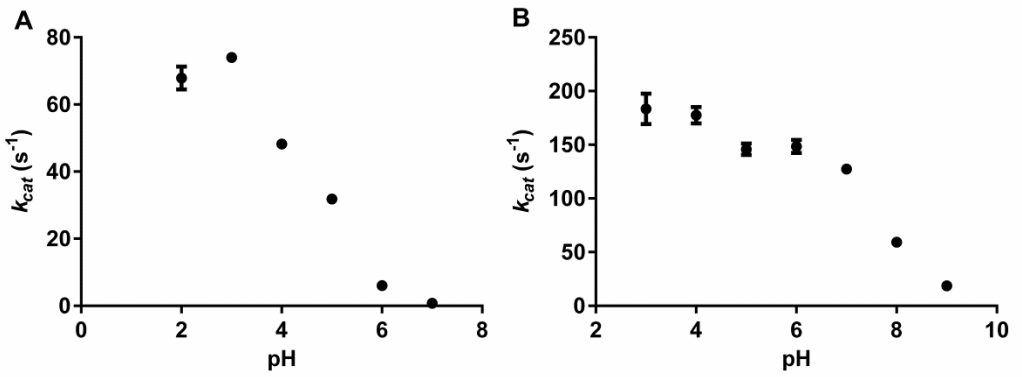

Figure 7.7 BOD and laccase pH activity profiles. A) Biochemical k_{cat} of laccase at varying pH. B) Biochemical k_{cat} of BOD at varying pH. Experiments performed in 0.1 M sodium phosphate buffer for pH 5.0-9.0 and 0.1 M citrate buffer for pH 2.0-4.0.

Multicopper oxidase inhibition by anionic molecules has been reported to proceed through competitive inhibition by binding at the T1 copper-containing active site or to the His-Cys-His chain that is used to intramolecularly transfer electrons between the 2 active sites.[346, 347] To combat these instabilities, PBPE could be applied to reduce interactions with anionic compounds. The modification of protein surfaces through PBPE has been shown to augment enzyme activities and stabilities.[215, 217-219, 222] Toward the stabilization of laccase through PBPE, we grew poly(oligo(ethylene glycol)methyl ether methacrylate (pOEGMA) from ATRP initiator-modified laccase.[215] OEGMA monomer (Mn = 475) and tris(2-pyridylmethyl)amine (TPMA) were purchased from Sigma Aldrich with OEGMA passed through a basic aluminum oxide column to remove inhibitors prior to use. The resulting laccase-pOEGMA conjugates were adsorbed onto carbon paper strips (AVCarb© MEGL370; Fuel Cell Earth) by incubating 0.5 cm x 2 cm strips in 1 mg mL^{-1} laccase solution for 4 h then drying overnight and electrochemical characteristics compared to those similarly functionalized with native laccase (**Figure 7.8**).

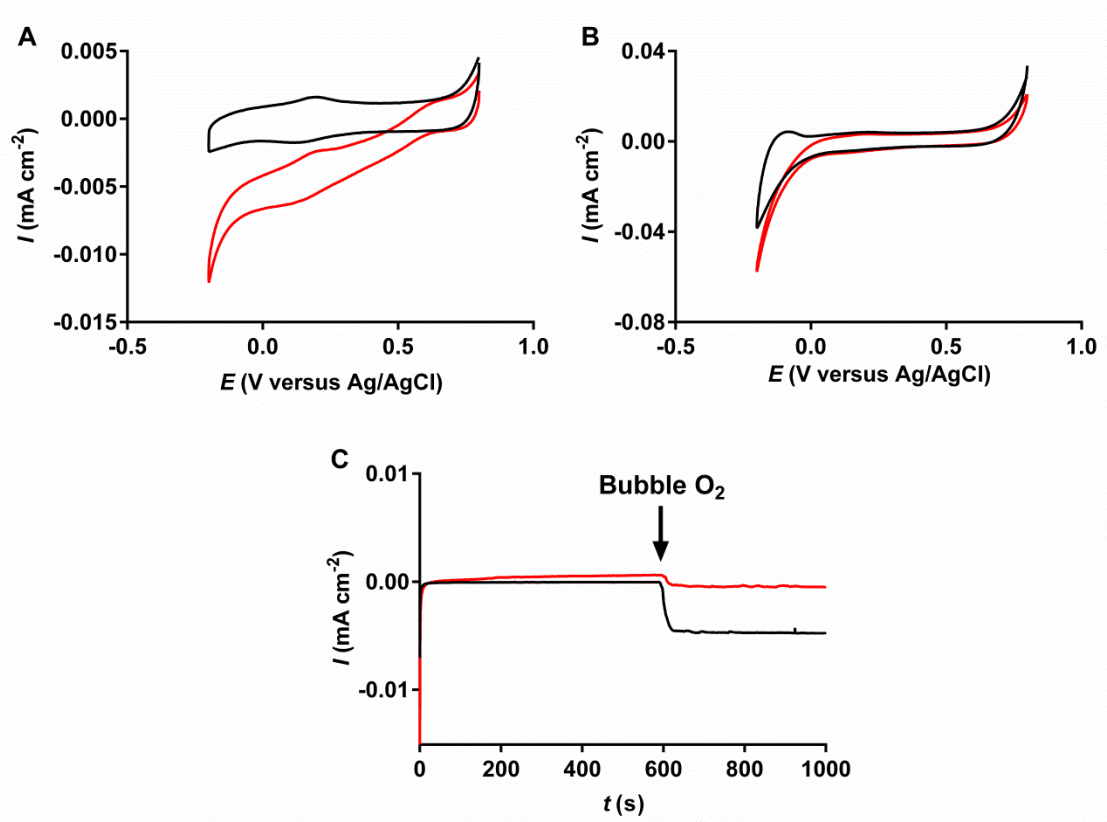

Figure 7.8 Electrochemical characterization of laccase-pOEGMA-carbon paper electrodes. A) Typical CV traces of laccase-carbon paper electrodes in argon-saturated solution (black) and in oxygen saturated solution (red). B) Typical CV traces of laccase-pOEGMA-carbon paper electrodes in argon-saturated solution (black) and oxygen saturated solution (red). C) Characteristic amperometric evaluation of laccase-carbon paper electrodes (black) and laccase-pOEGMA-carbon paper electrodes (red) in argon-saturated solution upon oxygen bubbling (indicated by arrow). Experiments performed in 0.1 M citrate buffer (pH 3.0).

Unfortunately, electrochemical characterizations of the laccase-pOEGMA-carbon paper electrodes exhibited significantly hindered DET capabilities (**Figure 7.8**). Specifically, CV traces with and without oxygen showed a greatly decreased capacity for oxygen reduction by the pOEGMA-modified laccase (**Figure 7.8A,B**). Native laccase exhibited 2 separate onset potentials for oxygen reduction: the first around 0.6 V versus Ag/AgCl and the second around 0 V versus Ag/AgCl (**Figure 7.8A**). Laccase-pOEGMA-carbon paper electrode CV traces only

yielded weak oxygen reduction beginning at 0 V versus Ag/AgCl (**Figure 7.8B**). Indeed, comparative amperometric evaluations with applied cell potential held at 0.2 V versus Ag/AgCl resulted in greatly decreased current densities by the polymer-modified laccase upon addition of oxygen (**Figure 7.8C**).

The observed electrochemical performances were likely a result of decreased biochemical activities upon modification and reduced DET efficiencies caused by the polymer coating. Careful design of cathodic enzyme-polymer conjugates incorporating efficient electron transfer pathways while imparting stability against anionic inhibitors is necessary for the development of stable enzyme-based cathodes. Some studies have suggested that incorporation of negatively charged polymers into the cathodic systems can provide resistance toward anionic inhibition of these cathodic enzymes.[70] Thus, future studies should focus on the targeted modification of BOD and laccase with negatively charged polymers such as poly(styrenesulfonate) (PSS) or poly(carboxylacrylamide) (pCAM) while maintaining DET capabilities. The successful development of such methods could prove vital to the continuous powering of implantable devices by EBFCs.

7.2 Overall Conclusions

In this work, carbon nanomaterial-based structures and polymer-based protein engineering (PBPE) were applied toward the development of next-generation enzymatic biosensors and enzymatic biofuel cells (EBFCs). Key goals throughout the completion of this dissertation were to increase the level of understanding on the impacts of electrode material properties on resulting biochemical and electrochemical characteristics in enzyme-based systems, and to develop a tailorable method of electroactive enzyme redox-functionalization using PBPE. Utilization of graphene/single-wall carbon nanotube (SWNCT) cogels with suitable

pore size and high available specific surface area (SSA) allowed the fabrication of EBFCs capable of producing rechargeable power densities within one order of magnitude of the highest reported systems to date. Material properties of the fabricated 3-dimensional structures allowed extremely high loadings of the anodic working enzyme glucose oxidase (GOX) and served to surround the enzymes with conductive material to promote direct electron transfer. Further EBFC investigations using graphene-coated SWCNT gels and gold nanoparticle/multi-wall carbon nanotube-coated polyacrylonitrile fiber paddles provided a comparative evaluation of electrode material properties such as SSA, pore size and support surface curvature to exhibit their specific influence on the biochemical and electrochemical characteristics of immobilized enzyme. It was discovered that the support surface curvature governed the retained biochemical kinetics with extended influence on electrochemical rates while total enzyme loadings were a function of SSA and pore size. For the design of GOX-redox polymer conjugates, PBPE techniques were applied toward the development of tailorable methods of electroactive enzyme functionalization for enhanced electron transfer efficiencies. Poly(*N*-(3-dimethyl(ferrocenyl) methylammonium bromide)propyl acrylamide) (pFcAc) was grown directly from the surface of GOX through atom-transfer radical polymerization in a "grafting from" approach. The resulting GOX-pFcAc conjugates showed a 24-fold increase in electron transfer efficiency and provided a 4-fold increase in EBFC power density relative to native GOX. The modified electrochemical properties exhibited by GOX-pFcAc conjugates were further applied to the fabrication of reliable and selective enzymatic glucose-based biosensors. The conjugation of redox polymers directly to the surface of the electroactive enzymes combined the characteristics of diffusively mediated enzymatic systems with those based on redox polymer networks. An in-depth study of potential sources of instability allowed the identification of strengths and weaknesses toward the

continuous operation of these enzyme-redox polymer conjugate based materials. GOX-pFcAc-modified electrodes were found to be resistant to common sources of instability exhibited by diffusively mediated systems with deactivation of the ferrocene mediator determined to be the key source of instability. Refinement of this PBPE approach leading to controllable enzyme functionalization would provide an additional layer of optimization capacity to enzymatic biosensors and EBFCs. Promising approaches to produce such a synthesis method were evaluated. Future studies toward this goal should focus on the development and combination of polymer-functionalized anodic and cathodic enzyme-polymer conjugates with suitable, advantageous electrode materials with high accessible surface areas to produce fully optimizable enzymatic systems. The potential implications of these methods could lead to next-generation sensing technologies and power sources for implantable devices with broadened implementation of enzyme-based bioelectronics.

References

[1] Wang, J., 2008, "Electrochemical glucose biosensors," Chem. Rev., 108(2), pp 814-825.

[2] Sheldon, R. A., and Van Pelt, S., 2013, "Enzyme immobilisation in biocatalysis: why, what and how," Chem. Soc. Rev., 42(15), pp 6223-6235.

[3] Kirk, O., Borchert, T. V., and Fuglsang, C. C., 2002, "Industrial enzyme applications," Curr. Opin. Biotechnol., 13(4), pp 345-351.

[4] Robles-Medina, A., Gonzalez-Moreno, P. A., Esteban-Cerdan, L., and Molina-Grima, E., 2009, "Biocatalysis: Towards ever greener biodiesel production," Biotechnol. Adv., 27(4), pp 398-408.

[5] End, N., and Schoning, K. U., 2004, "Immobilized biocatalysts in industrial research and production," Top. Curr. Chem., 242(1), pp 273-317.

[6] Min, K., and Yoo, Y. J., 2014, "Recent progress in nanobiocatalysis for enzyme immobilization and its application," Biotechnol. Bioproc. Eng., 19(4), pp 553-567.

[7] Mello, L. D., and Kubota, L. T., 2002, "Review of the use of biosensors as analytical tools in the food and drink industries," Food Chem., 77(2), pp 237-256.

[8] Bandodkar, A. J., and Wang, J., 2016, "Wearable Biofuel Cells: A Review," Electroanal., 28(6), pp 1188-1200.

[9] Liang, J. F., Li, Y. T., and Yang, V. C., 2000, "Biomedical application of immobilized enzymes," J. Pharm. Sci., 89(8), pp 979-990.

[10] Clark, L. C., and Lyons, C., 1962, "Electrode Systems for Continuous Monitoring in Cardiovascular Surgery," Ann. N. Y. Acad. Sci., 102(1), pp 29-45.

[11] Heller, A., 2004, "Miniature biofuel cells," Phys. Chem. Chem. Phys., 6(2), pp 209-216.

[12] Kim, J., Jia, H. F., and Wang, P., 2006, "Challenges in biocatalysis for enzyme-based biofuel cells," Biotechnol. Adv., 24(3), pp 296-308.

[13] Rasmussen, M., Abdellaoui, S., and Minteer, S. D., 2016, "Enzymatic biofuel cells: 30 years of critical advancements," Biosens. Bioelectron., 76, pp 91-102.

[14] Osman, M. H., Shah, A. A., and Walsh, F. C., 2011, "Recent progress and continuing challenges in bio-fuel cells. Part I: Enzymatic cells," Biosens. Bioelectron., 26(7), pp 3087-3102.

[15] Wang, J., 2001, "Glucose biosensors: 40 years of advances and challenges," Electroanal., 13(12), pp 983-988.

[16] Bullen, R. A., Arnot, T. C., Lakeman, J. B., and Walsh, F. C., 2006, "Biofuel cells and their development," Biosens. Bioelectron., 21(11), pp 2015-2045.

[17] Luckarift, H. R., Atanassov, P. B., and Johnson, G. R. Enzymatic fuel cells: from fundamentals to applications. (Wiley, 2014).

[18] Shukla, A. K., Suresh, P., Berchmans, S., and Rajendran, A., 2004, "Biological fuel cells and their applications," Curr. Sci., 87(4), pp 455-468.

[19] Rabaey, K., and Verstraete, W., 2005, "Microbial fuel cells: novel biotechnology for energy generation," Trends Biotechnol., 23(6), pp 291-298.

[20] Logan, B. E., Hamelers, B., Rozendal, R. A., Schrorder, U., Keller, J., Freguia, S., Aelterman, P., Verstraete, W., and Rabaey, K., 2006, "Microbial fuel cells: Methodology and technology," Environ. Sci. Technol., 40(17), pp 5181-5192.

[21] Newman, J. D., and Setford, S. J., 2006, "Enzymatic biosensors," Mol. Biotechnol., 32(3), pp 249-268.

[22] Minteer, S. D., Liaw, B. Y., and Cooney, M. J., 2007, "Enzyme-based biofuel cells," Curr. Opin. Biotechnol., 18(3), pp 228-234.

[23] Rocchitta, G., Spanu, A., Babudieri, S., Latte, G., Madeddu, G., Galleri, G., Nuvoli, S., Bagella, P., Demartis, M. I., Fiore, V., Manetti, R., and Serra, P. A., 2016, "Enzyme Biosensors for Biomedical Applications: Strategies for Safeguarding Analytical Performances in Biological Fluids," Sens., 16(6), pp 780-801.
[24] Liu, G., Wan, Y., Gau, V., Zhang, J., Wang, L. H., Song, S. P., and Fan, C. H., 2008, "An enzyme-based E-DNA sensor for sequence-specific detection of femtomolar DNA targets," J. Am. Chem. Soc., 130(21), pp 6820-6825.
[25] So, K., Kawai, S., Hamano, Y., Kitazumi, Y., Shirai, O., Hibi, M., Ogawa, J., and Kano, K., 2014, "Improvement of a direct electron transfer-type fructose/dioxygen biofuel cell with a substrate-modified biocathode," Phys. Chem. Chem. Phys., 16(10), pp 4823-4829.
[26] Wu, X. E., Guo, Y. Z., Chen, M. Y., and Chen, X. D., 2013, "Fabrication of flexible and disposable enzymatic biofuel cells," Electrochim. Acta, 98, pp 20-24.
[27] Das, M., Barbora, L., Das, P., and Goswami, P., 2014, "Biofuel cell for generating power from methanol substrate using alcohol oxidase bioanode and air-breathed laccase biocathode," Biosens. Bioelectron., 59, pp 184-191.
[28] Neto, S. A., Suda, E. L., Xu, S., Meredith, M. T., De Andrade, A. R., and Minteer, S. D., 2013, "Direct electron transfer-based bioanodes for ethanol biofuel cells using PQQ-dependent alcohol and aldehyde dehydrogenases," Electrochim. Acta, 87, pp 323-329.
[29] Azevedo, A. M., Prazeres, D. M. F., Cabral, J. M. S., and Fonseca, L. P., 2005, "Ethanol biosensors based on alcohol oxidase," Biosens. Bioelectron., 21(2), pp 235-247.
[30] Grieshaber, D., Mackenzie, R., Voros, J., and Reimhult, E., 2008, "Electrochemical biosensors - Sensor principles and architectures," Sens., 8(3), pp 1400-1458.
[31] Thevenot, D. R., Toth, K., Durst, R. A., and Wilson, G. S., 2001, "Electrochemical biosensors: recommended definitions and classification," Biosens. Bioelectron., 16(1-2), pp 121-131.
[32] Wang, J. Analytical electrochemistry, Edn. 3rd. (Wiley-VCH, Hoboken, N.J.; 2006).
[33] Leskovac, V., Trivic, S., Wohlfahrt, G., Kandrac, J., and Pericin, D., 2005, "Glucose oxidase from Aspergillus niger: the mechanism of action with molecular oxygen, quinones, and one-electron acceptors," Int. J. Biochem. Cell. Biol., 37(4), pp 731-750.
[34] Updike, S. J., and Hicks, G. P., 1967, "Enzyme Electrode," Nature, 214(5092), pp 986-&.
[35] Guilbault, G. G., and Lubrano, G. J., 1973, "Enzyme Electrode for Amperometric Determination of Glucose," Anal. Chim. Acta, 64(3), pp 439-455.
[36] Matuleviciene, V., Joseph, J. I., Andelin, M., Hirsch, I. B., Attvall, S., Pivodic, A., Dahlqvist, S., Klonoff, D., Haraldsson, B., and Lind, M., 2014, "A Clinical Trial of the Accuracy and Treatment Experience of the Dexcom G4 Sensor (Dexcom G4 System) and Enlite Sensor (Guardian REAL-Time System) Tested Simultaneously in Ambulatory Patients with Type 1 Diabetes," Diabetes Technol. Therap., 16(11), pp 759-767.
[37] Bailey, T. S., Ahmann, A., Brazg, R., Christiansen, M., Garg, S., Watkins, E., Welsh, J. B., and Lee, S. W., 2014, "Accuracy and Acceptability of the 6-Day Enlite Continuous Subcutaneous Glucose Sensor," Diabetes Technol. Therap., 16(5), pp 277-283.
[38] Yoo, E. H., and Lee, S. Y., 2010, "Glucose Biosensors: An Overview of Use in Clinical Practice," Sens., 10(5), pp 4558-4576.
[39] Kavanagh, P., and Leech, D., 2013, "Mediated electron transfer in glucose oxidising enzyme electrodes for application to biofuel cells: recent progress and perspectives," Phys. Chem. Chem. Phys., 15(14), pp 4859-4869.

[40] Cass, A. E. G., Davis, G., Francis, G. D., Hill, H. a. O., Aston, W. J., Higgins, I. J., Plotkin, E. V., Scott, L. D. L., and Turner, A. P. F., 1984, "Ferrocene-Mediated Enzyme Electrode for Amperometric Determination of Glucose," Anal. Chem., 56(4), pp 667-671.
[41] Frew, J. E., and Hill, H. a. O., 1987, "Electrochemical Biosensors," Anal. Chem., 59(15), pp 933A-944A.
[42] Milton, R. D., Abdellaoui, S., Khadka, N., Dean, D. R., Leech, D., Seefeldt, L. C., and Minteer, S. D., 2016, "Nitrogenase bioelectrocatalysis: heterogeneous ammonia and hydrogen production by MoFe protein," Energ. Environ. Sci., 9(8), pp 2550-2554.
[43] Sassolas, A., Blum, L. J., and Leca-Bouvier, B. D., 2012, "Immobilization strategies to develop enzymatic biosensors," Biotechnol. Adv., 30(3), pp 489-511.
[44] Zhang, W. J., and Li, G. X., 2004, "Third-generation biosensors based on the direct electron transfer of proteins," Anal. Sci., 20(4), pp 603-609.
[45] Ghindilis, A. L., Atanasov, P., and Wilkins, E., 1997, "Enzyme-catalyzed direct electron transfer: Fundamentals and analytical applications," Electroanal., 9(9), pp 661-674.
[46] Luong, J. H. T., Glennon, J. D., Gedanken, A., and Vashist, S. K., 2017, "Achievement and assessment of direct electron transfer of glucose oxidase in electrochemical biosensing using carbon nanotubes, graphene, and their nanocomposites," Microchim. Acta, 184(2), pp 369-388.
[47] Wohlfahrt, G., Witt, S., Hendle, J., Schomburg, D., Kalisz, H. M., and Hecht, H. J., 1999, "1.8 and 1.9 angstrom resolution structures of the Penicillium amagasakiense and Aspergillus niger glucose oxidases as a basis for modelling substrate complexes," Acta Crystallogr. D, 55(5), pp 969-977.
[48] Holzinger, M., Le Goff, A., and Cosnier, S., 2014, "Nanomaterials for biosensing applications: a review," Front. Chem., 2(63), pp 1-10.
[49] Yahiro, A. T., Lee, S. M., and Kimble, D. O., 1964, "Bioelectrochemistry .I. Enzyme Utilizing Bio-Fuel Cell Studies," Biochim. Biophys. Acta, 88(2), pp 375-383.
[50] Laane, C., Pronk, W., Franssen, M., and Veeger, C., 1984, "Use of a Bioelectrochemical Cell for the Synthesis of (Bio)Chemicals," Enzyme Microb. Technol., 6(4), pp 165-168.
[51] Le Goff, A., Holzinger, M., and Cosnier, S., 2015, "Recent progress in oxygen-reducing laccase biocathodes for enzymatic biofuel cells," Cell. Mol. Life Sci., 72(5), pp 941-952.
[52] Cooney, M. J., Svoboda, V., Lau, C., Martin, G., and Minteer, S. D., 2008, "Enzyme catalysed biofuel cells," Energ. Environ. Sci., 1(3), pp 320-337.
[53] Cosnier, S., Le Goff, A., and Holzinger, M., 2014, "Towards glucose biofuel cells implanted in human body for powering artificial organs: Review," Electrochem. Commun., 38, pp 19-23.
[54] Jia, W. Z., Bandodkar, A. J., Valdes-Ramirez, G., and Wang, J., 2014, "Wearable biosensors and biofuel cells for continuous non-invasive epidermal monitoring," Abstr. Pap. Am. Chem. Soc., 248, pp
[55] Chen, C., Xie, Q. J., Yang, D. W., Xiao, H. L., Fu, Y. C., Tan, Y. M., and Yao, S. Z., 2013, "Recent advances in electrochemical glucose biosensors: a review," RSC Adv., 3(14), pp 4473-4491.
[56] Xu, L. H., Zhu, Y. H., Yang, X. L., and Li, C. Z., 2009, "Amperometric biosensor based on carbon nanotubes coated with polyaniline/dendrimer-encapsulated Pt nanoparticles for glucose detection," Mater. Sci. Eng. C Biomim. Supramol. Sys., 29(4), pp 1306-1310.
[57] Pedrosa, V. A., Yan, J., Simonian, A. L., and Revzin, A., 2011, "Micropatterned Nanocomposite Hydrogels for Biosensing Applications," Electroanal., 23(5), pp 1142-1149.

[58] Lin, J. H., He, C. Y., Zhao, Y., and Zhang, S. S., 2009, "One-step synthesis of silver nanoparticles/carbon nanotubes/chitosan film and its application in glucose biosensor," Sens. Actuators B, 137(2), pp 768-773.
[59] Che, X., Yuan, R., Chai, Y. Q., Li, J. J., Song, Z. J., Li, W. J., and Zhong, X., 2011, "A glucose biosensor based on chitosan-Prussian blue-multiwall carbon nanotubes-hollow PtCo nanochains formed by one-step electrodeposition," Colloids Surf. B, 84(2), pp 454-461.
[60] Ping, J. F., Wang, Y. X., Fan, K., Wu, J., and Ying, Y. B., 2011, "Direct electrochemical reduction of graphene oxide on ionic liquid doped screen-printed electrode and its electrochemical biosensing application," Biosens. Bioelectron., 28(1), pp 204-209.
[61] Pang, X., Imin, P., Zhitomirsky, I., and Adronov, A., 2012, "Conjugated polyelectrolyte complexes with single-walled carbon nanotubes for amperometric detection of glucose with inherent anti-interference properties," J. Mater. Chem., 22(18), pp 9147-9154.
[62] Fu, Y. C., Zou, C., Xie, Q. J., Xu, X. H., Chen, C., Deng, W. F., and Yao, S. Z., 2009, "Highly Sensitive Glucose Biosensor Based on One-Pot Biochemical Preoxidation and Electropolymerization of 2,5-Dimercapto-1,3,4-thiadiazole in Glucose Oxidase-Containing Aqueous Suspension," J. Phys. Chem. B, 113(5), pp 1332-1340.
[63] Fu, Y. C., Li, P. H., Xie, Q. J., Xu, X. H., Lei, L. H., Chen, C., Zou, C., Deng, W. F., and Yao, S. Z., 2009, "One-Pot Preparation of Polymer-Enzyme-Metallic Nanoparticle Composite Films for High-Performance Biosensing of Glucose and Galactose," Adv. Funct. Mater., 19(11), pp 1784-1791.
[64] Vashist, S. K., Zheng, D., Al-Rubeaan, K., Luong, J. H. T., and Sheu, F. S., 2011, "Technology behind commercial devices for blood glucose monitoring in diabetes management: A review," Anal. Chim. Acta, 703(2), pp 124-136.
[65] Wu, J. M., and Yin, L. W., 2011, "Platinum Nanoparticle Modified Polyaniline-Functionalized Boron Nitride Nanotubes for Amperometric Glucose Enzyme Biosensor," ACS Appl. Mater. Interfaces, 3(11), pp 4354-4362.
[66] Zeng, Q., Cheng, J. S., Liu, X. F., Bai, H. T., and Jiang, J. H., 2011, "Palladium nanoparticle/chitosan-grafted graphene nanocomposites for construction of a glucose biosensor," Biosens. Bioelectron., 26(8), pp 3456-3463.
[67] Zebda, A., Gondran, C., Le Goff, A., Holzinger, M., Cinquin, P., and Cosnier, S., 2011, "Mediatorless high-power glucose biofuel cells based on compressed carbon nanotube-enzyme electrodes," Nat. Commun., 2, pp
[68] Reuillard, B., Le Goff, A., Agnes, C., Holzinger, M., Zebda, A., Gondran, C., Elouarzaki, K., and Cosnier, S., 2013, "High power enzymatic biofuel cell based on naphthoquinone-mediated oxidation of glucose by glucose oxidase in a carbon nanotube 3D matrix," Phys. Chem. Chem. Phys., 15(14), pp 4892-4896.
[69] Prasad, K. P., Chen, Y., and Chen, P., 2014, "Three-Dimensional Graphene-Carbon Nanotube Hybrid for High-Performance Enzymatic Biofuel Cells," ACS Appl. Mater. Interfaces, 6(5), pp 3387-3393.
[70] Kwon, C. H., Lee, S. H., Choi, Y. B., Lee, J. A., Kim, S. H., Kim, H. H., Spinks, G. M., Wallace, G. G., Lima, M. D., Kozlov, M. E., Baughman, R. H., and Kim, S. J., 2014, "High-power biofuel cell textiles from woven biscrolled carbon nanotube yarns," Nat. Commun., 5, pp
[71] Halamkova, L., Halamek, J., Bocharova, V., Szczupak, A., Alfonta, L., and Katz, E., 2012, "Implanted Biofuel Cell Operating in a Living Snail," J. Am. Chem. Soc., 134(11), pp 5040-5043.

[72] Zebda, A., Cosnier, S., Alcaraz, J. P., Holzinger, M., Le Goff, A., Gondran, C., Boucher, F., Giroud, F., Gorgy, K., Lamraoui, H., and Cinquin, P., 2013, "Single Glucose Biofuel Cells Implanted in Rats Power Electronic Devices," Sci. Rep., 3, pp 1516.
[73] Tamaki, T., 2012, "Enzymatic Biofuel Cells Based on Three-Dimensional Conducting Electrode Matrices," Top. Catal., 55(16-18), pp 1162-1180.
[74] Kropff, J., and Devries, J. H., 2016, "Continuous Glucose Monitoring, Future Products, and Update on Worldwide Artificial Pancreas Projects," Diabetes Technol. Therap., 18, pp 53-63.
[75] Swoboda, B. E. P., and Massey, V., 1965, "Purification and Properties of Glucose Oxidase from Aspergillus Niger," J. Biol. Chem., 240(5), pp 2209-2215.
[76] Zhang, X., Ju, H., and Wang, J. Electrochemical sensors, biosensors, and their biomedical applications, Edn. 1st. (Academic Press, Amsterdam ; Boston; 2008).
[77] Bankar, S. B., Bule, M. V., Singhal, R. S., and Ananthanarayan, L., 2009, "Glucose oxidase - An overview," Biotechnol. Adv., 27(4), pp 489-501.
[78] Frederick, K. R., Tung, J., Emerick, R. S., Masiarz, F. R., Chamberlain, S. H., Vasavada, A., Rosenberg, S., Chakraborty, S., Schopter, L. M., and Massey, V., 1990, "Glucose-Oxidase from Aspergillus-Niger - Cloning, Gene Sequence, Secretion from Saccharomyces-Cerevisiae and Kinetic-Analysis of a Yeast-Derived Enzyme," J. Biol. Chem., 265(7), pp 3793-3802.
[79] Kriechbaum, M., Heilmann, H. J., Wientjes, F. J., Hahn, M., Jany, K. D., Gassen, H. G., Sharif, F., and Alaeddinoglu, G., 1989, "Cloning and DNA-Sequence Analysis of the Glucose-Oxidase Gene from Aspergillus-Niger NRRL-3," FEBS Lett., 255(1), pp 63-66.
[80] Hecht, H. J., Kalisz, H. M., Hendle, J., Schmid, R. D., and Schomburg, D., 1993, "Crystal-Structure of Glucose-Oxidase from Aspergillus-Niger Refined at 2 .3 Angstrom Resolution," J. Mol. Biol., 229(1), pp 153-172.
[81] Kalisz, H. M., Hecht, H. J., Schomburg, D., and Schmid, R. D., 1990, "Crystallization and Preliminary-X-Ray Diffraction Studies of a Deglycosylated Glucose-Oxidase from Aspergillus-Niger," J. Mol. Biol., 213(2), pp 207-209.
[82] Bright, H. J., 1974, "Flavoprotein Oxidases," Adv. Chem. Series,(136), pp 305-323.
[83] Bourdillon, C., Demaille, C., Moiroux, J., and Saveant, J. M., 1993, "New Insights into the Enzymatic Catalysis of the Oxidation of Glucose by Native and Recombinant Glucose-Oxidase Mediated by Electrochemically Generated One-Electron Redox Cosubstrates," J. Am. Chem. Soc., 115(1), pp 2-10.
[84] Wohlfahrt, G., Trivic, S., Zeremski, J., Pericin, D., and Leskovac, V., 2004, "The chemical mechanism of action of glucose oxidase from Aspergillus niger," Mol. Cell. Biochem., 260(1-2), pp 69-83.
[85] Gibson, Q. H., Massey, V., and Swoboda, B. E. P., 1964, "Kinetics and Mechanism of Action of Glucose Oxidase," J. Biol. Chem., 239(11), pp 3927-3934.
[86] Bright, H. J., and Appleby, M., 1969, "Ph Dependence of Individual Steps in Glucose Oxidase Reaction," J. Biol. Chem., 244(13), pp 3625-3634.
[87] Christenson, A., Shleev, S., Mano, N., Heller, A., and Gorton, L., 2006, "Redox potentials of the blue copper sites of bilirubin oxidases," BBA Bioenergetics, 1757(12), pp 1634-1641.
[88] Datta, S., Christena, L. R., and Rajaram, Y. R. S., 2013, "Enzyme immobilization: an overview on techniques and support materials," 3 Biotech., 3(1), pp 1-9.
[89] Asuri, P., Bale, S. S., Karajanagi, S. S., and Kane, R. S., 2006, "The protein-nanomaterial interface," Curr. Opin. Biotechnol., 17(6), pp 562-568.

[90] Asuri, P., Karajanagi, S. S., Yang, H. C., Yim, T. J., Kane, R. S., and Dordick, J. S., 2006, "Increasing protein stability through control of the nanoscale environment," Langmuir, 22(13), pp 5833-5836.
[91] Campbell, A. S., Dong, C. B., Meng, F. K., Hardinger, J., Perhinschi, G., Wu, N. Q., and Dinu, C. Z., 2014, "Enzyme Catalytic Efficiency: A Function of Bio-Nano Interface Reactions," ACS Appl. Mater. Interfaces, 6(8), pp 5393-5403.
[92] Qian, X., Rameshbabu, U., Dordick, J. S., and Siegel, R. W., 2016, "Selective characterization of proteins on nanoscale concave surfaces," Biomater., 75, pp 305-312.
[93] Sheldon, R. A., 2007, "Enzyme immobilization: The quest for optimum performance," Adv. Synth. Catal., 349(8-9), pp 1289-1307.
[94] Milton, R. D., Wang, T., Knoche, K. L., and Minteer, S. D., 2016, "Tailoring Biointerfaces for Electrocatalysis," Langmuir, 32(10), pp 2291-2301.
[95] Zhou, L. Y., Jiang, Y. J., Gao, J., Zhao, X. Q., Ma, L., and Zhou, Q. L., 2012, "Oriented immobilization of glucose oxidase on graphene oxide," Biochem. Eng. J., 69, pp 28-31.
[96] Martins, M. V. A., Pereira, A. R., Luz, R. a. S., Iost, R. M., and Crespitho, F. N., 2014, "Evidence of short-range electron transfer of a redox enzyme on graphene oxide electrodes," Phys. Chem. Chem. Phys., 16(33), pp 17426-17436.
[97] Ramirez, P., Mano, N., Andreu, R., Ruzgas, T., Heller, A., Gorton, L., and Shleev, S., 2008, "Direct electron transfer from graphite and functionalized gold electrodes to T1 and T2/T3 copper centers of bilirubin oxidase," BBA Bioenergetics, 1777(10), pp 1364-1369.
[98] Arrocha, A. A., Cano-Castillo, U., Aguila, S. A., and Vazquez-Duhalt, R., 2014, "Enzyme orientation for direct electron transfer in an enzymatic fuel cell with alcohol oxidase and laccase electrodes," Biosens. Bioelectron., 61, pp 569-574.
[99] Li, Y., Zhang, J. W., Huang, X. R., and Wang, T. H., 2014, "Construction and direct electrochemistry of orientation controlled laccase electrode," Biochem. Biophys. Res. Comm., 446(1), pp 201-205.
[100] Shleev, S., Tkac, J., Christenson, A., Ruzgas, T., Yaropolov, A. I., Whittaker, J. W., and Gorton, L., 2005, "Direct electron transfer between copper-containing proteins and electrodes," Biosens. Bioelectron., 20(12), pp 2517-2554.
[101] Cosnier, S., Gondran, C., Le Pellec, A., and Senillou, A., 2001, "Controlled fabrication of glucose and catechol microbiosensors via electropolymerized biotinylated polypyrrole films," Anal. Lett., 34(1), pp 61-70.
[102] Asuri, P., Bale, S. S., Pangule, R. C., Shah, D. A., Kane, R. S., and Dordick, J. S., 2007, "Structure, function, and stability of enzymes covalently attached to single-walled carbon nanotubes," Langmuir, 23(24), pp 12318-12321.
[103] Delvaux, M., and Demoustier-Champagne, S., 2003, "Immobilisation of glucose oxidase within metallic nanotubes arrays for application to enzyme biosensors," Biosens. Bioelectron., 18(7), pp 943-951.
[104] Ferreira, L., Ramos, M. A., Dordick, J. S., and Gil, M. H., 2003, "Influence of different silica derivatives in the immobilization and stabilization of a Bacillus licheniformis protease (Subtilisin Carlsberg)," J. Mol. Catal. B Enzym., 21(4-6), pp 189-199.
[105] Wong, L. S., Khan, F., and Micklefield, J., 2009, "Selective Covalent Protein Immobilization: Strategies and Applications," Chem. Rev., 109(9), pp 4025-4053.
[106] Dinu, C. Z., Borkar, I. V., Bale, S. S., Campbell, A. S., Kane, R. S., and Dordick, J. S., 2012, "Perhydrolase-nanotube-paint sporicidal composites stabilized by intramolecular crosslinking," J. Mol. Catal. B Enzym., 75, pp 20-26.

[107] Xiao, Y., Patolsky, F., Katz, E., Hainfeld, J. F., and Willner, I., 2003, ""Plugging into enzymes": Nanowiring of redox enzymes by a gold nanoparticle," Science, 299(5614), pp 1877-1881.
[108] Patolsky, F., Weizmann, Y., and Willner, I., 2004, "Long-range electrical contacting of redox enzymes by SWCNT connectors," Angew. Chem., 43(16), pp 2113-2117.
[109] Choi, H. N., Kim, M. A., and Lee, W. Y., 2005, "Amperometric glucose biosensor based on sol-gel-derived metal oxide/Nafion composite films," Anal. Chim. Acta, 537(1-2), pp 179-187.
[110] Liu, S. Q., and Sun, Y. M., 2007, "Co-immobilization of glucose oxidase and hexokinase on silicate hybrid sol-gel membrane for glucose and ATP detections," Biosens. Bioelectron., 22(6), pp 905-911.
[111] Shen, Q. Y., Yang, R. J., Hua, X., Ye, F. Y., Zhang, W. B., and Zhao, W., 2011, "Gelatin-templated biomimetic calcification for beta-galactosidase immobilization," Process Biochem., 46(8), pp 1565-1571.
[112] Wang, Z. G., Wan, L. S., Liu, Z. M., Huang, X. J., and Xu, Z. K., 2009, "Enzyme immobilization on electrospun polymer nanofibers: An overview," J. Mol. Catal. B Enzym., 56(4), pp 189-195.
[113] Wen, H., Nallathambi, V., Chakraborty, D., and Barton, S. C., 2011, "Carbon fiber microelectrodes modified with carbon nanotubes as a new support for immobilization of glucose oxidase," Microchim. Acta, 175(3-4), pp 283-289.
[114] Gerard, M., Chaubey, A., and Malhotra, B. D., 2002, "Application of conducting polymers to biosensors," Biosens. Bioelectron., 17(5), pp 345-359.
[115] Amer, W. A., Wang, L., Amin, A. M., Ma, L. A., and Yu, H. J., 2010, "Recent Progress in the Synthesis and Applications of Some Ferrocene Derivatives and Ferrocene-Based Polymers," J. Inorg. Organomet. Polym. Mater., 20(4), pp 605-615.
[116] Sirkar, K., and Pishko, M. V., 1998, "Amperometric biosensors based on oxidoreductases immobilized in photopolymerized poly(ethylene glycol) redox polymer hydrogels," Anal. Chem., 70(14), pp 2888-2894.
[117] Heller, A., 2006, "Electron-conducting redox hydrogels: design, characteristics and synthesis," Curr. Opin. Chem. Biol., 10(6), pp 664-672.
[118] Ge, J., Lu, D. N., Liu, Z. X., and Liu, Z., 2009, "Recent advances in nanostructured biocatalysts," Biochem. Eng. J., 44(1), pp 53-59.
[119] Wen, D., Liu, W., Herrmann, A. K., and Eychmuller, A., 2014, "A Membraneless Glucose/O-2 Biofuel Cell Based on Pd Aerogels," Chem. Eur. J., 20(15), pp 4380-4385.
[120] Cosnier, S., 2003, "Biosensors based on electropolymerized films: new trends," Anal. Bioanal. Chem., 377(3), pp 507-520.
[121] Trojanowicz, M., and Krawczyk, T. K. V., 1995, "Electrochemical biosensors based on enzymes immobilized in electropolymerized films," Mikrochim. Acta, 121(1-4), pp 167-181.
[122] Degani, Y., and Heller, A., 1987, "Direct Electrical Communication between Chemically Modified Enzymes and Metal-Electrodes .1. Electron-Transfer from Glucose-Oxidase to Metal-Electrodes Via Electron Relays, Bound Covalently to the Enzyme," J. Phys. Chem., 91(6), pp 1285-1289.
[123] Degani, Y., and Heller, A., 1988, "Direct Electrical Communication between Chemically Modified Enzymes and Metal-Electrodes .2. Methods for Bonding Electron-Transfer Relays to Glucose-Oxidase and D-Amino-Acid Oxidase," J. Am. Chem. Soc., 110(8), pp 2615-2620.

[124] Kim, J. H., Hong, S. G., Wee, Y., Hu, S., Kwon, Y., Ha, S., and Kim, J., 2017, "Enzyme precipitate coating of pyranose oxidase on carbon nanotubes and their electrochemical applications," Biosens. Bioelectron., 87, pp 365-372.
[125] Kim, R. E., Hong, S. G., Ha, S., and Kim, J., 2014, "Enzyme adsorption, precipitation and crosslinking of glucose oxidase and laccase on polyaniline nanofibers for highly stable enzymatic biofuel cells," Enzyme Microb. Technol., 66, pp 35-41.
[126] Fischback, M., Kwon, K. Y., Lee, I., Shin, S. J., Park, H. G., Kim, B. C., Kwon, Y., Jung, H. T., Kim, J., and Ha, S., 2012, "Enzyme precipitate coatings of glucose oxidase onto carbon paper for biofuel cell applications," Biotechnol. Bioeng., 109(2), pp 318-324.
[127] Kim, B. C., Zhao, X. Y., Ahn, H. K., Kim, J. H., Lee, H. J., Kim, K. W., Nair, S., Hsiao, E., Jia, H. F., Oh, M. K., Sang, B. I., Kim, B. S., Kim, S. H., Kwon, Y., Ha, S., Gu, M. B., Wang, P., and Kim, J., 2011, "Highly stable enzyme precipitate coatings and their electrochemical applications," Biosens. Bioelectron., 26(5), pp 1980-1986.
[128] Broun, G., Thomas, D., Gellf, G., Domurado, D., Berjonne.Am, and Guillon, C., 1973, "New Methods for Binding Enzyme Molecules into a Water-Insoluble Matrix - Properties after Insolubilization," Biotechnol. Bioeng., 15(2), pp 359-375.
[129] Gouda, M. D., Kumar, M. A., Thakur, M. S., and Karanth, N. G., 2002, "Enhancement of operational stability of an enzyme biosensor for glucose and sucrose using protein based stabilizing agents," Biosens. Bioelectron., 17(6-7), pp 503-507.
[130] El Ichi-Ribault, S., Zebda, A., Laaroussi, A., Reverdy-Bruas, N., Chaussy, D., Belgacem, M. N., Suherman, A. L., Cinquin, P., and Martin, D. K., 2016, "Laccase-based biocathodes: Comparison of chitosan and Nafion," Anal. Chim. Acta, 937, pp 43-52.
[131] El Ichi, S., Zebda, A., Alcaraz, J. P., Laaroussi, A., Boucher, F., Boutonnat, J., Reverdy-Bruas, N., Chaussy, D., Belgacem, M. N., Cinquin, P., and Martin, D. K., 2015, "Bioelectrodes modified with chitosan for long-term energy supply from the body," Energ. Environ. Sci., 8(3), pp 1017-1026.
[132] El Ichi, S., Zebda, A., Laaroussi, A., Reverdy-Bruas, N., Chaussy, D., Belgacem, M. N., Cinquin, P., and Martin, D. K., 2014, "Chitosan improves stability of carbon nanotube biocathodes for glucose biofuel cells," Chem. Commun., 50(93), pp 14535-14538.
[133] Zhao, S., Zhang, K., Bai, Y., Yang, W. W., and Sun, C. Q., 2006, "Glucose oxidase/colloidal gold nanoparticles immobilized in Nafion film on glassy carbon electrode: Direct electron transfer and electrocatalysis," Bioelectrochem., 69(2), pp 158-163.
[134] Yu, Y. Y., Chen, Z. G., He, S. J., Zhang, B. B., Li, X. C., and Yao, M. C., 2014, "Direct electron transfer of glucose oxidase and biosensing for glucose based on PDDA-capped gold nanoparticle modified graphene/multi-walled carbon nanotubes electrode," Biosens. Bioelectron., 52, pp 147-152.
[135] Deng, C. Y., Chen, J. H., Nie, Z., and Si, S. H., 2010, "A sensitive and stable biosensor based on the direct electrochemistry of glucose oxidase assembled layer-by-layer at the multiwall carbon nanotube-modified electrode," Biosens. Bioelectron., 26(1), pp 213-219.
[136] Patil, D., Dung, N. Q., Jung, H., Ahn, S. Y., Jang, D. M., and Kim, D., 2012, "Enzymatic glucose biosensor based on CeO2 nanorods synthesized by non-isothermal precipitation," Biosens. Bioelectron., 31(1), pp 176-181.
[137] Holzinger, M., Le Goff, A., and Cosnier, S., 2012, "Carbon nanotube/enzyme biofuel cells," Electrochim. Acta, 82, pp 179-190.

[138] Wooten, M., Karra, S., Zhang, M. G., and Gorski, W., 2014, "On the Direct Electron Transfer, Sensing, and Enzyme Activity in the Glucose Oxidase/Carbon Nanotubes System," Anal. Chem., 86(1), pp 752-757.
[139] Minteer, S. D., Atanassov, P., Luckarift, H. R., and Johnson, G. R., 2012, "New materials for biological fuel cells," Mater. Today, 15(4), pp 166-173.
[140] Walcarius, A., Minteer, S. D., Wang, J., Lin, Y. H., and Merkoci, A., 2013, "Nanomaterials for bio-functionalized electrodes: recent trends," J. Mater. Chem. B, 1(38), pp 4878-4908.
[141] Feng, W., and Ji, P. J., 2011, "Enzymes immobilized on carbon nanotubes," Biotechnol. Adv., 29(6), pp 889-895.
[142] Ansari, S. A., and Husain, Q., 2012, "Potential applications of enzymes immobilized on/in nano materials: A review," Biotechnol. Adv., 30(3), pp 512-523.
[143] Sarma, A. K., Vatsyayan, P., Goswami, P., and Minteer, S. D., 2009, "Recent advances in material science for developing enzyme electrodes," Biosens. Bioelectron., 24(8), pp 2313-2322.
[144] Kuila, T., Bose, S., Khanra, P., Mishra, A. K., Kim, N. H., and Lee, J. H., 2011, "Recent advances in graphene-based biosensors," Biosens. Bioelectron., 26(12), pp 4637-4648.
[145] Goran, J. M., Mantilla, S. M., and Stevenson, K. J., 2013, "Influence of Surface Adsorption on the Interfacial Electron Transfer of Flavin Adenine Dinucleotide and Glucose Oxidase at Carbon Nanotube and Nitrogen-Doped Carbon Nanotube Electrodes," Anal. Chem., 85(3), pp 1571-1581.
[146] Liang, B., Guo, X. S., Fang, L., Hu, Y. C., Yang, G., Zhu, Q., Wei, J. W., and Ye, X. S., 2015, "Study of direct electron transfer and enzyme activity of glucose oxidase on graphene surface," Electrochem. Commun., 50, pp 1-5.
[147] Razmi, H., and Mohammad-Rezaei, R., 2013, "Graphene quantum dots as a new substrate for immobilization and direct electrochemistry of glucose oxidase: Application to sensitive glucose determination," Biosens. Bioelectron., 41, pp 498-504.
[148] Murata, K., Kajiya, K., Nakamura, N., and Ohno, H., 2009, "Direct electrochemistry of bilirubin oxidase on three-dimensional gold nanoparticle electrodes and its application in a biofuel cell," Energ. Environ. Sci., 2(12), pp 1280-1285.
[149] Reuillard, B., Abreu, C., Lalaoui, N., Le Goff, A., Holzinger, M., Ondel, O., Buret, F., and Cosnier, S., 2015, "One-year stability for a glucose/oxygen biofuel cell combined with pH reactivation of the laccase/carbon nanotube biocathode," Bioelectrochem., 106, pp 73-76.
[150] Aoki, A., and Heller, A., 1993, "Electron-Diffusion Coefficients in Hydrogels Formed of Cross-Linked Redox Polymers," J. Phys. Chem., 97(42), pp 11014-11019.
[151] Kim, J., Kim, S. I., and Yoo, K. H., 2009, "Polypyrrole nanowire-based enzymatic biofuel cells," Biosens. Bioelectron., 25(2), pp 350-355.
[152] Schuhmann, W., 1994, "Conducting Polymers and Their Application in Amperometric Biosensors," Diagnostic Biosensor Polymers, 556, pp 110-123.
[153] Bidan, G., 1992, "Electroconducting Conjugated Polymers - New Sensitive Matrices to Build up Chemical or Electrochemical Sensors - a Review," Sens. Actuators B, 6(1-3), pp 45-56.
[154] Bartlett, P. N., and Cooper, J. M., 1993, "A Review of the Immobilization of Enzymes in Electropolymerized Films," J. Electroanal. Chem., 362(1-2), pp 1-12.
[155] Ramanathan, K., Pandey, S. S., Kumar, R., Gulati, A., Surya, A., Murthy, N., and Malhotra, B. D., 2000, "Covalent immobilization of glucose oxidase to Poly(O-Amino benzoic acid) for application to glucose biosensor," J. Appl. Polym. Sci., 78(3), pp 662-667.

[156] Chaubey, A., Pande, K. K., Singh, V. S., and Malhotra, B. D., 2000, "Co-immobilization of lactate oxidase and lactate dehydrogenase on conducting polyaniline films," Anal. Chim. Acta, 407(1-2), pp 97-103.
[157] Heller, A., 1990, "Electrical Wiring of Redox Enzymes," Accounts Chem. Res., 23(5), pp 128-134.
[158] Osadebe, I., Conghaile, P. O., Kavanagh, P., and Leech, D., 2015, "Glucose oxidation by osmium redox polymer mediated enzyme electrodes operating at low potential and in oxygen, for application to enzymatic fuel cells," Electrochim. Acta, 182, pp 320-326.
[159] Saleem, M., Yu, H. J., Wang, L., Zain-Ul-Abdin, Khalid, H., Akram, M., Abbasi, N. M., and Huang, J., 2015, "Review on synthesis of ferrocene-based redox polymers and derivatives and their application in glucose sensing," Anal. Chim. Acta, 876, pp 9-25.
[160] Mao, F., Mano, N., and Heller, A., 2003, "Long tethers binding redox centers to polymer backbones enhance electron transport in enzyme "wiring" hydrogels," J. Am. Chem. Soc., 125(16), pp 4951-4957.
[161] Merchant, S. A., Glatzhofer, D. T., and Schmidtke, D. W., 2007, "Effects of electrolyte and pH on the behavior of cross-linked films of ferrocene-modified poly(ethylenimine)," Langmuir, 23(22), pp 11295-11302.
[162] Schuhmann, W., Ohara, T. J., Schmidt, H. L., and Heller, A., 1991, "Electron-Transfer between Glucose-Oxidase and Electrodes Via Redox Mediators Bound with Flexible Chains to the Enzyme Surface," J. Am. Chem. Soc., 113(4), pp 1394-1397.
[163] Milton, R. D., Hickey, D. P., Abdellaoui, S., Lim, K., Wu, F., Tan, B. X., and Minteer, S. D., 2015, "Rational design of quinones for high power density biofuel cells," Chem. Sci., 6(8), pp 4867-4875.
[164] Hou, C. T., Lang, Q. L., and Liu, A. H., 2016, "Tailoring 1,4-naphthoquinone with electron-withdrawing group: toward developing redox polymer and FAD-GDH based hydrogel bioanode for efficient electrocatalytic glucose oxidation," Electrochim. Acta, 211, pp 663-670.
[165] Guzik, U., Hupert-Kocurek, K., and Wojcieszynska, D., 2014, "Immobilization as a Strategy for Improving Enzyme Properties-Application to Oxidoreductases," Molecules, 19(7), pp 8995-9018.
[166] Falk, M., Blum, Z., and Shleev, S., 2012, "Direct electron transfer based enzymatic fuel cells," Electrochim. Acta, 82, pp 191-202.
[167] Ferapontova, E. E., Shleev, S., Ruzgas, T., Stoica, L., Christenson, A., Tkac, J., Yaropolov, A. I., and Gorton, L., 2005, "Direct Electrochemistry of Proteins and Enzymes," Persp. Bioanal., 1, pp 517-598.
[168] Chaubey, A., and Malhotra, B. D., 2002, "Mediated biosensors," Biosens. Bioelectron., 17(6-7), pp 441-456.
[169] Schuhmann, W., Wohlschlager, H., Lammert, R., Schmidt, H. L., Loffler, U., Wiemhofer, H. D., and Gopel, W., 1990, "Leaching of Dimethylferrocene, a Redox Mediator in Amperometric Enzyme Electrodes," Sens. Actuators B, 1(1-6), pp 571-575.
[170] Badia, A., Carlini, R., Fernandez, A., Battaglini, F., Mikkelsen, S. R., and English, A. M., 1993, "Intramolecular Electron-Transfer Rates in Ferrocene-Derivatized Glucose-Oxidase," J. Am. Chem. Soc., 115(16), pp 7053-7060.
[171] Okawa, Y., Nagano, M., Hirota, S., Kobayashi, H., Ohno, T., and Watanabe, M., 1999, "Tethered mediator biosensor. Mediated electron transfer between redox enzyme and electrode via ferrocene anchored to electrode surface with long poly(oxyethylene) chain," Biosens. Bioelectron., 14(2), pp 229-235.

[172] Heller, A., 1992, "Electrical Connection of Enzyme Redox Centers to Electrodes," J. Phys. Chem., 96(9), pp 3579-3587.
[173] Deng, H. M., Shen, W., and Gao, Z. Q., 2012, "Synthesis of water-soluble and cross-linkable ferrocenyl redox polymers for uses as mediators in biosensors," Sens. Actuators B, 168, pp 238-242.
[174] Merchant, S. A., Meredith, M. T., Tran, T. O., Brunski, D. B., Johnson, M. B., Glatzhofer, D. T., and Schmidtke, D. W., 2010, "Effect of Mediator Spacing on Electrochemical and Enzymatic Response of Ferrocene Redox Polymers," J. Phys. Chem. C, 114(26), pp 11627-11634.
[175] Soukharev, V., Mano, N., and Heller, A., 2004, "A four-electron O-2-electroreduction biocatalyst superior to platinum and a biofuel cell operating at 0.88 V," J. Am. Chem. Soc., 126(27), pp 8368-8369.
[176] Aoki, A., Rajagopalan, R., and Heller, A., 1995, "Effect of Quaternization on Electron-Diffusion Coefficients for Redox Hydrogels Based on Poly(4-Vinylpyridine)," J. Phys. Chem., 99(14), pp 5102-5110.
[177] Rajagopalan, R., Aoki, A., and Heller, A., 1996, "Effect of quaternization of the glucose oxidase "wiring" redox polymer on the maximum current densities of glucose electrodes," J. Phys. Chem., 100(9), pp 3719-3727.
[178] Forster, R. J., and Vos, J. G., 1993, "Charge Transport-Properties of Electrodes Modified with Osmium Containing Polymer-Films," NATO ASI Series, 385, pp 615-621.
[179] Bunte, C., and Ruhe, J., 2009, "Photochemical Generation of Ferrocene-Based Redox-Polymer Networks," Macromol. Rapid Comm., 30(21), pp 1817-1822.
[180] Takahashi, S., and Anzai, J., 2013, "Recent Progress in Ferrocene-Modified Thin Films and Nanoparticles for Biosensors," Mater., 6(12), pp 5742-5762.
[181] Berezin, I. V., Bogdanovskaia, V. A., Varfolomeev, S. D., Tarasevich, M. R., and Iaropolov, A. I., 1978, "Bioelectrocatalysis - Equilibrium Oxygen Potential in Presence of Laccase," Dokl. Akad. Nauk. SSSR, 240(3), pp 615-618.
[182] Brocato, S., Lau, C., and Atanassov, P., 2012, "Mechanistic study of direct electron transfer in bilirubin oxidase," Electrochim. Acta, 61, pp 44-49.
[183] Filip, J., and Tkac, J., 2014, "Direct electron transfer of bilirubin oxidase on graphene and carbon black," J Biotechnol, 185, pp S21-S22.
[184] Pita, M., Shleev, S., Ruzgas, T., Fernandez, V. M., Yaropolov, A. I., and Gorton, L., 2006, "Direct heterogeneous electron transfer reactions of fungal laccases at bare and thiol-modified gold electrodes," Electrochem. Commun., 8(5), pp 747-753.
[185] Shleev, S., Jarosz-Wilkolazka, A., Khalunina, A., Morozova, O., Yaropolov, A., Ruzgas, T., and Gorton, L., 2005, "Direct electron transfer reactions of laccases from different origins on carbon electrodes," Bioelectrochem., 67(1), pp 115-124.
[186] Shleev, S., Wang, Y., Gorbacheva, M., Christenson, A., Haltrich, D., Ludwig, R., Ritzgas, T., and Gorton, L., 2008, "Direct heterogeneous electron transfer reactions of Bacillus halodurans bacterial blue multicopper oxidase," Electroanal., 20(9), pp 963-969.
[187] Pereira, A. R., Martins, M. V. A., and Crespilho, F. N., 2014, "Direct electron transfer of glucose oxidase on graphene oxides-modified flexible carbon fiber electrode," Abstr. Pap. Am. Chem. Soc., 247, pp
[188] Goran, J. M., Phan, E. N. H., Favela, C. A., and Stevenson, K. J., 2015, "H2O2 Detection at Carbon Nanotubes and Nitrogen-Doped Carbon Nanotubes: Oxidation, Reduction, or Disproportionation?," Anal. Chem., 87(12), pp 5989-5996.

[189] Gao, Y. F., Yang, T., Yang, X. L., Zhang, Y. S., Xiao, B. L., Hong, J., Sheibani, N., Ghourchian, H., Hong, T., and Moosavi-Movahedi, A. A., 2014, "Direct electrochemistry of glucose oxidase and glucose biosensing on a hydroxyl fullerenes modified glassy carbon electrode," Biosens. Bioelectron., 60, pp 30-34.
[190] Mani, V., Devadas, B., and Chen, S. M., 2013, "Direct electrochemistry of glucose oxidase at electrochemically reduced graphene oxide-multiwalled carbon nanotubes hybrid material modified electrode for glucose biosensor," Biosens. Bioelectron., 41, pp 309-315.
[191] Jose, M. V., Marx, S., Murata, H., Koepsel, R. R., and Russell, A. J., 2012, "Direct electron transfer in a mediator-free glucose oxidase-based carbon nanotube-coated biosensor," Carbon, 50(11), pp 4010-4020.
[192] Liu, W. S., Wang, L., and Jiang, R. R., 2012, "Specific Enzyme Immobilization Approaches and Their Application with Nanomaterials," Top. Catal., 55(16-18), pp 1146-1156.
[193] Riklin, A., Katz, E., Willner, I., Stocker, A., and Buckmann, A. F., 1995, "Improving Enzyme-Electrode Contacts by Redox Modification of Cofactors," Nature, 376(6542), pp 672-675.
[194] Abuchowski, A., Vanes, T., Palczuk, N. C., and Davis, F. F., 1977, "Alteration of Immunological Properties of Bovine Serum-Albumin by Covalent Attachment of Polyethylene-Glycol," J. Biol. Chem., 252(11), pp 3578-3581.
[195] Abuchowski, A., Mccoy, J. R., Palczuk, N. C., Vanes, T., and Davis, F. F., 1977, "Effect of Covalent Attachment of Polyethylene-Glycol on Immunogenicity and Circulating Life of Bovine Liver Catalase," J. Biol. Chem., 252(11), pp 3582-3586.
[196] Sumerlin, B. S., 2012, "Proteins as Initiators of Controlled Radical Polymerization: Grafting-from via ATRP and RAFT," ACS Macro Lett., 1(1), pp 141-145.
[197] Matyjaszewski, K., and Tsarevsky, N. V., 2014, "Macromolecular Engineering by Atom Transfer Radical Polymerization," J. Am. Chem. Soc., 136(18), pp 6513-6533.
[198] Matyjaszewski, K., 2012, "Atom Transfer Radical Polymerization (ATRP): Current Status and Future Perspectives," Macromol., 45(10), pp 4015-4039.
[199] Siegwart, D. J., Oh, J. K., and Matyjaszewski, K., 2012, "ATRP in the design of functional materials for biomedical applications," Prog. Polym. Sci., 37(1), pp 18-37.
[200] Cobo, I., Li, M., Sumerlin, B. S., and Perrier, S., 2015, "Smart hybrid materials by conjugation of responsive polymers to biomacromolecules," Nat. Mater., 14(2), pp 143-159.
[201] Pelegri-O'day, E. M., Lin, E. W., and Maynard, H. D., 2014, "Therapeutic Protein-Polymer Conjugates: Advancing Beyond PEGylation," J. Am. Chem. Soc., 136(41), pp 14323-14332.
[202] Kim, J., and Grate, J. W., 2004, "Single enzyme nanoparticles.," Abstr. Pap. Am. Chem. Soc., 227, pp U251-U251.
[203] Matyjaszewski, K., and Spanswick, J., 2005, "Controlled/living radical polymerization," Mater. Today, 8(3), pp 26-33.
[204] Georges, M. K., Veregin, R. P. N., Kazmaier, P. M., and Hamer, G. K., 1993, "Narrow Molecular-Weight Resins by a Free-Radical Polymerization Process," Macromol., 26(11), pp 2987-2988.
[205] Hawker, C. J., Bosman, A. W., and Harth, E., 2001, "New polymer synthesis by nitroxide mediated living radical polymerizations," Chem. Rev., 101(12), pp 3661-3688.
[206] Wang, J. S., and Matyjaszewski, K., 1995, "Controlled Living Radical Polymerization - Atom-Transfer Radical Polymerization in the Presence of Transition-Metal Complexes," J. Am. Chem. Soc., 117(20), pp 5614-5615.

[207] Destarac, M., Charmot, D., Franck, X., and Zard, S. Z., 2000, "Dithiocarbamates as universal reversible addition-fragmentation chain transfer agents," Macromol. Rapid Comm., 21(15), pp 1035-1039.
[208] Chiefari, J., Chong, Y. K., Ercole, F., Krstina, J., Jeffery, J., Le, T. P. T., Mayadunne, R. T. A., Meijs, G. F., Moad, C. L., Moad, G., Rizzardo, E., and Thang, S. H., 1998, "Living free-radical polymerization by reversible addition-fragmentation chain transfer: The RAFT process," Macromol., 31(16), pp 5559-5562.
[209] Averick, S., Simakova, A., Park, S., Konkolewicz, D., Magenau, A. J. D., Mehl, R. A., and Matyjaszewski, K., 2012, "ATRP under Biologically Relevant Conditions: Grafting from a Protein," ACS Macro Lett., 1(1), pp 6-10.
[210] Li, M., Li, H. M., De, P., and Sumerlin, B. S., 2011, "Thermoresponsive Block Copolymer-Protein Conjugates Prepared by Grafting-from via RAFT Polymerization," Macromol. Rapid Comm., 32(4), pp 354-359.
[211] Lele, B. S., Murata, H., Matyjaszewski, K., and Russell, A. J., 2005, "Synthesis of uniform protein-polymer conjugates," Biomacromolecules, 6(6), pp 3380-3387.
[212] Heredia, K. L., Bontempo, D., Ly, T., Byers, J. T., Halstenberg, S., and Maynard, H. D., 2005, "In situ preparation of protein - "Smart" polymer conjugates with retention of bioactivity," J. Am. Chem. Soc., 127(48), pp 16955-16960.
[213] Gao, W. P., Liu, W. G., Mackay, J. A., Zalutsky, M. R., Toone, E. J., and Chilkoti, A., 2009, "In situ growth of a stoichiometric PEG-like conjugate at a protein's N-terminus with significantly improved pharmacokinetics," Proc. Natl. Acad. Sci., 106(36), pp 15231-15236.
[214] Peeler, J. C., Woodman, B. F., Averick, S., Miyake-Stoner, S. J., Stokes, A. L., Hess, K. R., Matyjaszewski, K., and Mehl, R. A., 2010, "Genetically Encoded Initiator for Polymer Growth from Proteins," J. Am. Chem. Soc., 132(39), pp 13575-13577.
[215] Murata, H., Cummings, C. S., Koepsel, R. R., and Russell, A. J., 2013, "Polymer-Based Protein Engineering Can Rationally Tune Enzyme Activity, pH-Dependence, and Stability," Biomacromolecules, 14(6), pp 1919-1926.
[216] Carmali, S., Murata, H., Cummings, C., Matyjaszewski, K., and Russell, A. J., 2017, "Polymer-Based Protein Engineering: Synthesis and Characterization of Armored, High Graft Density Polymer-Protein Conjugates," Methods in Enzymology, pp in press.
[217] Cummings, C., Murata, H., Koepsel, R., and Russell, A. J., 2013, "Tailoring enzyme activity and stability using polymer-based protein engineering," Biomater., 34(30), pp 7437-7443.
[218] Cummings, C., Murata, H., Koepsel, R., and Russell, A. J., 2014, "Dramatically Increased pH and Temperature Stability of Chymotrypsin Using Dual Block Polymer-Based Protein Engineering," Biomacromolecules, 15(3), pp 763-771.
[219] Cummings, C. S., Murata, H., Matyjaszewski, K., and Russell, A. J., 2016, "Polymer-Based Protein Engineering Enables Molecular Dissolution of Chymotrypsin in Acetonitrile," ACS Macro Lett., 5(4), pp 493-497.
[220] Falatach, R., Li, S. H., Sloane, S., Mcglone, C., Berberich, J. A., Page, R. C., Averick, S., and Konkolewicz, D., 2015, "Why synthesize protein-polymer conjugates? The stability and activity of chymotrypsin-polymer bioconjugates synthesized by RAFT," Polym., 72, pp 382-386.
[221] Hu, J., Wang, G. L., Zhao, W. G., Liu, X. Y., Zhang, L. B., and Gao, W. P., 2016, "Site-specific in situ growth of an interferon-polymer conjugate that outperforms PEGASYS in cancer therapy," Biomater., 96, pp 84-92.

[222] Murata, H., Cummings, C. S., Koepsel, R. R., and Russell, A. J., 2014, "Rational Tailoring of Substrate and Inhibitor Affinity via ATRP Polymer-Based Protein Engineering," Biomacromolecules, 15(7), pp 2817-2823.
[223] Li, H. M., Bapat, A. P., Li, M., and Sumerlin, B. S., 2011, "Protein conjugation of thermoresponsive amine-reactive polymers prepared by RAFT," Polym. Chem., 2(2), pp 323-327.
[224] Cummings, C. S., Campbell, A. S., Baker, S. L., Carmali, S., Murata, H., and Russell, A. J., 2017, "Design of Stomach Acid-Stable and Mucin-Binding Enzyme Polymer Conjugates," Biomacromolecules, 18(2), pp 576-586.
[225] Meredith, M. T., and Minteer, S. D., 2012, "Biofuel Cells: Enhanced Enzymatic Bioelectrocatalysis," Annu. Rev. Anal. Chem., 5, pp 157-179.
[226] Ammam, M., 2014, "Electrochemical and electrophoretic deposition of enzymes: Principles, differences and application in miniaturized biosensor and biofuel cell electrodes," Biosens. Bioelectron., 58(1), pp 121-131.
[227] Leech, D., Kavanagh, P., and Schuhmann, W., 2012, "Enzymatic fuel cells: Recent progress," Electrochim. Acta, 84, pp 223-234.
[228] De Poulpiquet, A., Ciaccafava, A., and Lojou, E., 2014, "New trends in enzyme immobilization at nanostructured interfaces for efficient electrocatalysis in biofuel cells," Electrochim. Acta, 126, pp 104-114.
[229] Miyake, T., Haneda, K., Yoshino, S., and Nishizawa, M., 2013, "Flexible, layered biofuel cells," Biosens. Bioelectron., 40(1), pp 45-49.
[230] Jenkins, P., Tuurala, S., Vaari, A., Valkiainen, M., Smolander, M., and Leech, D., 2012, "A mediated glucose/oxygen enzymatic fuel cell based on printed carbon inks containing aldose dehydrogenase and laccase as anode and cathode," Enzyme Microb. Technol., 50(3), pp 181-187.
[231] Mano, N., Mao, F., and Heller, A., 2003, "Characteristics of a miniature compartment-less glucose-O-2 biofuel cell and its operation in a living plant," J. Am. Chem. Soc., 125(21), pp 6588-6594.
[232] Kim, J., and Yoo, K. H., 2013, "Glucose oxidase nanotube-based enzymatic biofuel cells with improved laccase biocathodes," Phys. Chem. Chem. Phys., 15(10), pp 3510-3517.
[233] Bunte, C., Hussein, L., and Urban, G. A., 2014, "Performance of non-compartmentalized enzymatic biofuel cell based on buckypaper cathode and ferrocene-containing redox polymer anode," J. Power Sources, 247, pp 579-586.
[234] Gao, F., Viry, L., Maugey, M., Poulin, P., and Mano, N., 2010, "Engineering hybrid nanotube wires for high-power biofuel cells," Nat. Commun., 1, pp
[235] Zhang, Y. J., Chu, M., Yang, L., Tan, Y. M., Deng, W. F., Ma, M., Su, X. L., and Xie, Q. J., 2014, "Three-Dimensional Graphene Networks as a New Substrate for Immobilization of Laccase and Dopamine and Its Application in Glucose/O-2 Biofuel Cell," ACS Appl. Mater. Interfaces, 6(15), pp 12808-12814.
[236] Brunauer, S., Emmett, P. H., and Teller, E., 1938, "Adsorption of gases in multimolecular layers," J. Am. Chem. Soc., 60, pp 309-319.
[237] Kim, K. H., Oh, Y., and Islam, M. F., 2013, "Mechanical and Thermal Management Characteristics of Ultrahigh Surface Area Single-Walled Carbon Nanotube Aerogels," Adv. Funct. Mater., 23(3), pp 377-383.
[238] Kim, K. H., Oh, Y., and Islam, M. F., 2012, "Graphene coating makes carbon nanotube aerogels superelastic and resistant to fatigue," Nat. Nanotechnol., 7(9), pp 562-566.

[239] Bryning, M. B., Milkie, D. E., Islam, M. F., Hough, L. A., Kikkawa, J. M., and Yodh, A. G., 2007, "Carbon nanotube aerogels," Adv. Mater., 19(5), pp 661-+.
[240] Islam, M. F., Rojas, E., Bergey, D. M., Johnson, A. T., and Yodh, A. G., 2003, "High weight fraction surfactant solubilization of single-wall carbon nanotubes in water," Nano Lett, 3(2), pp 269-273.
[241] Hummers, W. S., and Offeman, R. E., 1958, "Preparation of Graphitic Oxide," J. Am. Chem. Soc., 80(6), pp 1339-1339.
[242] Marcano, D. C., Kosynkin, D. V., Berlin, J. M., Sinitskii, A., Sun, Z. Z., Slesarev, A., Alemany, L. B., Lu, W., and Tour, J. M., 2010, "Improved Synthesis of Graphene Oxide," Acs Nano, 4(8), pp 4806-4814.
[243] Chen, D. T. N., Chen, K., Hough, L. A., Islam, M. F., and Yodh, A. G., 2010, "Rheology of Carbon Nanotube Networks During Gelation," Macromol., 43(4), pp 2048-2053.
[244] Hough, L. A., Islam, M. F., Janmey, P. A., and Yodh, A. G., 2004, "Viscoelasticity of single wall carbon nanotube suspensions," Phys. Rev. Lett., 93(16), pp
[245] Fan, F. R. F., and Bard, A. J., 1999, "Imaging of biological macromolecules on mica in humid air by scanning electrochemical microscopy," Proc. Natl. Acad. Sci., 96(25), pp 14222-14227.
[246] Gong, C. S., He, Y. M., Zhou, J. Y., Chen, W. J., Han, W. H., Zhang, Z. X., Zhang, P., Pan, X. J., Wang, Z. G., and Xie, E. Q., 2014, "Synthesis on Winged Graphene Nanofibers and Their Electrochemical Capacitive Performance," ACS Appl. Mater. Interfaces, 6(17), pp 14844-14850.
[247] Rabaey, K., Boon, N., Siciliano, S. D., Verhaege, M., and Verstraete, W., 2004, "Biofuel cells select for microbial consortia that self-mediate electron transfer," Appl. Environ. Microb., 70(9), pp 5373-5382.
[248] Laviron, E., 1979, "General Expression of the Linear Potential Sweep Voltammogram in the Case of Diffusionless Electrochemical Systems," J. Electroanal. Chem., 101(1), pp 19-28.
[249] Rahimi, P., Rafiee-Pour, H. A., Ghourchian, H., Norouzi, P., and Ganjali, M. R., 2010, "Ionic-liquid/NH2-MWCNTs as a highly sensitive nano-composite for catalase direct electrochemistry," Biosens. Bioelectron., 25(6), pp 1301-1306.
[250] Vivian, J. T., and Callis, P. R., 2001, "Mechanisms of tryptophan fluorescence shifts in proteins," Biophys J, 80(5), pp 2093-2109.
[251] Beechem, J. M., and Brand, L., 1985, "Time-Resolved Fluorescence of Proteins," Annu. Rev. Biochem., 54, pp 43-71.
[252] Cracknell, J. A., Mcnamara, T. P., Lowe, E. D., and Blanford, C. F., 2011, "Bilirubin oxidase from Myrothecium verrucaria: X-ray determination of the complete crystal structure and a rational surface modification for enhanced electrocatalytic O-2 reduction," Dalton T, 40(25), pp 6668-6675.
[253] Ramasamy, R. P., Luckarift, H. R., Ivnitski, D. M., Atanassov, P. B., and Johnson, G. R., 2010, "High electrocatalytic activity of tethered multicopper oxidase-carbon nanotube conjugates," Chem. Commun., 46(33), pp 6045-6047.
[254] Shleev, S., El Kasmi, A., Ruzgas, T., and Gorton, L., 2004, "Direct heterogeneous electron transfer reactions of bilirubin oxidase at a spectrographic graphite electrode," Electrochem. Commun., 6(9), pp 934-939.
[255] Ammam, M., and Fransaer, J., 2013, "Combination of laccase and catalase in construction of H2O2-O-2 based biocathode for applications in glucose biofuel cells," Biosens. Bioelectron., 39(1), pp 274-281.

[256] Zheng, W., Zhao, H. Y., Zhou, H. M., Xu, X. X., Ding, M. H., and Zheng, Y. F., 2010, "Electrochemistry of bilirubin oxidase at carbon nanotubes," J. Solid State Electrochem., 14(2), pp 249-254.
[257] Devadas, B., Mani, V., and Chen, S. M., 2012, "A Glucose/O-2 Biofuel Cell Based on Graphene and Multiwalled Carbon Nanotube Composite Modified Electrode," Int. J. Electrochem. Sci., 7(9), pp 8064-8075.
[258] Palanisamy, S., Cheemalapati, S., and Chen, S. M., 2012, "An Enzymatic Biofuel cell Based On Electrochemically Reduced Graphene Oxide and Multiwalled Carbon nanotubes/Zinc oxide Modified Electrode," Int. J. Electrochem. Sci., 7(11), pp 11477-11487.
[259] Dudzik, J., Chang, W. C., Kannan, A. M., Filipek, S., Viswanathan, S., Li, P. Z., Renugopalakrishnan, V., and Audette, G. F., 2013, "Cross-linked glucose oxidase clusters for biofuel cell anode catalysts," Biofabr., 5(3), pp
[260] Shan, G. B., Surampalli, R. Y., Tyagi, R. D., and Zhang, T. C., 2009, "Nanomaterials for environmental burden reduction, waste treatment, and nonpoint source pollution control: a review," Front. Environ. Sc.i Eng., 3(3), pp 249-264.
[261] Schubart, I. W., Gobel, G., and Lisdat, F., 2012, "A pyrroloquinolinequinone-dependent glucose dehydrogenase (PQQ-GDH)-electrode with direct electron transfer based on polyaniline modified carbon nanotubes for biofuel cell application," Electrochim. Acta, 82, pp 224-232.
[262] Min, K., Ryu, J. H., and Yoo, Y. J., 2010, "Mediator-free Glucose/O-2 Biofuel Cell Based on a 3-Dimensional Glucose Oxidase/SWNT/Polypyrrole Composite Electrode," Biotechnol. Bioproc. Eng., 15(3), pp 371-375.
[263] Deng, L., Shang, L., Wang, Y. Z., Wang, T., Chen, H. J., and Dong, S. J., 2008, "Multilayer structured carbon nanotubes/poly-L-lysine/laccase composite cathode for glucose/O-2 biofuel cell," Electrochem. Commun., 10(7), pp 1012-1015.
[264] Scherbahn, V., Putze, M. T., Dietzel, B., Heinlein, T., Schneider, J. J., and Lisdat, F., 2014, "Biofuel cells based on direct enzyme-electrode contacts using PQQ-dependent glucose dehydrogenase/bilirubin oxidase and modified carbon nanotube materials," Biosens. Bioelectron., 61, pp 631-638.
[265] Campbell, A. S., Dong, C. B., Dordick, J. S., and Dinu, C. Z., 2013, "BioNano engineered hybrids for hypochlorous acid generation," Process Biochem., 48(9), pp 1355-1360.
[266] Yang, X. Y., Tian, G., Jiang, N., and Su, B. L., 2012, "Immobilization technology: a sustainable solution for biofuel cell design," Energ. Environ. Sci., 5(2), pp 5540-5563.
[267] Wu, X. L., Ge, J., Yang, C., Hou, M., and Liu, Z., 2015, "Facile synthesis of multiple enzyme-containing metal-organic frameworks in a biomolecule-friendly environment," Chem. Commun., 51(69), pp 13408-13411.
[268] Li, Z. X., Zhang, Y. F., Su, Y. C., Ouyang, P. K., Ge, J., and Liu, Z., 2014, "Spatial co-localization of multi-enzymes by inorganic nanocrystal-protein complexes," Chem. Commun., 50(83), pp 12465-12468.
[269] Ge, J., Lei, J. D., and Zare, R. N., 2012, "Protein-inorganic hybrid nanoflowers," Nat. Nanotechnol., 7(7), pp 428-432.
[270] Wu, X. L., Yang, C., Ge, J., and Liu, Z., 2015, "Polydopamine tethered enzyme/metal-organic framework composites with high stability and reusability," Nanoscale, 7(45), pp 18883-18886.
[271] Lyu, F. J., Zhang, Y. F., Zare, R. N., Ge, J., and Liu, Z., 2014, "One-Pot Synthesis of Protein-Embedded Metal-Organic Frameworks with Enhanced Biological Activities," Nano Lett, 14(10), pp 5761-5765.

[272] Wu, X. L., Hou, M., and Ge, J., 2015, "Metal-organic frameworks and inorganic nanoflowers: a type of emerging inorganic crystal nanocarrier for enzyme immobilization," Catal. Sci. Technol., 5(12), pp 5077-5085.
[273] Ge, J., Yang, C., Zhu, J. Y., Lu, D. a. N., and Liu, Z., 2012, "Nanobiocatalysis in Organic Media: Opportunities for Enzymes in Nanostructures," Top. Catal., 55(16-18), pp 1070-1080.
[274] Zhu, L., Gong, L., Zhang, Y. F., Wang, R., Ge, J., Liu, Z., and Zare, R. N., 2013, "Rapid Detection of Phenol Using a Membrane Containing Laccase Nanoflowers," Chem. Asian J., 8(10), pp 2358-2360.
[275] Wang, R., Zhang, Y. F., Lu, D. N., Ge, J., Liu, Z., and Zare, R. N., 2013, "Functional protein-organic/inorganic hybrid nanomaterials," Wiley Nanomed. Nanobiotechnol., 5(4), pp 320-328.
[276] Falk, M., Andoralov, V., Blum, Z., Sotres, J., Suyatin, D. B., Ruzgas, T., Arnebrant, T., and Shleev, S., 2012, "Biofuel cell as a power source for electronic contact lenses," Biosens. Bioelectron., 37(1), pp 38-45.
[277] Falk, M., Andoralov, V., Silow, M., Toscano, M. D., and Shleev, S., 2013, "Miniature Biofuel Cell as a Potential Power Source for Glucose-Sensing Contact Lenses," Anal. Chem., 85(13), pp 6342-6348.
[278] Campbell, A. S., Jeong, Y. J., Geier, S. M., Koepsel, R. R., Russell, A. J., and Islam, M. F., 2015, "Membrane/Mediator-Free Rechargeable Enzymatic Biofuel Cell Utilizing Graphene/Single-Wall Carbon Nanotube Cogel Electrodes," ACS Appl. Mater. Interfaces, 7(7), pp 4056-4065.
[279] Marx, S., Jose, M. V., Andersen, J. D., and Russell, A. J., 2011, "Electrospun gold nanofiber electrodes for biosensors," Biosens. Bioelectron., 26(6), pp 2981-2986.
[280] Wilson, E., and Islam, M. F., 2015, "Ultracompressible, High-Rate Supercapacitors from Graphene-Coated Carbon Nanotube Aerogels," ACS Appl. Mater. Interfaces, 7(9), pp 5612-5618.
[281] Mano, N., 2012, "Features and applications of bilirubin oxidases," Appl. Microbiol. Biot., 96(2), pp 301-307.
[282] Bard, A. J., and Faulkner, L. R. Electrochemical methods : fundamentals and applications, Edn. 2nd. (Wiley, New York; 2001).
[283] Stoller, M. D., Park, S. J., Zhu, Y. W., An, J. H., and Ruoff, R. S., 2008, "Graphene-Based Ultracapacitors," Nano Lett, 8(10), pp 3498-3502.
[284] Laviron, E., and Roullier, L., 1980, "General Expression of the Linear Potential Sweep Voltammogram for a Surface Redox Reaction with Interactions between the Adsorbed Molecules - Applications to Modified Electrodes," J. Electroanal. Chem., 115(1), pp 65-74.
[285] Heller, A., and Degani, Y., 1987, "Direct Electrical Communication between Redox Enzymes and Metal-Electrodes," J. Electrochem. Soc., 134(8B), pp C494-C495.
[286] Barton, S. C., Gallaway, J., and Atanassov, P., 2004, "Enzymatic biofuel cells for Implantable and microscale devices," Chem. Rev., 104(10), pp 4867-4886.
[287] Filip, J., and Tkac, J., 2014, "Is graphene worth using in biofuel cells?," Electrochim. Acta, 136, pp 340-354.
[288] Campbell, A. S., Jose, M. V., Marx, S., Cornelius, S., Koepsel, R. R., Islam, M. F., and Russell, A. J., 2016, "Improved power density of an enzymatic biofuel cell with fibrous supports of high curvature," RSC Adv., 6(12), pp 10150-10158.

[289] Mcmillan, D. G. G., Marritt, S. J., Kemp, G. L., Gordon-Brown, P., Butt, J. N., and Jeuken, L. J. C., 2013, "The impact of enzyme orientation and electrode topology on the catalytic activity of adsorbed redox enzymes," Electrochim. Acta, 110, pp 79-85.
[290] Ivnitski, D., Atanassov, P., and Apblett, C., 2007, "Direct bioelectrocatalysis of PQQ-dependent glucose dehydrogenase," Electroanal., 19(15), pp 1562-1568.
[291] Baghayeri, M., Zare, E. N., and Lakouraj, M. M., 2015, "Monitoring of hydrogen peroxide using a glassy carbon electrode modified with hemoglobin and a polypyrrole-based nanocomposite," Microchim. Acta, 182(3-4), pp 771-779.
[292] Baghayeri, M., Zare, E. N., and Lakouraj, M. M., 2014, "Novel superparamagnetic PFu@Fe3O4 conductive nanocomposite as a suitable host for hemoglobin immobilization," Sens. Actuators B, 202, pp 1200-1208.
[293] Baghayeri, M., Zare, E. N., and Lakouraj, M. M., 2014, "A simple hydrogen peroxide biosensor based on a novel electro-magnetic poly(p-phenylenediamine)@Fe3O4 nanocomposite," Biosens. Bioelectron., 55, pp 259-265.
[294] Baghayeri, M., Zare, E. N., and Namadchian, M., 2013, "Direct electrochemistry and electrocatalysis of hemoglobin immobilized on biocompatible poly(styrene-alternative-maleic acid)/functionalized multi-wall carbon nanotubes blends," Sens. Actuators B, 188, pp 227-234.
[295] Baghayeri, M., 2015, "Glucose sensing by a glassy carbon electrode modified with glucose oxidase and a magnetic polymeric nanocomposite," RSC Adv., 5(24), pp 18267-18274.
[296] Abdellaoui, S., Milton, R. D., Quah, T., and Minteer, S. D., 2016, "NAD-dependent dehydrogenase bioelectrocatalysis: the ability of a naphthoquinone redox polymer to regenerate NAD," Chem. Commun., 52(6), pp 1147-1150.
[297] Chen, J., Bamper, D., Glatzhofer, D. T., and Schmidtke, D. W., 2015, "Development of Fructose Dehydrogenase-Ferrocene Redox Polymer Films for Biofuel Cell Anodes," J. Electrochem. Soc., 162(3), pp F258-F264.
[298] Hardy, C. G., Ren, L. X., Tamboue, T. C., and Tang, C. B., 2011, "Side-Chain Ferrocene-Containing (Meth)acrylate Polymers: Synthesis and Properties," J. Polym. Sci. A Polym. Chem., 49(6), pp 1409-1420.
[299] Herfurth, C., Voll, D., Buller, J., Weiss, J., Barner-Kowollik, C., and Laschewsky, A., 2012, "Radical Addition Fragmentation Chain Transfer (RAFT) Polymerization of Ferrocenyl (Meth)Acrylates," J. Polym. Sci. A Polym. Chem., 50(1), pp 108-118.
[300] Matyjaszewski, K., and Xia, J. H., 2001, "Atom transfer radical polymerization," Chem. Rev., 101(9), pp 2921-2990.
[301] Ciampoli.M, and Nardi, N., 1967, "Complexes of Bivalent Iron Cobalt Nickel and Copper with Bis(2-Dimethylaminoethyl) Oxide," Inorg. Chem., 6(3), pp 445-&.
[302] Ahmad, S., Gromiha, M., Fawareh, H., and Sarai, A., 2004, "ASAView: Database and tool for solvent accessibility representation in proteins," Bmc Bioinformatics, 5, pp
[303] Lins, L., Thomas, A., and Brasseur, R., 2003, "Analysis of accessible surface of residues in proteins," Protein Sci., 12(7), pp 1406-1417.
[304] Li, H., Robertson, A. D., and Jensen, J. H., 2005, "Very fast empirical prediction and rationalization of protein pK(a) values," Proteins, 61(4), pp 704-721.
[305] Gotti, G., Fajerwerg, K., Evrard, D., and Gros, P., 2014, "Electrodeposited gold nanoparticles on glassy carbon: Correlation between nanoparticles characteristics and oxygen reduction kinetics in neutral media," Electrochim. Acta, 128, pp 412-419.

[306] Hezard, T., Fajerwerg, K., Evrard, D., Colliere, V., Behra, P., and Gros, P., 2012, "Gold nanoparticles electrodeposited on glassy carbon using cyclic voltammetry: Application to Hg(II) trace analysis," J. Electroanal. Chem., 664, pp 46-52.
[307] Kumar, T. N., Sivabalan, S., Chandrasekaran, N., and Phani, K. L. N., 2014, "Ferrocene-functionalized polydopamine as a novel redox matrix for H_2O_2 oxidation," J. Mater. Chem. B, 2(36), pp 6081-6088.
[308] Koide, S., and Yokoyama, K., 1999, "Electrochemical characterization of an enzyme electrode based on a ferrocene-containing redox polymer," J. Electroanal. Chem., 468(2), pp 193-201.
[309] Zhang, Y. W., Li, Y. Q., Wu, W. J., Jiang, Y. R., and Hu, B. R., 2014, "Chitosan coated on the layers' glucose oxidase immobilized on cysteamine/Au electrode for use as glucose biosensor," Biosens. Bioelectron., 60, pp 271-276.
[310] Katz, E., and Willner, I., 2003, "Probing biomolecular interactions at conductive and semiconductive surfaces by impedance spectroscopy: Routes to impedimetric immunosensors, DNA-Sensors, and enzyme biosensors," Electroanal., 15(11), pp 913-947.
[311] Lang, N. J., Liu, B. W., and Liu, J. W., 2014, "Characterization of glucose oxidation by gold nanoparticles using nanoceria," J Colloid Interf Sci, 428, pp 78-83.
[312] Pasta, M., La Mantia, F., and Cui, Y., 2010, "Mechanism of glucose electrochemical oxidation on gold surface," Electrochim. Acta, 55(20), pp 5561-5568.
[313] Shrier, A., Giroud, F., Rasmussen, M., and Minteer, S. D., 2014, "Operational Stability Assays for Bioelectrodes for Biofuel Cells: Effect of Immobilization Matrix on Laccase Biocathode Stability," J. Electrochem. Soc., 161(4), pp H244-H248.
[314] Das, P., Das, M., Chinnadayyala, S. R., Singha, I. M., and Goswami, P., 2016, "Recent advances on developing 3rd generation enzyme electrode for biosensor applications," Biosens. Bioelectron., 79, pp 386-397.
[315] Casado, N., Hernandez, G., Sardon, H., and Mecerreyes, D., 2016, "Current trends in redox polymers for energy and medicine," Prog. Polym. Sci., 52, pp 107-135.
[316] Bartlett, P. N., Whitaker, R. G., Green, M. J., and Frew, J., 1987, "Covalent Binding of Electron Relays to Glucose-Oxidase," J. Chem. Soc. Chem. Comm.,(20), pp 1603-1604.
[317] Campbell, A. S., Murata, H., Carmali, S., Matyjaszewski, K., Islam, M. F., and Russell, A. J., 2016, "Polymer-based protein engineering grown ferrocene-containing redox polymers improve current generation in an enzymatic biofuel cell," Biosens. Bioelectron., 86, pp 446-453.
[318] Kleppe, K., 1966, "Effect of Hydrogen Peroxide on Glucose Oxidase from Aspergillus Niger," Biochem., 5(1), pp 139-143.
[319] Greenfield, P. F., Kittrell, J. R., and Lawrence, R. L., 1975, "Inactivation of Immobilized Glucose Oxidase by Hydrogen-Peroxide," Anal. Biochem., 65(1-2), pp 109-124.
[320] Chen, P. H., and Mccreery, R. L., 1996, "Control of electron transfer kinetics at glassy carbon electrodes by specific surface modification," Anal. Chem., 68(22), pp 3958-3965.
[321] Wang, Y. D., Joshi, P. P., Hobbs, K. L., Johnson, M. B., and Schmidtke, D. W., 2006, "Nanostructured biosensors built by layer-by-layer electrostatic assembly of enzyme-coated single-walled carbon nanotubes and redox polymers," Langmuir, 22(23), pp 9776-9783.
[322] Sirkar, K., Revzin, A., and Pishko, M. V., 2000, "Glucose and lactate biosensors based on redox polymer/oxidoreductase nanocomposite thin films," Anal. Chem., 72(13), pp 2930-2936.
[323] Dervisevic, M., Cevik, E., and Senel, M., 2015, "Development of glucose biosensor based on reconstitution of glucose oxidase onto polymeric redox mediator coated pencil graphite electrodes," Enzyme Microb. Technol., 68, pp 69-76.

[324] Cadet, M., Gounel, S., Stines-Chaumeil, C., Brilland, X., Rouhana, J., Louerat, F., and Mano, N., 2016, "An enzymatic glucose/O-2 biofuel cell operating in human blood," Biosens. Bioelectron., 83, pp 60-67.
[325] Binyamin, G., Chen, T., and Heller, A., 2001, "Sources of instability of 'wired' enzyme anodes in serum: urate and transition metal ions," J. Electroanal. Chem., 500(1-2), pp 604-611.
[326] Gerritsen, M., Jansen, J. A., Kros, A., Vriezema, D. M., Sommerdijk, N. a. J. M., Nolte, R. J. M., Lutterman, J. A., Van Hovell, S. W. F. M., and Van Der Gaag, A., 2001, "Influence of inflammatory cells and serum on the performance of implantable glucose sensors," J. Biomed. Mater. Res., 54(1), pp 69-75.
[327] Fernandez, L., and Carrero, H., 2005, "Electrochemical evaluation of ferrocene carboxylic acids confined on surfactant-clay modified glassy carbon electrodes: oxidation of ascorbic acid and uric acid," Electrochim. Acta, 50(5), pp 1233-1240.
[328] Colin-Orozco, E., Corona-Avendano, S., Ramirez-Silva, M. T., Romero-Romo, M., and Palomar-Pardave, M., 2012, "On the Electrochemical Oxidation of Dopamine, Ascorbic Acid and Uric Acid onto a Bare Carbon Paste Electrode from a 0.1 M NaCl Aqueous Solution at pH 7," Int. J. Electrochem. Sci., 7(7), pp 6097-6105.
[329] Desmet, C., Marquette, C. A., Blum, L. J., and Doumeche, B., 2016, "Paper electrodes for bioelectrochemistry: Biosensors and biofuel cells," Biosens. Bioelectron., 76, pp 145-163.
[330] Wilson, G. S., and Gifford, R., 2005, "Biosensors for real-time in vivo measurements," Biosens. Bioelectron., 20(12), pp 2388-2403.
[331] Grover, G. N., and Maynard, H. D., 2010, "Protein-polymer conjugates: synthetic approaches by controlled radical polymerizations and interesting applications," Curr. Opin. Chem. Biol., 14(6), pp 818-827.
[332] Smith, P. K., Krohn, R. I., Hermanson, G. T., Mallia, A. K., Gartner, F. H., Provenzano, M. D., Fujimoto, E. K., Goeke, N. M., Olson, B. J., and Klenk, D. C., 1985, "Measurement of Protein Using Bicinchoninic Acid," Anal. Biochem., 150(1), pp 76-85.
[333] Wiechelman, K. J., Braun, R. D., and Fitzpatrick, J. D., 1988, "Investigation of the Bicinchoninic Acid Protein Assay - Identification of the Groups Responsible for Color Formation," Anal. Biochem., 175(1), pp 231-237.
[334] Wilson, R., and Turner, A. P. F., 1992, "Glucose-Oxidase - an Ideal Enzyme," Biosens. Bioelectron., 7(3), pp 165-185.
[335] Rajagopalan, R., Aokl, A., and Heller, A., 1995, "Electron-Diffusion Coefficients in Enzyme Wiring Hydrogels," Abstr. Pap. Am. Chem. Soc., 210, pp B168-Inor.
[336] Flory, P. J. Principles of polymer chemistry. (Cornell University Press, Ithaca,; 1953).
[337] Sulak, M. T., Gokdogan, O., Gulce, A., and Gulce, H., 2006, "Amperometric glucose biosensor based on gold-deposited polyvinylferrocene film on Pt electrode," Biosens. Bioelectron., 21(9), pp 1719-1726.
[338] Gulce, H., Ozyoruk, H., Celebi, S. S., and Yildiz, A., 1995, "Amperometric Enzyme Electrode for Aerobic Glucose Monitoring Prepared by Glucose-Oxidase Immobilized in Poly(Vinylferrocenium)," J. Electroanal. Chem., 394(1-2), pp 63-70.
[339] Silveira, G. Q., Ronconi, C. M., Vargas, M. D., San Gil, R. a. S., and Magalhaes, A., 2011, "Modified Silica Nanoparticles with an Aminonaphthoquinone," J. Brazil Chem. Soc., 22(5), pp 961-U226.
[340] Conghaile, P. O., Kamireddy, S., Macaodha, D., Kavanagh, P., and Leech, D., 2013, "Mediated glucose enzyme electrodes by cross-linking films of osmium redox complexes and glucose oxidase on electrodes," Anal. Bioanal. Chem., 405(11), pp 3807-3812.

[341] Suzuki, A., Mano, N., and Tsujimura, S., 2017, "Lowering the potential of electroenzymatic glucose oxidation on redox hydrogel-modified porous carbon electrode," Electrochim. Acta, 232, pp 581-585.
[342] Prevoteau, A., and Mano, N., 2012, "Oxygen reduction on redox mediators may affect glucose biosensors based on "wired" enzymes," Electrochim. Acta, 68, pp 128-133.
[343] Ohara, T. J., Rajagopalan, R., and Heller, A., 1993, "Glucose Electrodes Based on Cross-Linked [Os(Bpy)(2)](+/2+) Complexed Poly(L-Vinylimidazole) Films," Anal. Chem., 65(23), pp 3512-3517.
[344] Arrocha, A. A., Cano-Castillo, U., Aguila, S.A., & Vazquez-Duhalt, R., 2014, "Enzyme orientation for direct electron transfer in an enzymatic fuel cell with alcohol oxidase and laccase electrodes," Biosens. Bioelectron., 61, pp 569-574.
[345] Mano, N., and Edembe, L., 2013, "Bilirubin oxidases in bioelectrochemistry: Features and recent findings," Biosens. Bioelectron., 50, pp 478-485.
[346] Milton, R. D., Giroud, F., Thumser, A. E., Minteer, S. D., and Slade, R. C. T., 2014, "Bilirubin oxidase bioelectrocatalytic cathodes: the impact of hydrogen peroxide," Chem. Commun., 50(1), pp 94-96.
[347] Milton, R. D., Giroud, F., Thumser, A. E., Minteer, S. D., and Slade, R. C. T., 2014, "Glucose oxidase progressively lowers bilirubin oxidase bioelectrocatalytic cathode performance in single-compartment glucose/oxygen biological fuel cells," Electrochim. Acta, 140, pp 59-64.